The Development of Transition Metal Catalyzed Reactions for Applications in Complex Molecule Synthesis, Methodological Development and Biomass Processing

by

Bryan Shigeru Matsuura

A dissertation submitted in partial fulfillment
of the requirements for the degree of
Doctor of Philosophy
(Chemistry)
in The University of Michigan
2015

Doctoral Committee:

Associate Professor Corey R. J. Stephenson, Chair
Assistant Professor Pavel Nagorny
Professor Melanie S. Sanford
Assistant Professor Matthew B. Soellner

To my family and friends

Acknowledgements

The work in this thesis is the product of 6 joyous years of research, which could not have been completed without the unconditional and loving support from a large group of caring individuals. First and foremost, I must extend my sincere gratitude to by advisor Corey Stephenson. I joined Corey's group in 2007 as one of his first students when we were at Boston University. By the time I had graduated, based on my credentials alone, I would not have been admitted into graduate school without help from my advisor. I thank you Corey, for going to the mat for me, and betting on the fact that I was worth the time and effort, an enabling me to pursue this degree.

My time as a graduate student has been enriched by the contributions of several faculty members during my time at Boston University and The University of Michigan. Thank you Prof. John Snyder for inspiring me to do chemistry and for your helpful discussions during the course of my PhD. Thank you Prof. Ramesh Jasti for your past and continued support during my PhD studies. I would also like to extend my gratitude to my Committee members, professors Melanie Sanford, Pavel Nagorny, and Matthew Soellner for their time and their helpful suggestions during my Data Meeting, Original Research Proposal, and my Oral Defense. I would also like to thank Prof. Corinna Schindler for her invaluable advice in the Post-Doctoral application process and for her continued support during my graduate and post graduate career. I would also like to thank Prof. Derek Pratt for his invaluable discussions and advice during the course of the resveratrol project and to Prof. Paolo Melchiorre for hosting my stay in his laboratory at ICIQ. Thank you to Dr. Chris Kojiro and Dr. Eugenio Alvarado for their assistance with the NMR facilities, Dr. James

Windak and Dr. Paul Lennon for their help with Mass Spectrometry, and Dr. Jeff Kampf for his help with X-Ray Crystallography.

I must also extend my gratitude to three lifetime mentors that have been immensely influential in my interest and desire to be a scientist. These people are Dr. Stacey Matsuura, Mr. Mori Constantino, and Prof. Mitchell Colgan. Thank you dad for being an ideal father, role model, and for teaching me the value of hard work and dedication. Thank you Uncle Mori, for continuously challenging my prejudices and predispositions. The sheer number of interests you have and continued fascination to with the world is something that I still aspire to. Thank you Dr. Colgan for your interest in my scientific development. Our discussions on a variety of topics have enriched my understanding of the natural world and motivated me to pursue my studies on a graduate level.

I have had the honor and privilege to work with the most wonderful colleagues in the world. It is without a doubt, the best part of graduate school and I could not have finished my degree without the support from a large group of graduate students and Post Docs. First and foremost, I have to thank Dr. Jagan Narayanam. You have been a fantastic mentor and a continued source of inspiration throughout my career as a scientist. I would like to acknowledge the following project collaborators, whom I am indebted to for their support: Dr. Laura Furst, Dr. Jagan Narayanam, Dr. Joe Tucker, Ms. Allison Condie, Mr. Ian McBee, Mr. Ryan Buff, Mr. Greg Karahalis, Dr. John Nguyen, Mr. Mitchell Keylor, Ms. Bo Li, Ms. YuXuan Lin, Ms. Shelby Allison, Ms. Kendra Souther, Mr. Chang Lee, Mr. Victor Chen, Ms. Becky Watson, Mr. Tim Monos, Mr. Gabe, Magallanes, Ms. Dharati Joshi, and Ms. Mariia Kirillova. I would also like to thank the following Post-Docs and visiting professors for their illuminating discussions and helpful advice: Dr. Jagan Narayanam, Prof. José Carlos Gonzáles-Gómez, Dr. David Freeman, Dr. Carl-Johan Wallentin,

Dr. James Douglas, Prof. Jim Devery, Dr. Elizabeth Swift, Dr. Milena Czyz, Dr. Markus Kärkäs, Dr. Daryl Staveness and Dr. Verner Loffstrand. I would also like to acknowledge the multitude of Stephenson Group graduate students and undergrads that I have had the immense pleasure to work with including Mr. Paul Fink, Mr. Mike Shinall, Dr. Laura Furst, Dr. Chunhui Dai, Mr. Ian McBee, Ms. Allison Condie, Dr. Joe Tucker, Dr. John Nguyen, Ms. Marlena Konieczynska, Mr. Mitchell Keylor, Mr. Joel Beatty, Mr. Sung Hun Park, Mr. Long Nguyen, Mr. Tim Monos, Mr. Gabe Magallanes, Mr. Martin Sevrin, and Ms. Theresa Williams. I am particularly indebted to the following students (in no particular order) Dr. Laura Furst, Dr. John Nguyen, Mr. Mitchell Keylor, Mr. Joel Beatty, Dr. Jagan Narayanam, Dr. David Freeman, Dr. Carl-Johan Wallentin, Dr. James Douglas, Dr. Markus Kärkäs, Dr. Elizabeth Swift, Dr. Milena Czyz, Mr. Alex Nett, Mr. Long Nguyen, Mr. Sung Hun Park, Mr. Ryan Buff, Ms. Beck Watson, Ms. Haley Albright, and Ms. Lara Cala for being wonderful colleagues and even better friends.

I would also like to thank my friends and family outside of my graduate studies who provided a loving and supportive environment for my growth as a scientist and as a person. I would like to acknowledge my mother Aileen Matsuura and my father Dr. Stacey Matsuura for being the best parents a son can ask for and for supporting my career as a scientist. They taught me the values of perseverance, determination and hard work as well as empathy, kindness and honesty - values that have made this entire endeavor possible. I would like to thank my siblings Brianna Matsuura, Blair Matsuura, and Brynn Matsuura for being the best brothers and sisters that I could ask for. My hope is that I can continue to be as good a sibling to them as they have been for me. I would also like to thank my friends (in no particular order) that have been with me since the beginning. My friends Eric Tsukamoto, Jim Connors, Andrew Swank, Brock Mantella, Ryan Dowd, Aaron Shiosaki, Daniel Cho, Tim Cho, Jordan Frease, and Ryan Ko have been the best group of friends

a guy can ask for. I am honored to call you all my friends and I don't think that any of this could have been done without the support from the aforementioned people. I love you all and I look forward to the future memories that we will make together.

Finally, I would like to thank the various people in the University of Michigan Chemistry Department, the Boston University CMLD and Vertex pharmaceuticals for financial support of my graduate studies.

Table of Contents

Chapter 2: A High-Valent Palladium Mediated Oxyarylation of Alkenes

Chapter 3: Development of a Mild, Photocatalytic Strategy Towards the Depolymerization of Lignin

List of Figures

List of Schemes

List of Tables

List of Abbreviations

abs	absorbance
Ac	acetyl
aq	aqueous
Ar	aryl
ATRA	atom transfer radical addition
AIBN	azobisisobutyronitrile
APPH	2,2'-azobis-(2-amidinopropane)-dihydrochloride
BF_4	tetrafluoroborate anion
BHT	2,6-di-*tert*-butyl-4-hydroxytoluene
Bn	benzyl
Boc	*tert*-butoxycarbonyl
BTX	benzene, toluene, xylene
Bu	*n*-butyl
bpy	2,2’-bipyridine
bpz	2,2’-bipyrazine
CAN	cerium(IV) ammonium nitrate
CFL	compact fluorescent lightbulb
cm	centimeter
°C	degree Celsius
CoA	coenzyme A
COD	1,5-cyclooctadiene
CPQM	cyclized *para*-quinone methide
Cu	copper
CV	cyclic voltammetry
d	doublet
DABCO	1,4-diazabicyclo[2.2.2]octane
DBU	1,8-diazabicyclo[5.4.0]undec-7-ene
DCM	dichloromethane
DDQ	2,3-dichloro-5,6-dicyano-1,4-benzoquinone
$dF(CF_3)ppy$	2-(2,4-difluorophenyl)-5-(trifluoromethyl)pyridine
DIPEA	*N*,*N*-diisopropylethylamine
DMF	dimethylformamide
DMP	Dess-Martin periodinane
DMSO	dimethylsulfoxide
DPPH	2,2-diphenyl-1-picrylhydrazyl
dr	diastereomeric ratio
dtbbpy	4,4'-di-tert-butyl-2,2'-bipyridine
δ	chemical shift in parts per million

$E_{0,0}$	zero-zero excitation energy
E_{red}	reduction potential
EDG	electron-donating group
ee	enantiomeric excess
eq	equation
equiv	equivalents
ESI	electrospray ionization
Et	ethyl
ET	
fac	facial
g	grams
h	hours
HAT	H-atom transfer
H_2B-PMHC	BODIPY-2,2,5,7,8-pentamethyl-6-hydroxy-chromane
HMDS	hexamethyldisilazide
HRMS	high resolution mass spectroscopy
Hz	hertz
Ir	iridium
IR	infrared
isc	intersystem crossing
J	coupling constant
K	Potassium
L	liters
LAH	lithium aluminium hydride
LBQM	linear bis *para*-quinone methide
LED	light emitting diode
Li	lithium
LMQM	linear mono *para*-quinone methide
λ_{ex}	excitation wavelength
λ_{max}	maximum wavelength
m	multiplet
m	meta
M	molar concentration
Me	methyl
MeOAMVN	2,2'-azobis-(4-methoxy-2,4-imethylvaleronitrile)
mg	milligrams
MHz	megahertz
NFSI	*N*-fluorobenzensulfonimide
μL	microliters
min	minutes
mL	milliliters
MLCT	metal to ligand charge transfer
mm	millimeters
mmol	millimoles
mol	moles
MW	molecular weight

NBS	*N*-bromosuccinimide
nm	nanometers
ns	nanosecond
NMR	nuclear magnetic resonance
o	ortho
[O]	oxidant
p	para
PC	photocatalyst
PCET	proton-coupled electron transfer
PF_6	hexafluorophosphate anion
Ph	phenyl
phen	phenanthroline
PIDA	phenyliodine diacetate
PMB	*para*-methoxybenzyl
PMHC	2,2,5,7,8-pentamethyl-6-hydroxy-chromane
PMP	*para*-methoxyphenyl
ppm	parts per million
ppy	2-phenylpyridine
Pr	propyl
q	quartet
rt or RT	room temperature
RTA	radical-trapping antioxidant
Ru	ruthenium
s	singlet
SC	super critical
SCE	saturated calomel electrode
SelectFluor	1-chloromethyl-4-fluoro-1,4-diazoniabicyclo[2.2.2]octane
SET	single electron transfer
SPLET	sequential proton-loss electron transfer
t	triplet
^{t}Bu	*tert*-butyl
TBS	*tert*-butyldimethylsilyl
TBDPS	*tert*-butyldimethylsilyl
TEMPO	2,2,6,6-tetramethylpiperidyl-1-oxyl
Tf	triflyl
THF	tetrahydrofuran
THP	tetrahydropyran
TLC	thin layer chromatography
α-TOH	α-Tocopherol
TPP	tetraphenyl porphyrin
$_R$	residence time
Ts	*para*-toluene sulfonate
UV	ultraviolet light
V	volts
W	watt

Abstract

Described herein are four projects: Chapter 1 will discuss the development of an intermolecular C–H functionalization of indoles with diethyl bromomalonate mediated by the photoredox catalyst, $Ru(bpy)_3Cl_2$. The direct functionalization of indoles is of interest to the greater synthetic community due to their ubiquity within the natural world. The difficulty in developing an intermolecular radical alkylation reaction is principally due to competitive side reactions such as reductive dehalogenation. Our approach enables a room temperature alkylation of a wide variety of electron rich heterocycles that is high-yielding, scalable and functional group tolerant. Chapter 2 will describe the development of an unusual vicinal olefin difunctionalization reaction using high-valent palladium catalysis for the synthesis of highly functionalized spirocyclohexadienones and polycyclic aromatic compounds. This synthetic approach has applications in the total synthesis of the antibiotic platensimysin. It will also provide commentary on the differences in reactivity between conventional $Pd^{II/0}$ alkene difunctionalization and ones that are mediated by higher oxidation states of palladium. Chapter 3 will present the application of visible light photoredox catalysis towards the degradation of lignin. Lignin is the second most abundant biopolymer on earth and is the only renewable feedstock for aromatic compounds. However, there are no currently implemented technologies that exploit this resource for the purpose of producing renewable fine chemicals. This chapter will discuss our lab's first successes in the validation of this concept. Specifically, in the development of a two-stage, chemoselective benzylic alcohol oxidation/photocatalytic reductive C–O bond cleavage reaction. The final chapter

will discuss a collaborative project between the Stephenson group and the Pratt group concerning a scalable biomimetic total synthesis of the resveratrol dimers quadrangularin A and pallidol. The beneficial properties of resveratrol are often attributed to its purported ability to act as a radical trapping antioxidant and maintain redox homeostasis within the body. As a result of our synthesis, we were able to provide sufficient material for the rigorous evaluation of its antioxidant activity and challenge this hypothesis.

Chapter 1: A Photocatalytic, Intermolecular Malonation of Indole

*Portions of this thesis were published in:
• Furst, L.; Matsuura, B. S.; Narayanam, J. M. R.; Tucker, J. W.; Stephenson, C. R. J. Visible Light-Mediated Intermolecular C−H Functionalization of Electron-Rich Heterocycles with Malonates. *Org. Lett.* **2010**, *12*, 3104

1.1 Introduction to Photoredox Catalysis

The electron transfer behavior of polypyridyl transition metal complexes, as typified by ruthenium (II) tris(2,2'-bipyridine) **1**, have been studied extensively since the mid 1930's.[1] Their unique redox behavior and photophysical properties have wide ranging applications in the development of dye-sensitized solar cells,[2] water-splitting catalysts,[3] novel semiconducting materials,[4] and advanced organic light-emitting diodes.[5] In their ground state, photoredox catalysts are relatively inert and are poor single electron oxidants or reductants. However, these transition metal complexes can absorb light from within the visible region, giving rise to a long-lived photoexcited state. This excited state, which can be thought of as both an oxidant and a reductant, is formally a charge separated state – and the fundamental property by which all of these applications are connected. Until recently, photoactive complexes such as $Ru(bpy)_3Cl_2$ had been almost exclusively studied by physical chemists and inorganic chemists within the context of studying electron transfer or for applications in energy research.[6] Although there were sporadic reports within the synthetic organic literature that span over the last four decades, it wasn't until 2008, when MacMillian, and Yoon simultaneously reported the use of $Ru(bpy)_3Cl_2$ to perform the enantioselective α-alkylation of aldehydes and the intramolecular radical [2+2] cycloaddition of α,β-unsaturated ketones, that it became a widely adopted strategy in organic chemistry.

The utility of photoredox catalysis largely hinges on its ability to promote single electron transfer chemistry to generate reactive radical species under conditions where they would not normally occur. Prior to the development of photoredox catalysis, organic radicals were typically generated using trialkylstannanes/AIBN, under high-energy UV irradiation, or through the use of pyrophoric alkylborane/O_2 conditions.[7] Generating radicals under classical conditions are often not compatible with many functional groups or required heating to initiate the radical chain reaction. Despite these drawbacks, the utility of radical chemistry was not underestimated, pioneering work by chemists such as Barton or Curran had demonstrated their ability to form bond disconnections that would otherwise not be possible.[8] However, the toxicity associated with stannanes and the unpredictable or uncontrollable reactivity of UV-photochemistry had perhaps unjustly prejudiced the wider synthetic community, who considered radicals to be too reactive for general synthetic purposes.

Photoredox catalysts are highly versatile and can promote reactions that are outside of the purview of traditional radical chemistry. Aside from net reductions or oxidations, photoredox catalysts can also mediate redox neutral reactions where the same catalyst can transiently accept an electron from one substrate, and then reintroduce it as some other point in the reaction. Often times with radical reactions that rely on chain propagation as a mechanism, photoredox catalysts can reinitiate the reactions that would normally terminate prematurely.[9] Photoredox catalysts can also sensitize the formation of high-energy triplet states in organic substrates through energy transfer, enabling chemistry that would otherwise require UV-light. From a practical standpoint, photoredox reactions are typically ran at ambient temperature and are insensitive to the presence of water, are compatible with a wide range of solvents, and only require irradiation with visible

light. These considerations have led to the resurgence in popularity of photoredox catalysis as a novel approach towards organic synthesis.

1.2 The Photochemistry of Visible-Light Photoredox Catalysts

Photoredox reactions can be mediated by several structurally distinct transition metal complexes and organic dyes. Although the photophysical properties of a photocatalyst are highly dependent on the catalyst structure and substitution, the mechanisms of catalyst excitation and electron transfer are generally the same and can be extended to non-polypyridyl photosensitizers. For the sake of simplicity, the following section will describe the photochemistry of the best studied photocatalyst, $Ru(bpy)_3^{2+}$ (**1**).

The excitation of $Ru(bpy)_3^{2+}$ begins with absorption of a photon of light from the ground state, which promotes an electron from the metal center's t_{2g} orbital to the low lying ligand-centered π^* orbital in a process that is called metal-to-ligand charge transfer (MLCT, Figure 1, A). Depending on the energy of the photon, the electron can initially occupy one of several excited states, but will eventually relax through its lowest lying singlet state ($^1MLCT_1$) through internal conversion (IC).[6] Thus, irradiation of the photocatalyst does not require a specific wavelength, since relaxation will occur through the same singlet state, which is why the broad spectrum irradiation by a household lightbulb is usually sufficient to initiate a reaction. For $Ru(bpy)_3^{2+}$ absorption occurs maximally in the blue region at 452 nm. The $Ru(bpy)_3^{2+*}$ $^1MLCT_1$ undergoes rapid intersystem crossing (ISC), followed by internal conversion to lowest lying triplet state, $^3MLCT_1$. This triplet state is very long lived, on the order of 800μs, since relaxation (usually through phosphorescence) to the ground state of the complex is spin forbidden.[6]

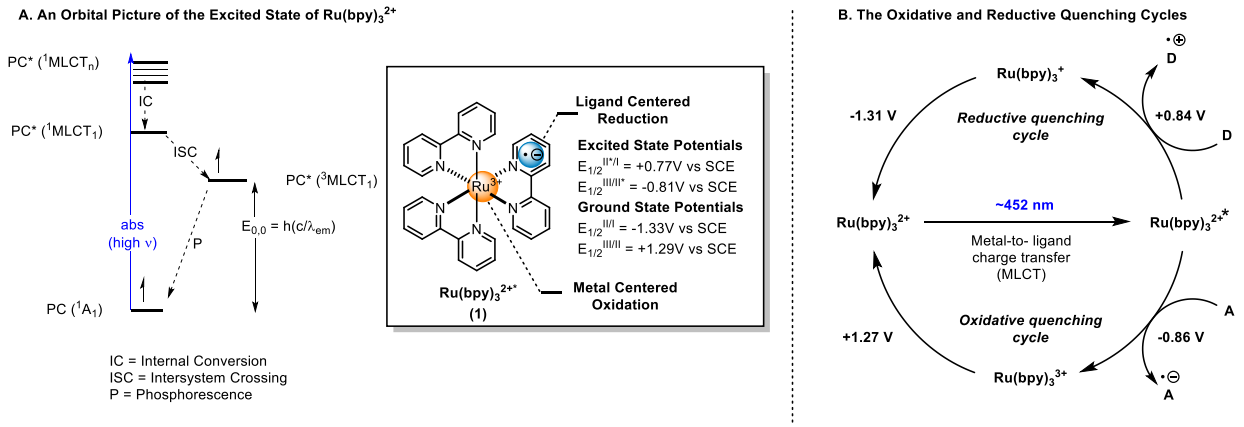

Figure 1 A simple depiction of the excited state of $Ru(bpy)_3$

This excited state of $Ru(bpy)_3^{2+*}$ ($^3MLCT_1$), which is electron deficient at the metal center and is electron rich in the ligand, has the remarkable ability to simultaneously act as an oxidant and as a reductant. In the presence of an of an electron donor, $Ru(bpy)_3^{2+*}$ can act as an oxidant and accept an electron, reducing the complex to the Ru(I) oxidation in what is called the reductive quenching cycle (Figure 1, B). In the presence of an electron acceptor, $Ru(bpy)_3^{2+*}$ can act as a reductant and donate an electron, oxidizing the complex to the Ru(III) oxidation state in what is called the oxidative quenching cycle (Figure 1, B). It should be noted that Ru(I) and Ru(III) are exceptionally strong single electron reductant/oxidants (respectively) in their own right. The reduction potentials of $Ru(bpy)_3^{2+}$ are summarized in Figure 1, wherein the term "reduction potential" is describing the electrochemical half-reaction where the more oxidized species is being reduced: $Ru^{III} + e^- \rightarrow Ru^{II}$ ($E_{1/2}$ = +1.29V vs SCE) referenced to the saturated calomel electrode.

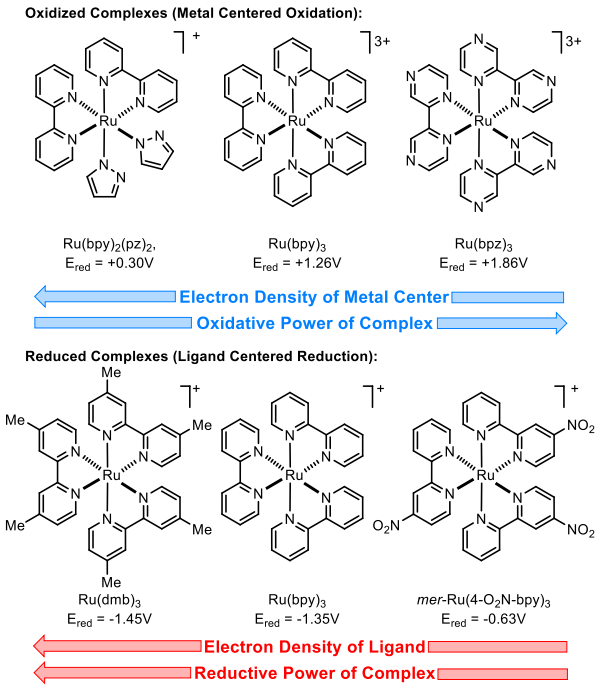

Figure 2 Effects of ligand substitution on photophysical properties (adapted from Ref [10])

Due to their extensive history in the context water splitting catalysis and solar energy applications, the photophysical properties and electrochemical potentials of hundreds of photocatalysts have been characterized.[6,11,12] These values, which include the excited state and ground state reduction potentials, the absorption wavelength, quantum yield, and excited state lifetime, are all highly dependent on the identity of the metal center and ligand structure. For instance, ligands with electron donating groups tend to shift reduction potentials in the negative direction. Ligands that are electron poor, shift reduction potentials in the positive direction (Figure 2). This provides a convenient means to choose an appropriate catalyst based on the reduction potentials of the catalyst and the reduction potentials of the substrate.[10] This is by no means an absolute rule, and a catalyst with insufficient reduction potentials can often reduce or oxidize substrates that appear to be outside of their electrochemical window.

1.3 Project Background

The application of photoredox catalysis within the context of synthetic chemistry received very limited attention prior to 2008. Several groups including Deronzier,[13] Kellogg,[14] Okada and Oda,[15] and Fukuzimi[16] were amongst the first to recognize the potential utility of $Ru(bpy)_3Cl_2$ in developing new radical reactions, including the reduction of aryl diazonium salts, carbon–halogen bonds, and N–O bonds. Unfortunately, these reports appear sporadically across the literature and went relatively unnoticed by the broader synthetic community.

Then in 2008, Nicewicz and MacMillan described an elegant enantioselective α-alkylation of aldehydes through the merger of organocatalysis and photoredox catalysis.[17] They demonstrated that $Ru(bpy)_3$ could reduce activated C–Br bonds, such as one found on diethyl bromomalonate, the resultant electron deficient radical could add enantioselectively to a chiral, electron rich enamine **5**, generated from an imidazolidinone organocatalyst (**3**) and an aldehyde. The resulting α-amino radical can then act as a single electron reductant, quenching the excited state of the photocatalyst, followed by hydrolysis to yield product **4**. Overall, this process is redox neutral, since the reduction of the C–Br bond is couple with the oxidation of the enamine. This reaction worked on a range of aliphatic aldehydes and enjoyed broad substrate scope with respect to the activated alkylbromides, occurring in high yields and *ee*'s. Shortly thereafter, this approach was expanded to include the enantioselective trifluoromethylation and perfluoroalkylation of aliphatic aldehydes.[18]

In a paper published simultaneously, Yoon and co-workers disclosed a novel intramolecular formal [2+2] cycloaddition of tethered α,β–unsaturated enones (**6**) to make fused cyclobutanones (**7**) through the use of the reductive quenching cycle of $Ru(bpy)_3Cl_2$.[19]

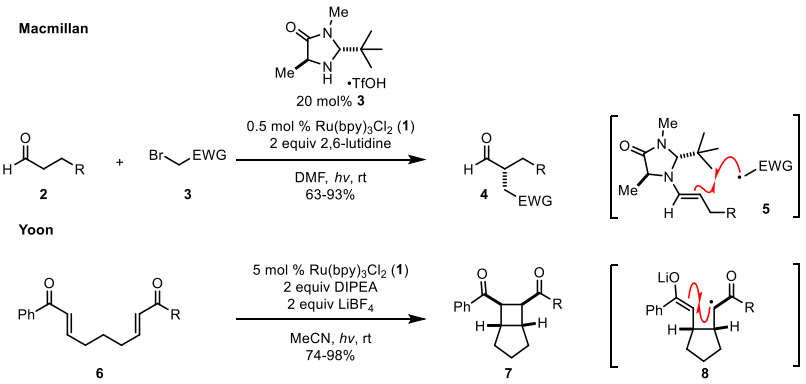

Figure 3 MacMillan and Yoon seminal publications

They found that the addition of $LiBF_4$ was an essential component of the reaction, acting as Lewis acid, which could activate the α,β–unsaturated enone by lowering its LUMO, enabling the catalyst to more efficiently reduce the ketone generating a stabilized, electron rich radical anion which could undergo an intramolecular radical conjugate addition forming (**8**), a second radical cyclization followed by oxidation of the ketyl radical yields the desired product **7**. It is important to note, that although 2 equivalents of DIPEA are used as a reductive quencher, this reaction is still redox neutral, since the overall oxidation state of the product does not change from the starting material. The intermolecular, crossed [2+2] cycloaddition variant was also subsequently reported.[20]

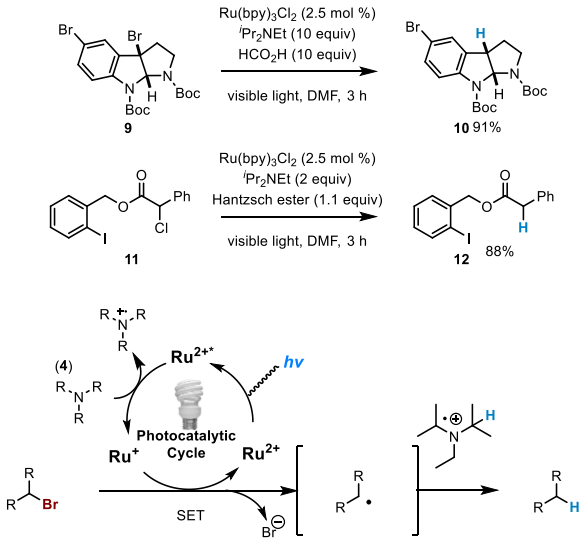

Figure 4 Stephenson's photocatalytic reductive dehalogenation

Shortly thereafter, Stephenson and co-workers described a tin-free reductive dehalogenation of activated carbon–halogen bonds.[21] The report disclosed a general set of reduction conditions that unified the pioneering studies of Fukuzumi, Kellogg, and Sauvage on the same topic. The developed reaction conditions were able to reduce a range of activated alkyl bromide, chloride and iodide bonds in good to excellent yields. Perhaps most importantly, this method displays superb chemoselectivity, preferentially reducing activated halides whilst preserving aryl and olefinic C–Br and C–I bonds, which would be impossible using the tributyltin hydride/AIBN reaction conditions. They disclosed two general reaction conditions: 1) 1 mol% $Ru(bpy)_3Cl_2$, 10 equivalents of diisopropylethylamine (DIPEA), and 10 equivalents of formic acid. 2) 2.5 mol% $Ru(bpy)_3Cl_2$, 2 equivalents of DIPEA, and 1.1 equivalents of Hantzsch ester, with the latter conditions being used in cases where nucleophilic displacement of C–X bonds by formic acid was problematic.

They proposed the reaction was going through the reductive quenching of $Ru(bpy)_3^{2+*}$ by DIPEA, forming Ru(I) and the corresponding amine radical cation. The Ru(I) ground state reduces

the activated carbon–halide bond, generating an alkyl radical. Through the use of deuterium labelling studies, they were able to determine that the H-atom donor came from the α-amine C–H from the radical cation of DIPEA, likely one of the methines on the isopropyl groups.

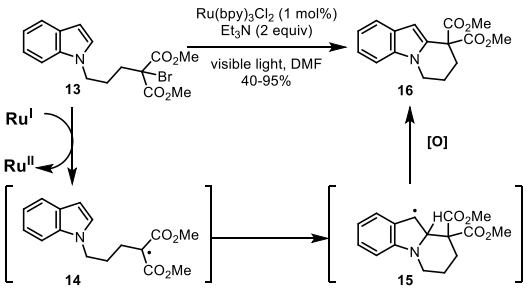

Figure 5 Stephenson's intramolecular radical cyclization of indoles

After the tin-free reductive dehalogenation, the Stephenson group published a method concerning the intramolecular C–H malonation of electron rich indoles and pyrroles.[22] Using the reaction conditions they had developed in their previous paper, they observed significant reductive dehalogenation of the starting material when DIPEA was used as an electron donor. In order to suppress this side reaction, they replaced DIPEA with triethylamine as the reductive quencher, which they knew from previous experience to be a less efficient H-atom donor.[21] These slightly modified reaction conditions enabled the radical cyclization of a variety of substituted indoles and pyrroles in moderate to good yields. Using **13** as their substrate, they were able to initiate a radical cyclization cascade, generating the corresponding bicyclic indole **16** in 79% yield. The reaction mechanism was proposed to go through the reductive quenching cycle, wherein triethylamine transfers an electron to the excited state of $Ru(bpy)_3^{2+*}$, generating the ground state Ru(I). Single electron transfer from this complex to the activated C–Br bond of the indole-malonate **13** affords the electron-deficient radical intermediate **14**. Intramolecular radical cyclization onto the indole forms the radical intermediate **15**, which upon single electron oxidation and proton loss results in the formation of the desired product. This publication demonstrated the potential of photoredox

catalysis to enable the C–H alkylation of electron rich aromatic compounds. The reactions reported in this publication served as the basis for the intermolecular alkylation of indole derivatives, which we were interested in developing for applications in the total synthesis of indole alkaloids.

It is important to note that this background section only provides the context by which Laura and I started the chemistry described in this chapter. At the time there were ~15 total publications stemming from 2008 from the labs of MacMillan, Yoon, and Stephenson. The field of photoredox catalysis has since developed enormously in the intervening years with contributions from many groups around the world. This research is outside of the context of this introduction and have been summarized expertly in the following reviews.[23–25]

1.4 Reaction Design Strategy

The indole nucleus is a highly prevalent motif in natural products chemistry and pharmaceuticals.[26] Therefore, methodologies aimed at the selective functionalization of indole are of considerable importance in the context of the total synthesis. Although there are several ways to synthesize indoles, the selective functionalization of substituted indoles, remains a challenging task. In particular, functionalization of the C2 position is difficult, since indole typically reacts in the C3 position.[27–30] The alkylation of indoles with activated alkyl halides is overall a redox neutral process. If the photocatalyst cannot reduce the desired C–X bond using its photoexcited state, it is often possible to do so under reductive quenching conditions. The reduced ground state of a photocatalyst often has several advantages over excited state electron transfer since it does not quench through energy transfer, is not limited by the excited state lifetime, and has stronger electrochemical potential, enabling it to engage in single electron reduction chemistry with a wider variety of electrophiles. In order to achieve this, however, there must be a sacrificial reductive quencher in sufficient quantities to quench the excited state. Typically this is achieved with

trialkylamine such as triethylamine, tributylamine, or diisopropylethylamine. However, performing a redox neutral transformation using trialkylamine reductive quenchers is problematic since the oxidation of amines, though reversible, results in the formation of radical cations which have

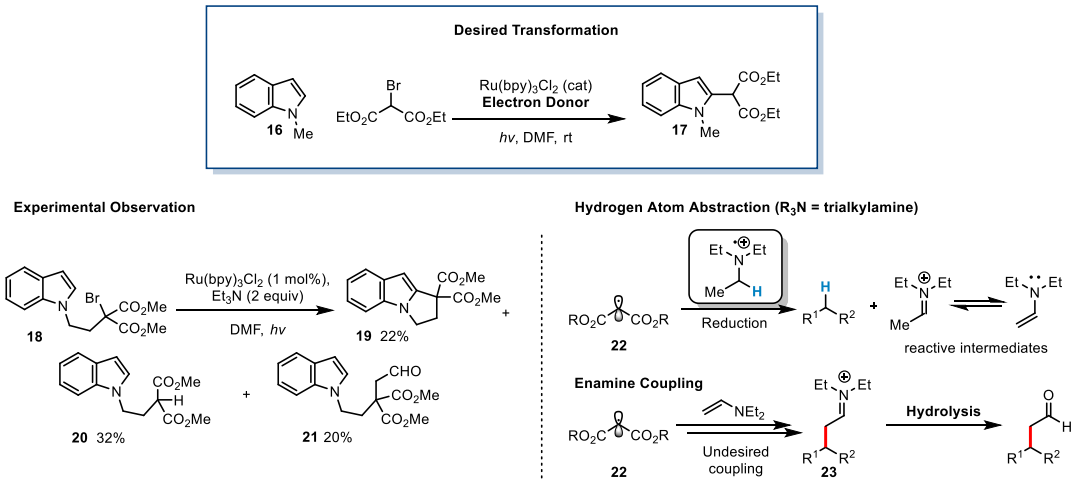

Figure 6 Side reactivity of amine radical cations

several decomposition pathways and can interfere with the reaction (Figure 6). During our lab's initial studies on the alkylation of indole, we found that although intramolecular malonation reaction was efficient using triethylamine as a reductive quencher, the intermolecular variant did not work, even when superstoichiometric quantities of indole were used as a reaction partner. This was due to the competitive reductive dehalogenation of the C–Br bond of diethyl bromomalonate.[21] The oxidation of trialkylamines to their amine radical cation derivatives significantly lowers the pKa of their α-protons, which can either be deprotonated to make an α-amine radical, a good single electron reductant, or can serve as an H-atom donor.[31,32] In the case of the intermolecular indole malonation, these amine radical cations were reducing the photocatalytically generated malonyl radicals (**22**) through H-atom transfer. During our studies

on intramolecular indole cyclization chemistry, we had observed that while substrates that cyclized to form 6-membered rings were generally efficient, substrate **18** was converted to **19** in only 22% yield. In addition to reductive dehalogenation, we observed significant reductive dehalogenation to **20** and formation of unusual product **21**. We hypothesized that the acetaldehyde moiety was generated from the oxidation of triethylamine to its corresponding iminium ion, upon interconversion into the corresponding enamine, it would react with **22** forming iminium **23**, which hydrolyzes generating **21** (Figure 6).

The inability of trialkylamines to serve as reductive quenchers for intermolecular alkylation chemistry can be attributed to the presence of the α-protons, which act as parasitic reducing equivalents in a reaction that is redox-neutral. To overcome this limitation, we sought to identify a new class of reductive quencher that could effectively quench the excited state of $Ru(bpy)_3Cl_2$, but did not interfere with subsequent reaction processes. We hypothesized that this could be accomplished if we could identify a reductive quencher that did not possess any C–H bonds that could reduce electron deficient radicals via H-atom abstraction. With this goal in mind, my colleague and mentor Dr. Laura Furst and I set out to discover such a reagent.

1.5 The identification of *N,N*-diphenylanisidine as a reductive quencher

In contrast to trialkylamines, triarylamines immediately stood out as promising candidates as electron donors, due to their lack of α-amine C–H bonds. These compounds, which have been used as *p*-type materials in the preparation of organic semiconductors, are capable of undergoing highly reversible oxidation/reduction reactions due to resonance stabilization of the corresponding arene radical cation.[33] In fact, triarylamine radical cation (**24**), known as the Ledwith–Weitz salt, is a stable amine radical cation that has been used in the context of organic synthesis as a single electron oxidant and as a radical shuttle for radical-cation mediated Diels-Alder reactions

(Figure 7).[34–36] However, triarylamines generally possess more positive reduction potentials compared to trialkylamines as a result of conjugation of their lone pair with its arene rings and the reversible nature of the amine/aminium redox couple could potentially be problematic if the back electron transfer reaction could outcompete reduction of the diethyl bromomalonate.

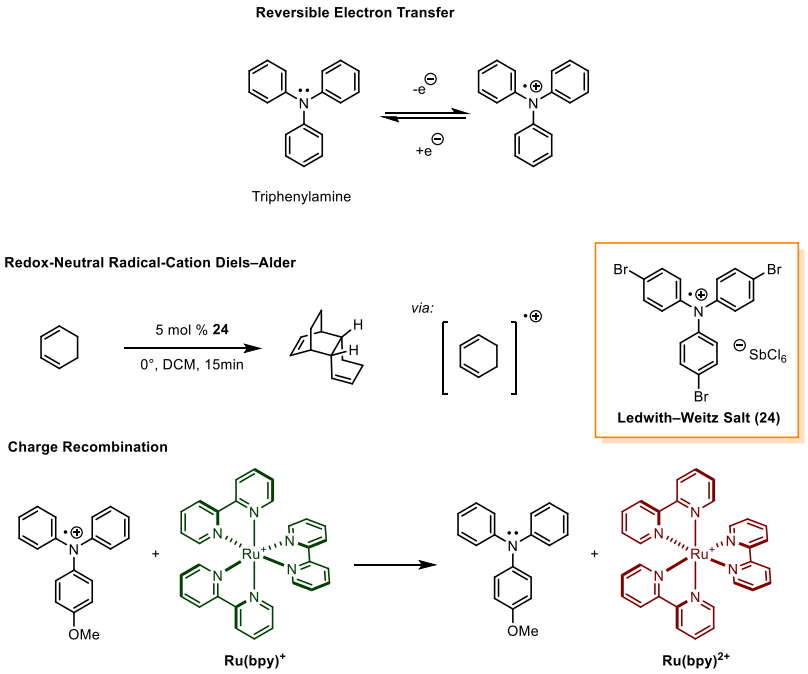

Figure 7 Reversible redox behavior of triarylamines

After some initial optimization, we found that the commercially available triarylamine, *N*,*N*-diphenylanisidine (**25**) was an effective electron donor. Using 2 equivalents of **25**, 1 mol% of $Ru(bpy)_3Cl_2$ (**1**) and 2 equivalents of diethyl bromomalonate, we were able alkylate *N*-methyl indole (**16**) to isolate 82% of 2-malonylindole **17** under blue LED irradiation (Figure 8). In contrast, when 5 equivalents of *N*-methyl indole (**16**) is reacted with 1 equivalent of diethyl bromomalonate using triethylamine as a reductive quencher afforded alkylated product **17** in only 25% yield**.** In theory, **25** should be able to

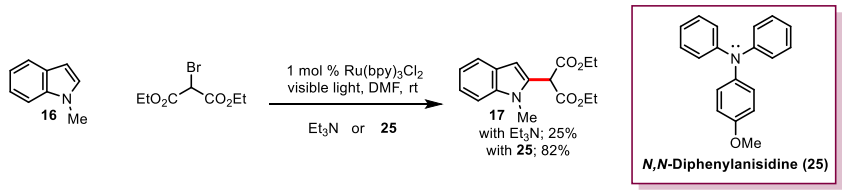

Figure 8 Malonation of *N*-methylindole using trialkylamine and triarylamine reductive quenchers

act as a catalytic electron donor, however, the use of 1 equivalent of **25,** the reaction affords comparable product yields with prolonged reaction time. We hypothesized that the extra equivalent of base is also acting as a buffer against the HBr that forms during the course of the reaction, therefore necessitating the use of 2 equivalents. Using blue LEDs accelerated the reaction considerably, since $Ru(bpy)_3Cl_2$ absorbs maximally at these wavelengths.[6] Control experiments revealed that without the presence of $Ru(bpy)_3Cl_2$, light or 25, no conversion of **16** was observed, indicating that each of those conditions are essential. With these optimized results in hand, we set out to explore the full scope of the intermolecular malonation of indoles.

1.6 Reaction Scope

In general, our reaction conditions were efficient in the malonation of electron rich heterocycles such as indoles, pyrroles, and even 5-bromo-7-azaindole, albeit in lower yield since it is more electron poor (Table 1). The reaction was exceptionally functional group tolerant and was efficient in the presence of acid sensitive Boc groups, unprotected amides, free carboxylic acids and methyl esters (Entries 6–8). The reduction was also highly selective for the malonyl C–Br bond, and indole substrates containing aliphatic or aromatic C–Br survived the reaction conditions unmolested.[21] The reaction was also found to be scalable, affording 73% of **30** on a 2 mmol scale. These reaction conditions were also competent in the malonation of highly functionalized diketopiperidine **36** and dipeptide **37**, which are motifs that are commonly found in natural products. Furthermore, we were able to able to isolate 40% of **33** when water was used as

a solvent. The low yield of this reaction was likely due to the fact that nearly all components of the reaction were insoluble. However, this result suggests that photoredox catalysis or radical alkylation chemistry could potentially serve as an approach to bioorthoginal chemistry, in particular in the selective tagging of tryptophan residues on proteins.

Table 1 Photoredox catalyzed intermolecular radical C–H functionalization of electron rich heterocycles

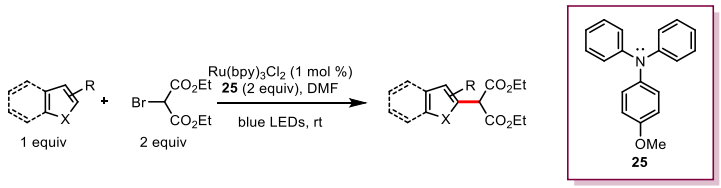

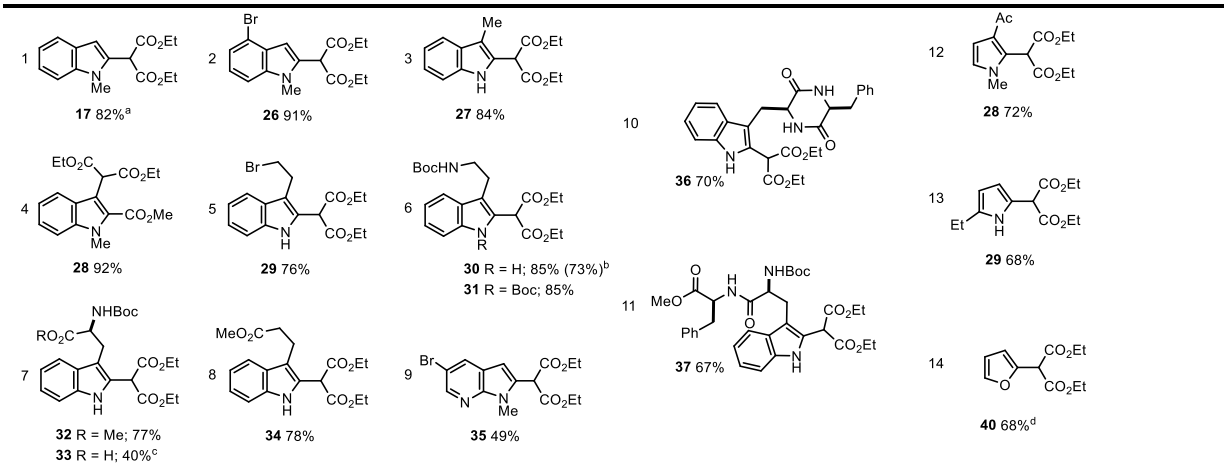

[a]Isolated yield after purification by chromatography on SiO_2; [b]2.0 mmol scale; [c]Reaction was performed in water, isolated as the methyl ester and yield based upon recovered SM; [d]5 equiv furan used.

When less reactive α-bromophenylacetic acid **41** was subjected to our optimized conditions, we were unable to observe any product formation. We reasoned this was due to competitive charge recombination between $Ru(bpy)_3^+$ and the corresponding amine radical cation. To test this hypothesis, Laura synthesized the more electron rich triarylamine, 4,4'-

dimethoxytriphenyl amine **42**. In principle, this more electron rich triarylamine should have a more negative reduction potential, making it a more

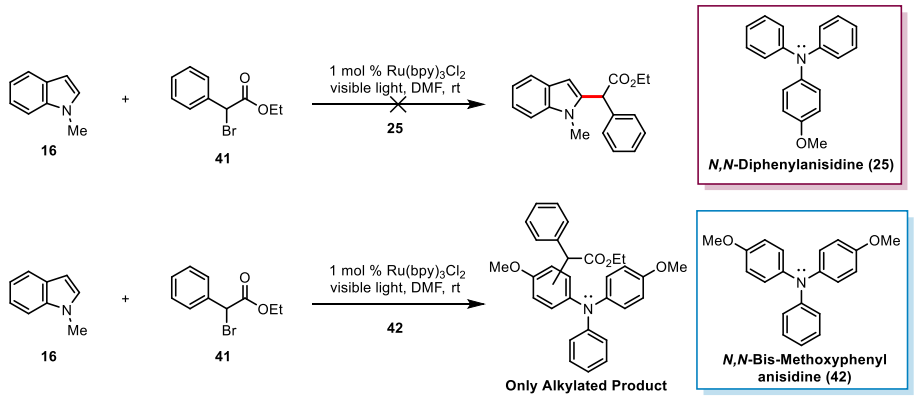

Figure 9 Attempted Alkylation of **16** with less activated alkylhalides with an electronically tuned triarylamine

efficient reductive quencher, whereas the corresponding amine radical cation should also be a weaker oxidant, making back electron transfer less efficient. Unfortunately, we were unable to identify any indole alkylation with **41** using triarylamine **42** reductive quencher and instead observed triarylamine alkylation. This result suggested that charge recombination could be suppressed by modifying the electron structure of our electron donor. However, this comes at the price of increasing the reactivity of the reductive quencher towards the electron deficient α-ketoradicals, introducing unwanted side reactivity. To our disappointment, we were unable to expand the scope of the alkylating reagents beyond diethyl bromomalonate, significantly limiting the generality of this reaction.

1.7 Reaction Mechanism

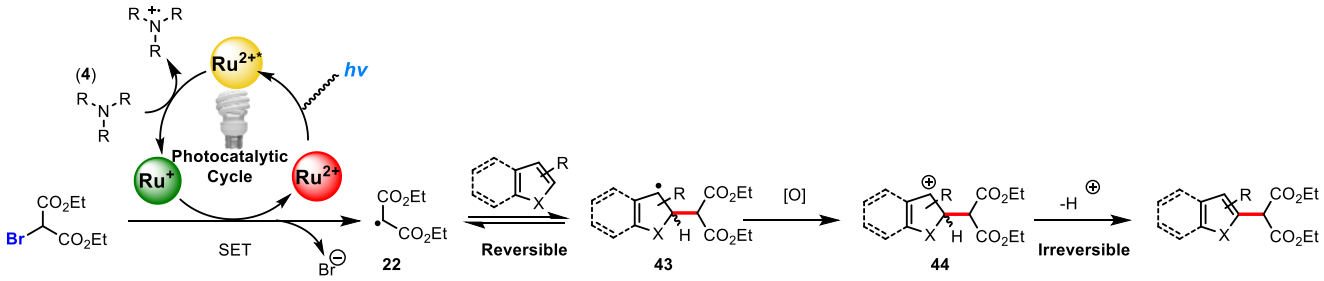

Figure 10 Mechanism of indole malonation with photoredox catalysis

Based our results, a plausible mechanism for our indole malonation is presented in Figure 10. Irradiation of $Ru(bpy)_3^{2+}$ promotes it from its ground state to excited state via a metal-to-ligand charge transfer (MLCT). This long lived excited state can either fluoresce, returning to its ground state, or can accept an electron from **25** forming its radical cation and the ground state reductant $Ru(bpy_3)^{+}$. The Ru(I) complex can then reduce diethyl bromomalonate forming the electron deficient malonyl radical **22**, with loss of a bromide ion. This reactive intermediate can undergo reversible radical addition to the electron rich π-system of the electron-rich arene. This typically occurs on the C2 carbon on indole, presumably due to the formation of a more stable benzylic radical intermediate **43**. Substrates that are substituted on the C2-position undergo functionalization on the benzylic C3-carbon (Entry 4, Table 1). Oxidation of the benzylic radical followed by irreversible deprotonation of cation **44 furnishes** the desired product.

1.8 Conclusions and Outlook

In conclusion, we have developed an efficient intermolecular radical C–H alkylation of electron rich heterocyles with diethyl bromomalonate using visible-light photoredox catalysis. This methodology is scalable and highly functional group tolerant, enabling rapid access to complex indole containing motifs that are commonly found in natural products. Furthermore, this

reaction can be conducted in aqueous media and therefore is a promising lead towards the development of novel bioconjugation and protein modification chemistry. Although the scope of the bromomalonate substrate partner is currently limited, this method further validates the utility of radical C–H functionalization for the synthesis of complex aromatic heterocycles. Expanding the scope of the alkylhalide coupling partner will significantly broaden the utility of this reaction. This will likely involve the identification of more strongly reducing photocatalysts or the identification of reductive quenchers that do not react with alkyl radicals and have favorable charge recombination dynamics. Ideally, this reductive quencher will behave either as an initiator or as a redox catalyst, obviating the need to use superstoichiometric quantities. It is highly likely that this reactivity will have to be optimized synergistically with a photoredox catalyst that has suitable photophysical properties.

1.9 Experimental Section

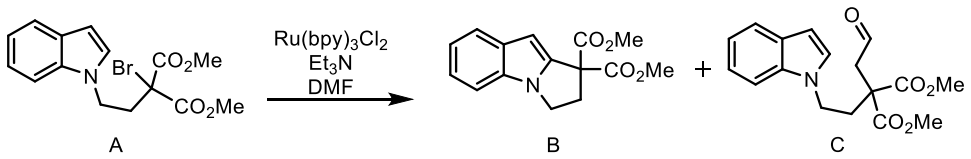

Dimethyl 2,3-dihydro-1H-pyrrolo[1,2-a]indole-1,1-dicarboxylate (**B**)[1] and **dimethyl 2-(2-(1H-indol-1-yl)ethyl)-2-(2-oxoethyl)malonate** (**C**) (Figure 2).

A flame dried 10 mL round bottom flask was equipped with a rubber septum and magnetic stir bar and was charged with tris(2,2´-bipyridyl)ruthenium(II) chloride hexahydrate (1.6 mg, 2.1 μmol, 0.010 equiv), **A** (75 mg, 0.21 mmol, 1.0 equiv), Et_3N (58 μL, 0.42 mmol, 2.0 equiv) and DMF (4.2 mL). The mixture was degassed by the freeze-pump-thaw procedure, and placed at a distance of ~10 cm from a 15 W fluorescent lamp. After the reaction was complete (12 h, as judged by TLC analysis), the mixture was poured into a separatory funnel containing 25 mL of Et_2O and 25 mL of H_2O. The layers were separated and the aqueous layer was extracted with Et_2O (2 X 50 mL). The combined organic layers were dried (Na2SO4) and concentrated. The residue was purified by chromatography on SiO_2 (95:5, hexanes/EtOAc) to provide **B** (13 mg, 22%) and **C** (13 mg, 20%) as colorless solids.

Data for **B**:

R_f (7:3 Hexanes/EtOAc) 0.39;

^{1}H NMR (400 MHz): δ 7.59 – 7.62 (m, 1 H), 7.26 – 7.28 (m, 1 H), 7.16 – 7.20 (m, 1 H), 7.08 – 7.12 (m, 1 H), 7.55 (d, *J* = 0.8 Hz, 1 H), 4.21 (t, *J* = 6.8 Hz, 2 H), 3.80 (s, 6 H), 3.19 (t, *J* = 6.8 Hz, 2 H).

Data for **C**:

Rf (7:3 Hexanes/EtOAc) 0.18;

IR (neat): 2955, 1732, 1462, 1352, 1215, 764 cm^{-1};

^{1}H NMR (300 MHz): 9.64 (s, 1 H), 7.60 (d, *J* = 7.8 Hz, 1 H), 7.34 (d, *J* = 7.8 Hz, 1 H), 7.21 (t, *J* = 7.4 Hz, 1 H), 7.09 (t, *J* = 7.4 Hz, 1 H), 7.03 (d, *J* = 3.3 Hz, 1 H), 6.47 (d, *J* = 3.3 Hz, 1 H), 4.19 – 424 (m, 2 H), 3.72 (s, 6 H), 3.02 (s, 2 H), 2.47 – 2.52 (m, 2 H);

^{13}C NMR (75 MHz): δ 198.0, 170.3, 135.6, 128.7, 127.4, 121.5, 119.5, 109.3, 101.7, 53.3, 53.1, 46.9, 42.5, 34.2, 29.7;

HRMS (ESI) *m/z* calculated for $C_{14}H_{19}NaNO_5^+$ ($[M+Na]^+$) 340.1161, found 340.1177.

[1] Magolan, J.; Kerr, M. A. *Org. Lett.* **2006**, *8*, 4561.

General Procedure for Photoredox Catalyzed Alkylation of Heteroaromatics

A flame dried 10 mL round bottom flask was equipped with a rubber septum and magnetic stir bar and was charged with the heteroaromatic compound (0.15 mmol, 1.0 equiv), tris(2,2´-bipyridyl)ruthenium(II) chloride hexahydrate (1.5 µmol, 0.01 equiv), 4-methoxytriphenylamine (0.30 mmol, 2.0 equiv), diethyl bromomalonate (0.30 mmol, 2.0 equiv) and DMF (1.5 mL). The mixture was degassed via the freeze-pump-thaw method and placed at a distance of ~2-5 cm from blue light emitting diodes (LEDs) [2]. After the reaction was complete (as judged by TLC analysis), the mixture was poured into a separatory funnel containing 25 mL of EtOAc and 25 mL of H_2O. The layers were separated and the aqueous layer was extracted with EtOAc (2 X 50 mL). The combined organic layers were washed with 25 mL of water and 25 mL of brine, dried (Na_2SO_4) and concentrated. The residue was purified by chromatography on silica gel, using the solvent system indicated, to afford the desired alkylated product.

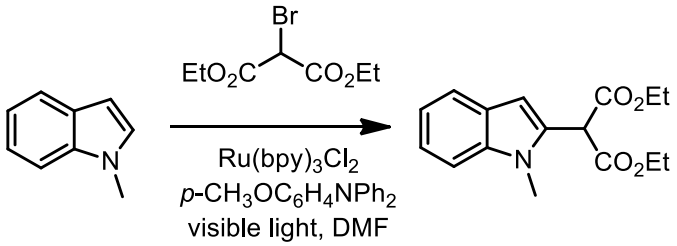

Diethyl 2-(1-methyl-1H-indol-2-yl)malonate (Table 1, entry 1). According to the general procedure, *N*-methylindole (0.10 g, 0.76 mmol), diethyl bromomalonate (0.20 mL, 1.2 mmol)**,** 4-methoxytriphenylamine (0.42 g, 1.6 mmol) and tris(2,2´-bipyridyl)ruthenium(II) chloride hexahydrate (6.0 mg, 7.6 µmol) afforded the coupled product (0.18 g, 82%) as a yellow-orange oil after purification on SiO_2 (95:5, hexanes/EtOAc) (18 h reaction time).

R_f (95:5 Hexanes/EtOAc) = 0.17;

IR (neat): 3409, 5979, 2935, 1692, 1508, 1457, 1392, 1366, 1244, 1167, 1028, 741 cm^{-1};

^{1}H NMR (400 Mhz): δ 7.78 (d, *J* = 7.8 Hz, 1 H), 7.59 – 7.46 (m, 1 H), 7.47 – 7.33 (m, 1 H), 7.37 – 7.25 (m,1 H), 6.78 (s, 1 H), 5.12 (s, 1 H), 4.64 – 4.30 (m, 4 H), 3.91 (s, 3 H), 1.49 (t, *J* = 7.1 Hz, 6 H);

^{13}C NMR (100 MHz): δ 167.6, 156.2, 136.4, 136.3, 127.7, 125.9, 122.9, 119.8, 119.2, 122.6, 111.5, 62.7, 62.7, 49.5, 41.3, 28.7, 25.0, 14.3;

HRMS (ESI) *m/z* calculated for $C_{16}H_{19}NO_4$ $[M+1]^+$ 290.1392, found 290.1394.

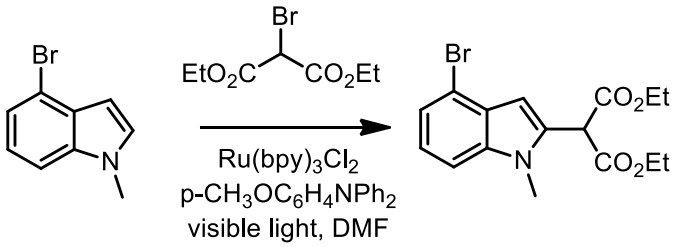

Diethyl 2-(4-bromo-1-methyl-1H-indol-2-yl)malonate (Table 1 Entryl 2). According to the general procedure, 4-bromo-1-methylindole (50 mg, 0.24 mmol), diethyl bromomalonate (0.08 mL, 0.48 mmol)**,** 4-methoxytriphenylamine (0.13 g, 0.48 mmol) and tris(2,2´-bipyridyl)ruthenium(II) chloride hexahydrate (2.0 mg, 2.4 µmol) afforded the coupled product (88 mg, 91%) as an orange oil after purification on SiO_2 (98:2, hexanes/EtOAc) (4 days reaction time).

R_f (90:10 Hexanes/EtOAc) = 0.16;

IR (neat): 2981, 2928, 1732, 1653, 1537, 1457, 1424, 1368, 1344, 1214, 1150, 1030, 764 cm^{-1};

^{1}H NMR (400 MHz): δ 7.17 – 7.21 (m, 1 H), 7.00 – 7.03 (m,1 H), 6.59 (s, 1 H), 4.89 (s, 1 H), 4.18 – 4.34 (m, 4 H), 3.64 (s, 3 H), 1.25 (t, *J* = 7.1 Hz, 6 H);

^{13}C NMR (100 MHz): δ 166.9, 131.9, 128.2, 123.1, 122.9, 115.0, 108.8, 103.7, 62.6, 51.6, 31.1;

HRMS (ESI) *m/z* calculated for $C_{16}H_{18}BrNO_4$ $[M+1]^+$ 368.0497, found 368.0500.

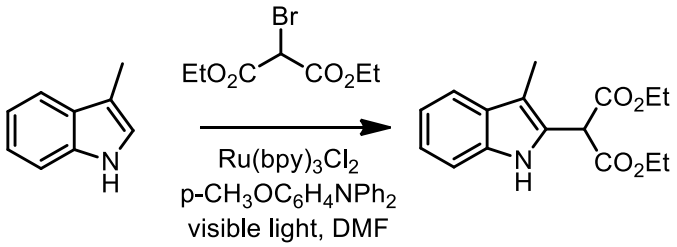

Diethyl 2-(1,3-dimethyl-1H-indol-2-yl)malonate (Table 1, Entry 3). According to the general procedure, 3-methylindole (50 mg, 0.38 mmol), diethyl bromomalonate (91 µL, 0.53 mmol,)**,** 4-methoxytriphenylamine (0.21 g, 0.53 mmol) and tris(2,2´-bipyridyl)ruthenium(II) chloride hexahydrate (3.0 mg, 3.8 µmol) afforded the coupled product (92 mg, 84%) as a yellow oil after purification on SiO_2 (90:5:5 hexanes/EtOAc/AcOH) (8 h reaction time).

R_f (93:5:2, Hexanes/EtOAc/AcOH) = 0.50;

IR (neat): 3414, 3060, 2982, 2936, 1731, 1621, 1460,1369, 1318, 1243 cm^{-1};

^{1}H NMR (400 MHz): δ 8.93 (br s, 1 H, NH), 7.55 (dd, *J* = 7.8, 1.2 Hz, 1 H), 7.42 – 7.30 (m, 1 H), 7.23 – 7.16 (m, 1 H), 7.16 – 7.04 (m, 1 H), 4.38 – 4.13 (m, 4 H), 2.39 – 2.21 (m, 3 H), 1.36 – 1.20 (m, 6 H);

^{13}C NMR (100 MHz) δ 167.4, 135.8, 128.2, 124.5, 122.4, 119.2, 118.8, 111.1, 110.6, 62.3, 49.3, 49.3, 14.0, 8.5;

HRMS (ESI) *m/z* calculated for $C_{16}H_{19}NO_4$ $[M+1]^+$ 290.1392, found 290.1390.

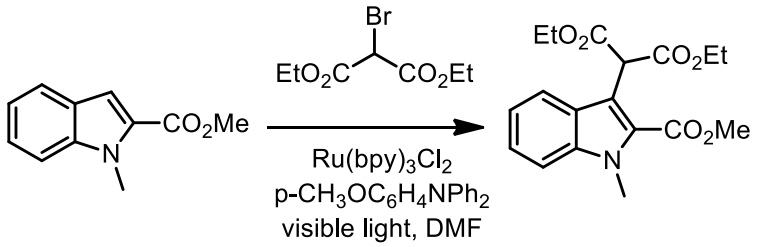

Diethyl 2-(2-(methoxycarbonyl)-1-methyl-1H-indol-3-yl)malonate (Table 1, Entry 4). According to the general procedure, methyl 1-methylindole-2-carboxylate (50 mg. 0.26 mmol), diethyl bromomalonate (90 μL, 0.53 mmol,)**,** 4-methoxytriphenylamine (0.14 g, 0.53 mmol) and tris(2,2´-bipyridyl)ruthenium(II) chloride hexahydrate (2.0 mg, 2.6 μmol) afforded the coupled product (84 mg, 93%) as a light green solid after purification on SiO_2 (1:9 hexanes/EtOAc) (24 h reaction time).

R_f (90:10, Hexanes/EtOAc) = 0.14;

IR (neat): 2983, 2956, 2362, 2331, 1732, 1714, 1532, 1468, 1441, 1398, 1368, 1311, 1241, 1150, 1109, 1050, 862, 745 cm^{-1};

^{1}H NMR (400 MHz): δ 7.78 – 7.64 (m, 1 H), 7.43 – 7.30 (m, 2 H), 7.20 – 7.10 (m, 1 H), 5.75 (s, 1 H), 4.32 – 4.15 (m, 4 H), 4.02 (s, 3 H), 3.94 (s, 3 H), 1.24 (t, *J* = 7.1 Hz, 6 H);

^{13}C NMR (100 MHz): δ 168.8, 162.7, 138.9, 126.4, 125.9, 125.6, 122.2, 121.0, 114.7, 110.6, 61.9, 52.0, 50.2, 32.5, 14.3;

HRMS (ESI) *m/z* calculated for $C_{18}H_{21}NNaO_6$ $[M+Na]^+$ 370.1267, found 370.1272.

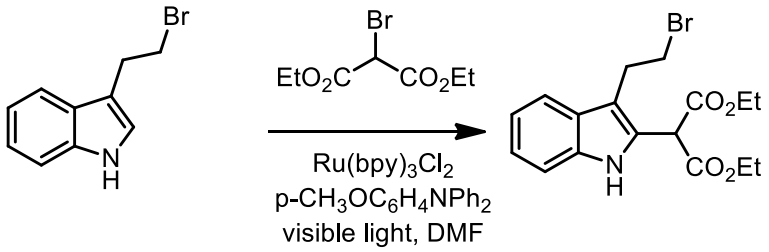

Diethyl 2-(3-(2-bromoethyl)-1H-indol-2-yl)malonate (Table 1, Entry 5). According to the general procedure, 3-(2-bromoethyl)indole (50 mg, 0.22 mmol), diethyl bromomalonate (75 µL, 0.45 mmol,)**,** 4-methoxytriphenylamine (0.12 g, 0.45 mmol) and tris(2,2´-bipyridyl)ruthenium(II) chloride hexahydrate (3.0 mg, 2.2 µmol) afforded the coupled product (64 mg, 76%) as a light pink solid after purification on SiO_2 (95:5 hexanes/acetone) (12 h reaction time).

R_f (90:10 Hexanes/EtOAc) 0.13;

IR (neat): 3399, 2982, 1729, 1459, 1310, 1242, 1204, 1151, 1030 cm^{-1};

^{1}H NMR (400 MHz): δ 9.03 (br s, 1 H, NH), 7.56 (d, *J* = 8.0 Hz, 1 H), 7.38 (dd, *J* = 8.1, 0.9 Hz, 1 H), 7.22 (tt, *J* = 7.6, 1.0 Hz, 1 H), 7.17 – 7.10 (m, 1 H), 5.00 (s, 1 H), 4.36 – 4.12 (m, 4 H), 3.65 – 3.51 (m, 2 H), 3.40 – 3.29 (m, 2 H), 1.29 (t, *J* = 6.6 Hz, 6 H);

^{13}C NMR (100 MHz): δ 167.0, 135.8, 125.9, 122.7, 119.8, 118.4, 112.2, 111.4, 77.2, 62.5, 49.2, 32.3, 28.3, 14.0;

HRMS (ESI) *m/z* calculated for $C_{17}H_{21}BrNO_4$ $[M+1]^+$ 382.0654, found 382.0650.

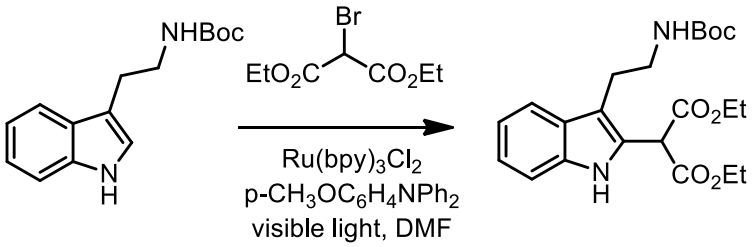

Diethyl 2-(3-(2-((tert-butoxycarbonyl)amino)ethyl)-1H-indol-2-yl)malonate (Table 1, Entry 6; R = H). According to the general procedure, *N*-Boc-tryptamine (0.50 g, 2.0 mmol), diethyl bromomalonate (0.70 mL, 4.1 mmol)**,** 4-methoxytriphenylamine (1.1 g, 4.1 mmol) and tris(2,2´-bipyridyl)ruthenium(II) chloride hexahydrate (18 mg, 0.02 mmol) afforded The coupled productthe coupled product (0.62 g, 73%) as a white solid after purification on SiO_2 (4:1 hexanes/EtOAc) (12 h reaction time).

R_f (70:30 Hexanes/EtOAc) = 0.40;

IR (neat): 3409, 2979, 2935, 1692, 1508, 1457, 1392, 1366, 1244, 1167, 1028, 741 cm^{-1};

^{1}H NMR (400 MHz): δ 8.94 (br s, 1 H, NH), 7.59 (d, *J* = 7.8 Hz, 1 H), 7.37 (dd, *J* = 8.1, 0.7 Hz, 1 H), 7.2 (m, 1 H), 7.12 (m, 1 H), 4.96 (s, 1 H), 4.75 (br s, 1 H, NH), 4.25 (m, 4 H), 3.42 (br s, 2H), 2.96 (t, *J* = 6.6 Hz, 2 H), 1.44 (s, 9 H), 1.29 (td, *J* = 7.1, 0.7 Hz, 6 H);

^{13}C NMR (100 MHz): δ 167.6, 156.2, 136.4, 136.3, 127.7, 125.9, 122.9, 119.8, 119.2, 122.6, 111.5, 62.7, 62.7, 49.5, 41.3, 28.7, 25.0, 14.3;

HRMS (ESI) *m/z* calculated for $C_{22}H_{30}N_2O_6Na$ $[M+Na]^+$ 441.2002, found 441.2010.

Spectral data is in accordance with previously reported data [3].

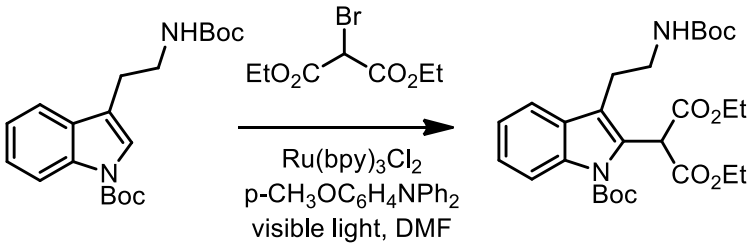

Diethyl 2-(1-(tert-butoxycarbonyl)-3-(2-((tert-butoxycarbonyl)amino)ethyl)-1H-indol-2yl) malonate (Table 1, Entry 6; R = Boc). According to the general procedure, *N,N'*-di-Boc-tryptamine (50 mg, 0.14 mmol), diethyl bromomalonate (50 μL, 0.28 mmol)**,** 4-methoxytriphenylamine (77 mg, 0.28 mmol) and tris(2,2´-bipyridyl)ruthenium(II) chloride hexahydrate (1.0 mg, 1.4 μmol) afforded the coupled product (62 mg, 85%) as a beige solid after purification on SiO_2 (4:1 hexanes/EtOAc) (12 h reaction time).

R_f (80:20 Hexanes/EtOAc) = 0.25;

IR (neat): 3363, 2980, 2360, 2342, 1722, 1456, 1366, 1329, 1233, 1162, 1131, 1039, 757 cm^{-1};

^{1}H NMR (400 MHz): δ 8.02 (d, *J* = 8.4 Hz, 1 H), 7.57 (d, *J* = 7.7 Hz, 1 H), 5.21 (s, 1 H), 4.89 (br s, 1 H, NH), 4.35 – 4.14 (m, 4 H), 3.40 (d, *J* = 5.7 Hz, 2 H), 2.88 (t, *J* = 6.4 Hz, 2 H), 1.66 (s, 9 H), 1.43 (s, 9 H), 1.24 (t, *J* = 7.2 Hz, 3 H);

^{13}C NMR (100 MHz): δ 166.5, 156.0, 150.5, 135.6, 129.1, 129.0, 124.7, 122.6, 119.5, 118.9, 115.8, 84.4, 79.2, 77.2, 61.8, 49.9, 40.2, 28.4, 28.2, 24.7, 14.1;

HRMS (ESI) *m/z* calculated for $C_{27}H_{39}N_2O_8$ $[M+1]^+$ 519.2706, found 519.2706.

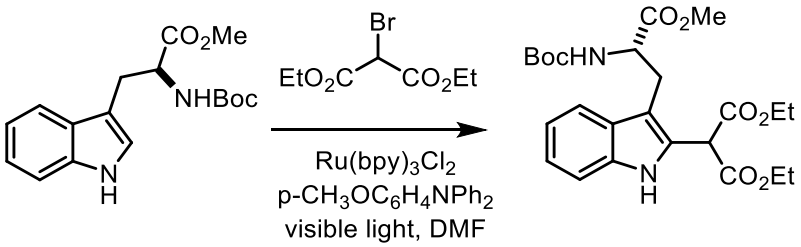

(*S*)-Diethyl 2-(3-(2-((tert-butoxycarbonyl)amino)-3-methoxy-3-oxopropyl)-1H-indol-2-yl) malonate (Table 1, Entry 7). According to the general procedure, *N*-Boc-tryptophan methyl ester (50 mg, 0.16 mmol), diethyl bromomalonate (53 µL, 0.31 mmol)**,** 4-methoxytriphenylamine (87 mg, 0.31 mmol) and tris(2,2´-bipyridyl)ruthenium(II) chloride hexahydrate (1.0 mg, 1.6 µmol) afforded the coupled product (60 mg, 77%) as a tan solid after purification on SiO_2 (4:1 hexanes/EtOAc) (20 h reaction time).

R_f (75:25 hexanes/EtOAc) = 0.24;

IR (neat): 3399, 2982, 1748, 1640, 1368, 1267, 1028 cm^{-1};

^{1}H NMR (400 Mhz): δ 8.93 (br s, 1 H, NH), 7.52 (d, *J* = 8.0 Hz, 1 H), 7.33 (d, *J* = 8.0 Hz, 1 H), 7.17 (td, *J* = 7.5, 1.2 Hz, 1 H), 7.12 – 7.04 (m, 1 H), 5.24 (d, *J* = 8.0 Hz, 1 H), 4.96 (s, 1 H, NH), 4.70 – 4.57 (m, 1 H); 4.33 – 4.13 (m, 4 H); 3.59 (s, 3 H); 3.26 (d, *J* = 5.9 Hz, 2 H); 1.39 (s, 6 H); 1.27 (td, *J* = 7.1, 1.5 Hz, 6 H);

^{13}C NMR (100 MHz): δ 172.6, 167.3, 155.2, 136.0, 127.7, 126.6, 122.7, 119.7, 119.0, 111.2, 109.4, 79.8, 62.5, 54.1, 52.3, 49.3, 28.3, 28.0, 27.0, 14.1, 14.0;

HRMS (ESI) *m/z* calculated for $C_{24}H_{32}N_2O_8$ $[M+Na]^+$ 499.2056, found 499.2046.

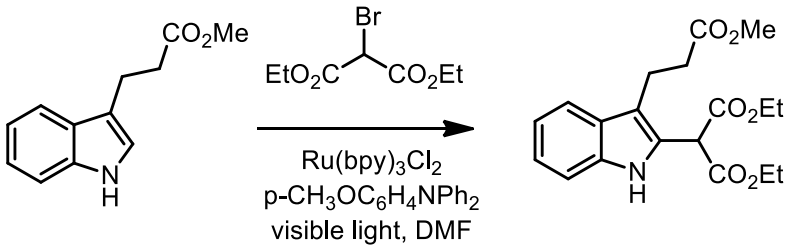

Diethyl 2-(3-(3-methoxy-3-oxopropyl)-1H-indol-2-yl)malonate (Table 1, Entry 8). According to the general procedure, methyl indole-3-propionate (50 mg, 0.25 mmol), diethyl bromomalonate (83 μL, 0.50 mmol)**,** 4-methoxytriphenylamine (0.14 g, 0.50 mmol) and tris(2,2´-bipyridyl)ruthenium(II) chloride hexahydrate (2.0 mg, 2.5 μmol) afforded the coupled product (70 mg, 78%) as a brown semi-solid oil after purification on SiO_2 (9:1 hexanes/EtOAc) (18 h reaction time).

R_f (90:10 Hexanes/EtOAc) = 0.19;

IR (neat): 3399, 2983, 1734, 1460, 1369, 1267, 1202, 1029, 744 cm^{-1};

^{1}H NMR (400 MHz): δ 8.91 (br s, 1 H, NH), 7.56 (m, 1 H), 7.36 (m, 1 H), 7.19 (ddd, *J* = 8.1, 7.1, 1.2 Hz, 1 H), 7.1 (m, 1H), 5.1 (s, 1H) 4.23 (m, 4H), 3.64 (s, 3H), 3.09 (t, *J* = 7.5 Hz, 2H), 2.66 (t, *J* = 7.5 Hz, 2H), 1.28 (t, *J* = 3.0 Hz, 6H);

^{13}C NMR (100 MHz): δ 173.9, 167.6, 136.2, 127.4, 127.4, 125.5, 122.7, 119.7, 118.8, 113.7, 111.6, 62.6, 51.8, 49.4, 35.0, 19.7, 14.2;

HRMS (ESI) *m/z* calculated for $C_{19}H_{23}NO_6$ $[M+Na]^+$ 384.1423, found 384.1435.

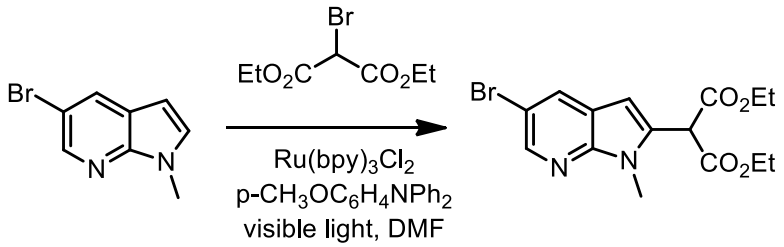

Diethyl 2-(4-bromo-1-methyl-1H-pyrrolo[2,3-b]pyridin-2-yl)malonate (Table 1, Entry 9). According to the general procedure, 5-bromo-1-methyl-7-azaindole (0.10 g, 0.45 mmol), diethyl bromomalonate (0.15 mL, 0.90 mmol)**,** 4-methoxytriphenylamine (0.25 g, 0.90 mmol,) and tris(2,2´-bipyridyl)ruthenium(II) chloride hexahydrate (3.4 mg, 4.5 µmol) afforded the coupled product (0.95 g, 49%) as a yellow oil after purification on SiO_2 (9:1 hexanes/EtOAc) (18 h reaction time).

R_f (90:10 Hexanes/EtOAc) = 0.31;

IR (neat cm-1) 2982, 2927, 2854, 2361, 2340, 1738, 1533, 1476, 1402, 1369, 1311, 1216, 1155, 1031, 761 cm^{-1};

^{1}H NMR (500 MHz): δ 8.25 (d, *J* = 2.2 Hz, 1 H), 7.89 (dd, *J* = 2.2, 0.5 Hz, 1 H), 6.44 (s, 1 H), 4.84 (s, 1 H), 4.30 – 4.11 (m, 4 H), 3.73 (s, 3 H), 1.22 (t, *J* = 7.1 Hz, 6 H);

^{13}C NMR (100 MHz): δ 166.4, 147.0, 143.7, 133.3, 130.6, 121.3, 111.9, 100.4, 62.6, 51.3, 28.8, 14.1;

HRMS (ESI) *m/z* calculated for $C_{15}H_{18}BrN_2O_4$ $[M+1]^+$ 369.0450, found 369.0452.

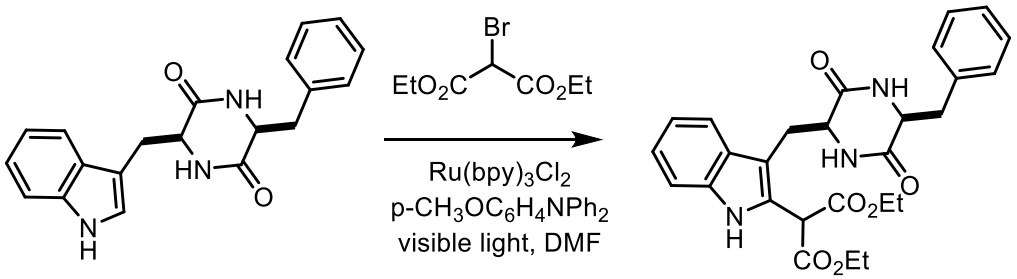

Diethyl 2-(3-(((2*S*,5*R*)-5-benzyl-3,6-dioxopiperazin-2-yl)methyl)-1H-indol-2-yl)malonate (Table 1, Entry 10). According to the general procedure, tryptophan/phenylalanine diketopiperzine (50 mg, 0.15 mmol), diethyl bromomalonate (51 μL, 0.30 mmol)**,** 4-methoxytriphenylamine (83 mg, 0.30 mmol) and tris(2,2´-bipyridyl)ruthenium(II) chloride hexahydrate (1.1 mg, 1.5 μmol) afforded the coupled product (49 mg, 68%) as a grayish solid after purification on SiO_2 (1:1 hexanes/EtOAc →100% CH_2Cl_2 → 9:1 CH_2Cl_2/MeOH) (18 h reaction time).

R_f (90:10 CH_2Cl_2/MeOH) = 0.55;

IR (neat): 3297, 2983, 2364, 1730, 1674, 1456, 2323, 1215, 1092, 1028, 910, 740 cm^{-1};

^{1}H NMR (300 MHz): δ 9.15 (s, 1 H, NH), 7.59 (d, *J* = 7.7 Hz, 1 H), 7.49 – 6.99 (m, 6 H), 6.84 (d, *J* = 1.6 Hz, 1 H), 6.39 (d, *J* = 1.8 Hz, 1 H), 4.80 (s, 1 H), 4.44 – 4.02 (m, 4 H), 3.34 (dd, *J* = 14.8, 2.6 Hz, 1 H), 3.05 (dd, *J* = 13.7, 3.8 Hz, 1 H), 2.70 (dd, *J* = 13.6, 6.7 Hz, 1 H), 2.11 (dd, *J* = 14.6, 9.3 Hz, 1 H), 1.96 (br s, 1 H), 1.52 – 1.27 (m, 6 H);

^{13}C NMR (100 MHz): δ 167.9, 167.7, 167.6, 166.2, 136.4, 135.6, 130.5, 129.2, 127.7, 127.2, 127.1, 123.4, 120.4, 119.2, 111.7, 109.5, 76.9, 63.3, 62.8, 56.6, 55.9, 49.3, 40.3, 29.7, 14.3;

HRMS (ESI) *m/z* calculated for $C_{24}H_{29}N_3NaO_6$ $[M+Na]^+$ 514.1954, found 514.1954.

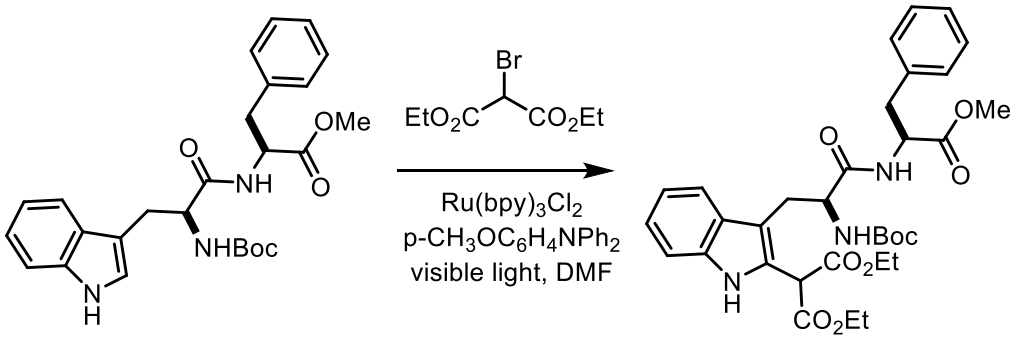

Diethyl 2-(3-((*S*)-2-((tert-butoxycarbonyl)amino)-3-(((*S*)-1-methoxy-1-oxo-3-phenylpropan-2-yl)amino)-3-oxopropyl)-1H-indol-2-yl)malonate (Table 1, Entry 11). According to the general procedure, tryptophan-phenylalanine dipeptide (50 mg, 0.10 mmol), diethyl bromomalonate (51 μL, 0.20 mmol)**,** 4-methoxytriphenylamine (59 mg, 0.20 mmol) and tris(2,2´-bipyridyl)ruthenium(II) chloride hexahydrate (0.8 mg, 8.0 μmol) afforded the coupled product (45 mg, 67%) as a tan solid after purification on SiO_2 (7:3 hexanes/EtOAc) (12 h reaction time).

R_f (70:30 Hexanes/EtOAc) = 0.25;

IR (neat): 3388, 3064, 2982, 2936, 1745, 1674, 1497, 1459, 1368, 1246, 1211, 1180, 1028, cm^{-1};

^{1}H NMR (300 MHz): δ 9.03 (s, 1 H, NH), 7.57 (d, *J* = 7.8 Hz, 1 H), 7.33 (d, *J* = 8.1 Hz, 1 H), 7.23 – 7.00 (m, 4 H), 6.80 (br s, 2 H), 6.19 (d, *J* = 7.2 Hz, 1 H), 5.36 (br s, 1 H, NH), 5.14 (br s, 1 H, NH), 4.47 (d, *J* = 5.6 Hz, 2 H), 4.35 – 4.01 (m, 4 H), 3.48 (s, 2 H), 3.38 – 3.19 (m, 1 H), 3.17 – 2.99 (m, 1 H), 2.89 (d, *J* = 5.1 Hz, 2 H), 1.77 (br s, 1H), 1.42 (s, 9 H), 1.36 – 1.11 (m, 6 H);

^{13}C NMR (100 MHz): δ 171.4, 171.3, 171.2, 155.4, 136.3, 135.6, 129.1, 128.4, 127.5, 127.0, 123.4, 122.2, 119.6, 118.8, 111.3, 110.2, 80.1, 60.4, 55.2, 53.2, 52.2, 37.9, 28.3, 21.0, 14.2;

HRMS (ESI) *m/z* calculated for $C_{33}H_{41}N_3NaO_9$ $[M+Na]^+$ 646.2740, found 646.2738.

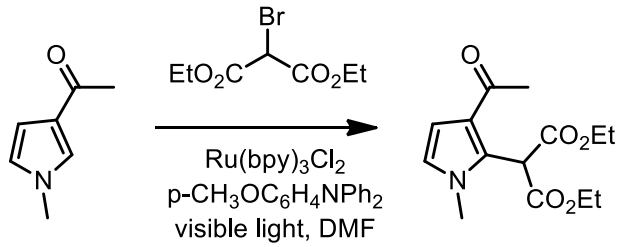

Diethyl 2-(3-acetyl-1-methyl-1H-pyrrol-2-yl)malonate (Table 1, Entry 12). According to the general procedure, 3-acetyl-1-methylpyrrole (50 mg, 0.25 mmol), diethyl bromomalonate (83 μL, 0.50 mmol)**,** 4-methoxytriphenylamine (0.14 g, 0.50 mmol) and tris(2,2´-bipyridyl)ruthenium(II) chloride hexahydrate (2.0 mg, 2.5 μmol) afforded the coupled product (70 mg, 78%) as a brown oil after purification on SiO_2 (9:1 hexanes/EtOAc) (18 h reaction time).

R_f (90:10 Hexanes/EtOAc) = 0.14;

IR (neat) : 3410, 1727, 1647, 1504, 1219, 1146, 1021 cm^{-1};

^{1}H NMR (300 MHz): δ 6.61 (s, 1 H), 6.53 (dd, *J* = 15.3, 2.9 Hz,1 H), 4.38 – 4.05 (m, 4 H), 3.63 (s, 3 H), 2.40 (s, 3 H), 1.27 (t, *J* = 7.1 Hz, 6 H);

^{13}C NMR (100 MHz): δ 195.5, 167.5, 127.8, 123.7, 122.5, 110.4, 61.9, 48.5, 35.2, 28.4, 14.0, 13.9;

HRMS (ESI) *m/z* calculated for $C_{14}H_{20}NO_5$ $[M+1]^+$ 282.1297, found 282.1317.

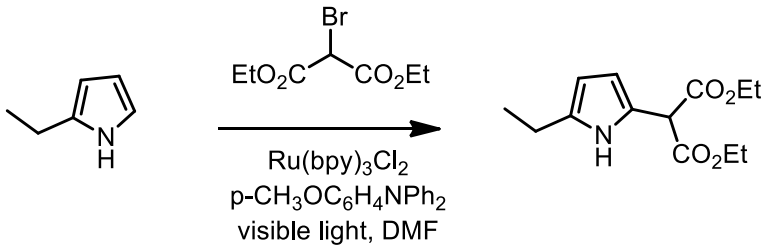

Diethyl 2-(5-ethyl-1H-pyrrol-2-yl) malonate (Table 1, Entry 13). According to the general procedure, 2-ethylpyrrole (50 mg, 0.53 mmol), diethyl bromomalonate (0.25 mL, 1.0 mmol,)**,** 4-methoxytriphenylamine (0.29 g, 1.0 mmol) and tris(2,2´-bipyridyl)ruthenium(II) chloride hexahydrate (3.9 mg, 5.3 µmol) afforded the coupled product (90 mg, 68%) as a dark oil after purification on SiO_2 (9:1 hexanes/EtOAc) (12 h reaction time).

R_f (90:10 Hexanes/EtOAc) = 0.28;

IR (neat) 3398, 2981, 2936, 1736, 1466, 1370, 1304, 1190, 1150 cm^{-1};

^{1}H NMR (400 MHz): δ 8.72 (br s, 1 H, NH), 6.02 (dd, *J* = 2.9 Hz, 1 H), 5.83 (t, *J* = 3.0 Hz, 1 H), 4.69 (s, 1 H), 4.40 – 4.08 (m, 4 H), 2.63 (q, *J* = 7.6 Hz, 2 H), 1.41 – 1.14 (m, 6 H);

^{13}C NMR (100 MHz): δ 168.2, 135.6, 120.0, 108.9, 104.4, 62.2, 51.4, 30.0, 21.1, 14.2, 13.7, 13.6;

HRMS (ESI) *m/z* calculated for $[M+1]^+$ 254.1392, found 254.1398.

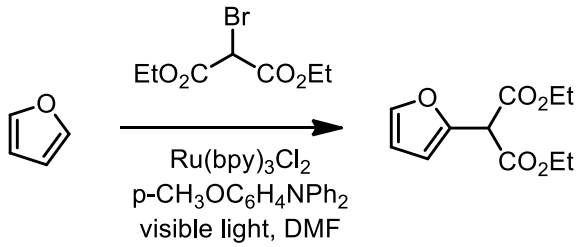

Diethyl 2-(furan-2-yl)malonate (Table 1, Entry 14). A flame dried 10 mL round bottom flask was equipped with a rubber septum and magnetic stir bar and was charged with tris(2,2´-bipyridyl)ruthenium(II) chloride hexahydrate (5.9 µmol, 0.01 equiv), 4-methoxytriphenylamine (1.2 mmol, 2.0 equiv), diethyl bromomalonate (0.59 mmol, 1.0 equiv) and DMF (2 mL). The mixture was degassed via the freeze-pump-thaw method, *after which* freshly distilled furan (0.22 mL, 3.0 mmol) was added and exposed to blue light for 24 h. The reaction mixture was worked up in accordance with the general procedure. The coupled product (87 mg, 67%) was isolated as a yellow oil after purification on SiO_2 (95:5 hexanes/EtOAc).

R_f (90:10 Hexanes/EtOAc) = 0.13;

^{1}H NMR (300 MHz): δ 7.47 – 7.38 (m, 1 H), 6.44 (dd, *J* = 3.3, 0.7 Hz, 1 H), 6.41 – 6.35 (m, 1 H), 4.77 (s, 1 H), 4.25 (q, *J* = 7.1 Hz, 4 H), 1.41 – 1.18 (m, 7 H).

Luminescence Quenching of $Ru(bpy)_3Cl_2$

Emission intensities were measured using a J**obin Yvon Horiba FluoroMax 3 Fluorimeter** equipped with an excitation/emission monochromator. Samples were excited at 452 nm and emission peaks were observed at 617 nm. Typical procedure: A stock solution of 1.47 mM $Ru(bpy)_3Cl_2$ in DMF was prepared and degassed three times via freeze-pump-thaw method. The stock solution was then added to varying amounts of the tested quencher in a 1 cm quartz cuvette. Samples were prepared in five concentrations: 0.36M, 0.18M, 0.09M, 0.045M, and 0.0225M.

Figure S1: Luminescence Quenching of Ru(II)* by 4-Methoxytriphenylamine

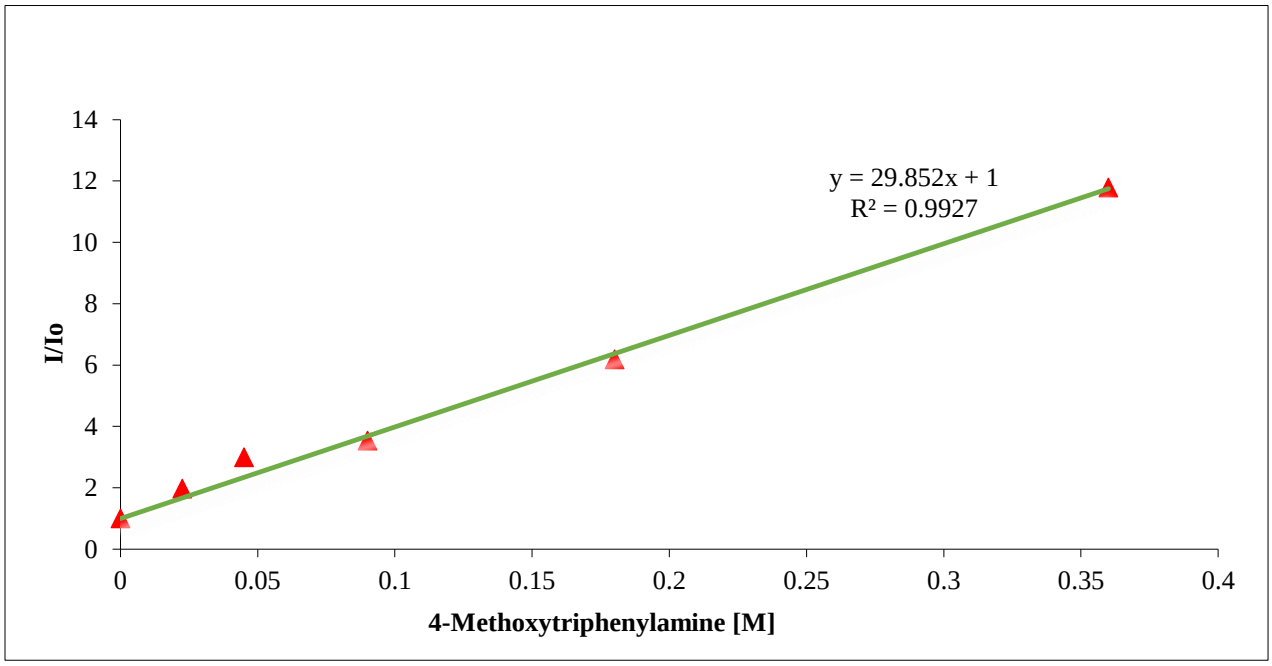

References and Notes

[1] Perrin, D. D.; Armarego, W. L. F. *Purification of Laboratory Chemicals*, 3rd ed.; Pergamon Press: Oxford, 1988.

[2] Blue LEDs were purchased at http://www.creativelightings.com.

[3] Reyes-Guiterrez, P. E.; Torres-Ochoa, R. O.; Martinez, R.; Miranda, L. D. *Org. Biomol.Chem.* **2009**, *7*, 1388.

Chapter 2: A High-Valent Palladium Mediated Oxyarylation of Alkenes

*Portions of this thesis were published in:
• Matsuura, B. S.; Condie, A. G.; McBee, I. A.; Buff, R. C.; Karahalis, G. J.; Stephenson, C. R. J.
Org. Lett. **2011**, *13* (23), 6320

2.1 Introduction

The ubiquity of alkenes in commodity/fine chemicals and their ease of synthesis has made them an indispensable functional group in nearly all disciplines of organic chemistry. The functionalization of unactivated olefins is particularly desirable as a means to rapidly generate molecular complexity from simple starting materials. There are several classic olefin difunctionalization methodologies that have become a staple of organic synthesis including hydrogenation, epoxidation, dihydroxylation, aziridination, and dihalogenation. The fact that these areas are still a subject of intense research is an enduring reminder that although alkene difunctionalization is an old concept, it is still far from maturity. Recent trends in catalytic alkene functionalization chemistry has attempted to move away from the use of expensive (rhodium, iridium, platinum) or highly toxic (osmium, lead) metals towards cheaper and safer alternatives. In this regard, palladium catalysis has emerged as a highly versatile olefin functionalization catalyst. Advances in the catalytic, oxidative amino acetoxylation,[37–39] dihydroxylation,[40,41] and diamination[42,43] chemistry has greatly expanded the utility of palladium catalysis within the context of synthesis. Despite many years of research, the catalytic carbofunctionalization of unactivated alkenes remains challenging. Within this context we were interested in developing a new oxyarylation reaction using high valent palladium catalysis.

In the mid 1970's Hegedus and co-workers reported the intermolecular amination of alkenes using stoichiometric palladium (II) salts.[44] Under these conditions, they were able to alkylate secondary amines using a variety of terminal and internal olefins. Hegedus and co-workers suggested that this transformation was going through a Wacker-type mechanism, wherein the coordination of palladium to the alkene forms π-complex **45**, followed by the *anti*-nucleophilic attack of the amine onto the alkene. The resultant alkylpalladium complex **46** was stable at low temperature and could be reduced with hydrogen gas, liberating the desired amine **47** in mid to high yields (Figure 11, A). Using *o*-allyl anilines and stoichiometric $(MeCN)_2PdCl_2$ induced a 5-*exo*-trig cyclization resulting the formation of alkylpalladium **48**, β–hydride elimination followed by isomerization enabled the synthesis of a series of 2-alkyl indole derivatives (Figure 11, A). In these circumstances, the amine did not need to be protected.[45] The intramolecular cyclization of alkylamines required the presence of an electron withdrawing group, but was able to efficiently construct 5 and 6 membered rings.[46] Remarkably, $(MeCN)_2PdCl_2$ was

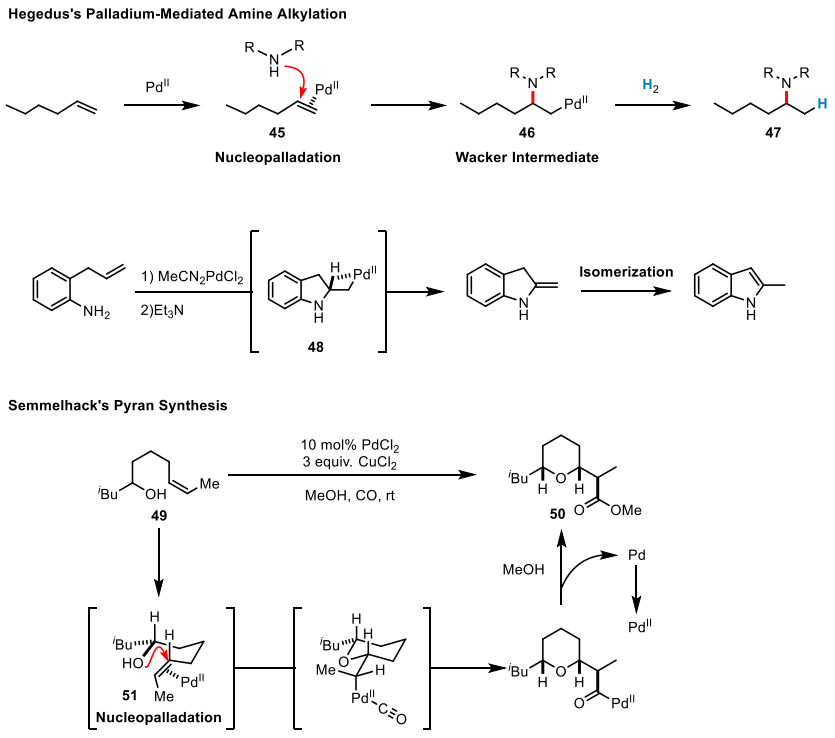

Figure 11 A) Hegedus' indole synthesis via a Wacker cyclization B) The Semmelhack Reaction

also highly efficient in mediating the intermolecular alkylation of lithium enolates with simple terminal olefins.[47,48]

One drawback of this early chemistry was that it required stoichiometric quantities of the palladium salt as a reaction promotor and terminal oxidant. Further reaction development by the Hegedus group yielded general catalytic conditions for this cyclization chemistry using benzoquinone as a stoichiometric co-oxidant in the early 1980's (Figure 11, B).[46] Concurrently, the Semmelhack group developed an analogous catalytic oxidative carbonylative tetrahydropyran synthesis using racemic alcohol **49**, using $PdCl_2$ as the catalyst, with copper(II) chloride as a co-oxidant under an atmosphere of carbon monoxide to furnish product **50** in good to excellent yields. [49] Unlike the Hegedus reaction, which typically terminate via a β-hydride elimination, the Semmelhack reaction could easily functionalize both carbons in the pendant alkene. The reaction was capable of mediating both 6-*endo* and 6-*exo* carbonylative cyclizations, which were typically highly stereoselective for the *syn*-diastereomer of the resultant tetrahydropyran, presumably due to the minimization of *syn*-pentane interactions. This synthetic logic could also be extended to the stereoselective synthesis of tetrahydrofuans.[50] Although stoichiometric and catalytic variants of the carbonylative Wacker-type olefin difunctionalization had been previously reported, these were usually special cases. In later disclosures, Semmelhack demonstrated that the Wacker intermediate could be intercepted with other coupling partners such as olefins, enabling the synthesis of highly substituted pyrans, via the vicinal difunctionalization of simple unsaturated alcohols.[51] The ubiquity of tetrahydrofurans and pyrans in natural products, and in particular macrocyclic polyketides, has made this reaction an attractive strategy in complex molecule synthesis.[52–54]

The research efforts by these two groups provided a very important framework for modern palladium difunctionalization chemistry, particularly in respect to the reaction mechanism.[55] In the intervening years, there were very few reports that expanded on the scope of this reaction. Despite the utility of the Wacker-type olefin difunctionalization reaction, there were some limitations that prevented more widespread use in synthesis. 1) After the initial nucleopalladation step, the resulting Wacker intermediate **48** or **51** can only undergo a limited number of reactions – typically a Heck reaction onto methacrylate or a carbonylative esterification reaction (Figure 11). 2) The corresponding intermolecular reaction had not been described. 3) There were only a limited number of oxidants identified at the time that were capable of oxidizing Pd^0 back to Pd^{II} while being unreactive in the presence of amines or free alcohols. Until these issues could be addressed, this full potential of this chemistry could not be realized.

2.1.1 Oxidizing the Wacker Intermediate: Development of a Conceptually Novel Oxyamination Reaction

A significant breakthrough occurred in 2005, when a team led by Sorensen described a palladium-mediated oxidative, intramolecular oxyamination of tosylcarbamates.[37] The authors were aware of the inherent disadvantages of using a traditional $Pd^{II/0}$ catalytic cycle, which risked undesirable β–hydride elimination. A recent report by Sanford and co-workers had demonstrated that iodine (III) based oxidants such as phenyliodine diacetate (PIDA) could oxidize alkylpalladium(II) species into the corresponding high-valent palladium(IV) intermediate (Figure 12, A).[56] They therefore hypothesized if they could prevent β-hydride elimination if they oxidized the Wacker intermediate. When reacted with 2 equivalents of PIDA, 1 equivalent of NBu_4OAc, 10 mol% of palladium acetate in DCM, *N*-nosylated amine (**52**) cyclized to the corresponding acetoxylated piperidine (**53**) and azepane (**54**) as a 1.7:1 mixture in 79% yield. This reaction was found to be very general and several amine equivalents could effectively participate in the initial

nucleopalladation step including *O*-allylated tosylcarbamates, amides, amines, and anilines. Yields were general moderate to good (60-80% yield) and could generate 5, 6, and 7 membered rings. For their mechanism, they proposed an initial *trans*-nucleopalladation of the tosylamine to generate an aza-Wacker intermediate **55**. They proposed that the oxidation of this intermediate to Pd(IV) was followed by direct C–O reductive elimination, retaining the configuration at that center. Only a few months after the Sorensen contribution, Muñiz and co-workers described a similar intramolecular Pd(IV) mediated diamination of alkene with tethered tosylated ureas (Figure 12, B).[42] The reported reaction conditions were very similar to the Sorensen report, reacting alkene **56** with 5 mol% $Pd(OAc)_2$, 2.2 equivalents PIDA, and 1 equivalents Bu_4NCl/NaOAc in DCM to yield cyclic urea **57** in 92% yield. This reaction was very high yielding (~90% average), and the aminopalladation reaction could cyclize to form

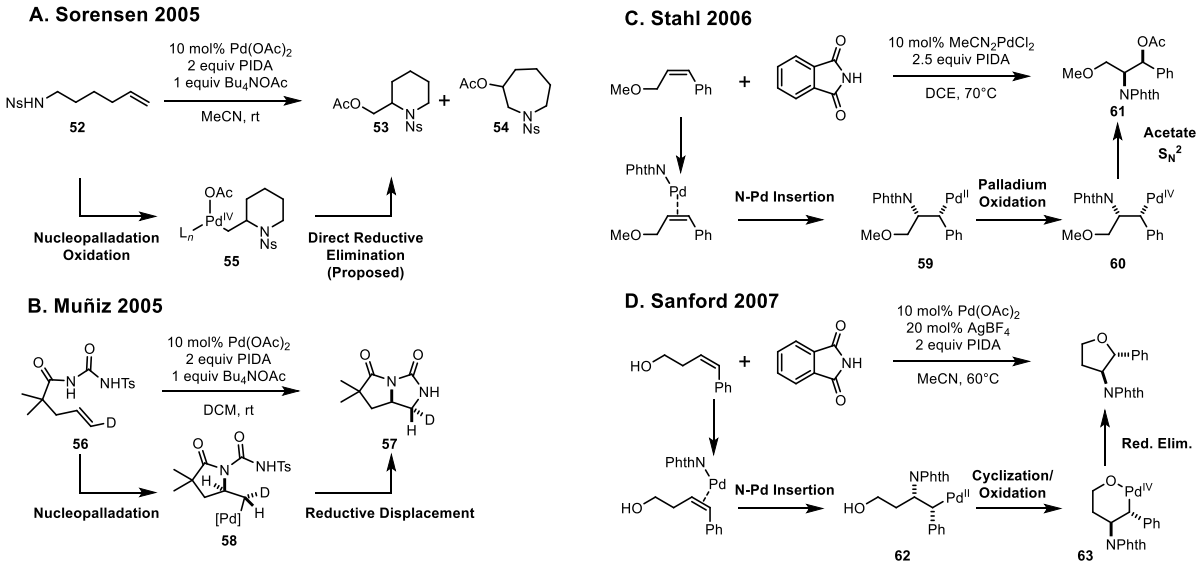

Figure 12 Seminal contributions to high-valent palladium mediated olefin difunctionalization

5, 6, and 7 membered rings, and react with 1,1-disubstituted alkenes to afford tertiary amines. They proposed an initial *trans*-nucleopalladation of **56**, as in the Sorensen report, however, they showed through a deuterium labelling experiment that the observed stereoisomer was *inverted*,

suggesting that the reductive elimination of intermediate **58** to **57** proceeded from an S_N2 type mechanism.

In 2006 and 2007, Stahl[38] and Sanford[39] reported the intermolecular and intramolecular aminooxygenation of alkenes using Pd(IV) catalysis (Figure 12, C and D). The reaction conditions between these two differed slightly, Stahl employing 5 mol% $(MeCN)_2PdCl_2$/2.5 equivalents PIDA in DCE and Sanford using 10 mol% $Pd(OAc)_2$/20 mol% $AgBF_4$/3 equivalents PIDA. In both reaction conditions, phthalimide was the limiting reagent. The greatest significance of these papers, aside from their obvious synthetic utility, was their contribution to the field's understanding on the reactivity of high-valent palladium. Through a series of mechanistic experiments, both Sanford and Stahl concluded, at least when phthalimide is the nucleophile, the initial step is *not* a *trans*-nucleopalladation, but rather the result of *cis*-amino palladation, through a migratory insertion process to form Wacker intermediates **59** and **62** (Figure 12, C and D). This finding, though subtle, is important because it was contrary to the common assumption that the initial palladation step would occur by a Wacker-type *trans*-nucleopalladation. In Stahl's method, which was an amino acetoxylation, he observed that the acetoxylation step occurred with *inversion* of configuration, suggesting the C–O reductive elimination of intermediate **60** was occurring in an S_N2 fashion. In contrast the Sanford communication was forming an aliphatic C–O bond and in this case was postulated to undergo stereoretentive reductive elimination of palladacycle **63**. Sanford and co-workers have studied the mechanism of C–O bond reductive elimination on sp^3-hybridized carbons. They found that for acetate and other soft oxygen nucleophiles, an S_N2 mechanism is operative.[57] Mechanistic studies of the reductive elimination of C–F bonds suggest that the mechanism of direct alkoxide reductive elimination is probably analogous.[58] Taken together, these reports indicated that the mechanistic picture of these Pd(IV) mediated alkene

difunctionalization reactions are quite a bit more complex than initially realized. In light of these more recent investigations, the mechanism of the Sorensen report could go through a *cis*-amino palladation of alkene **52**, followed by an S_N2-type reductive elimination of intermediate **55** with inversion of configuration at the C–Pd bond.

2.1.2 High-valent Palladium Mediated Amino Arylation and Alkynylation Reactions

In 2009, Michael and co-workers described a novel aminoarylation of γ-unsaturated aliphatic carbamoylated amines.[59] Key to this innovation was the identification of NFSI as an external oxidant to favor intermolecular arylation versus carbon–heteroatom bond reductive elimination. Using 1 equivalent of amine **64**, 10 mol% $Pd(TFA)_2$, 2 equivalents of NFSI, and 1 equivalent of 2,6-di-*tert*-butyl-4-hydroxy toluene (BHT), they were able to isolate substituted pyrrolidine **65** 82% yield when toluene was used as a solvent (Figure 13). Similar to other reactions in this class, the Wacker-type cyclization could efficiently generate 5,6 and 7 membered rings, however, products containing multiple stereocenters were isolated as a mixture of diastereomers, indicating the initial aminopalladation step did not occur with high levels of stereoselectivity. Although the reaction required solvent quantities of arene, functionalized arenes could also be successfully incorporated in the

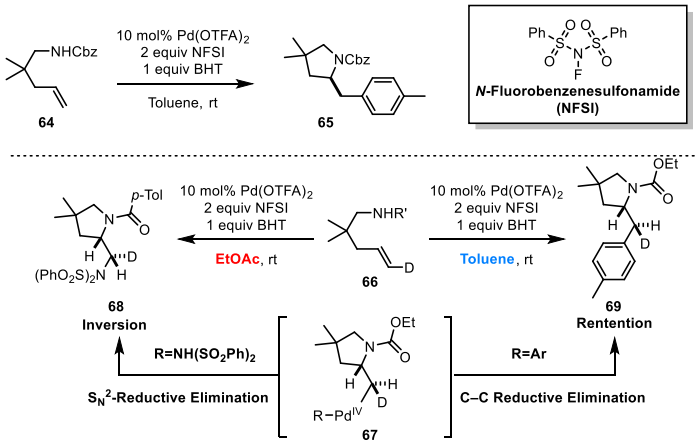

Figure 13 Michael's intermolecular aminoarylation and mechanism

reaction products if desired. In later mechanistic studies using deuterated amine **66**, they were able to establish that the cyclization occurs through a *trans*-nucleopalladation to form an aza-Wacker intermediate **67**.[60] This intermediate had divergent reactivity depending on the reaction conditions. In a previous report, they described the diamination of the same alkene substrates using NFSI; in this case, the solvent was ethylacetate instead of toluene, preventing the arylation reaction.[61] In the absence of an arene, Pd(IV) complex **67** underwent nucleophilic displacement to form *syn*-diamination products **68**, whereas in the presence of an arene, the reductive elimination occurs with retention of configuration at the C–Pd bond during the formation of **69**. Furthermore, they note that Pd(II) complex **67** was unreactive to arenes, suggesting that the C–H metalation step occurs in the Pd(IV) oxidation state.

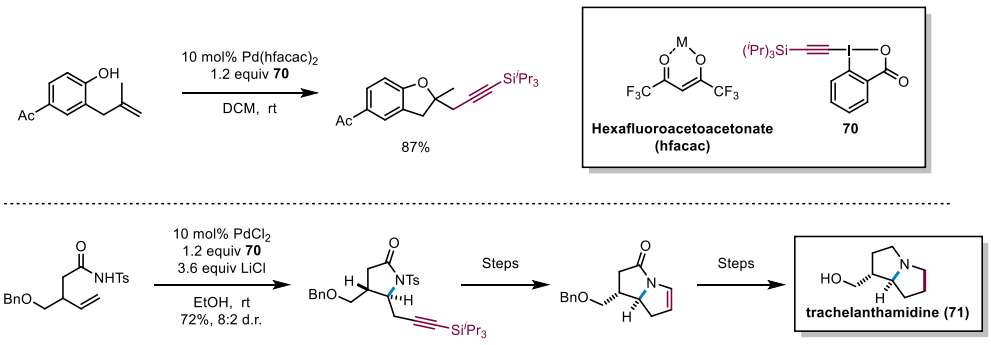

Figure 14 Waser's palladium catalyzed oxyalkynylation using a novel λ^3-iodane

Finally, in 2010 Waser and co-workers described an oxyalkynylation reaction[62] mediated by Pd(IV) and an unusual alkynyl-λ_3-iodane oxidant (**70**) based off of Togni's reagent.[63] Waser and co-workers found that several palladium salts traditionally used in high-valent palladium catalysis, such as $Pd(TFA)_2$ and $(MeCN)_2PdCl_2$ were ineffective at mediating their desired transformation. Identification of palladium bis-hexafluoroacetoacetonate (hfacac) complex was essential to the successful realization of this transformation (Figure 14). Several nucleopalladation

substrates were competent reaction partners including phenols, aliphatic alcohols, aryl/alkyl carboxylic acid, and a protected hydroxamic acid. Yields ranged from 30% to 87% with carboxylic acid containing substrates providing the most consistently good yields. Phenols exhibited less generality, requiring 1,1-disubstituted alkenes for good yields. This methodology was extended to include N-acylsulfonamides, which they later applied in the synthesis of the natural product trachelanthamidine (**71**, Figure 14).[64]

2.2 Concluding Remarks

The mid 2000's heralded the revival of the palladium mediated alkene difunctionalization chemistry. Primarily inspired by the efforts of Hegedus and Semmelhack, the utility chemistry expanded as new concepts in palladium catalysis were introduced, including high-valent palladium catalysis. The variety of distinct vicinal difunctionalization reactions that are now available was concurrent with the development of novel oxidation reagents, notably λ^3-iodanes (PIDA, Togni's reagent, diaryliodonium salts), milder fluorination reagents (Selectfluor, *N*-fluoropyridinium, NFSI), oxone, among others. The combined efforts of these groups has made alkene difunctionalization chemistry a practical solution towards the synthesis of complex molecules. Although outside of the scope of this overview, it would be remiss to not acknowledge the critical advances palladium (0/II) mediated oxyarylation[65–67] and aminoarylation[68,69] chemistry, which were largely driven by innovation in ligand design.[70,71] The contributions of the Wolfe group have been particularly influential, enabling access to highly functionalized oxygen and nitrogen containing heterocycles in racemic and enantioselective fashion.[72]

2.3 Strategy

Our lab's foray into high-valent palladium catalysis was stimulated by our efforts towards the synthesis of the natural product platensimycin (**72**).[73] This novel terpenoid natural product possessed broad-spectrum antibiotic activity against gram-positive bacteria through potent inhibition of FabF, an enzyme involved in bacterial fatty acid synthesis. Being the first compound of a new class of antibiotics discovered in years, many were optimistic that it could provide a new line of defense against the looming threat of deadly multiresistant strains of bacteria. The unique caged pentacyclic structure was unprecedented at the time, which when coupled with its promising biological activity, instantly made it a popular target amongst synthetic chemists.[74] The lab's synthetic approach started from the simple commercially available starting materials methylvinyl oxirane and an *O*-protected bromoarene (Figure 15). A copper catalyzed vinylogous conjugate addition of the brominated arene to methylvinyl oxirane would lead to alyllic alcohol **73**. A

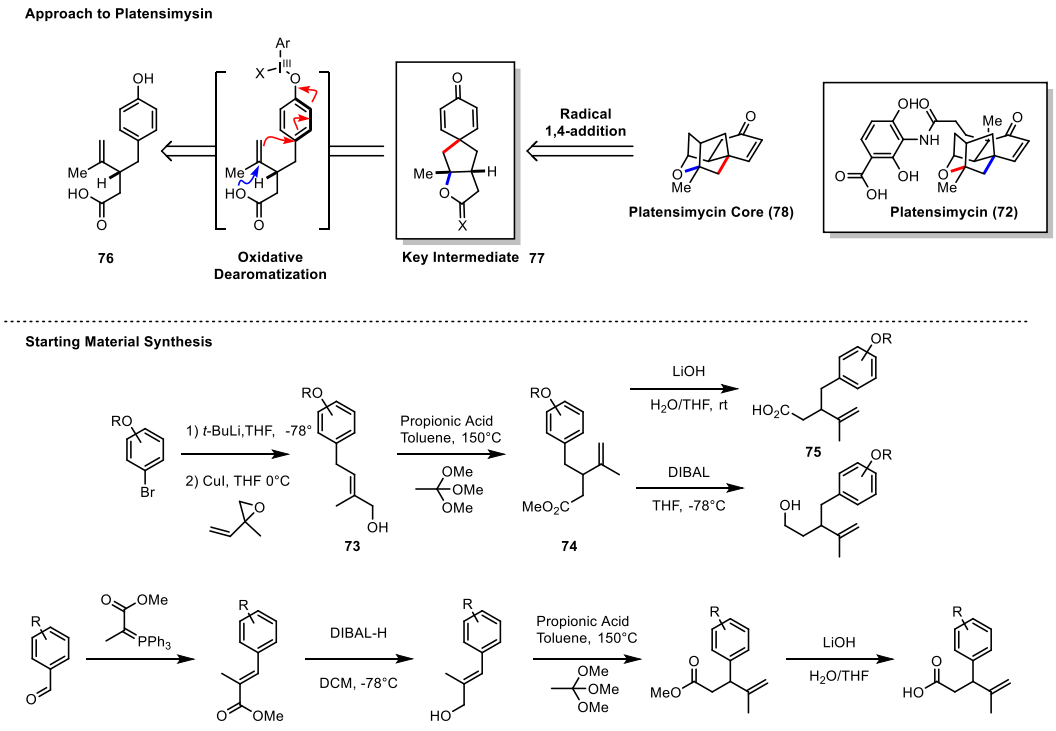

Figure 15 A) Synthetic approach towards the synthesis of platensimycin B) Substrate synthesis

subsequent Johnson Orthoester Claisen reaction followed by saponification would produce butenoic acid **75** in four steps. Our proposed key step was an oxidative dearomatization/cyclization of phenol **76** to form spirocyclohexadienone **77** as a precursor for an intramolecular radical or anionic conjugate addition towards pentacycle **78**. Despite our best efforts, strategies involving hypervalent iodine, halocyclization/dearomative alkylation or conventional Wacker cyclization reaction were unsuccessful, resulting in the decomposition of our starting material. Although the Semmelhack chemistry did not provide our desired product, we were reasonably convinced that the intended nucleopalladation was indeed working, but the subsequent Wacker intermediate was not reactive enough to engage the pendant phenol. The emergence of high-valent palladium catalysis in alkene functionalization suggested that oxidizing the Wacker intermediate could make the alkylpalladium species significantly more reactive, potentially overcoming the issues with the prior Pd-based strategies. This afforded an opportunity to develop a novel dearomative alkene difunctionalization reaction. This project was passed through many capable hands before my own and I am indebted to the guidance of my senior colleagues Allison Condie, and Ian McBee during the course of this project. I also had the pleasure of working with the talented undergraduates Ryan Buff and Greg Karahalis.

2.4.1 The Development of a High-Valent Palladium Mediated Synthesis of Spirocyclic Dienones

Reaction optimization began with **79**, prepared in 5 steps from 4-bromophenol. As alluded to previously, effecting the cyclization cascade using λ^3-iodanes or traditional Wacker cyclization chemistry were ineffective. Our results implementing high-valent palladium catalysis were initially disappointing, although very small quantities (5–10% yield) of cyclohexadienone **80** could be isolated using 10 mol% $Pd(OAc)_2$, 2 equivalents of PIDA in MeCN (Table 1). The fact that PIDA was an ineffective oxidant is perhaps unsurprising since it has been frequently used as a

reagent for the direct oxidative dearomatization of phenols and in the palladium mediated acetoxylation of sp^2 and sp^3 hybridized carbons. After an extensive reaction optimization, we found that the electrophilic fluorination regent Selectfluor provided spirocycle **80** in 43% yield as a single diastereomer (Figure 15). The use of Selectfluor provided many benefits that were not clear at the time. Qualitatively, Selectfluor was less reactive to the presence of our substrate as compared to λ^3-iodinanes. Although it can effectively oxidize Pd^{II} complexes to higher oxidation states,[75] the corresponding C–F reductive elimination is very difficult.[76,77] This property has enabled chemists to use fluoride as a "by standing" ligand for the selective reductive elimination of difficult C–X bonds and was likely a contributing factor to the success of this reaction.[78–80]

Table 2 Optimization for Oxidative Dearomatization

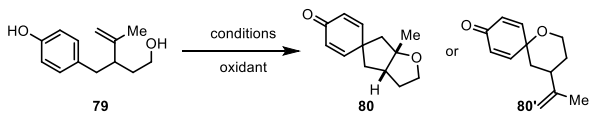

79 80 80'

entry	conditions	yield of **2**[a]
1	$Pd(OAc)_2$ (10 mol %), $PhI(OAc)_2$ (2.0 equiv) PhMe, rt, 12 h	0%
2	$Pd(OAc)_2$ (10 mol %), $PhI(OAc)_2$ (2.0 equiv) CH_3CN, rt, 12 h	5–10%
3	$Pd(OAc)_2$ (10 mol %), PhI=O, (3.0 equiv) CH_3CN, rt, 12 h	N. R.
4	$Pd(OAc)_2$ (10 mol %), Selectfluor (2.0 equiv) CH_3CN, rt, 12 h	43%
5	$PhI(OAc)_2$ (1.1 equiv), CH_3CN	0%[b]
6	$PhI(O_2CCF_3)_2$ (1.1 equiv), $(F_3C)_2CHOH$	0%[b]

[a]Isolated yield (%) after purification by chromatography on SiO_2; [b]**2a** was the only isolable product.

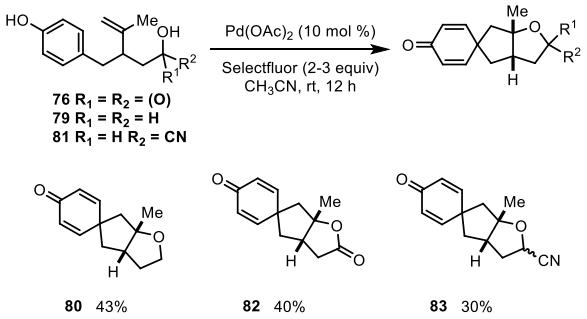

Figure 16 Synthesis of spirocyclohexadienones via high-valent palladium catalysis

The scope of this particular transformation was very limited, reacting substrate **76** containing a pendant carboxylic acid, afforded spirodieneone in a comparable 40% yield (**82**, Figure 16). Surprisingly, the reaction conditions were tolerant to the presence of cyanohydrins, cyclizing in somewhat lower yield as a 1:1 mixture of diastereomers (**83**, Figure 16). Despite the narrow substrate scope and low synthetic yield, this methodology enables the synthesis of complex polycyclic compounds from readily available starting materials. It would be difficult to imagine an alternative approach to this compound class using more traditional methods. Also, this methodology is a unique approach towards high-valent palladium catalysis and vicinal olefin difunctionalization.

2.4.2 Development of a High-Valent Palladium Mediated Oxy-Arylation via C–H Functionalization

During the optimization of the spirocyclohexadienone synthesis, we found that γ-unsaturated carboxylate **84** produced the desired dearomatization product **85** in 20% yield. Analysis of the reaction mixture revealed that the majority of the reaction product was in fact the C–H functionalization product **86**, isolated as 1:1 mixture of diastereomers in 68% yield. Intrigued by this alternative reactivity along with inherent incompatibility of free phenols towards the strongly oxidizing conditions necessary for high-valent palladium catalysis we were prompted to explore

Table 3 Substrate Scope for C–H Functionalization

entry	substrate	product	yield[b]
1	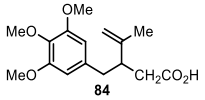 **84**	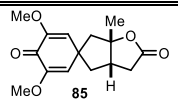 **85** 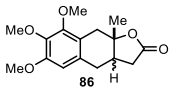 **86**	20% 68% [d,e]
2	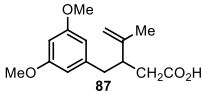 **87**	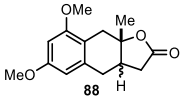 **88**	92%[c]
3	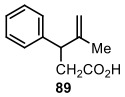 **89**	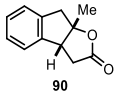 **90**	60%
4	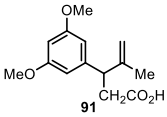 **91**	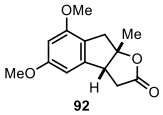 **92**	60%
5	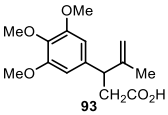 **93**	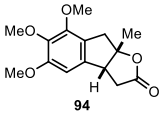 **94**	53%
6	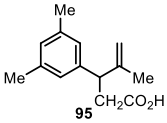 **95**	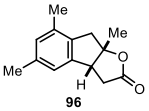 **96**	57%
7	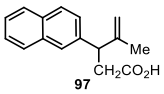 **97**	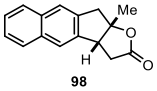 **98**	56%
8	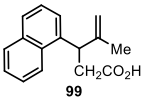 **99**	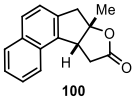 **100**	51%
9	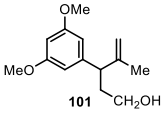 **101**	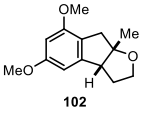 **102**	46%

[a]Reaction Conditions: $Pd(OAc)_2$ (10 mol %), $PhI(OAc)_2$ (2.0 equiv), CH_3CN, rt, 12 h; [b]Isolated yield (%) after purification by chromatography on SiO_2; [c]dr 1.75:1; [d]dr 1.3:1; [e] When Selectfluor was used as the stoichiometric oxidant, there was extensive decomposition of the starting material

our catalytic system in the presence of less reactive arenes. By modifying the functionalization of the arene ring, we sought to suppress dienone formation in favor of this interesting alternative reaction pathway.

While PIDA was ineffective for the oxidative spirocyclohexadienone cyclization, it proved to optimal for the oxyarylation of less activated arenes. Using 10 mol% $Pd(OAc)_2$, 2 equivalents of PIDA in acetonitrile cleanly cyclized substrate **87** to lactone **88** in 92% yield as a 1.3:1 mixture of diastereomers. Again, attempts to use conventional Wacker oxidation conditions were ineffective in mediating this transformation. These reaction conditions could effectively cyclize substrates containing electron rich and electron neutral arenes in moderate to good yields (Table 3). Substrates that formed smaller [3.3.0] bicyclooctanes (Table 3, Entries 3–9) showed a consistent decline in yield compared with substrates **84** and **87**. The isolation of pyranone **103** and traces quantities of acetoxylated side product **104** during the conversion of **92** indicated that some of this yield loss could be attributed to undesired off cycle processes (

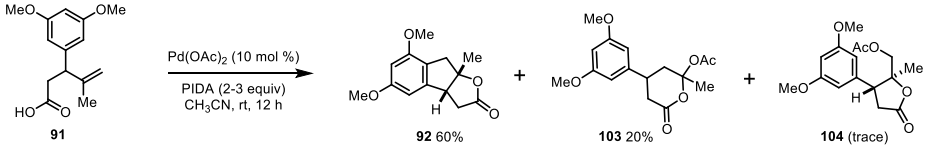

Figure **17**). Suppression of these reaction pathways proved challenging, however it provided some indirect insight into the mechanism of this reaction.

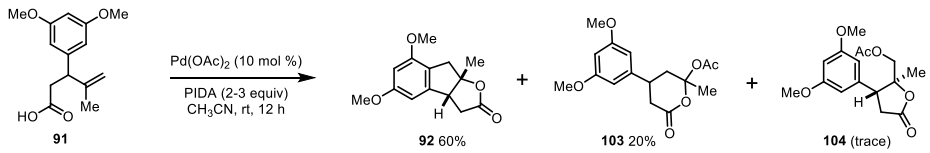

Figure 17 Isolation of a pyranone byproduct

2.5 Reaction Mechanism

Although the exact mechanisms for these two reactions is not entirely clear, a plausible catalytic cycle is outlined below (Figure **18**, A). Palladium (II) coordinates to the olefin of the substrate and undergoes a nucleopalladation forming Wacker intermediate **105**. For the C–H functionalization reaction (Path B), we proposed a C–H metalation of **105** followed by oxidation to Pd(IV) was operative. Reductive elimination of palladacycle **106** produces the desired product, regenerating the catalyst. In the case of the oxidative dearomatization, oxidation of the alkylpalladium intermediate by Selectfluor generates a high-valent palladium intermediate **107**. The presence of highly electron withdrawing fluoride ancillary ligands likely stabilizes **107** in the absence of any other groups capable of undergoing competitive reductive elimination. Spirocycle **108** can then be formed by an S_N2–type reductive elimination.[57]

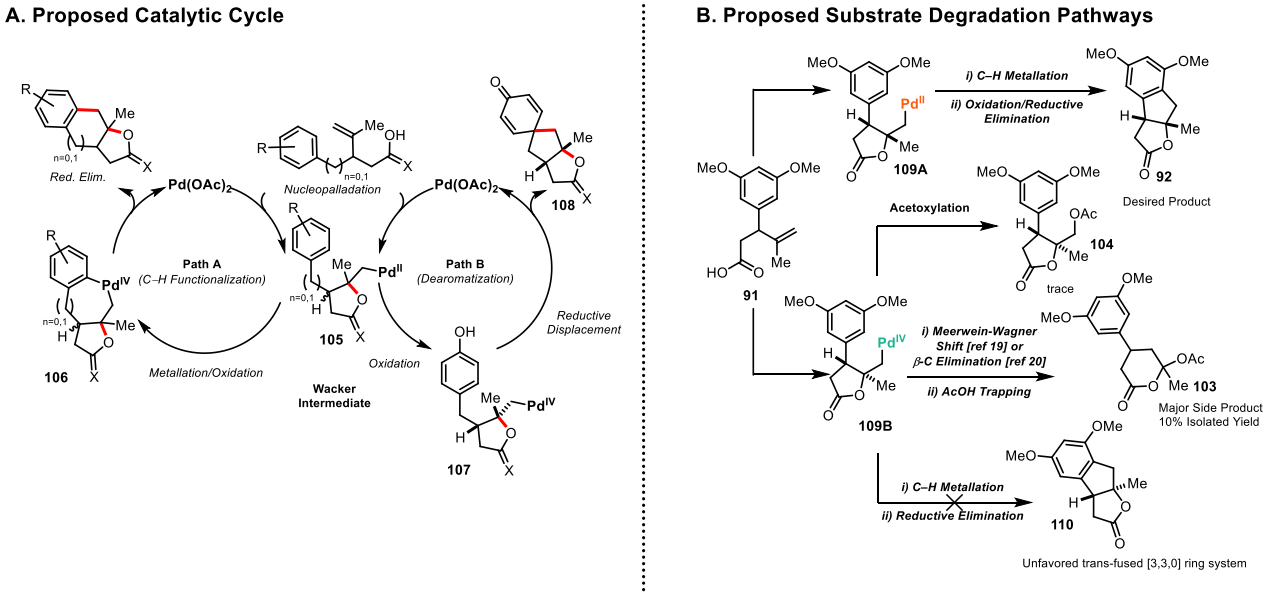

Figure 18 Mechanistic proposal and rationale for observed side products

After establishing a plausible mechanistic hypothesis, we began to speculate on the origins of the pyranone (**103**) and acetoxylated (**104**) side products (Figure 18). Given that products **86** and **88**, which possess a [4.3.0] bicyclononane cores, were as a mixture of diastereomers suggested that the nucleopalladation step was not stereoselective. The formation of **103** and **104** could therefore be the consequence of the formation of a diastereomeric nucleopalladation step of substrate **91**, producing *cis*-lactone **109A** or its *trans*-diastereomer (**109B**). Since the C–H functionalization of **109B** would produce a highly strained *trans* [3.3.0] bicyclooctane (**110**), intermediate **109B** can undergo a Meerwein–Wagner Shift to form an oxocarbenium with concomitant trapping with acetate forming byproduct **103**. Direct reductive elimination (likely through an S_N2 type mechanism) rationalizes the formation of **104**.

2.6 Conclusions and Outlook

In conclusion, we developed a high-valent palladium mediated alkene oxyarylation reaction. Arenes possessing a hydroxyl group in the 4-position underwent an unprecedented oxidative C–C Bond forming dearomatization affording complex spirocyclohexadienones. These substrates have potential applications in the synthesis of natural products, in particular platencin and platensimycin. Despite the success of high-valent palladium catalysis within the context of alkene difunctionalization, there are more opportunities for advancement of this field. For instance, there is a relative paucity of enantioselective Pd(IV) mediated alkene difunctionalization. Additionally, the use of strong oxidants in several alkene difunctionalization reactions has precluded its use in synthesis due to substrate incompatibility. It would be interesting to see the role that photoredox catalysis might play in the future of high-valent palladium catalysis.[81] The emergence of photoredox catalysis within the context of transition metal chemistry opens up the

opportunity to develop new reactions under exceptionally mild conditions.[82–84] This could be highly beneficial within context high-valent palladium catalysis and circumvent the need to use of highly reactive stoichiometric oxidants.

2.7 Experimental Section

General Information

Chemicals were either used as received or purified according to *Purification of Common Laboratory Chemicals*[1]. Glassware was dried in an oven at 150°C or flame dried and cooled under a dry atmosphere prior to use. All reactions were performed using common dry, inert atmosphere techniques. Reactions were monitored by TLC and visualized by a dual short wave/long wave UV lamp and stained with an ethanolic solution of potassium permanganate or p-anisaldehyde. Column flash chromatography was performed using 230-400 mesh silica gel. NMR spectra were recorded on Varian Mercury 300, Varian Unity Plus 400, and Varian Mercury 400 spectrometers. Chemical shifts for ^{1}H NMR were reported as δ, parts per million, relative to the signal of $CHCl_3$ at 7.26 ppm. Chemical shifts for ^{13}C NMR were reported as δ, parts per million, relative to the center line signal of the $CDCl_3$ triplet at 77.0 ppm. Proton and carbon assignments were established using spectral data of similar compounds. The abbreviations s, br. s, d, dd, br. d, ddd, t, q, br. q, m, and br. m stand for the resonance multiplicity singlet, broad singlet, doublet, doublet of doublets, broad doublet, doublet of doublet of doublets, triplet, quartet, broad quartet, multiplet and broad multiplet, respectively. IR spectra were recorded on an Avatar 360 FT-IR spectrometer. Mass spectra were recorded at the Mass Spectrometry Facility at the Department of Chemistry of the Boston University in Boston, MA on a Waters Q-Tof API-US with ESI high resolution mass spectrometer. Concentration refers to removal of solvent under reduced pressure (house vacuum at ca. 20 mmHg)

General Procedure for Preparation of Starting materials

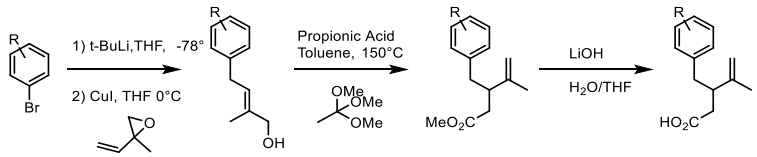

General Procedure for Preparation of Starting Materials for Substrates 1a-6a

Formation of Allylic Arene

To an argon-purged, flame dried round bottom flask equipped with a rubber septum and magnetic stirbar, aryl bromide (1 equiv) was added as a solution in dry THF under argon (50mL/g of substrate). The flask was cooled to -78°C and a solution of *t*-butyl lithium (2.2 equiv, 1.7M solution in hexanes) was added dropwise and stirred for 5 minutes. In a separate, argon-purged, flame dried flask, copper(I) iodide (15 mol %) and vinyl oxirane (1.5 equiv) were dissolved in THF and cooled to 0°C. To this, the aryl lithium solution was transferred dropwise via cannula over a span of 10 minutes. The solution stirred for 45 minutes and was quenched with a saturated solution of ammonium chloride. The THF was evaporated in vacuo and the aqueous layer was extracted with ethyl acetate (3 X). The aqueous layer was discarded and the organic layer was washed with water (2 X) and brine. The organic layer was concentrated in vacuo and the residue was purified by column chromatography on SiO_2.

Johnson Claisen Rearrangement

To a sealed tube, allylic arene (1 equiv) was added to a solution of toluene and of trimethyl orthoacetate (10 equiv). To this, propionic acid (0.1 equiv) was added and the reaction was refluxed at 150°C for 12 hours. The reaction was diluted with ethyl acetate and washed with water (2 X), brine (1 X), and dried over $Mg(SO_4)_2$. The residue was concentrated in vacuo and purified by column chromatography.

Saponification

To a round bottom flask, the Claisen product (1 equiv) and LiOH (4 equiv) were dissolved in 4:1 mixture of THF and water. To this, enough methanol was added to make the mixture a homogenous solution. Remaining solution was then diluted with ethyl acetate. The aqueous layer was washed with 1M aqueous solution of NaOH, and then extracted with ethyl acetate (3 X). The aqueous layer was acidified to a ~pH 3, using an aqueous 3M HCl solution, which was then extracted with ethyl acetate (3 X). The acidified ethyl acetate was then washed with water (3 X), with brine (1 X), and dried over $Mg(SO_4)_2$ and concentrated in vacuo. The residue was then purified using column chromatography to afford the starting material.

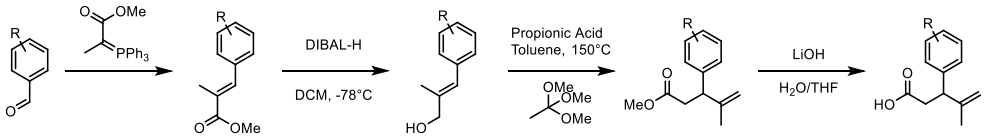

General Procedure for Preparation of Starting Materials for Compounds 9a-16a

Formation of the α,β unsaturated ester

To a slurry of DBU (3.6 equiv) and LiCl (3.6 equiv) in THF (0.6M with respect to benzaldehyde), 1.2 equivalents of phosphonate was added under nitrogen. The reaction was stirred for 1 hour upon which benzaldehyde (1 equiv) was added dropwise as a solution in THF. The reaction after 12 hours, the reaction was quenched with a saturated solution of NH_4Cl. The aqueous layer was extracted with ether (3 X), washed with brine (1 X) and dried over $Mg(SO_4)_2$. The filtrate was concentrated in vacuo and purified by column chromatography

Reduction of the α,β unsaturated ester

A solution ofα,β unsaturated ester in dichloromethane (15 mL per mmol of substrate) was cooled to -78°C under argon. To this, DIBAL-H (2.25 equiv) was added dropwise. After 1 hour the reaction was quenched with a saturated solution of Rochelle's salt and warmed to room temperature over a period of 2 hours. The aqueous layer was extracted with dichloromethane (3 X) and the organic layers were combined and washed with brine (1 X) and dried over $Mg(SO_4)_2$. The organic layer was then concentrated in vacuo and purified by column chromatography.

Johnson Claisen Rearrangement

To a sealed tube, allylic arene (1 equiv) was added to a solution of toluene and of trimethyl orthoacetate (10 equiv). To this, propionic acid (0.1 equiv) was added and the reaction was refluxed

at 150°C for 12 hours. The reaction was diluted with ethyl acetate and washed with water (2 X), one time with brine, and dried over $Mg(SO_4)_2$. The residue was concentrated in vacuo and purified by column chromatography.

Saponification

To a round bottom flask, the Claisen product (1 equiv) and LiOH (4 equiv) were dissolved in 4:1 mixture of THF and water. To this, enough methanol was added to make the mixture a homogenous solution. Remaining solution was then diluted with ethyl acetate. The aqueous layer was washed with 1M aqueous solution of NaOH, and then extracted with ethyl acetate (3 X). The aqueous layer was acidified to a ~pH 3, using an aqueous 3M HCl solution, which was then extracted with ethyl acetate (3 X). The acidified ethyl acetate was then washed with water (3 X), with brine (1 X), and dried over $Mg(SO_4)_2$ and concentrated in vacuo. The residue was then purified using column chromatography to afford the starting material.

Data for Starting Materials

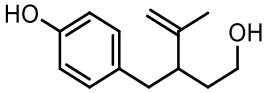

4-(2-(2-hydroxyethyl)-3-methylbut-3-en-1-yl)phenol (Table 2, Entries 1–6)

R_f (Hexane/EtOAc 4:1): 0.23

IR (Neat): 3343, 2936, 2360, 2342, 1645, 1614, 1598, 1514, 1449, 1375, 1240, 1047, 893, 828 cm^{-1};

^1H NMR ($CDCl_3$, 500MHz) δ: 6.99 (d, *J* = 8.5 Hz, 2 H), 6.73 (d, *J* = 8.5, 2 H), 3.92 (br. s., 1 H), 4.74 (m, 1 H), 4.69 (m, 1 H), 3.59 (m, 2 H), 2.69 (dd, *J* = 13.7, 7.6 Hz, 1 H), 2.57 (dd, *J* = 13.4, 7.0 Hz, 1 H), 2.47 (dtd, *J* = 9.5, 7.5, 7.5, 5.2 Hz, 1 H), 1.68 (m, 3 H), 1.64 (m, 2 H);

^{13}C NMR ($CDCl_3$, 125MHz) δ: 154.0, 147.2, 132.2, 130.0, 115.1, 112.2, 61.5, 46.2, 39.7, 34.7, 18.6;

HRMS (ESI) not found.

LRMS (ESI) *m/z* for $C_{13}H_{13}O_2Na^+$ ($[M+Na]^+$) found 229.15

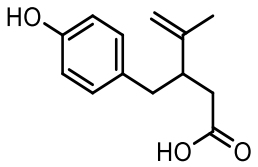

3-(4-hydroxybenzyl)-4-methylpent-4-enoic acid (Figure 16)

R_f (Hexane/EtOAc 7:3): 0.36;

IR (Neat): 3251, 1706, 1648, 1613, 1514, 1442, 1229, 896, 829, 611cm^{-1};

^{1}H NMR ($CDCl_3$, 500 MHz) δ: 7.01 (d, *J* = 8.5 Hz, 2 H), 6.73 (d, *J* = 8.5 Hz, 2 H), 4.74 (m, 2 H), 2.8 (qint, *J* = 7.5 X 4 Hz, 1 H), 2.7, (m, 1 H), 2.56 (m, 1 H), 2.13 (m, 2 H), 1.71 (s, 3 H);

^{13}C NMR ($CDCl_3$, 125MHz) δ: 178.1, 153.9, 145.9, 131.8, 130.2, 115.1, 112.0, 45.0, 39.1, 37.7, 20.0;

HRMS (ESI) not found.

LRMS (ESI) *m/z* for $C_{14}H_{17}O_2^+$ ($[M+H]^+$) found 220.10.

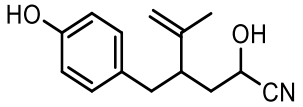

2-hydroxy-4-(4-hydroxybenzyl)-5-methylhex-5-enenitrile (isolated as a 1:1 mixture of diastereomers) (Figure 16)

R_f (DCM/Acetone 9:1): 0.56;

IR (Neat): 2402, 2927, 2248, 1708, 1645, 1613, 1598, 1515, 1447, 1378, 1227, 1173, 1081, 905, 830, 734 cm^{-1};

^{1}H NMR ($CDCl_3$, 500MHz) δ: 7.00 (d, *J* = 8.4 Hz, 2 H), 6.74 (d, *J* = 8.4 Hz 2 H), 4.86 (t, *J* = 1.5 Hz, 1 H, diastereomer 1), 4.81 (t, *J* = 1.5 Hz, 1 H. diastereomer 1), 4.80 (s, 1 H, diastereomer 2), ;4.78 (s, 1 H, diastereomer 2), 4.41 (dd, *J* = 7.0, 5.8 Hz, 1 H, diastereomer 1), 4.36 (dd, *J* = 9.3, 6.3 Hz, 1 H, diastereomer 2), 2.70 (m, 2 H), 2.58 (m, 2 H), 1.89 (m, 2 H, overlap);

^{13}C NMR ($CDCl_3$, 125MHz) δ: 154.0, 145.9, 145.2, 131.5, 130.0, 115.3, 114.22, 113.7, 60.8, 59.7, 45.5, 44.9, 39.4, 39.3, 37.6, 37.4, 30.9, 18.6, 18.6;

HRMS (ESI) not found.

LRMS (ESI) *m/z* for $C_{14}H_{18}NO_2$ ($[M+H]^+$) found 232.12.

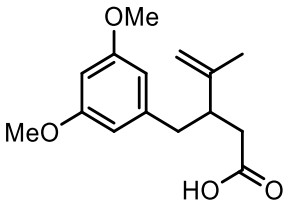

4-methyl-3-(3,5-dimethoxybenzyl)pent-4-enoic acid (Table 3, Entry 2)

R_f (Hexane/EtOAc 1:1): 0.44;

IR (Neat): 29378, 2838, 1704, 1594, 1459, 1428, 1292, 1204, 1146, 1057, 830, 753 cm^{-1};

^{1}H NMR ($CDCl_3$, 300MHz) δ: 6.32 (m, 3 H), 4.79 (t, *J* = 2 X 2.2 Hz, 1 H), 4.74 (s, 1 H), 3.77 (s, 6 H), 2.85 (ddd, *J* = 14.9, 7.9, 7.1 Hz, 1 H), 2.72 (dd, *J* = 13.5, 6.9 Hz, 1 H), 2.56 (dd, *J* = 13.5, 8.1 Hz, 1 H), 2.44-2.41 (m, 2 H), 1.73 (s, 3 H);

^{13}C NMR ($CDCl_3$, 100MHz) δ: 178.9, 160.6, 145.9, 142.0, 112.0, 107.1, 98.1, 55.2, 44.5, 40.2, 37.9, 20.0;

HRMS (ESI) *m/z* calculated for $C_{15}H_{21}O_4^+$ ($[M+H]^+$) 265.1440, found 265.1443.

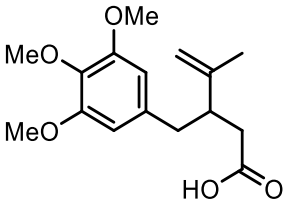

4-methyl-3-(3,4,5-trimethoxybenzyl)pent-4-enoic acid (Table 3, Entry 1)

R_f (Hexane/EtOAc 4:1): 0.13;

IR (Neat): 3014, 2938, 2839, 1706, 1590, 1508, 1458, 1420, 1326, 1236, 1124, 1005, 749, 666 cm^{-1};

^{1}H NMR ($CDCl_3$, 500MHz) δ: 6.37 (s, 2 H), 4.81 (s, 1 H), 4.75 (s, 1 H), 3.84 (s, 6 H), 3.82 (s, 3 H), 2.84 (dddd, *J* = 7.2 Hz, 1 H), 2.72 (dd, *J* = 13.9, 6.9 Hz, 1 H), 2.57(dd, *J* = 13.6, 8.0 Hz, 1 H), 2.48-2.35 (m, 2 H),1.74 (s, 3 H);

^{13}C NMR ($CDCl_3$, 75MHz) δ: 160.7, 147.5, 145.6, 110.6, 106.1, 98.0, 61.2, 55.2, 49.1, 35.7, 21.1;

HRMS (ESI) *m/z* calculated for $C_{16}H_{23}O_5^+$ ($[M+H]^+$) 237.1491, found 237.1498.

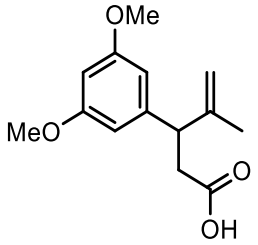

3-(3,5-dimethoxyphenyl)-4-methylpent-4-enoic acid (Table 3, Entry 4)

R_f (Hexane/EtOAc 3:1): 0.25;

IR (Neat):2941, 2838, 1708, 1596, 1461, 1430, 1291, 1205, 1157, 1067, 897, 835, 740, 698 cm^{-1};

^{1}H NMR ($CDCl_3$, 500MHz) δ: 6.39 (d, *J* = 2.1 Hz, 2 H), 6.34 (m, 1 H), 4.92 (d, *J* = 5.2 Hz, 2 H), 3.79 (s, 6 H), 3.74, (m, 1 H), 2.88 (dd, *J* = 15.6, 8.5 Hz, 1 H), 2.75 (dd, *J* = 15.6, 8.5 Hz, 1 H), 1.66 (s, 3 H);

^{13}C NMR ($CDCl_3$, 75MHz) δ: 178.2, 160.8, 146.1, 144.2, 110.7, 105.8, 98.5, 55.2, 48.3, 38.9, 21.7;

HRMS (ESI) *m/z* calculated for $C_{14}H_{19}O_4^+$ ($[M+H]^+$) 251.1295, found 251.1295.

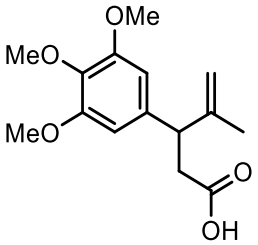

4-methyl-3-(3,4,5-trimethoxyphenyl)pent-4-enoic acid (Table 3, Entry 5)

R_f (Hexane/EtOAc 3:1): 0.1;

IR (Neat): 2640, 2839, 1709, 1648, 1591, 1509, 1461, 1422, 1330, 1239, 1127, 1010, 903, 663 cm^{-1};

^{1}H NMR ($CDCl_3$, 500MHz) δ: 6.43 (s, 2 H), 4.92 (s, 2 H), 3.83 (s, 6 H), 3.83 (m, 9 H), 2.87 (dd, *J* = 15.8, 8.2 Hz, 1 H), 2.72 (dd, *J* = 15.9, 7.3 Hz, 1 H), 1.65 (s, 3 H);

^{13}C NMR ($CDCl_3$, 75MHz) δ: 178.1, 153.1, 146.3, 137.5, 136.7, 110.6, 104.6, 60.8, 56.1, 48.4, 39.3, 21.8;

HRMS (ESI) not found.

LRMS (ESI) *m/z* for $C_{15}H_{21}O_5^+$ ($[M+H]^+$) found 281.13.

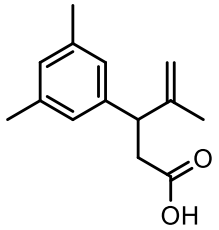

3-(3,5-dimethylphenyl)-4-methylpent-4-enoic acid (Table 3, Entry 6)

R_f (Hexane/EtOAc 9:1): 0.08;

IR (Neat): 3018, 2919, 1709, 1606, 1416, 1300, 1252, 1176, 893, 849, 704 cm^{-1};

^{1}H NMR ($CDCl_3$, 400MHz) δ: 11.53(s, 1 H, OH), 6.87 (s, 1 H), 6.83(s, 2 H), 4.93 (s, 1 H), 4.89 (s, 1 H), 3.71 (t, *J* = 7.8 Hz, 1 H), 2.88 (dd, *J* = 15.7, 8.5 Hz, 1 H), 2.73 (dd, *J* = 15.7, 7.1 Hz, 1 H), 2.29 (s, 6 H), 1.63 (s, 3 H);

^{13}C NMR ($CDCl_3$, 75MHz) δ: 178.4, 146.5, 141.7, 137.9, 128.5, 125.4, 110.4, 48.0, 39.1, 21.7, 21.3;

HRMS (ESI) not found.

LRMS (ESI) *m/z* for $C_{14}H_{19}O_2^+$ ($[M+H]^+$) found 241.13.

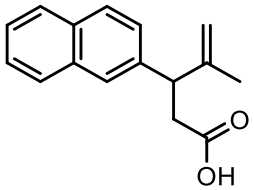

4-methyl-3-(naphthalen-1-yl)pent-4-enoic acid (Table 3, Entry 7)

R_f (Hexane/EtOAc/AcOH 81:15:4): 0.25;

IR (Neat): 3054, 2972, 2918, 1707, 1648, 1600, 1508, 1415, 1375, 1274, 1175, 945, 896, 858, 819, 746 cm^{-1};

^{1}H NMR ($CDCl_3$, 500MHz)δ: 7.80 (m, overlap, 3 H), 7.67 (s, 1 H), 7.45 (m, 2 H), 7.35 (dd, *J* = 8.6, 1.7 Hz, 2 H), 5.00 (s, 1 H), 4.95 (s, 1 H), 3.94 (t, *J* = 7.8 Hz, 1 H), 2.98 (dd, *J* = 15.9, 8. 6 Hz, 1 H), 2.86 (dd, *J* = 15.9, 7.8 Hz, 1 H), 1.64 (s, 3 H);

^{13}C NMR ($CDCl_3$, 125MHz) δ: 176.7, 146.3, 139.2, 133.4, 132.5, 128.2, 127.6, 126.2, 126.0, 126.0, 125.6, 110.9, 106.2, 48.3, 38.7, 21.7;

HRMS (ESI) *m/z* calculated for $C_{16}H_{17}O_2^+$ ($[M+H]^+$) 241.1229, found 241.1231.

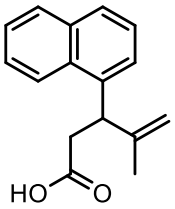

4-methyl-3-(naphthalen-1-yl)pent-4-enoic acid (Table 3, Entry 8)

R_f (Hexane/EtOAc 4:1): 0.31;

IR (Neat): 3044, 2968, 1706, 16495, 1511, 1415, 1027, 1026, 897, 798, 779 cm^{-1};

^{1}H NMR ($CDCl_3$, 500MHz) δ: 7.90 (d, *J* = 8.3 Hz, 1 H), 7.78 (d, *J* = 8.3 Hz, 1 H), 7.66 (d, *J* = 7.8 Hz, 1 H), 7.55 (ddd, *J* = 8.1, 6.9, 1.2 Hz, 1 H), 7.49 (ddd, *J* = 8.3, 7.1, 1.2 Hz, 1 H), 7.33 (d, *J* = 8.3 Hz, 1 H), 4.09 (dd, *J* = 9.8, 2.7 Hz, 1 H), 3.61 (d, *J* = 17.6 Hz, 1 H), 3.33 (d, *J* = 17.4 Hz, 1 H), 3.28 (dd, *J* = 18.1, 9.8 Hz, 1 H), 2.94 (d, *J* = 18.2, 2.8 Hz, 1 H), 1.75 (s, 3 H);

^{13}C NMR ($CDCl_3$, 125MHz) δ: 146.0, 137.6, 134.0, 131.7, 128.9, 127.5, 126.2, 125.6, 125.4, 124.2, 123.1, 111.8, 43.3, 39.0, 22.0;

HRMS (ESI) *m/z* calculated for $C_{16}H_{17}O_2^+$ ($[M+H]^+$) 241.1229, found 241.1229.

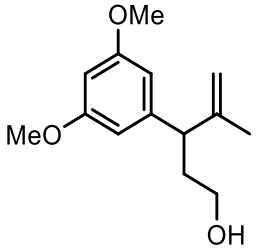

3-(3,5-dimethoxyphenyl)-4-methylpent-4-en-1-ol (Table 3, Entry 9)

R_f (Hexane/EtOAc 4:1): 0.24;

IR (Neat): 3392, 2941, 2838, 2361, 1596, 1462, 1429, 1291, 1205, 1157, 1057, 894, 834, 698 cm^{-1};

^{1}H NMR ($CDCl_3$, 400MHz) δ: 6.39 (d, *J* = 2.3 Hz, 1 H), 6.32 (t, *J* = 2.3 Hz, 1 H), 4.94(s, 1 H), 4.86 (t, *J* = 1.5 Hz, 1 H), 3.77 (s, 6 H), 3.60 (m, 2 H), 3.34 (t, *J* = 7.6 Hz, 1 H), 2.09 (dq, *J* = 13.7, 6.9 Hz, 1 H), 1.95 (ddt, *J* = 13.6, 7.9, 6.4 Hz, 1 H), 3.20 (s, 3 H);

^{13}C NMR ($CDCl_3$, 75MHz) δ: 160.7, 147.5, 145.6, 110.6, 106.1, 98.0, 61.2, 55.2, 49.1, 35.7, 21.1;

HRMS (ESI) *m/z* calculated for $C_{14}H_{21}O_3$($[M+H]^+$) 237.1491, found 237.1498.

General Procedure for Palladium Mediated Cyclizations

A flame dried 100 mL round bottom flask is equipped with a rubber septum and magnetic stir bar and is charged with the aryl cyclization precursor (0.15 mmol, 1.0 equiv) and suspended in 100ml of acetonitrile. To this, iodobenzene diacetate (0.45 mmol, 3.0 equiv) and palladium diacetate (0.015 mmol, 0.10 equiv) were added and the reaction was stirred at room temperature for 12 hours. After the reaction is complete (as judged by TLC analysis), the mixture was concentrated *in vacuo*. The resultant residue was separated by column chromatography on silica gel, using the solvent system indicated, to afford the desired cyclized product.

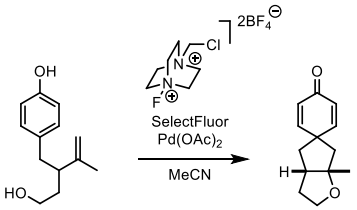

6a'-methyl-2',3',3a',4',6',6a'-hexahydrospiro[cyclohexa[2,5]diene-1,5'-cyclopenta[b]furan]-4-one According the general procedure, the aryl alcohol (100 mg, 0.49 mmol, 1.0 equiv), Selectfluor (258 mg, 0.73 mmol, 3.0 equiv) and palladium diacetate (11 mg, 0.05 mmol, 0.10 equiv) in dry acetonitrile (78 mL) afforded the cyclized product 43 mg in 43% yielda as a yellow oil after purification by chromatography on SiO_2 (80:20, Hexanes/EtOAc) (12 h reaction time).

R_f (DCM/Acetone 95:5): 0.72;

IR (Neat): 2963, 2930, 2863, 2360, 1662, 1451, 1408, 1376, 1259, 1179, 1141, 1110, 1018, 860 cm^{-1};

^{1}H NMR ($CDCl_3$, 500MHz) δ: 7.02 (m, 1 H), 6.93 (m, 1 H), 6.20 (m, 2 H), 3.97(m, 2 H), 2.64 (q, *J* = 8.31 Hz, 1 H), 2.17 (m, 2 H), 2.05 (dd, *J* = 13.3, 8.4 Hz, 1 H), 1.91 (d, *J* = 14.2 Hz, 1 H), 1.75 (m, 2 H), 1.4 (s, 3 H);

^{13}C NMR ($CDCl_3$, 75 MHz) δ: 153.1, 151.3, 128.7, 128.1, 94.9, 49.6, 48.1, 44.8, 44.4, 35.5, 26.3;

HRMS (ESI) not found.

LRMS (ESI) *m/z* for $C_{13}H_{17}O_2^+$ ($[M+H]^+$) found 205.13.

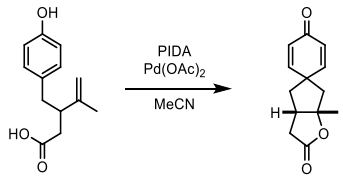

6a'-methyl-2',3',3a',4',6',6a'-hexahydrospiro[cyclohexa[2,5]diene-1,5'-cyclopenta[b]furan]-4-one According the general procedure, the aryl carboxylic acid (85 mg, 0.38 mmol, 1.0 equiv), phenyliodine diacetate (373 mg, 1.16 mmol, 3.0 equiv) and palladium diacetate (24 mg, 0.12 mmol, 0.30 equiv) in dry acetonitrile (85 mL) afforded 17 mgs of cyclized product **5b** after purification by chromatography on SiO_2(65:35 EtOAc/Hex) (2 hour reaction time).

R_f (EtOAc/Hexane 65:35): 0.23;

IR (Neat): 1769, 1665, 1623, 1442, 12267, 1232, 1133, 1096, 952, 861, 740, 703 cm^{-1};

^{1}H NMR ($CDCl_3$, 500 MHz) δ: 6.87 (ddd, *J* = 16.4, 10.0, 2.7 Hz, 2 H), 6.25 (ddd, *J* = 10.0, 5.7, 1.7 Hz, 2 H), 2.94 (dd, *J* = 17.6, 9.3 Hz, 1 H), 2.86 (ddd, *J* = 8.9 Hz, 1 H), 2.50 (d, *J* = 5.6 Hz, 1 H), 2.47 (d, *J* = 2.69 Hz, 1 H), 2.22 (dd, *J* = 13.7, 8.1 Hz, 1 H), 2.08 (d, *J* = 15.2, 1 H), 1.87 (s, 3 H);

^{13}C NMR ($CDCl_3$, 75 MHz) δ: 153.1, 151.3, 128.7, 128.1, 94.9, 49.6, 48.1, 44.8, 44.4, 35.5, 26.3;

HRMS (ESI) *m/z* calculated for $C_{13}H_{15}O_3$ ($[M+H]^+$) 219.1021, found 219.1012.

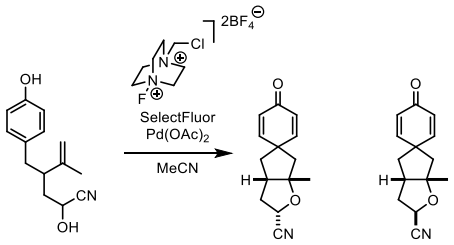

6a'-methyl-4-oxo-2',3',3a',4',6',6a'-hexahydrospiro[cyclohexa[2,5]diene-1,5'-cyclopenta[b]furan]-2'-carbonitrile According the general procedure, the aryl cyanohydrin (80 mg, 0.35mmol, 1.0 equiv), SelectFluor (184 mg, 0.52 mmol, 1.5 equiv) and palladium diacetate (7.7 mg, 0.035 mmol, 0.10 equiv) in dry acetonitrile (40 mL) afforded the cyclized product **13b** as a mixture of diastereoisomers (13 mg and 11 mg, 30% combined) as a yellow oil after purification by chromatography on SiO_2 (80:20, Hexanes/EtOAc) (12 h reaction time).

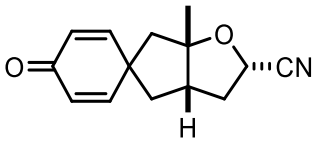

R_f (DCM/Acetone 95:5): 0.24;

IR (Neat): 2973, 2362, 2340, 1663, 1623, 1452, 1408, 1380, 1259, 1182, 1101, 1071, 1024, 860 cm^{-1};

^{1}H NMR ($CDCl_3$, 500MHz) δ: 6.91 (dd, *J* = 10.3, 2.93 Hz, 1 H), 6.86 (dd, *J* =10.3, 2.9 Hz, 1 H), 6.22 (dd, *J* = 4.9, 2.0 Hz, 1 H), 6.20 (dd, *J* = 4.7, 2.0 Hz, 1 H), 4.89 (t, *J* = 7.5 Hz, 1 H), 2.87 (qd, *J* = 8.4, 2.0 Hz, 1 H), 2.62 (dt, *J* = 13.5, 7.6 Hz, 1 H), 2.35 (ddd, *J* = 13.4, 7.8, 2.1 Hz, 1 H), 2.29 (d, *J* = 14.7 Hz, 1 H), 2.12 (dd, *J* = 13.7, 8.3 Hz, 1 H), 1.97 (d, *J* = 14.9 Hz, 1 H), 1.75 (dd, *J* = 13.7, 9.1 Hz, 1 H), 1.58 (s, 3 H);

^{13}C NMR ($CDCl_3$, 100MHz) δ: 185.6, 154.3, 151.6, 128.2, 127.6, 119.8, 96.4, 65.6, 50.3, 49.2, 49.1, 43.4, 36.8, 26.7;

HRMS (ESI) *m/z* calculated for $C_{14}H_{16}NO_2^+$ ([M+H$^+$]) 230.1181, found 230.1185.

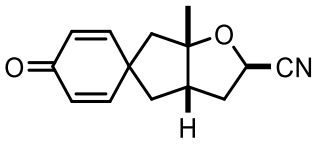

R_f (DCM/Acetone 95:5): 0.30;

IR (Neat): 2967, 2933, 2871, 1660, 1622, 1452, 1408, 1380, 1259, 1181, 1100, 1070, 1024, 859 cm^{-1};

^{1}H NMR ($CDCl_3$, 500MHz) δ: 7.02 (dd, *J* = 9.9, 3.1 Hz, 2 H), 6.93 (dd, *J* = 9.9, 3.1 Hz, 3 H), 6.26 (ddd, *J* = 11.7, 10.3, 2.0 Hz, 4 H), 4.85 (dd, *J* = 8.7, 2.8 Hz, 2 H), 2.81 (dtd, *J* = 9.9, 8.3, 8.3, 1.3 Hz, 3 H), 2.58 (dt, *J* = 13.7, 8.1 Hz, 3 H), 2.53 (d, *J* = 14.7 Hz, 3 H), 2.32 (dd, *J* = 14.0, 10.0 Hz, 1 H), 2.26 (ddd, *J* = 13.5, 2.9, 1.2 Hz, 4 H), 2.12 (ddd, *J* = 13.7, 8.3, 1.5 Hz, 3 H), 2.00 (dd, *J* = 14.7, 1.5 Hz, 3 H);

^{13}C NMR ($CDCl_3$, 125MHz) δ:185.5, 153.9, 152.4, 127.8, 127.6, 119.5, 96.6, 65.2, 49.8, 48.9, 48.8, 43.4, 37.7, 25.8;

HRMS (ESI) *m/z* calculated for $C_{14}H_{16}NO_2^+$ ($[M+H]^+$) Calculated 230.1181, found 230.1178.

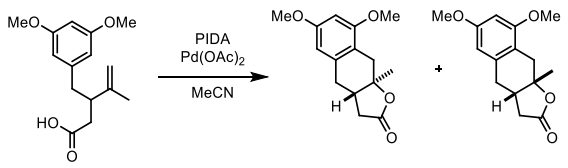

5,7-dimethoxy-3,3a,8,8a-tetrahydro-2 H-indeno[2,1-b]furan-2-one

According the general procedure, the aryl carboxylic acid (100 mg, 0.38 mmol, 1.0 equiv), phenyliodine diacetate (182.9 mg, 0.57 mmol, 1.5 equiv) and palladium diacetate (8.9 mg, 0.038 mmol, 0.10 equiv) in dry acetonitrile (100 m) afforded the cyclized product **2b** and **2b'** (51 mg and 39 mg, 91% combined) as a white precipitate after purification by chromatography on SiO_2 (80:20, Hexanes/EtOAc) (12 h reaction time).

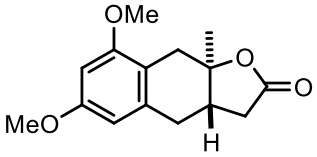

R_f (Hexane/EtOAc 4:1): 0.64;

IR (Neat): 2922, 2850, 1778, 1609, 1464, 1321, 1251, 1207, 1146, 1053, 945, 832, 741 cm^{-1};

^{1}H NMR ($CDCl_3$, 500MHz) δ: 6.33 (d, *J* = 2.2 Hz, 1 H), 6.26 (d, *J* = 2.2 Hz, 1 H), 3.78 (s, 3 H), 3.77 (s, 3 H), 3.11 (d, *J* = 15.7 Hz, 1 H), 2.97 (dd, *J* = 16.3, 3.8 Hz, 1 H), 2.67-2.78 (m, 2 H), 2.59-2.44 (m, 3 H), 1.20 (s, 3 H);

^{13}C NMR ($CDCl_3$, 75 MHz) δ: 176.1, 159.3, 157.8, 137.7, 115.3, 104.8, 96.9, 87.5, 55.5, 55.4, 39.9, 34.9, 34.9, 34.3, 32.4, 28.6;

HRMS (ESI) *m/z* calculated for $C_{15}H_{19}O_4^+$ ($[M+H]^+$) 263.1283, Found 263.1285.

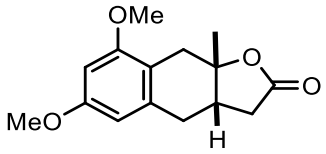

R_f (Hexane/EtOAc 4:1): 0.53;

IR (Neat):2927, 2848, 1766, 1596, 1496, 1464, 1323, 1204, 1147, 1095, 1052, 955, 835, 737 cm^{-1};

^{1}H NMR ($CDCl_3$, 500MHz) δ: 6.34 (d, *J* = 2.2 Hz, 1 H), 6.26 (d, *J* = 2.2 Hz, 1 H), 3.79 (s, 3 H), 3.78 (s, 3 H), 3.16 (d, *J* = 15.4 Hz, 1 H), 2.81 (dd, *J* = 18.5, 8.8 Hz, 1 H), 2.63 (d, *J* = 15.4 Hz, 1 H), 2.52 (m, 2 H), 1.12 (dd), *J* = 18.5, 5.0 Hz, 1 H), 1.50 (s, 3 H);

^{13}C NMR ($CDCl_3$, 75 MHz) δ: 176.2, 158.9, 136.4, 115.8, 104.7, 96.5, 84.8, 55.3, 62.1, 36.0, 32.9, 31.0, 17.8;

HRMS (ESI) *m/z* calculated for $C_{15}H_{19}O_4^+$ ($[M+H]^+$) 263.1283, Found 263.1277.

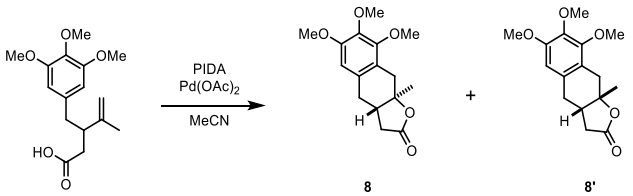

6,7,8-trimethoxy-9a-methyl-3a,4,9,9a-tetrahydronaphtho[2,3-b]furan-2(3 H)-one

According the general procedure, the aryl carboxylic acid (100 mg, 0.34 mmol, 1.0 equiv), phenyliodine diacetate (216 mg, 0.67 mmol, 2.0 equiv) and palladium diacetate (7.0 mg, 0.03mmol, 0.10 equiv) in dry acetonitrile (100 mL) afforded the cyclized products **3b** and **3b'** in 37 mg and 28 mg respectively, for a combined yield of 65%. Crude NMR analysis revealed a 1.8:1 diastereomeric ratio in favor for product **3b**. Both diastereomers were a tan solid after purification by chromatography on SiO_2 (80:20, Hexanes) (12 h reaction time).

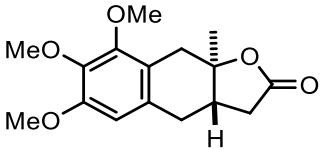

R_f (Hexane/EtOAc 4:1): 0.31;

IR (Neat): 2937, 1779, 1603, 1493, 1461, 1340, 1255, 1244, 1119, 1069, 1032, 668 cm^{-1} ;

^{1}H NMR ($CDCl_3$, 500MHz) δ: 6.52 (s, 1 H), 3.86 (s, 3 H), 3.84 (s, 3 H), 3.83 (s, 3 H), 3.11 (d, *J* = 15.6 Hz, 1 H), 3.84 (dd, *J* = 18.6, 10.4 Hz, 1 H), 2.75 (dd, *J* = 13.9, 4.7 Hz, 1 H), 2.63 (d, *J* = 15.3, 1 H), 2.56 (m, 1 H), 2.51 (dd, *J* = 14, 5.2 Hz), 2.20 (dd, *J* = 18.5, 4.7 Hz), 1.53 (s 3 H);

^{13}C NMR ($CDCl_3$, 75MHz) δ: 175.9, 152.1, 152.0, 140.7, 130.0, 120.8, 107.9, 84.5, 60.8, 60.5, 55.9, 42.3, 36.3, 32.9, 30.7, 17.6;

HRMS (ESI) *m/z* calculated for $C_{16}H_{21}O_5^+$ ($[M+H]^+$) 293.1389, Found 293.1386.

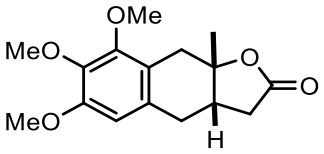

R_f (Hexane/EtOAc 4:1): 0.25;

IR (Neat): 2936, 1778, 1602, 1493, 1461, 1412, 1340, 1255, 1119, 1069, 1031, 987, 668 cm^{-1};

^{1}H NMR ($CDCl_3$, 500MHz) δ: 6.43 (s, 1 H), 3.85 (s, 3 H), 3.84 (s, 3 H), 3.82 (s, 3 H), 3.19 (d, *J* = 15.5 Hz, 1 H), 2.96 (dd, *J* = 16.0, 3.9 Hz, 1 H), 2.8 (d, *J* = 15.7, 1 H), 2.68 (m, 1 H), 2.57 (d, *J* = 8.4 Hz, 1 H), 2.48 (m, 1 H), 1.21 (s, 3 H)

^{13}C NMR ($CDCl_3$, 75MHz) δ: 175.9, 152.2, 151.5, 141.1, 131.3, 120.5, 107.7, 87.2, 61.3, 61.0, 56.1, 39.9, 34.9, 34.2, 33.4, 28.6;

HRMS (ESI) *m/z* calculated for $C_{16}H_{21}O_5^+$ ($[M+H]^+$) 292.1389, found 293.1376.

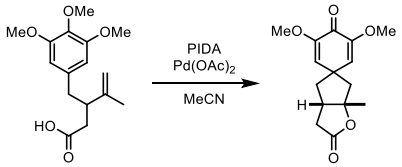

(3a'S,6a'S)-3,5-dimethoxy-6a'-methyl-3a',4',6',6a'-tetrahydrospiro[cyclohexa[2,5]diene-1,5'-cyclopenta[b]furan]-2',4(3'H)-dione According the general procedure, the aryl carboxylic acid (100 mg, 0.34 mmol, 1.0 equiv), phenyliodine diacetate (216 mg, 0.67 mmol, 2.0 equiv) and palladium diacetate (7.0 mg, 0.03mmol, 0.10 equiv) in dry acetonitrile (100 mL) afforded 23 mg of cyclized product **3c** as a brown solid in 32% yield, after purification by chromatography on SiO_2 (80:20, Hexanes/EtOAc → 99:1 EtOAc/MeOH) (12 h reaction time).

R_f (EtOAc/MeOH 99:1): 0.20;

IR (Neat): 2936, 1778, 1602, 1493, 1461, 1340, 1255, 1119, 1069, 987, 668 cm^{-1};

^{1}H NMR ($CDCl_3$, 500MHz) δ: 5.91-5.72 (m, 2 H), 3.66 (s, 6 H), 2.96 (dd, *J* = 18.1, 8.8 Hz, 1), 2.87 (dd, *J* = 8.5 Hz, 1 H), 2.49 (dd, *J* = 7.8, 6.6 Hz, 2 H), 2.22 (ddd, *J* = 13.5, 8.0, 1.5 Hz, 1 H), 2.11 (dd, *J* = 14.8, 1.6 Hz, 1 H), 1.91 (dd, *J* = 13.5, 9.3 Hz, 1 H), 1.6 (s, 3 H);

^{13}C NMR ($CDCl_3$, 75 MHz) δ: 176.0, 175.5, 150.3, 150.0, 120.9, 119.1, 94.9, 55.3, 55.2, 51.6, 46.4, 46.3, 44.8, 35.5, 26.5;

HRMS (ESI) *m/z* calculated for $C_{15}H_{18}O_5Na^+$ ([M+Na^+]) 301.1052, found 301.1061.

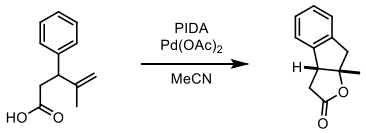

8a-methyl-3,3a,8,8a-tetrahydro-2 H-indeno[2,1-b]furan-2-one

According the general procedure, the aryl carboxylic acid (93 mg, 0.48 mmol, 1.0 equiv), phenyliodine diacetate (460 mg, 1.4 mmol, 3.0 equiv) and palladium diacetate (12 mg, 0.048 mmol, 0.10 equiv) in dry acetonitrile (100 mL) afforded the cyclized product **9b** (55 mg, 60%) as a white solid after purification by chromatography on SiO_2 (90:10, Hexanes/EtOAc) (12 h reaction time).

R_f (Hexane/EtOAc 7:3): 0.32;

IR (Neat): 3024, 2970, 2929, 1768, 1483, 1419, 1384, 1255, 1222, 1170, 1119, 1067, 945, 914, 775, 751, 681 cm^{-1};

^{1}H NMR ($CDCl_3$, 500 MHz) δ: 7.29-7.10 (m, 4 H), 3.63 (d, *J* = 8.7 Hz, 1 H), 3.39 (d, *J* = 17.5 Hz, 1 H), 3.13 (d, *J* = 17.5 Hz, 1 H), 3.05 (dd, *J* = 17.9, 9.0 Hz, 1 H), 2.70 (dt, *J* = 17.8, 0.7 Hz, 1 H), 1.63 (s, 3 H);

^{13}C NMR ($CDCl_3$, 75MHz) δ: 175.7, 142.5, 140.2, 128.2, 127.6, 125.0, 124.6, 93.7, 50.5, 44.8, 35.4, 24.4;

HRMS (ESI) not found.

LRMS (ESI) *m/z* for $C_{12}H_{13}O_2^+$ ($[M+H]^+$) found 189.09

Note: For characterization data for the starting material (compound **10**), see: Padwa, A.; Austin, D. J.; Price, A. T.; Semones, M. A.; Doyle, M. P.; Protopopova, M. N.; Winchester, W. R.; Tran, A. *J. Am. Chem. Soc.* **1993**, *115*, 8669.

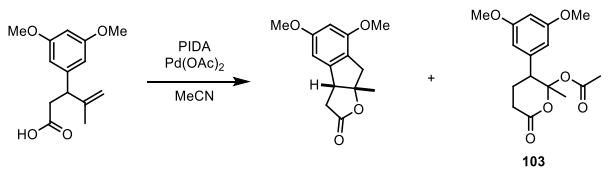

5,7-dimethoxy-3a,8a-dimethyl-3,3a,8,8a-tetrahydro-2 H-indeno[2,1-b]furan-2-one
According the general procedure, the aryl carboxylic acid (120 mg, 0.48 mmol, 1.0 equiv), phenyliodine diacetate (480 mg, 1.4 mmol, 3.0 equiv) and palladium diacetate (14 mg, 0.048 mmol, 0.10 equiv) in dry acetonitrile (100 mL) afforded the cyclized product **10b** (72 mg, 60%) as a white solid after purification by chromatography on SiO_2 (99.5:0.5, DCM/Et_2O) (12 h reaction time). Up to 20% of compound **103** could be isolated. See NMR at the end of the section.

R_f (Hexane/EtOAc/AcOH 68:30:2): 0.31;

IR (Neat): 2940, 1771, 1600, 1495, 1467, 1431, 1331, 1219, 1148, 1066, 946, 836, 737 cm^{-1};

^{1}H NMR ($CDCl_3$, 500 MHz) δ: 6.33 (d, *J* = 2.0 Hz, 1 H), 6.29 (d, *J* = 1.7 Hz, 1 H), 3.79 (s, 6 H), 3.61 (d, *J* = 9.0Hz, 1 H), 3.33 (d, *J* = 17.4 Hz, 1 H) , 3.04 (dd, *J* = 17.9, 9.3 Hz, 1 H), 2.96 (d, J = 17. 1 Hz, 1 H), 2.72 (dt, *J* = 17.9, 0.7 Hz, 1 H), 1.64 (s, 3 H);

^{13}C NMR ($CDCl_3$, 75MHz) δ: 175.7, 161.4, 156.7, 144.5, 120.2, 100.1, 98.0, 94.1, 55.6, 55.2, 51.1, 41.4, 35.1, 24.7;

HRMS (ESI) *m/z* calculated for $C_{14}H_{17}O_4^+$ ($[M+H]^+$) 249.1127, found 249.1118.

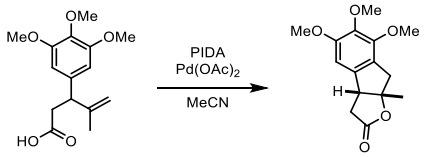

5,6,7-trimethoxy-8a-methyl-3,3a,8,8a-tetrahydro-2 H-indeno[2,1-b]furan-2-one

According the general procedure, the aryl carboxylic acid (100 mg, 0.35 mmol, 1.0 equiv), phenyliodine diacetate (276.5 mg, 1.25 mmol, 3.0 equiv) and palladium diacetate (9.6 mg, 0.043 mmol, 0.10 equiv) in dry acetonitrile (100 mL) afforded the cyclized product **11b** (51 mg, 52%) as a clear oil after purification by chromatography on SiO_2 (80:20 Hexanes/ Acetone) (12 h reaction time).

R_f (Hexane/EtOAc 4:1): 0.25;

IR (Neat): 2967, 2842, 1590, 1484, 1416, 1345, 1264, 1235, 1171, 1067, 947, 807, 710 cm^{-1};

^{1}H NMR ($CDCl_3$, 500MHz) δ: 6.45 (s, 1 H), 3.89 (s, 3 H), 3.84 (s, 3 H), 3.84 (s, 3 H), 3.60 (d, *J* = 8.7 Hz, 1 H), 3.41 (d, *J* = 17.1 Hz, 1 H), 2.96-3.15 (m, 2 H), 2.71 (d, *J* = 17.5 Hz, 1 H), 1.66 (s, 3 H);

^{13}C NMR ($CDCl_3$, 75 MHz) δ: 175.6, 154.2, 149.8, 141.6, 137.8, 124.7, 103.1, 94.0, 61.0, 60.4, 56.3, 50.9, 42.1, 35.3, 24.6;

HRMS (ESI) *m/z* calculated for $C_{15}H_{19}O_5^+$ ($[M+H]^+$) 279.1232, found 279.1233.

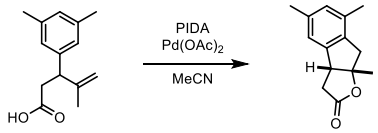

5,7,8a-trimethyl-3,3a,8,8a-tetrahydro-2 H-indeno[2,1-b]furan-2-one

According the general procedure, the aryl carboxylic acid (110 mg, 0.48 mmol, 1.0 equiv), phenyliodine diacetate (470 mg, 1.4 mmol, 3.0 equiv) and palladium diacetate (11 mg, 0.048 mmol, 0.10 equiv) in dry acetonitrile (100 mL) afforded the cyclized product **12b** (61 mg, 57%) as a white solid after purification by chromatography on SiO_2 (100% DCM) (12 h reaction time).

R_f (DCM): 0.28;

IR (Neat):2932, 2857, 2359, 1759, 1510, 1481, 1422, 1388, 1267, 1177, 1119, 1074, 1033, 945, 923, 857, 810, 729, 653 cm^{-1};

^{1}H NMR ($CDCl_3$, 500 MHz) δ: 6.88 (d, *J* = 0.6 Hz, 1 H), 6.81 (s, 1 H), 3.32 (d, *J* = 17.3 Hz, 1 H), 3.06 (dd, *J* = 17.8, 9.1 Hz, 1 H), 3.00 (d, *J* = 17.1 Hz, 1 H), 2.71 (dq, *J* = 17.6, 0.8 Hz, 1 H), 2.30 (s, 3 H), 2.20 (s, 3 H), 1.66 (s, 3 H);

^{13}C NMR ($CDCl_3$, 75MHz) δ: 175.9, 142.5, 137.7, 136.1, 134.2, 129.9, 122.4, 93.8, 50.6, 43.4, 35.5, 24.7, 21.2, 18.9;

HRMS (ESI) *m/z* calculated for $C_{14}H_{17}O_2^+$ ($[M+H]^+$) 217.1229, found 217.1234.

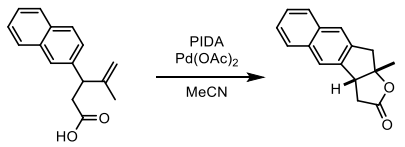

10a-methyl-3,3a,10,10a-tetrahydro-2 H-benzo[5,6]indeno[2,1-b]furan-2-one

According the general procedure, the aryl carboxylic acid (100 mg, 0.48 mmol, 1.0 equiv), phenyliodine diacetate (460 mg, 1.4 mmol, 3.0 equiv) and palladium diacetate (10.0 mg, 0.048 mmol, 0.10 equiv) in dry acetonitrile (100 mL) afforded the cyclized product **13b** (55 mg, 52%) as a white solid after purification by chromatography on SiO_2 (100% DCM) (12 h reaction time).

R_f (Hexane/EtOAc 4:1): 0.42;

IR (Neat): 2922, 2857, 2360, 2342, 1763, 1608, 1510, 1255, 1169, 1117, 1069, 945, 921, 872, 755 cm^{-1};

^{1}H NMR ($CDCl_3$, 400MHz) δ: 7.83-7.75 (m, 2 H), 7.65 (d, *J* = 9.0 Hz, 2 H), 7.48-7.40 (m, 2 H), 3.81 (d, *J* = 8.7 Hz, 1 H), 3.59 (d, *J* = 17.5 Hz, 1 H), 3.32 (d, *J* = 17.6 Hz, 1 H), 3.19 (dd, *J* = 17.8, 8.7 Hz, 1 H), 2.86 (d, *J* = 17.8 Hz, 1 H), 1.72 (s, 3 H);

^{13}C NMR ($CDCl_3$, 75MHz) δ: 175.5, 141.9, 138.8, 133.7, 133.2, 127.7, 127.6, 125.9, 125.6, 123.6, 123.5, 94.0, 50.13, 44.3, 36.1, 24.4;

HRMS (ESI) *m/z* calculated for $C_{16}H_{15}O_2^+$ ($[M+H]^+$) 239.1072, found 239.1073.

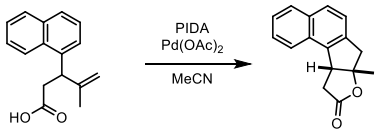

7a-methyl-10,10a-dihydro-7H-benzo[6,7]indeno[2,1-b]furan-9(7aH)-one

According the general procedure, the aryl carboxylic acid (120 mg, 0.50 mmol, 1.0 equiv), phenyliodine diacetate (320 mg, 0.99 mmol, 2.0 equiv) and palladium diacetate (11 mg, 0.05 mmol, 0.10 equiv) in dry acetonitrile (100 mL) afforded the cyclized product **14b** (63 mg, 53%) as a after purification by chromatography on SiO_2(90:10, Hexanes/EtOAc) (12 h reaction time).

R_f (Hexane/EtOAc 4:1): 0.13;

IR (Neat): 3057, 2979, 2931, 1773, 1517, 1384, 1267, 1241, 1178, 1072, 955, 814, 779, 739 cm^{-1};

^{1}H NMR ($CDCl_3$, 500MHz) δ: 7.90 (d, *J* = 8.3 Hz, 1 H), 7.78 (d, *J* = 8.3 Hz, 1 H), 7.66 (d, *J* = 7.8 Hz, 1 H), 7.55 (ddd, *J* = 8.1, 6.9, 1.2 Hz, 1 H), 7.49 (ddd, *J* = 8.3, 7.1, 1.2 Hz, 1 H), 7.33 (d, *J* = 8.3 Hz, 1 H), 4.09 (dd, *J* = 9.8, 2.7 Hz, 1 H), 3.61 (d, *J* = 17.6 Hz, 1 H), 3.33 (d, *J* = 17.4 Hz, 1 H), 3.28 (dd, *J* = 18.1, 9.8 Hz, 1 H), 2.94 (d, *J* = 18.2, 2.8 Hz, 1 H), 1.75 (s, 3 H);

^{13}C NMR ($CDCl_3$, 125MHz) δ: 175.9, 137.2, 137.0, 133.4, 129.5, 129.2, 129.2, 126.8, 125.4, 123.0, 123.0, 93.3, 50.1, 46.4, 34.7, 25.9;

HRMS (ESI) *m/z* calculated for $C_{16}H_{15}O_2^+$ ($[M+H]^+$) 239.1072, found 239.1076.

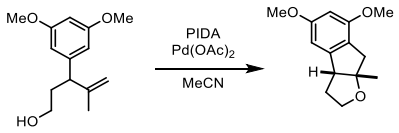

5,7-dimethoxy-8a-methyl-3,3a,8,8a-tetrahydro-2 H-indeno[2,1-b]furan

According the general procedure, the aryl carboxylic acid (110 mg, 0.48 mmol, 1.0 equiv), phenyliodine diacetate (480 mg, 1.4 mmol, 3.0 equiv) and palladium diacetate (16 mg, 0.048 mmol, 0.10 equiv) in dry acetonitrile (100 mL) afforded the cyclized product **15b** (52 mg, 46%) as a clear oil after purification by chromatography on SiO_2 (gradient of 90:10 → 80:20 Hexanes/EtOAc) (12 h reaction time).

R_f (Hexane/EtOAc 4:1): 0.43;

IR (Neat): 2940, 1660, 1596, 1462, 1429, 1344, 1205, 1157, 1059, 833, 744 cm^{-1};

^{1}H NMR ($CDCl_3$, 500MHz) δ: 6.32 (d, *J* = 1.5 Hz, 1 H), 6.29 (d, *J* = 1.9 Hz, 1 H), 3.91 (m, 2 H), 3.79 (s, 3 H), 3.78 (s, 3 H), 3.13 (td, *J* = 9.1, 9.1, 5.9 Hz, 1 H), 3.38, (dd, *J* = 8.6, 2.5 Hz, 2 H), 3.07 (d, *J* = 16.8 Hz, 1 H), 2.88 (d, *J* = 16.8Hz, 1 H), 2.23 (m, 1 H), 2.00 (ddt *J* = 12.1, 6.0, 2.8, 2.8 Hz, 1 H), 1.46 (s, 3 H);

^{13}C NMR ($CDCl_3$. 75MHz) δ: 160.7, 147.5, 145.6, 110.6, 106.1, 98.0, 61.3, 55.2, 49.2, 35.7, 21.1;

HRMS (ESI) not found.

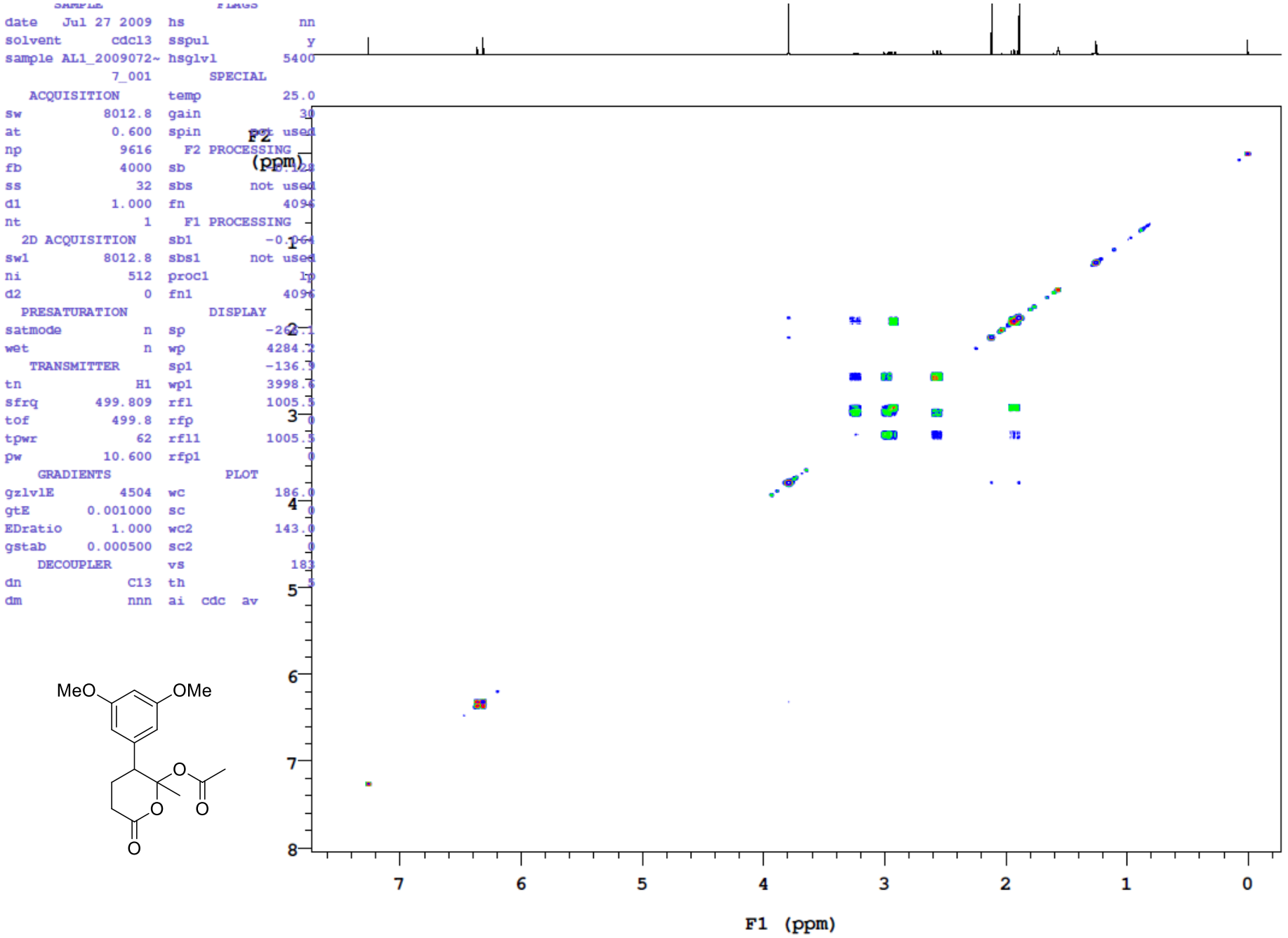
date Jul 27 2009
solvent cdcl3
sample AL1_2009072~7_001
ACQUISITION
sw 8012.8
at 0.600
np 9616
fb 4000
ss 32
d1 1.000
nt 1
2D ACQUISITION
sw1 8012.8
ni 512
d2 0
PRESATURATION
satmode n
wet n
TRANSMITTER
tn H1
sfrq 499.809
tof 499.8
tpwr 62
pw 10.600
GRADIENTS
gzlvlE 4504
gtE 0.001000
EDratio 1.000
gstab 0.000500
DECOUPLER
dn C13
dm nnn
hs nn
sspul y
hsglvl 5400
SPECIAL
temp 25.0
gain 30
spin not used
F2 PROCESSING
sb
sbs not used
fn 4096
F1 PROCESSING
sb1
sbs1 not used
proc1 lp
fn1 4096
DISPLAY
sp
wp 4284.2
sp1 -136.9
wp1 3998.6
rfl 1005.5
rfp 0
rfl1 1005.5
rfp1 0
PLOT
wc 186.0
sc 0
wc2 143.0
sc2 0
vs 183
th 5
ai cdc av
F2 (ppm)
F1 (ppm)
MeO
OMe
O
O
O
O

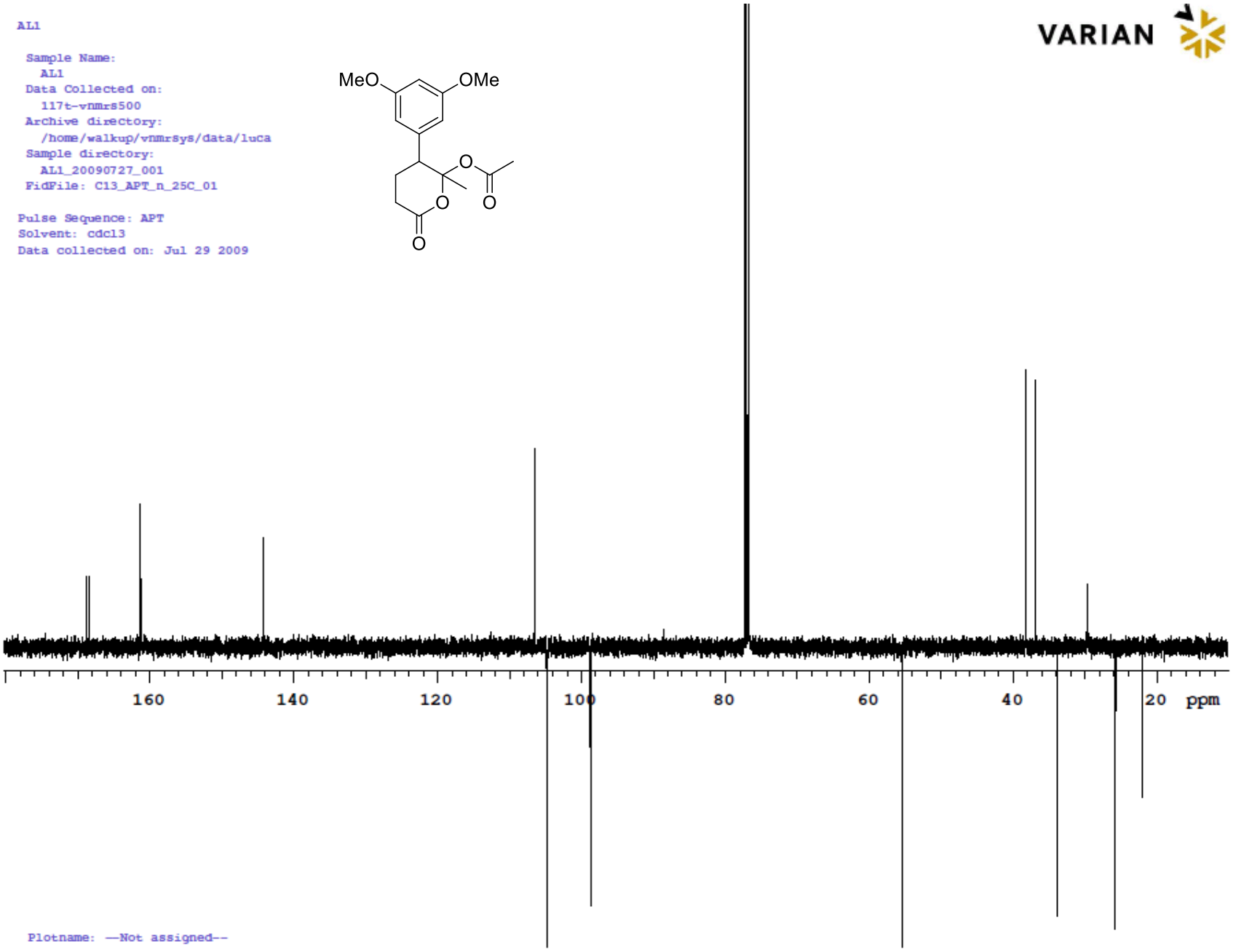
AL1
Sample Name:
AL1
Data Collected on:
117t-vnmrs500
Archive directory:
/home/walkup/vnmrsys/data/luca
Sample directory:
AL1_20090727_001
FidFile: C13_APT_n_25C_01
Pulse Sequence: APT
Solvent: cdcl3
Data collected on: Jul 29 2009
MeO
OMe
O
O
O
O
160
140
120
100
80
60
40
20
ppm
Plotname: --Not assigned--

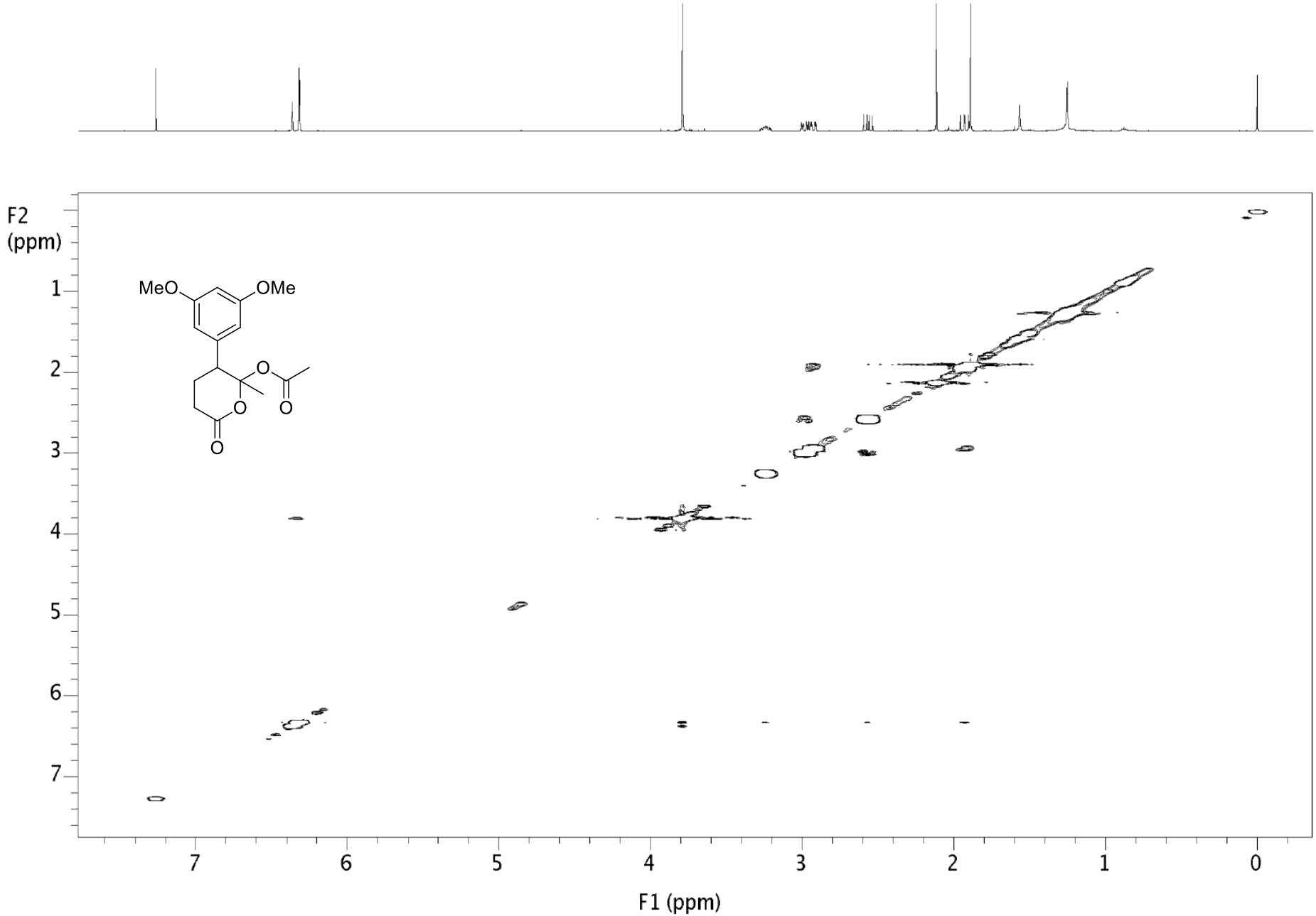
F2
(ppm)
1
2
3
4
5
6
7
MeO
OMe
O
O
O
O
7
6
5
4
3
2
1
0
F1 (ppm)

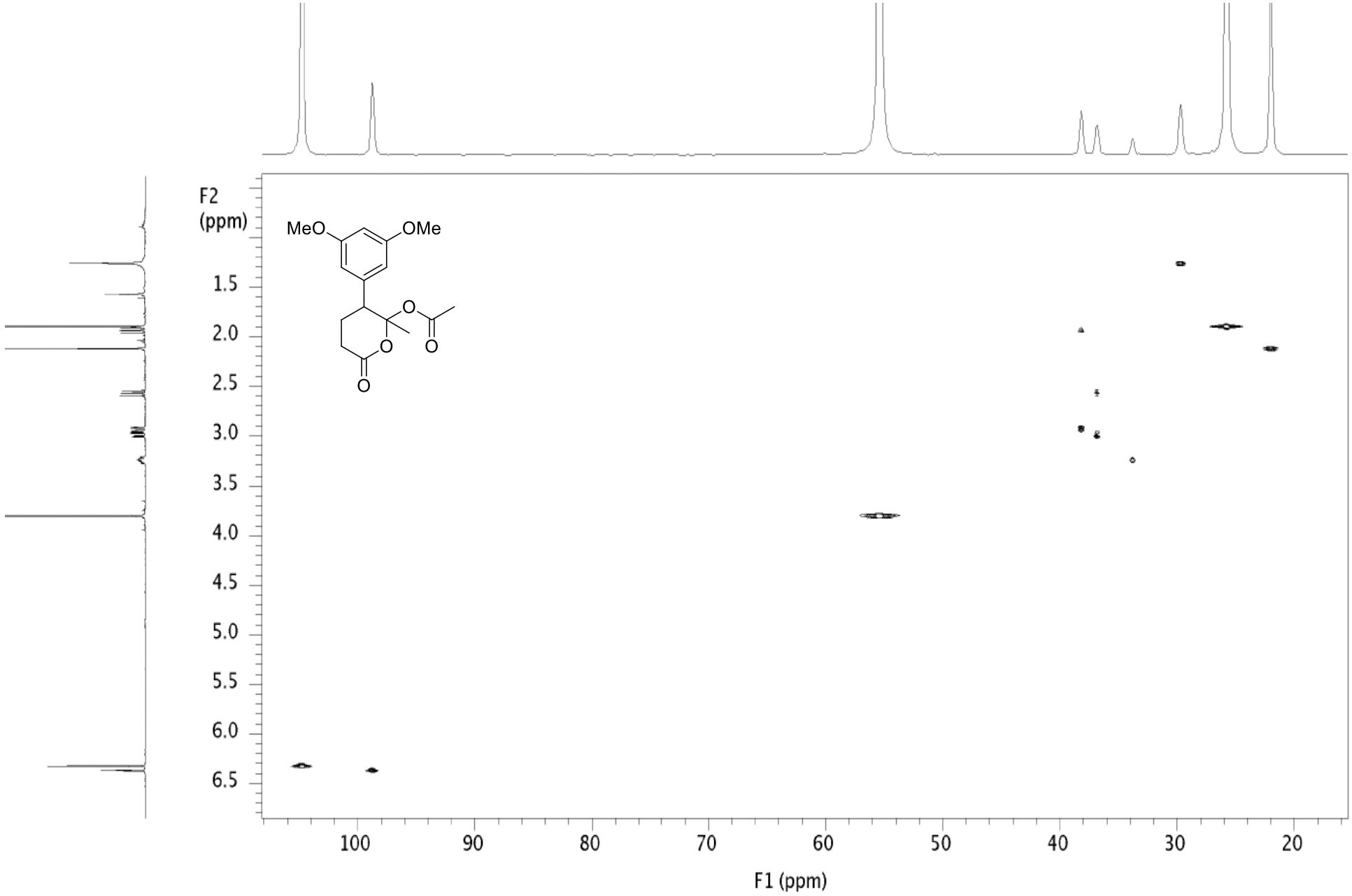
F2
(ppm)
MeO
OMe
O
O
O
O
1.5
2.0
2.5
3.0
3.5
4.0
4.5
5.0
5.5
6.0
6.5
100
90
80
70
60
50
40
30
20
F1 (ppm)

HSQC

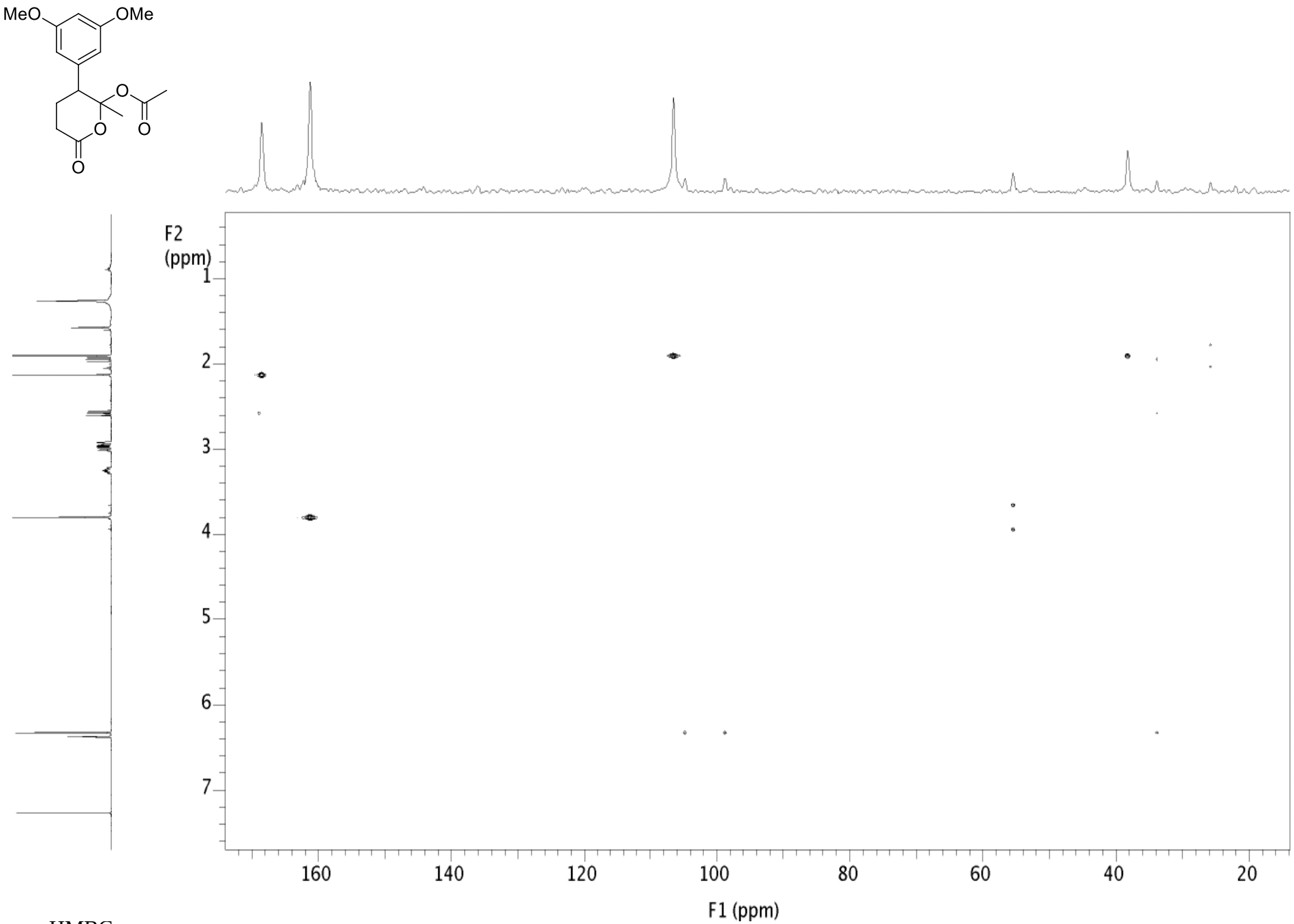

HMBC

Chapter 3: Development of a Mild, Photocatalytic Strategy Towards the Depolymerization of Lignin

*Portions of this thesis were published in:

Nguyen, J. D.[†]; Matsuura, B. S.[†]; Stephenson, C. R. J. *J. Am. Chem. Soc.* **2013**, *136*, 1218–1221.

3.1 Introduction

Concerns over energy security, environmental impact, rising cost, and dwindling supply of crude petroleum has prompted the scientific community to expand the role of biomass as a renewable resource for fuel and commodity chemicals.[1] As the only available renewable carbon feedstock, utilization of biomass for this purpose is considered essential to reducing humanity's un sustainable consumption of non-renewable resources. Currently, biomass is the largest source of renewable energy, supplying 3% of the total consumption of energy in the United States, surpassing hydroelectric and wind power. The United States has the capacity to produce 190 million tons of biomass each year, with the potential to increase production to 1 billion tons by 2050.[85] Although it is unlikely that biomass will replace the demand for petroleum outright, it possesses great potential as a replacement for crude oil as the carbon feedstock for the production of commodity chemicals, solvents, pharmaceuticals, and agrochemicals. Effective utilization of biomass for this purpose will require the development of new chemical processes that proceed with high yield, efficiency and selectivity on large scale.

Lignocellulosic biomass (dry plant matter) is the most abundant renewable carbon resource on earth. It is mainly composed of carbohydrate polymers cellulose and hemicellulose and the aromatic polymer lignin. While technologies to process cellulose and hemicellulose are well developed, lignin processing is a considerably more challenging task. Lignin is the second most

abundant biopolymer on earth, comprising of up to 20-35% of lignocellulosic biomass and over 40% of its energy content. Unlike polysaccharides or lipids, lignin is the only biopolymer possessing a high content of aromatic groups and is an ideal candidate as a renewable resource for aromatic commodity chemicals. Its highly branched and irregular structure play important roles in providing the plant biomechanical support, aiding in pathogenic defense and water transport. Lignin is constituted from three phenylpropanol alcohol precursors–coumaryl alcohol, coniferyl alcohol and sinapyl alcohol (

Figure 19)–which are collectively called *monolignols*. Although all monolignols are derived biosynthetically from the cinnamate pathway, the ratios of coumaryl, coniferyl and sinapyl; alcohol in lignin varies from species to species.[86] After biosynthesis, the monolignols are transported through the cell membrane to the cell wall through an unknown mechanism, where copolymerization occurs. It is generally accepted that polymerization is initiated by undirected oxidative radical polymerization of the cinnamyl alcohol precursors. The oxidation of the monolignol results in the formation of a highly stabilized phenoxyl radical that is best characterized by the resonance hybrids **A**, **B**, and **C** (

Figure 19, B). These radicals couple in a random, combinatorial fashion resulting in the formation of highly reactive quinone methide intermediates which undergo subsequent intermolecular nucleophilic substitution with water and other monolignols (causing cross linking) or intramolecular cyclization reactions yielding in a structurally diverse array of linkage motifs.[86] Consequently, the lignin polymer is random in both monomer sequence, linkage motif, and stereochemical configuration.[87] Of these linkages, the β–O–4 motif (Figure 19, B) is by far the most abundant comprising between 45-60% of all linkages found in lignin with the

dihydrobenzofuran, β-β' linkage, and the 5-5' linkages present in significant but less abundant quantities.[88]

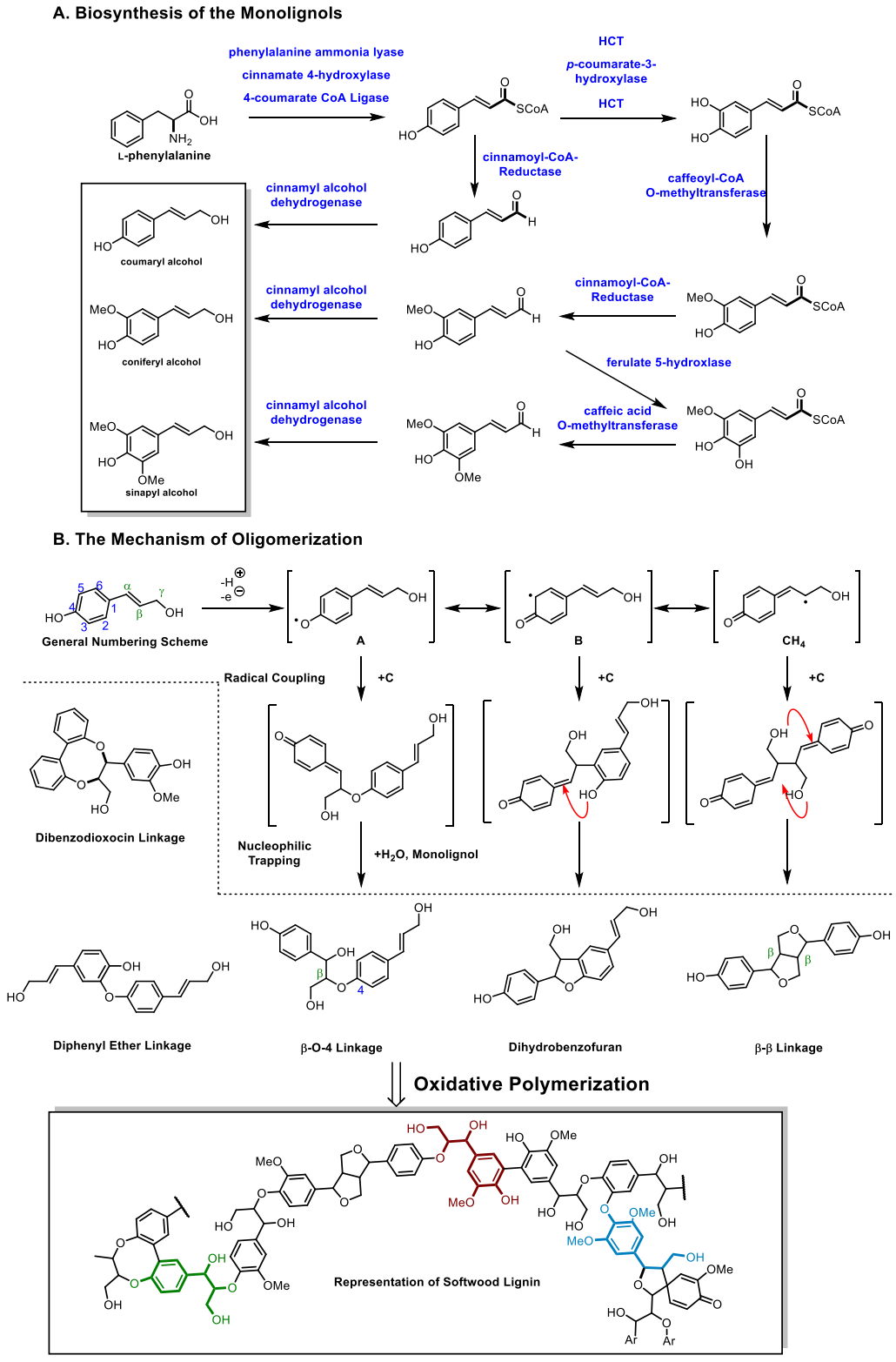

Figure 19 The biosynthesis of lignin A. Biosynthesis of the monolignols B. Mechanism of Oligomerization

Current biomass processing research is primarily focused on using cellulose as the main carbon source because it constitutes between 60-70% of biomass produced and is amenable to both chemical and enzymatic processing techniques.[89] Cellulose and oligosaccharides can be directly fermented to yield important commodity chemicals, such as ethanol, n-butanol and hydroxy methylfurfural. These can be further refined into saturated hydrocarbons, analogous to olefin-alkane distillates from petroleum refining.[90] Although the technologies to convert alkanes and alkenes into aromatic compounds exist,[91] these processes generally require high temperatures and are not energetically feasible to perform on a scale needed for commodity chemical synthesis. In contrast, the high aromatic content of lignin makes it the ideal feedstock for the renewable production of high value aromatics such as phenol, benzene, toluene or xylene (BTX) complementing the products obtained from cellulose or algal bio-oils processing. However, the highly complex and irregular structure of lignin has severely complicated the development of a controlled depolymerization of lignin for the production of fine chemicals. In the absence of any chemical processing technologies, pyrolysis of pretreated lignin yields syngas (a mixture of carbon monoxide and hydrogen gases) in about 15-20% yield, plus an intractable char that is rich in polyaromatic hydrocarbons.[92] This process, which is inefficient and highly energy intensive, could be used to generate synthetic alkanes through the Fischer–Tropsch process,[93] destroying the aromatic moieties of lignin in the process. The development of more suitable lignin conversion chemistry, that preserves its aromatic structures, is considered an essential objective in establishing the sustainable, carbon-neutral "bio-refinery" of the future (Figure 20).[94]

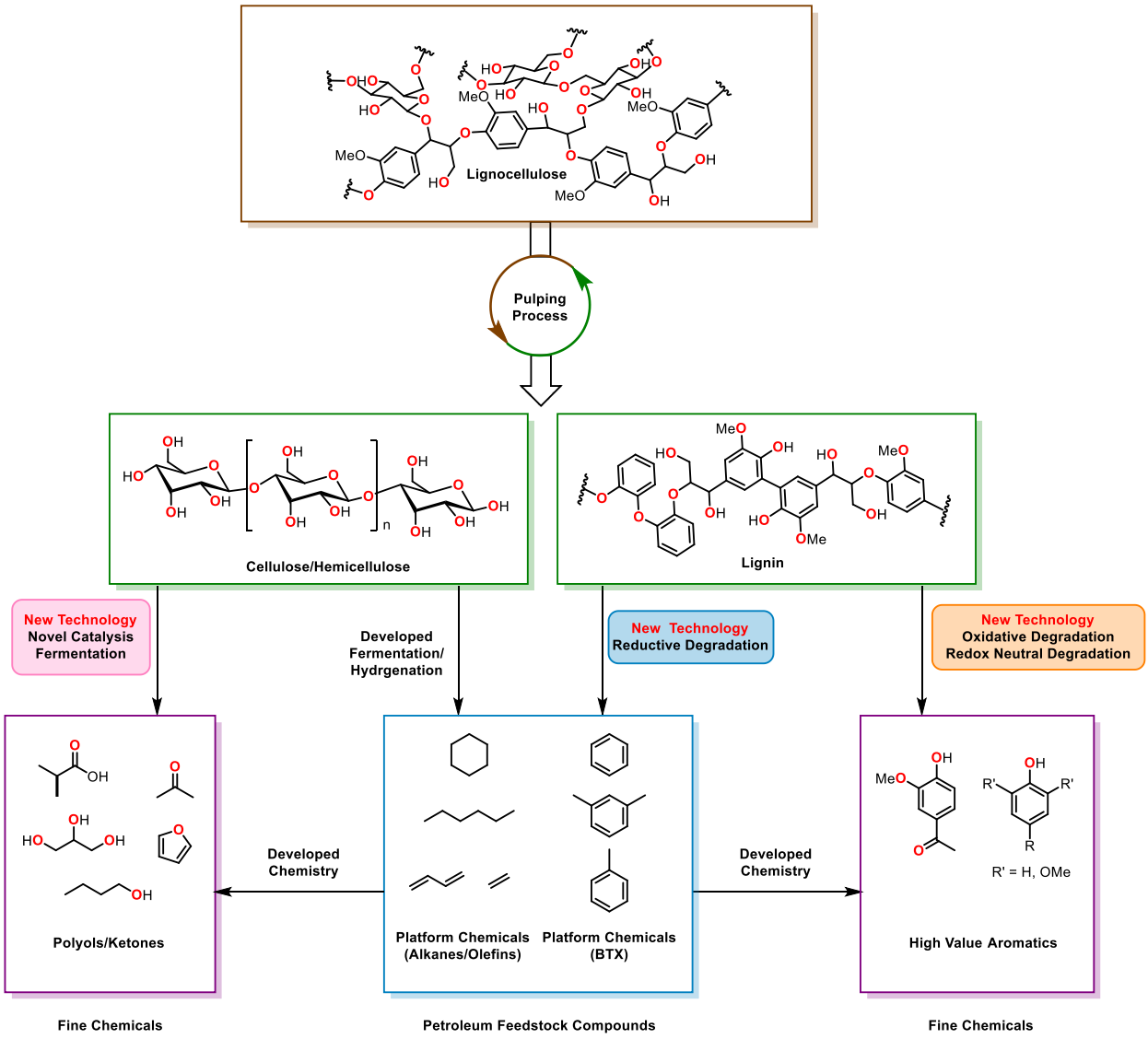

Figure 20 The Hypothetical Biorefinery

Lignin is separated from wood during the wood pulping by three industrial processes: the Kraft process, sulfite process, and the organosolv processes (Figure 21).[88] In the Kraft and sulfite processes, wood chips, corn stover, or plant bagasse are digested under high heat in either basic or acidic conditions to delignify cellulose and solubilize the lignin byproduct in water. Under these harsh conditions, lignin undergoes structural rearrangement, displacement of aryl ethers and

benzylic ethers with sulfides and sulfites, while simultaneously promoting other C–O and C–C bond cleavage reactions. The resultant Kraft or sulfite lignin is generally a highly intractable, water-soluble dark brown powder of unknown structure. In addition, these processes incorporate up to 4 wt% of sulfur into the lignin backbone. This adds additional difficulties in designing post-processing reactions since sulfur is a well-known poison for transition metal catalysts. These pulping processes, which were designed solely to delignify cellulose, renders lignin unsuitable for further processing. Due to these recalcitrant properties, lignin is largely used in applications such as fuel, as pulp for newspaper and composite boards where the bulk properties are more important than its chemical properties. Given the low cost and high volume this process is conducted on, nearly 40 million tons of lignin is produced annually as a byproduct of wood pulping. 95% of this biomass is burned as low value fuel. Attempts to valorize this waste stream led to the development of a short-lived industrial process for the synthesis of vanillin from the oxidation Kraft lignin in 7-10% yield, which was eventually abandoned due to high cost and low efficiency.[95] The organosolv process is a milder delignification process that occurs through the organic extraction of lignin with organic solvents such as ethanol, dioxane, or acetone. Like the Kraft and sulfite processes, organosolv pulping significantly alters the native structure of lignin. All three processes destroy the labile β–O–4 linkages and rendering the polymer even more intractable for further degradation. More advanced pulping technologies such as ball milling or the recently developed γ-valerolactone liquification[96] preserve the overall lignin structure. The development of more advanced preprocessing techniques such as these are going to be critical challenges to address for the development of a sustainable biorefinery. It is unlikely that these techniques will gain any widespread adoption in industry until it is economically viable to do so.

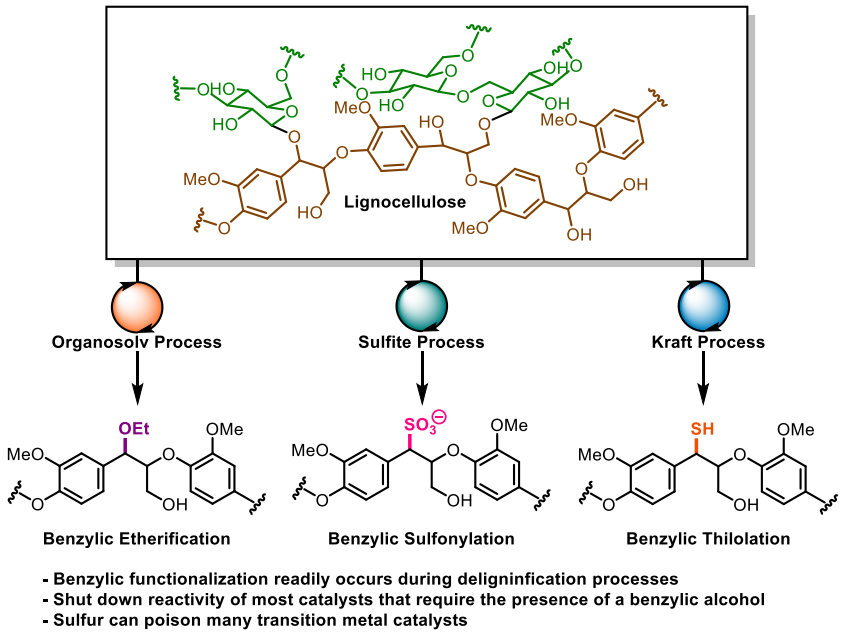

Figure 21 The Lignin Pulping Process

3.2 Strategies Towards the Catalytic Depolymerization of Lignin

The principle challenge of lignin depolymerization arises from its complex chemical structure. This highly branched polymer is not only composed of three different monomers, the linkage motifs between each monomer is structurally different and are non-uniform in sequence. The ideal depolymerization process would be able to selectively degrade lignin into discrete, high value small molecule products. In order to address these issues, the depolymerization catalyst has to be able to tolerate the functional groups found in lignin, react selectively, and resist catalyst deactivation. Depolymerization strategies can be categorized into three groups: oxidative, reductive, and redox neutral catalysis.

3.2.1 Oxidative Strategies Towards Lignin Depolymerization

In nature, there are several species of white-rot fungi that are capable of degrading lignin through the action of delignifying enzymes such as peroxide dependent ligninase or laccase.[97] These enzymes work through the single electron oxidation of the aromatic groups found in lignin, generating arene radical cation **112** (Figure 22, **A**) upon oxidation of **111**. This reactive intermediate can either undergo α–β cleavage, causing a break in the polymer backbone yielding aldehyde **113** and radical **114**. Alternatively, deprotonation of H_α forms ketyl radical **115** which can undergo a β–O–4 fragmentation yielding β-hydroxyketone **116** or undergo direct oxidation to the benzylic ketone **117**. Under these oxidative conditions, the cleaved products readily undergo further oxidation chemistry yielding carboxylic acid and quinones. The overall delignification process is relatively slow, taking many months to fully degrade higher molecular weight lignin, since the depolymerization process occurs on the heterogeneous surface of the wood itself. Despite the low contact surface area the fungi have to degrade lignin, especially in the early stages of wood decay, the depolymerization of lignin occurs efficiently. The relatively stable radical cations formed during arene oxidation can undergo reversible intramolecular or intermolecular electron transfer (Figure 22, **B**). This charge transfer phenomena allows the ligninase to initiate degradation at multiple sites within the polymer matrix despite having low surface contact with the substrate.[98]

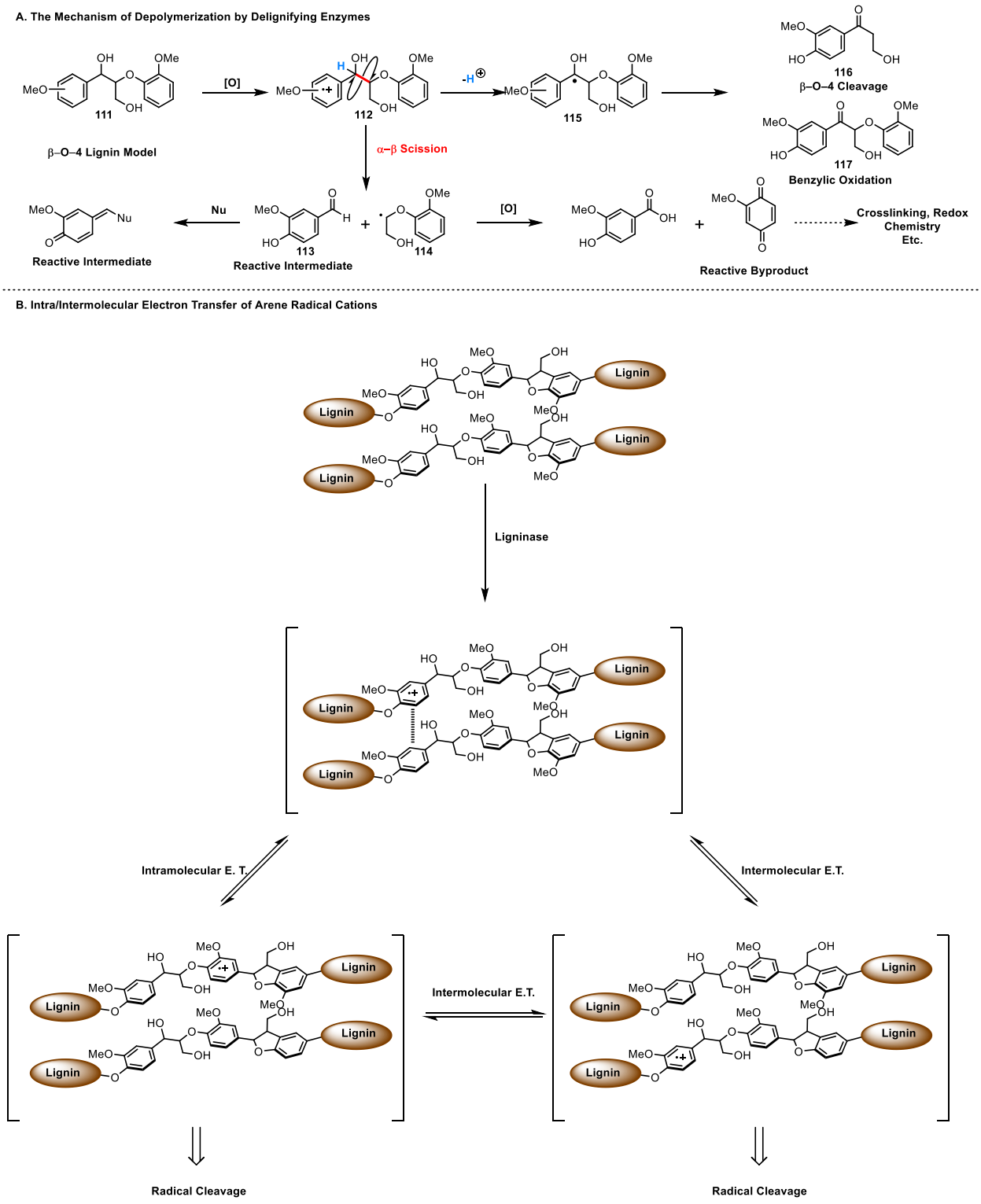

Figure 22 The mechanisms of lignin depolymerization in nature. A. Fragmentation of lignin radical cation B. Electron Relay within the lignin matrix

From a strategic standpoint, an oxidative approach towards the depolymerization of lignin has several advantages: 1) Several oxidation reactions are competent at low temperatures, which is critical for preserving lignin structure. 2) The use of oxygen as a terminal oxidant is essentially free and limitless. A viable lignin depolymerization process will, in theory, be conducted on a multi-ton scale, where the use of stoichiometric reagents can quickly become cost prohibitive. 3) Oxidative depolymerization is versatile and can cleave several linkage motifs. The main disadvantage of oxidative depolymerization is achieving high product chemoselectivity. Aromatic phenols are highly susceptible to over-oxidation to their corresponding quinones and benzaldehydes under facile oxidation to their corresponding benzoates. Furthermore, quinones and benzaldehydes are reactive in their own right and will readily undergo unwanted side reactions.

The first reports of oxidative depolymerization of lignin concentrated on the study of the mechanism of oxidative cleavage of β–O–4 model compounds by whole cell degradation, cell extract, or various enzymes such as horse radish peroxides[99] or ligninase.[100] These studies established the oxidative nature of lignin depolymerization and confirmed that it can engage in the fragmentation of several lignin motifs regardless of structure and/or stereoconfiguration. Following this lead, catalytic oxidative depolymerization strategies systems such as riboflavin/*hν*/O_2 reaction developed by Kutsuki,[101] Fe(TPP)Cl_3/^{t}BuOOH reported by Shimada and co-workers[102] or Co(II)/Mn(III) by DiCosimo and Szabo corroborated these findings.[103] Since the structure of lignin is highly complex and different from sample to sample, most chemists studying the depolymerization use the phenylpropanol compound **111** as a β–O–4 model system. These early oxidative degradation reactions tend to completely consume **111**; practical application of this strategy has been hampered by poor mass recovery or production of an intractable mixture of oxidation products. In addition, oxidation of lignin model systems often generates compound **117**

as a major product. This compound represents a dead-end reaction pathway as it is highly resistant to further oxidative degradation to more useful basic building blocks.

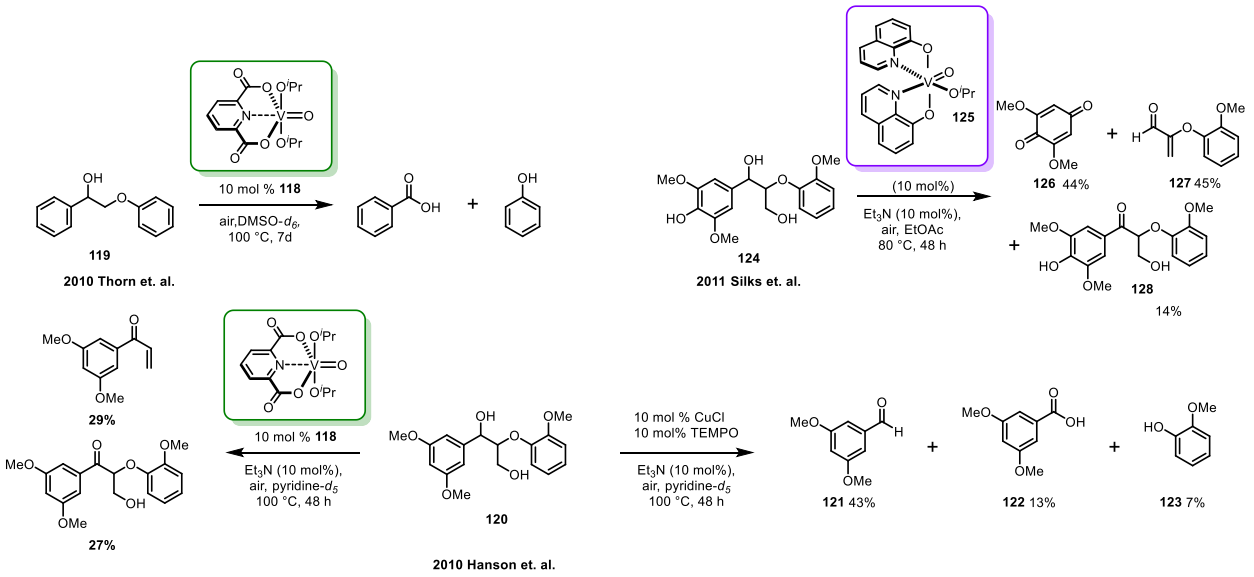

Scheme 1 Vanadium catalyzed oxidative studies in the oxidative fragmentation of lignin model compounds

Prior to the late 90's and early 2000's, efforts to controllably and selectively degrade lignin were relatively scarce. Attempts to oxidatively depolymerize lignin using heterogeneous catalysis, POM catalysts,[104] photocatalysis,[105] and enzymatic catalysis[98102] were all suffering from the same problems with chemoselectivity. During the mid-2000's, lignin depolymerization chemistry received significant contributions from inorganic and synthetic organic groups. This work was largely done using model compounds, such as **111**, in order to gain insight on the reactivity of defined homogenous catalysts on defined structural motifs. In 2010, Thorn and co-workers were the first to describe a novel vanadium dipicoline catalyst (**118**) capable of oxidatively cleaving simple β–O–4 model systems **119 (**Scheme 1). Unlike the corresponding oxidative cleavage of 1,2 vicinal diols, the catalytic oxidative cleavage of the 1,2 hydroxy ether functionality found in lignin had not been reported previously. This chemistry was further expanded by Hanson and co-workers in 2011 using a CuCl/TEMPO catalytic system to study the oxidative fragmentation of

more elaborate lignin model compound **120** (Scheme 1, C).[106] They discovered that unlike the vanadium catalyst **118**, the CuCl/TEMPO reaction conditions operated under a different mechanisms.[106] Where catalyst **118** primarily acts as a selective benzylic oxidant, the CuCl/TEMPO catalytic system directly cleaves the α–β bond through an apparent concerted C–C bond cleavage reaction yielding 3,5-dimethoxybenzlaldehyde (**121)** and along with minor quantities of benzoic acid **122** and guaiacol (**123**, Scheme 1).

Shortly thereafter, Silks and co-workers disclosed related work describing the aerobic oxidative cleavage of unprotected sinapyl β–O–4 model compound **124** using a novel vanadium quinolate complex **125.**[107] This catalyst was able to mediate a highly unusual α–1 fragmentation, yielding ~40% of quinone **126** and acrolein derivative **127**. This catalyst provided complimentary reactivity to a related vanadium catalyst described by Toste (discussed in section **3.2.3**) and yielded a mixture of the α–1 cleavage product **127** and the benzylic oxidation product **128**. These results allude to the tantalizing prospect of chemoselective, catalyst-controlled product synthesis from a common feedstock. Current work continues to advance this concept more thoroughly and is under intense investigation.[108,109,110,111]

3.2.2 Reductive Strategies Towards Lignin Depolymerization

The development of heterogeneous hydrogenation catalysis was key to establishment of modern wood chemistry. Prior to the mid 1930's the basic structure of lignin was not well understood. The challenge of elucidating the structure of lignin was no easy task during that time: NMR had not been available for analytical purposes, the polymeric nature of lignin rendered mass spectrometry and elemental analysis unsuitable, and the reactions available for the chemical degradation caused significant changes in the chemical structure of the lignin monomer. The aromatic structure of lignin had been deduced by oxidative degradation by Freudenberg[112] and

later by solvolysis by Hibbert.[113] However, these reactions caused significant structural rearrangements and degradation of the lignin monomers, preventing satisfactory identification of even the basic carbon skeleton of lignin. Then in 1938, Adkins and co-workers described the hydrogenation of aspen methanolsolv lignin over copper chromite yielded 1-(4-hydroxycyclohexyl)-propan-3-ol in ~40%.[114] This was provided the first compelling evidence for phenylpropanoid structure of the monolignols. Since that disclosure, several other groups reported varying conditions for the hydrogenation of lignin in rapid succession.[115] When Hibbert described the mild Raney-Nickel hydrogenation of lignin, which preserved the aromatic rings, it provided the final proof of the phenylpropanol structure of the monolignols.[116]

The pivotal role of hydrogenation in the structure elucidation of lignin greatly improved our understanding of the reactivity of lignin towards reduction chemistry. Like uncontrolled oxidative depolymerization, high pressure/high temperature hydrogenation can effectively depolymerize lignin, despite the diversity of linkage motifs and the presence of different monomers. Hydrogenolysis of lignin can be controlled to a much better degree than oxidative depolymerization reactions, and often have higher monomer yields and better product selectivity. Furthermore, there are highly recalcitrant linkage motifs such as the diarylethers or dibenzodioxocin (Figure 19, B) can be effectively cleaved using hydrogenation conditions. Historically, reductive depolymerization of lignin occurs with high temperatures and pressures and although this has been successful in producing phenylpropanols and medium weight alkanes, these reactions indiscriminately reduce benzylic ketones, aromatic ethers/hydroxyl groups, and olefins.

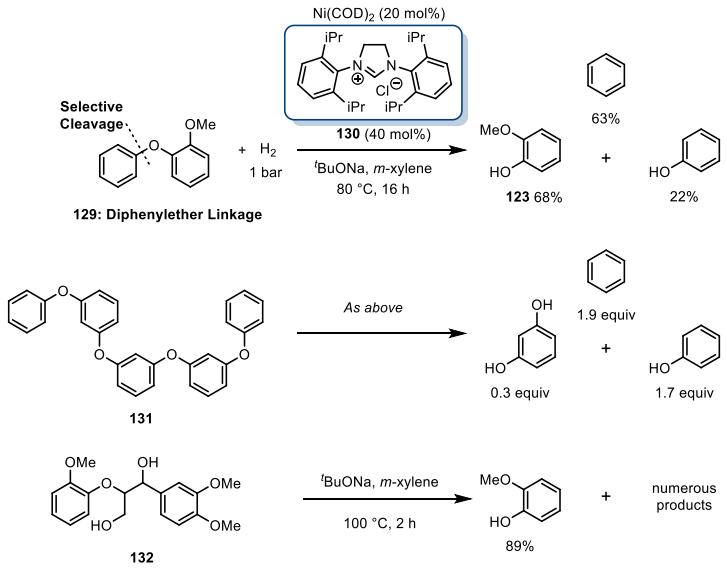

Scheme 2 Hartwig's Selective Hydrogenation of Diphenylether Linkages

Research in the reductive depolymerization of lignin has largely been dominated by heterogeneous hydrogenation. In 2011, Hartwig and co-workers disclosed a novel approach towards the depolymerization of diphenyl ether linkage found in lignin (Scheme 2).[117] They found that diphenyl ethers could be reductively cleaved by $Ni(COD)_2$, an NHC ligand **130**, with NaO^tBu as a stoichiometric base, into benzene, and phenol in quantitative yield under 1 bar of hydrogen. This catalyst system demonstrated exquisite chemoselectivity for the diphenylether motif over other similar functionalities such as methoxyphenyl groups and even benzylic ethers. For instance, 2-methoxydiphenylether (**129**) produced benzene and guaiacol, in high yield, with smaller quantities of anisole or phenol. It was also capable of reductively cleaving polyphenol ether **131** in high conversion. Unfortunately, the highly basic reaction conditions completely destroyed β–O–4 model system **132** in the absence of the catalyst. Nevertheless, this chemistry can almost certainly be used as a post processing step after an initial cleavage reaction to generate high value aromatics. They went on to further develop a ligandless variant of this reaction that possessed

complementary reactivity to this NHC catalyst.[118] Shortly after these publications, Wang and co-workers disclosed a similar hydrogenation reaction using $Fe(acac)_3$, NaO^tBu, and $LiAlH_4$.[119]

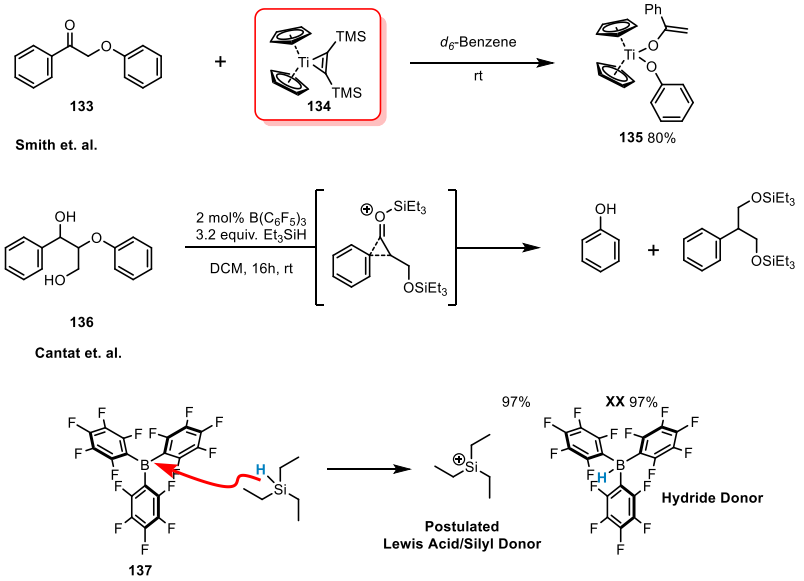

Scheme 3 Smith's titanium reductive cleavage and Cantat's metal free Kishi-type reduction

In 2012, Smith and co-workers demonstrated an unusual reductive cleavage of simple β–O–4 models system **133** using a low-valent titanium complex **134** (Scheme 3, Top) yielding complex **135** in 80% yield at room temperature.[120] This process presumably occurs through successive single electron reductions through a ketyl radical intermediate yielding the titanium enolate. Although the authors were not able to effect any reaction turn over, this reductive cleavage reaction served as a novel proof-of-concept for biomass processing.

After our publication,[121] Cantat disclosed an unusual catalytic fragmentation of β–O–4 model compound **136** using triethylsilane and trisperfluorophenyl borane **137** (Scheme 3, Bottom). The highly Lewis acidic **137** can efficiently ionize triethylsilane to the silyl cation, which in turn activates benzylic and aliphatic hydroxyl groups for a subsequent Kishi-type reduction. These reactions occurred with high yield and selectivity, however, the system required additional

equivalents of triethylsilane in the presence of methoxygroups since they observed significant demethylation.

3.2.3 Redox Neutral Strategies Towards Depolymerization

Redox neutral lignin depolymerization represents the ideal approach to biomass valorization because they do not require a terminal oxidant/reductant. This is a particularly important consideration in the context of commodity chemical/fine chemical synthesis, where the cost of stoichiometric reagents become prohibitively expensive on scale. There are several reactions that are encompassed by redox neutral processes ranging from simple acid/base catalysis or thermal cracking to more complex reaction methods such as transfer hydrogenation or multi-electron transfer chemistry. The earliest examples of redox neutral lignin depolymerization are the traditional Kraft, sulfite, and organosolv pulping which (ineffectively) depolymerize lignin with a combination of heating and treatment with acid or base. The development of controlled redox neutral depolymerization processes has been very slow no successful examples exist to date.

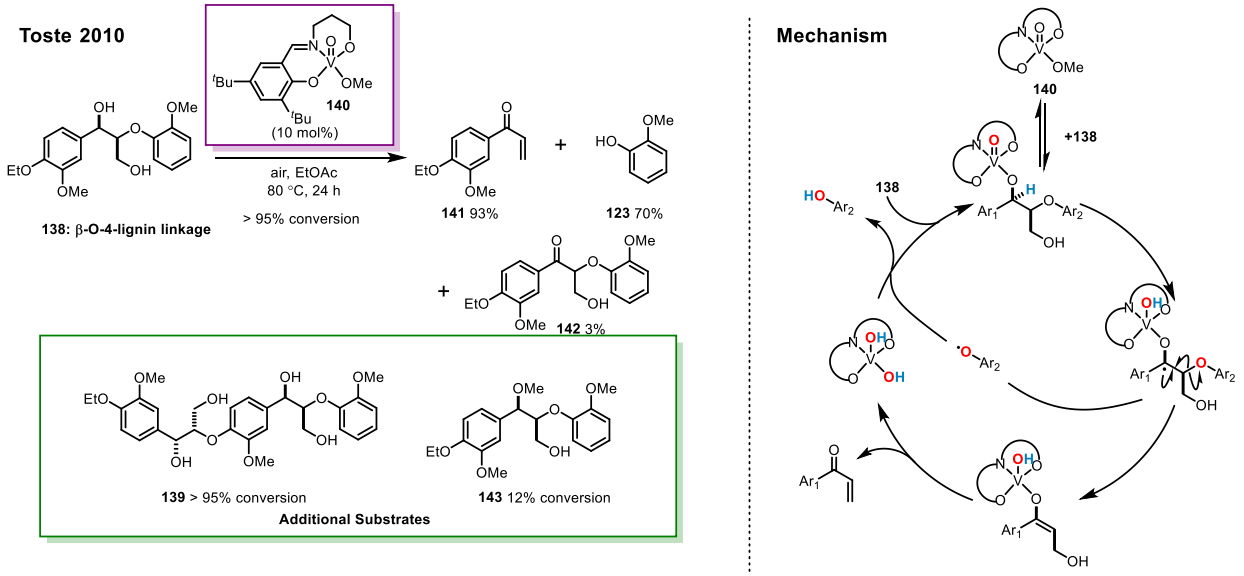

Figure 23 Toste's vanadium catalyzed redox-neutral depolymerization of lignin model compounds.

The pivotal point in redox neutral catalysis, and arguably modern lignin catalysis, came in 2010 when Toste and co-workers described a beautiful redox neutral fragmentation of dimeric (**138**) and trimeric (**139**) β–O–4 model compounds using vanadium complex **140** (Figure 23).[122,123] Reacting coniferyl model **138** with catalyst **140** in the presence of air yielded enone **141** and guaiacol in 93% and 70% yield respectively. A small quantity of undesired acetophenone derivative **142** was also observed as an undesired byproduct of the reaction. They demonstrated through a series of control experiments that the benzylic alcohol was a necessary component in their reaction, such as the case with low conversion of **142.** Based off of previous work in their lab, they suggested the mechanisms depicted in **Figure 23**. Interestingly, although oxygen was not necessary for catalyst turnover, it did increase reaction rate. Unfortunately, when this reaction system was applied to organosolv lignin (**143**), they observed low depolymerization and mixtures of redox neutral and oxidized monomers. Silks and co-workers (Section **3.2.1**) demonstrated that the presence of unprotected phenols perturbs the catalyst's reactivity and results in a mixture of redox neutral fragmentation and benzylic oxidation.[107]

Only a few months after the Toste report, Ellman and Bergman and co-workers disclosed a distinct transfer hydrogenation depolymerization reaction of the simple β–O–4 model system based on **119**.[124] Using an in-situ generated RuXantPhos catalyst **144**, they were able to fragment **119** in quantitative yield yielding acetophenone and the corresponding phenol. This reaction was extremely robust and could degrade a 7,000MW lignin model polymer **145** to 4-hydroxyacetophenone in 99% yield. They proposed that catalyst **144** oxidizes **119** to α-ketoether **133** upon which it oxidatively inserts into the C_β–O bond with concomitant hydrogenation to form the desired products. Follow up work by the James group revealed that this catalyst was

incompetent in the fragmentation of more elaborate lignin model systems containing the methylene oxo-moiety (**136**) due to the formation of unreactive off cycle intermediate **146.**[125,126] Despite this limitation, this work was also enormously influential in later efforts towards transfer-hydrogenation mediated lignin degradation.[127–129]

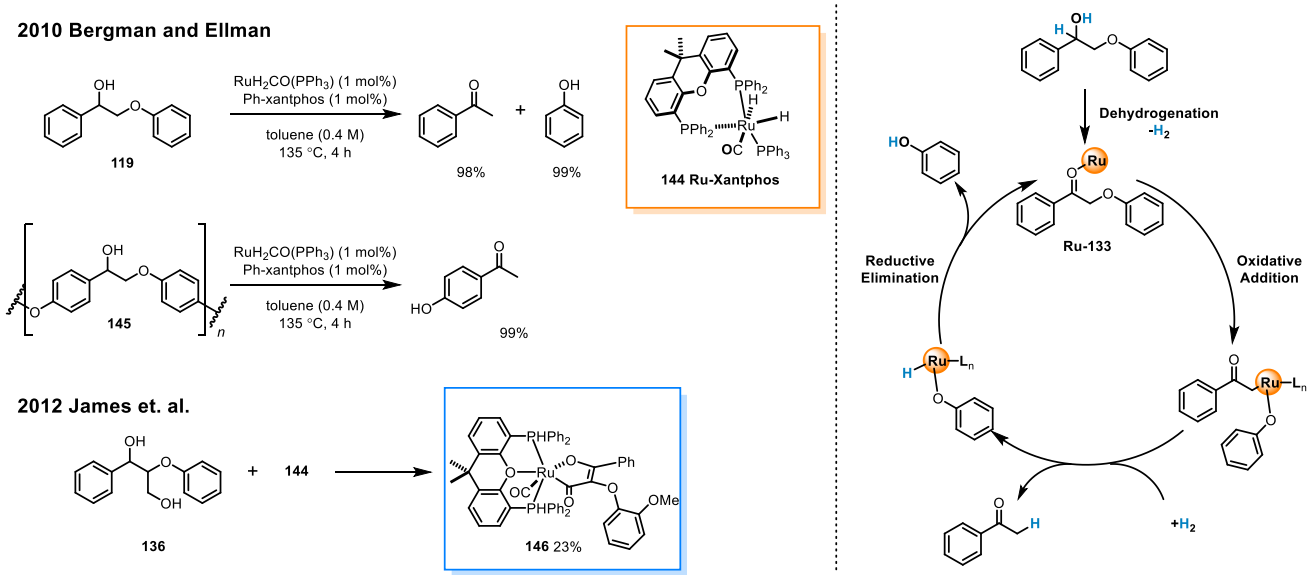

Figure 24 Redox neutral degradation of lignin model compounds with ruthenium catalysts

The reaction strategies delineated above reveal several trends regarding the depolymerization of lignin: 1) A majority of the approaches towards lignin depolymerization require elevated temperatures; 2) The presence of Lewis basic hydroxyl groups and unprotected phenols were deleterious to reactivity; 3) Most catalytic reactions required 5-10 mol% catalysts loadings; 4) Many reactions required the use of solvents where native lignin would not be soluble; 5) Achieving product selectivity is extremely challenging. With these challenges in mind, we envisioned that a photocatalytic approach to lignin degradation could address several of these issues. At the time, photoredox catalysts such as $Ru(bpy)_3Cl_2$ and $Ir(ppy)_2(dtbbpy)PF_6$ had stable at a wide range of

temperatures, pH, and solvents. In addition, photoredox catalysts have proven capable of mediating several reactions under extremely mild conditions with high degrees of chemoselectivity. In this regard, John and I saw an opportunity to apply these properties in the unique context of biomass processing.

3.3 Reaction Design Strategy

One of the most fascinating properties of photoredox catalysts is their ability to engage in both oxidation and reduction chemistry using visible light. A single catalyst has the ability to mediate overall redox neutral reactions through multiple electron transfer events. In this regard, photoredox catalysis possess the unique capacity to approach all three lignin depolymerization strategies using a unified reaction design logic. From the outset we was interested in using oxidative quenching, reductive quenching, and redox neutral catalysis to degrade β–O–4 model systems, given its ubiquity and abundance in lignin. Given the structure of the β–O–4 motif, photoredox catalysis is ideally suited for the cleavage of the C_α–C_β bond through oxidative catalysis and reduction of the C_β–O_{Ar} bond using either reductive or redox-neutral conditions. It was clear that the development of a selective oxidation of lignin was going to be the first priority. This process could be conceivably achieved through direct quenching of the excited state of the photocatalyst (PC*) or the oxidized photocatalyst (PC^+1) with the electron rich

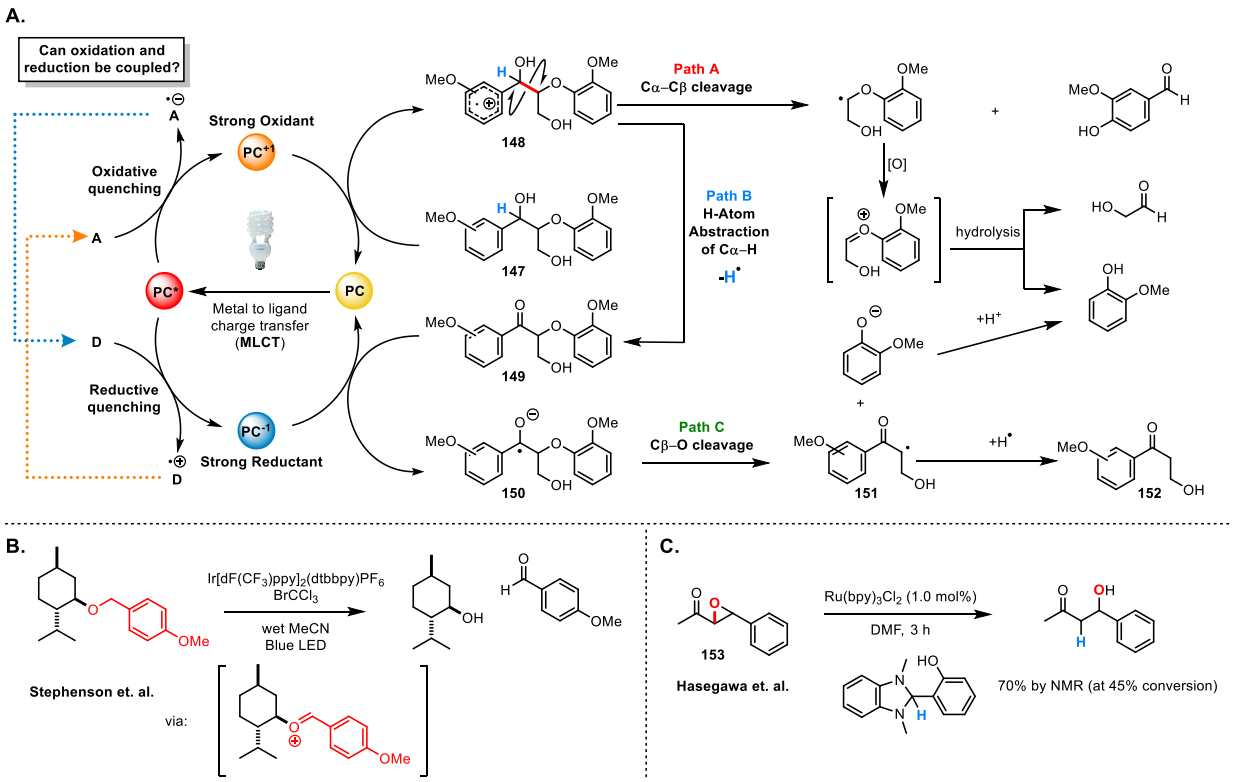

Figure 25 The photocatalytic strategy towards the depolymerization of lignin

arene from lignin compound **147** (Figure 25, A) generating the corresponding arene radical cation **148**, which our lab has demonstrated previously in a photocatalytic deprotection of PMB ethers (Figure 25, B). This intermediate can undergo β-scission, cleaving the C_α–C_β bond (Figure 25, Path A)[103,105] or form benzylic ketone **149** upon H-atom abstraction (Figure 25, Path B). The oxidation of the benzylic alcohol has important implications in the context of the proposed reductive C–O bond cleavage. DFT calculations predict that the bond dissociation energy of the C_β–O_{Ar} bond of **149** is ~14kcal/mol lower than the corresponding benzylic alcohol **147** making it significantly easier to cleave.[130] This benzylic ketone, which has been used as an electron acceptor in photoredox catalysis,[24] was an ideal substrate to test a new reductive cleavage of the C_β–O_{Ar} bond in lignin. This would be executed via the reductive photoredox catalysis wherein, the state of the photocatalyst (PC*) or the reduced ground state (PC^{-1}) could donate an electron to **149**, forming ketyl radical **150** (Figure 25). The subsequent elimination will form α-keto radical **151**,

which upon H-atom transfer or electron transfer/protonation will yield β-hydroxyketone **152** and guaiacol. Prior to this publication, there were no known methods to reduce aryl ether bonds utilizing photoredox catalysis, but there was precedent which indicated that C_β–O–4 bonds found in lignin could be reductively cleaved via single electron transfer. In 2006, Hasegawa demonstrated that $Ru(bpy)_3Cl_2$ can be used to cleave the strained C_β–O bond of an epoxide **153** activated by the presence of an α-carbonyl moiety (Figure 25, C).[131] A very similar report by Fensterbank and Ollivier were able to use this approach to reductively cleave activated epoxides and aziridines and trap with allylsulfones and H-atom donors.[132] With this precedent in mind, we hypothesized that if we could selectively generate benzylic ketone **149**, it would be possible to photochemically fragment the β–O–4 linkage in lignin using a strongly reducing photocatalyst. Furthermore, since this transformation is formally a redox neutral fragmentation, the tantalizing prospect of coupling the oxidation of **148** and with the reduction of **149** was, and is, highly sought after. From here, the path forward was clear and the success of this project would hinge on the identification of a mild and selective benzylic alcohol oxidation and a photocatalytic chemoselective C_β–O–4 bond reduction.

3.3.1 Development of a Selective Benzylic Oxidation of β–O–4 Model Systems

The heterogeneous structure of lignin possess diverse functionality within the polymer including primary, secondary, and benzylic alcohols, free phenols, electron rich aromatic groups, quinones, spirocyclohexadienones, benzofurans and dibenzodioxocin motifs. The free phenols, multitude of electron rich aromatic rings, and the aliphatic and benzylic alcohols are all oxidizable moieties that can potentially complicate a selective benzylic oxidation. Of all the linkage motifs found within lignin, the β–O–4 motif is the most prevalent, constituting anywhere from 45–60% of all the linkages in a given sample of lignin.[133] While the abundance of this linkage motif varies

from species to species, it is found ubiquitously within plant kingdom and is therefore the most important linkage motif from a depolymerization standpoint. It is important to acknowledge that the β–O–4 linkage is chemically unstable under forcing conditions and will readily undergo skeletal rearrangements under highly acidic or basic conditions in elevated temperatures. The resulting polymer is extremely resistant to further chemical degradation and unsuitable for processing into defined molecular entities. In order to preserve the β–O–4 linkage, an oxidation

Table 4 Preliminary attempts towards a chemoselective oxidation of benzylic alcohols

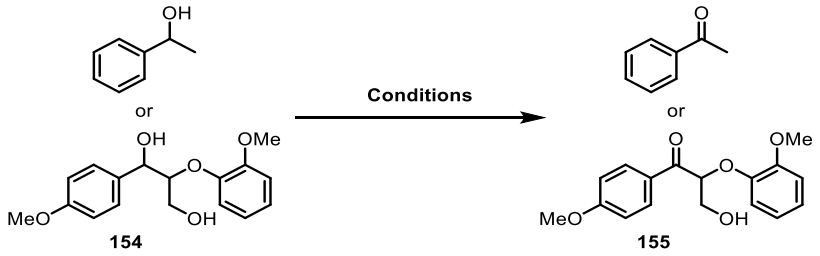

Entry	Reaction Conditions	Yield
1	1-phenylethyl alcohol (1 equiv), ammonium persulfate (1.5 equiv), visible light, H_2O, 24 h	15%
2	1-phenylethyl alcohol (1 equiv), ammonium persulfate (3.0 equiv), visible light, H_2O, 24 h	40%
3	1-phenylethyl alcohol (1 equiv.), **TiO_2** (anatase), visible light, air balloon, MeCN, 48 h	22%
4	1-phenylethyl alcohol (1 equiv.), **TiO_2** (anatase), visible light, air balloon, SiO_2, MeCN, 48 h	30%
5	1-phenylethyl alcohol (1 equiv.), **TiO_2** (anatase), visible light, continuous airflow, SiO_2, MeCN, 48 h	45%
6	1-(4-methylphenoxy)ethanol (1 equiv), 5.0 mol% methyl viologen dichloride, **$[Ir(ppy)_2(dtbbpy)]PF_6$**, visible light, MeCN, 12 h	80%
7	**154** (1 equiv), 5.0 mol% methyl viologen dichloride, visible light, **$[Ir(ppy)_2(dtbbpy)]PF_6$**, MeCN, 12 h	Decomp.

[a]Yields of products determined by ^1H NMR

method that was compatible near room temperature in near pH neutral conditions was sought. Under these principles, my colleague Dr. John Nguyen and I proceeded to develop the selective benzylic oxidation of β–O–4 model compounds.

Our first approaches towards the selective benzylic oxidation of lignin model systems (1-phenethylalcohol) used stoichiometric ammonium persulfate (**Table 4**, Entries 1 and 2 and photocatalytic oxidation using TiO_2 and air (**Table 4**, Entries 3–6). One particularly promising approach employed 1 mol% $[Ir(ppy)_2(dtbbpy)]PF_6$[134] as a photocatalyst, 5 mol% methylviologen as an oxidative quencher, and air as the terminal oxidant, affording acetophenone in 80% yield. Unfortunately, when applied to the more complex β–O–4 model system **154**, we observed decomposition of the starting material, consistent with non-selective oxidative α,β fragmentation observed previously.[103,105] During this time, Stahl and co-workers described a selective, catalytic, aerobic oxidation of β–O–4 model compounds using 4-NHAc-TEMPO/HNO_3/O_2 redox couple.[135] These reaction conditions could scalably oxidize the benzylic alcohol of several simple and complex β–O–4 models systems, such as **156**, with perfect selectivity to their corresponding benzylic ketones **157**. This methodology could effectively oxidize all three types of complexβ–O–4 model systems. Perhaps their most significant finding, however, was that these catalytic conditions could oxidize isolated lignin **158** in high yields. Spectacularly, they were able to depolymerize this "oxidized lignin" (**159**) using a sodium formate/formic acid/water system to generate 61 wt% of low molecular weight products.[136] Unfortunately, at this junction, John and I had not been able to identify photocatalytic oxidation conditions, so we shifted focus to adapt this reaction into our overall strategy. Initially, the reaction appeared to have the added benefit of using MeCN as the reaction solvent, opening up the possibility of performing a telescoped

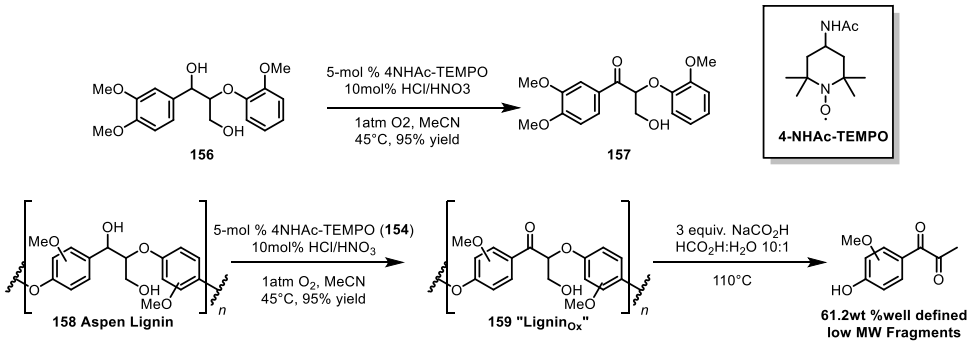

Figure 26 Stahls' catalytic, chemoselective oxidation of lignin using 4-NHAc-TEMPO

oxidation/photocatalytic reduction of β–O–4 model compounds.[137] Unfortunately, this proved to be untenable, and both John Nguyen and I were unable to successfully develop these conditions. We hypothesized that this was due to the presence of TEMPO, which is not only redox active, but is a highly efficient radical trapping agent. To circumvent these problems, we employed a procedure using [4-NHAcTEMPO]BF_4/silica developed by Bobbitt and co-workers.[138] These reaction conditions provided three main advantages: 1) It could be performed at room temperature 2) the TEMPO byproduct bound tightly to silica and could be filtered off and subsequently regenerated for future use 3) the oxidation product was pure by NMR after concentration and could be used directly in the next step without further purification. These reaction conditions were capable of oxidizing a variety of substrates with complete selectivity, including our desired complex model systems in nearly quantitative yield (Table 5 Entries 4–6).

Table 5 Oxidation of β–O–4 Model Systems of Bobbitt's Salt

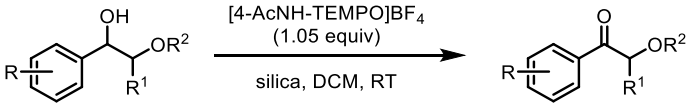

Entry	Substrate[a]	Time (h)	Product[b,c]	Yield
1	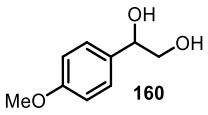 **160**	1.5	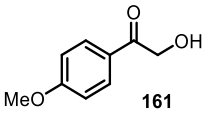 **161**	95%
2	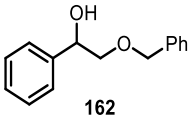 **162**	20	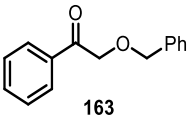 **163**	95%
3	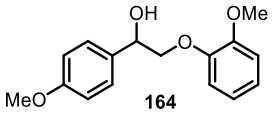 **164**	15	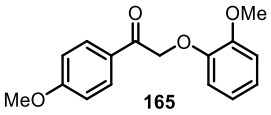 **165**	97%
4	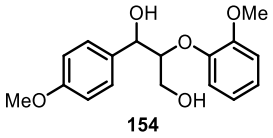 **154**	18	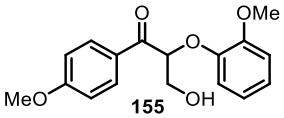 **155**	98%
5	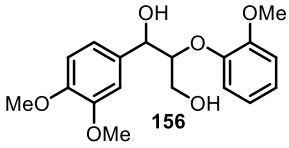 **156**	15	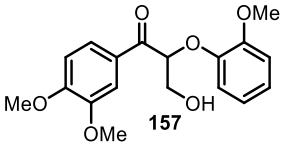 **157**	94%
6	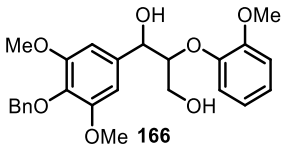 **166**	24	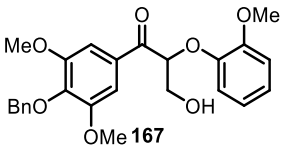 **167**	94%

[a]Unless otherwise noted, reactions were conducted on a 1.0 mmol scale. [b]Yields of products isolated by column chromatography. [c]Isolated yields based on an average of two runs.

3.3.2 Photocatalytic Reduction of Oxidized β–O–4 Model Systems

After the development of a generalized protocol chemoselective oxidation of benzylic alcohols, the next task was to identify reductive deoxygenation conditions for these substrates. As mentioned previously, prior work by Hasegawa[131] and Ollivier[132] demonstrated the feasibility of this transformation. However, in both of these cases, the desired substrate contained a highly strained epoxide, which could be reductively cleaved with $Ru(bpy)_3Cl_2$, a catalyst with moderate reactivity. Although there had been no reports of a reduction of an unstrained C–O bond at this point, previous work by John and others in our group had indicated the viability of this process.[137,139,140] I envisioned that using more strongly reducing metal complexes could enable the desired photochemical C–O bond reduction and provide a viable strategy to the larger goal of lignin biomass valorization.

We anticipated that catalysts possessing more strongly reducing excited state and ground state potentials would be more efficacious. Using conditions previously developed by John for the reduction of unactivated alkyl halides[140] were immediately effective. Using 1 mol% $Ir(ppy)_3$, 5 equivalents of tributylamine and formic acid in acetonitrile gave 100% conversion of simple model system **165** (Table 6). The quantities of both stoichiometric reagents could be dropped from 5 equivalents to 3 equivalents without a significant drop in reaction rate or yield. However, $Ir(ppy)_3$ is easily quenched by O_2, and therefore requires thorough degassing for the reaction to proceed. Photocatalysts like $Ru(bpy)_3Cl_2$, Eosin Y, and $[Ir(dF\{CF_3\}ppy)_2(dtbbpy)]PF_6$ were far less reactive, owing to their comparatively low ground state reduction potentials (Table 6, Entries 5, 6, and 8) ; whereas $Cu(dap)_2Cl_2$ was completely ineffective due to a well-known decomposition pathway in coordinating solvents (Table 6, Entry 7). Finally, $[Ir(ppy)_2(dtbbpy)]PF_6$ was found to

Table 6 Optimization of Reductive Cleavage

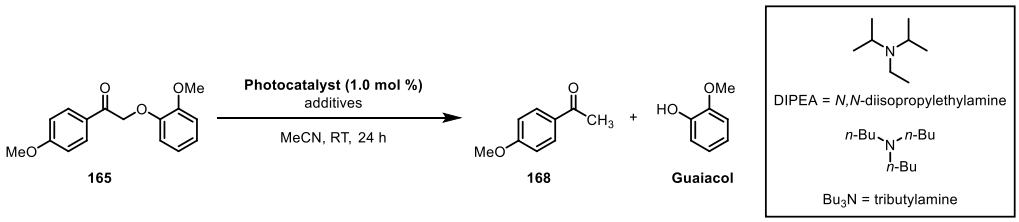

Entry	Conditions	Conversion
1	***fac*-Ir(ppy)$_3$**, Bu_3N (5 equiv), HCO_2H (5 equiv), visible light, degassed	100
2	***fac*-Ir(ppy)$_3$**, DIPEA (5 equiv), HCO_2H (5 equiv), visible light, degassed	100
3	***fac*-Ir(ppy)$_3$**, DIPEA (3 equiv), HCO_2H (3 equiv), visible light, degassed	100
4	***fac*-Ir(ppy)$_3$**, DIPEA (3 equiv), HCO_2H (3 equiv) visible light, not degassed	0
5	**Ru(bpy)$_3$Cl$_2$**, DIPEA (3 equiv), HCO_2H (3 equiv) visible light, not degassed	17
6	**[Ir{dF(CF$_3$)ppy}$_2$(dtbbpy)]PF$_6$**, DIPEA (3 equiv), HCO_2H (3 equiv) visible light, not degassed	37
7	**Cu(dap)$_2$Cl**, DIPEA (3 equiv), HCO_2H (3 equiv) visible light, not degassed	0
8	**eosin Y**, DIPEA (3 equiv), HCO_2H (3 equiv) visible light, not degassed	10
9	**[Ir(ppy)$_2$(dtbbpy)]PF$_6$**, DIPEA (3 equiv), HCO_2H (3 equiv) visible light, not degassed	100
10	[Ir(ppy)$_2$(dtbbpy)]PF_6, DIPEA (3 equiv) visible light, not degassed	80
11	[Ir(ppy)$_2$(dtbbpy)]PF_6, HCO_2H (3 equiv) visible light, not degassed	0
12	**No photocatalyst**, DIPEA (3 equiv), HCO_2H (3 equiv) visible light, not degassed	0
13	**[Ir(ppy)$_2$(dtbbpy)]PF$_6$**, DIPEA (3 equiv), HCO_2H (3 equiv) no light, not degassed	0
14	[Ir(ppy)$_2$(dtbbpy)]PF_6visible light, not degassed	0

be an equally competent to $Ir(ppy)_3$, without needing solvent degassing. Using 1 mol% $[Ir(ppy)_2(dtbbpy)]PF_6$, 3 equivalents of DIPEA and formic acid in MeCN under visible light irradiation could fragment **165** into 4-methoxyacetophenone (**168**) and guaiacol (**123**) in 88% and 89% isolated yield in 12h (**Table 6**, Entry 9).

With the optimized conditions in hand, John and I explored the scope of the reductive C_α-O bond cleavage reaction. As one might expect, reaction rate was highly dependent on the nature of the leaving group and carbonyl group. Substrate **165**, possessing an α-phenoxy substituent, converted completely within 12h, whereas substrate **169**, bearing an α-acetoxy group was complete in just 4h, due to the better leaving group ability of the acetate anion (

Table **7**, Entries 1 and 2). Conversely, when the electron acceptor was changed to a ketone (**170**), or ester (**171**), we observed no reactivity, presumably due to the lower reduction potential of ketones and esters compared to acetophenones (

Table **7**, Entries 3 and 4). Interestingly, the commercially available benzyloxyacetaldehyde underwent efficient reductive cleavage yielding 83% isolated benzyl alcohol (

Table **7**, Entry 5). Not only does this demonstrate that aldehydes are sufficient electrophiles for this reaction, but also that these reaction conditions are able to reduce much stronger C-O bonds of unactivated alkoxides. This result also suggests that this chemistry has potential application in the degradation of other biomass derived polymers such as polysaccharides, since **172** is a simple aldose. The complex substrates **155**, 157, and **128** are model compounds for coumaryl, coniferyl, and sinapyl β-O-4 linkage motifs commonly found in lignin. These substrates were found to effectively undergo reductive fragmentation yielding β–hydroxyl

ketone **173**, **174**, and **175** in 85%, 85%, and 90% yield respectively. These hydroxyketones were stable under the reaction conditions and did not undergo significant side reactions such as

Table 7 Substrate Scope of the Photocatalytic Reduction of β–O–4 Model Compounds

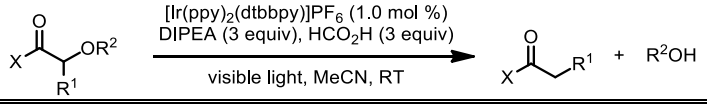

entry	substrate	time (h)	product 1[a,b]	product 2[a,b]
1	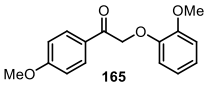 165	12	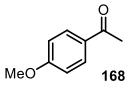 168 88%	 89%
2	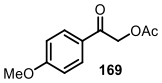 169	4	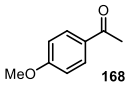 168 77%	 Not isolated
3	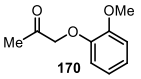 170	24	No reaction	
4	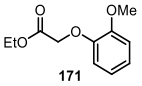 171	24	No reaction	
5	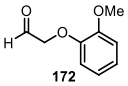 172	12	 Not isolated	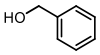 83%
6	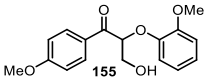 155	15	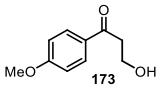 173 85%	 88%
7	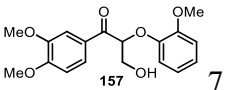 157 7	18	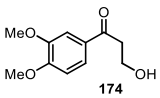 174 85%	 76%
8	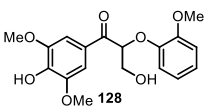 128	48	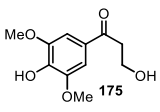 175 90%	 95%

9	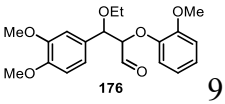	9	24	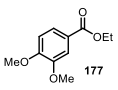	30%		70%

[a]Yields of products isolated by column chromatography. [b]Isolated yields based on an average of two runs.

retro-aldol reaction, pinacol coupling or oxidation. They also are unique fragmentation products which had only been observed in minute quantities previously. The reductive cleavage of **128** is significant because it possesses an unprotected phenol, which is problematic for several depolymerization strategies, particularly for oxidative and redox neutral methods. Substrate **176** unlike the previous entries, contains a benzylic ether, mimicking the structural modification lignin undergoes during ethanolsolv pulping and the α–O–4 linkage. Several depolymerization strategies using vanadium[122] or ruthenium catalysis,[124,129] rely on the presence of the alcohol to fragment the β–O–4 linkage via inner-sphere electron transfer process, however, lignin pulping techniques such as ethanolsolv pulping will displace this critical functionality. In order to address this challenge, we synthesized an oxidized ethanolsolv model system **176**. When subjected to our optimized reaction conditions, **176** yielded 70% of guaiacol. Attempts to isolate the anticipated cinnamaldehyde product were unsuccessful, perhaps due to subsequent degradation/polymerization. However, upon closer inspection, we were able to isolate 30% of 3,4-dimethoxymethylbenzoate **177**, presumably from the fragmentation of the Cα–Cβ upon fragmentation of the ketylradical of **178** (See below for mechanism). Taken together these results highlight several advantages of the developed catalytic system. 1) The reaction occurs at room temperature, lowering the probability of thermal and acidic decomposition of the β–O–4 linkage.

2) This reaction is highly versatile and able to effectively cleave substrates possessing sensitive functionality such as OH groups and cleave aryl ether bonds activated by both benzylic ketones and aldehydes. 3) The reaction is insensitive to the presence of oxygen or water. Although the reagent stoichiometry is not ideal, this reaction is an important proof-of-concept for the validity of photocatalysis as a viable strategy towards the longer term goal of biomass processing and lignin depolymerization as a whole.

3.3.3 The Development of a Telescoped Lignin Depolymerization using Flow Chemistry

Implementation of a single stage depolymerization of lignin is highly advantageous from a practical standpoint by reducing the number of processing steps, potentially improving atom economy, and increasing material throughput. However, devising a one-step depolymerization of lignin has proven challenging, often requiring high reaction temperatures and forcing conditions which can potentially modify the lignin structure, rendering it more difficult to process further. Splitting the depolymerization process into two milder steps, though more lengthy, can impart greater chemoselectivity with product distribution while preserving the lignin structure (Figure 27).

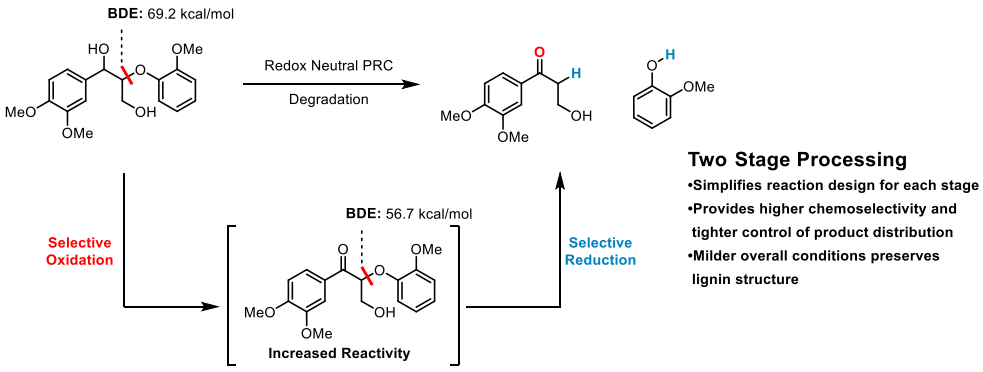

Figure 27 Two Stage Processing of Lignin

With both the benzylic oxidation and the reductive cleavage reactions optimized, we were immediately interested in streamlining these two processes and minimize product loss through unnecessary purification steps. The conditions we had employed for the oxidation of the benzylic alcohol, as described by Bobbitt and co-workers[138] were particularly amenable to this goal. In short, substrates could be reacted with 1.05 equiv. of [4-AcNH-TEMPO]BF_4 in DCM with 100 wt% of silica in respect to substrate (Table 5, vide supra). After reaction completion, the silica was filtered off and the reaction was concentrated in vacuo. The resulting crude mixture could be redissolved in MeCN, upon which [Ir(ppy)$_2$(dtbbpy)]PF_6, DIPEA and formic acid were directly added and the resultant solution was irradiated with blue LEDs, producing the desired fragmentation products in high yield. This streamlined reaction protocol was more efficient, leading to higher overall isolated yields. With the success of the batch-to-batch process, we were interested in exploring the reaction within a continuous flow reactor. Using a homemade flow reactor, John developed a simple batch-to-flow protocol[137] where the oxidation occurred in batch and the reduction occurred within a continuous flow reactor. Previous reports by our group and the Seeberger group had demonstrated that the use of a flow reactor can greatly accelerate photoredox catalyzed reactions due to the efficient irradiation of the reaction solution.[141,142] Performing the reaction in the flow reactor greatly accelerated the reaction rate when compared to the analogous batch-to-batch reaction.

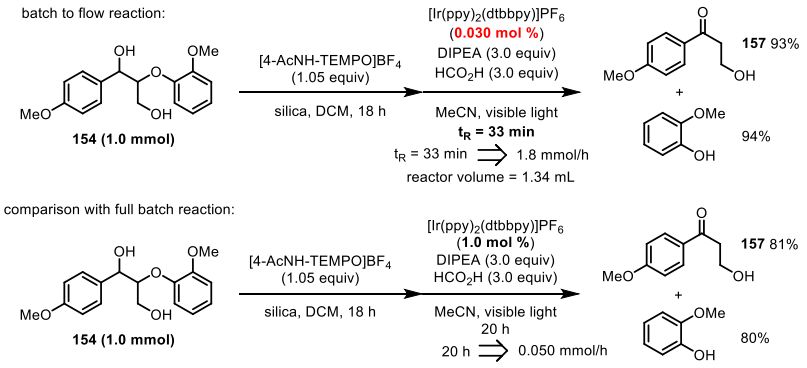

Scheme 4 Comparison of reaction throughput of batch-to-flow with batch-to-batch

When 1.0 mmol of coumaryl model system **154** was reacted in a batch-to-batch fashion, we observed an 81% yield of hydroxyketone **173** and 80% of guaiacol, corresponding to a reaction throughput of 0.05mmol/h. The batch to flow process, however, was able to convert the same quantity of 154 at a reaction throughput of 1.8mmol/h in a 1.34mL flow reactor with a residence time of 33min yielding slightly higher yields of hydroxyketone **157** and guaiacol. This corresponds to a nearly 50-fold rate acceleration *in spite of the fact that the catalyst loading was reduced to 0.03 mol%*. Gratifyingly, when the corresponding batch-to-batch reaction was ran on gram scale, a similar yield was observed, demonstrating that the reaction is scalable and requires very low catalyst loading.

One of the drawbacks of photoredox catalysis is the requirement for efficient irradiation of the reaction. This can become particularly troublesome in reactions where substrates that absorb within the same spectral window as the photocatalyst or in heterogeneous reactions where insoluble particles prevent efficient irradiation of the reaction medium. From the outset, we were concerned that the dark color of lignin could interfere with the photocatalyzed C–O bond reduction by preventing efficient irradiation of the reaction medium. To test this hypothesis, we attempted to reductively cleave β–O–4 model in the presence of 100 wt% of lignosulfonate using slightly modified reaction conditions, substituting the acetonitrile with a 4:3 mixture of acetonitrile in

water to fully solubilize the lignin. After 48h, no conversion of **165** into fragmentation products was observed (Scheme 5). When the same reaction was ran through a flow reactor, **165** cleanly fragmented into 4-methoxyacetophenone (**168**) and guaiacol in 90% and 92% yield respectively with a high reaction throughput of 8.9mmol/h. This result demonstrates the utility of flow chemistry within the context of photoredox catalysis. Though one can reasonably expect a reaction rate acceleration using a flow reactor, in this case it enables a reaction to proceed where the batch reaction could not. Furthermore, this reaction also demonstrates that the reductive cleavage chemistry is highly chemoselective and can occur in the presence of solvent quantities of water and in the presence of the several functionalities found in lignosulfonate including quinones, hydroxyl groups, sulfonic acid groups and electron rich aromatic groups.

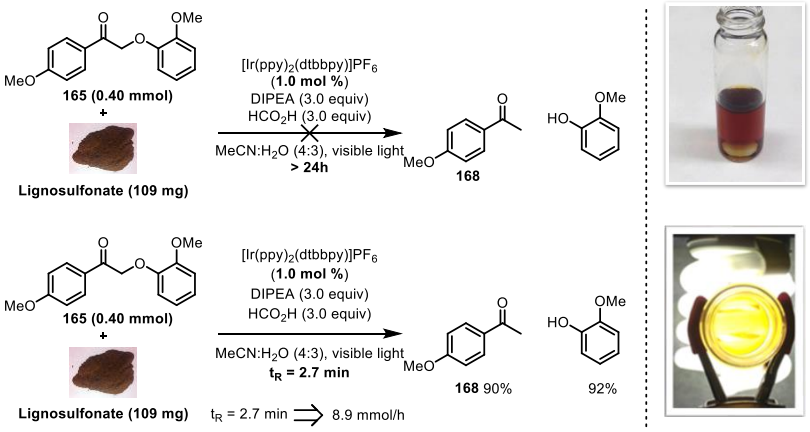

Scheme 5 Flow chemistry enables the reduction of **165** in the presence of lignin

3.4 Reaction Mechanism

The mechanism of the reductive cleavage of oxidized β–O–4 model systems can be rationalized by the well-understood reductive quenching cycle of $[Ir(ppy)_2(dtbbpy)]PF_6$ as described previously by my colleagues Dr. Jagan Narayanam,[21] Dr. Joseph Tucker,[139] and John

Nguyen.[140] Upon irradiation with visible light, $[Ir(ppy)_2(dtbbpy)]PF_6$ will undergo excitation, initiating a metal-to-ligand charge transfer (MLCT). This excited state $[Ir]^{3+*}$ then accepts an electron from DIPEA or the DIPEA•HCO_2H salt forming the ground state reductant $[Ir]^{2+}$ (-1.51 V vs. SCE). This $[Ir]^{2+}$ complex can then reduce the benzylic ketone **149** forming ketyl radical **150** which fragments into the phenoxide of guaiacol and radical **151**. Hydrogen atom transfer to α-keto radical **152** and protonation of guaiacol furnishes the desired products.

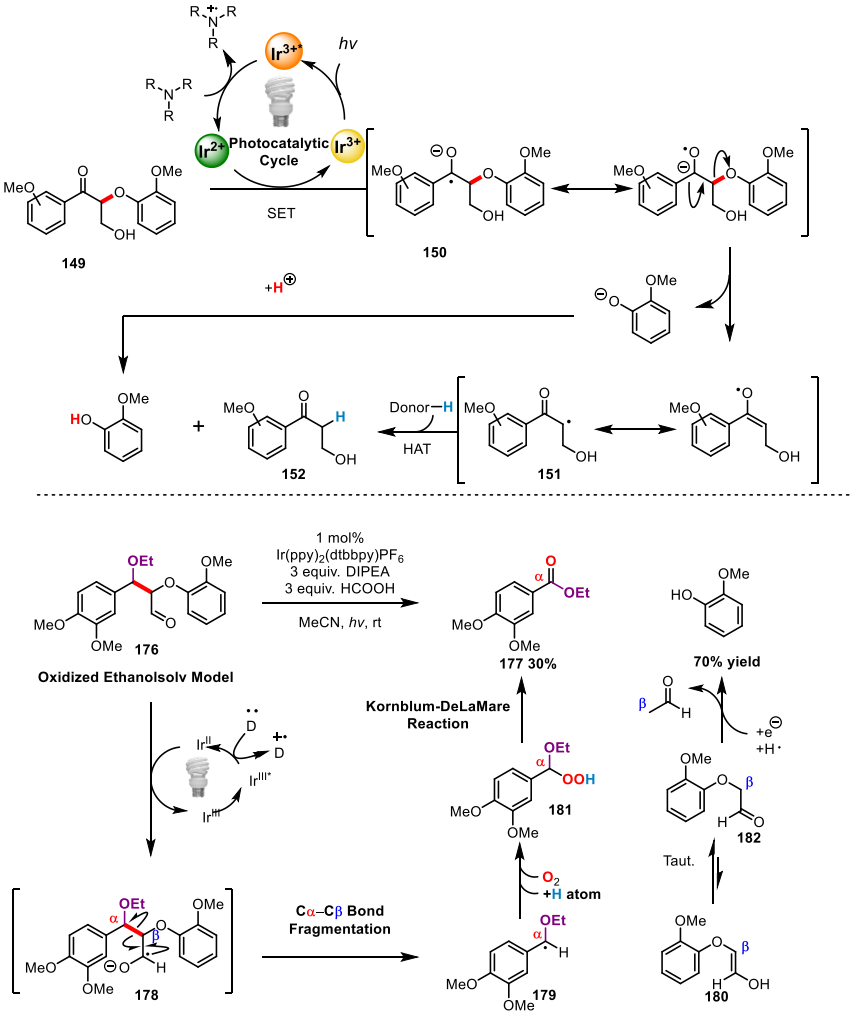

Figure 28 Mechanism of the photocatalytic reductive cleavage of the C_α–O bond

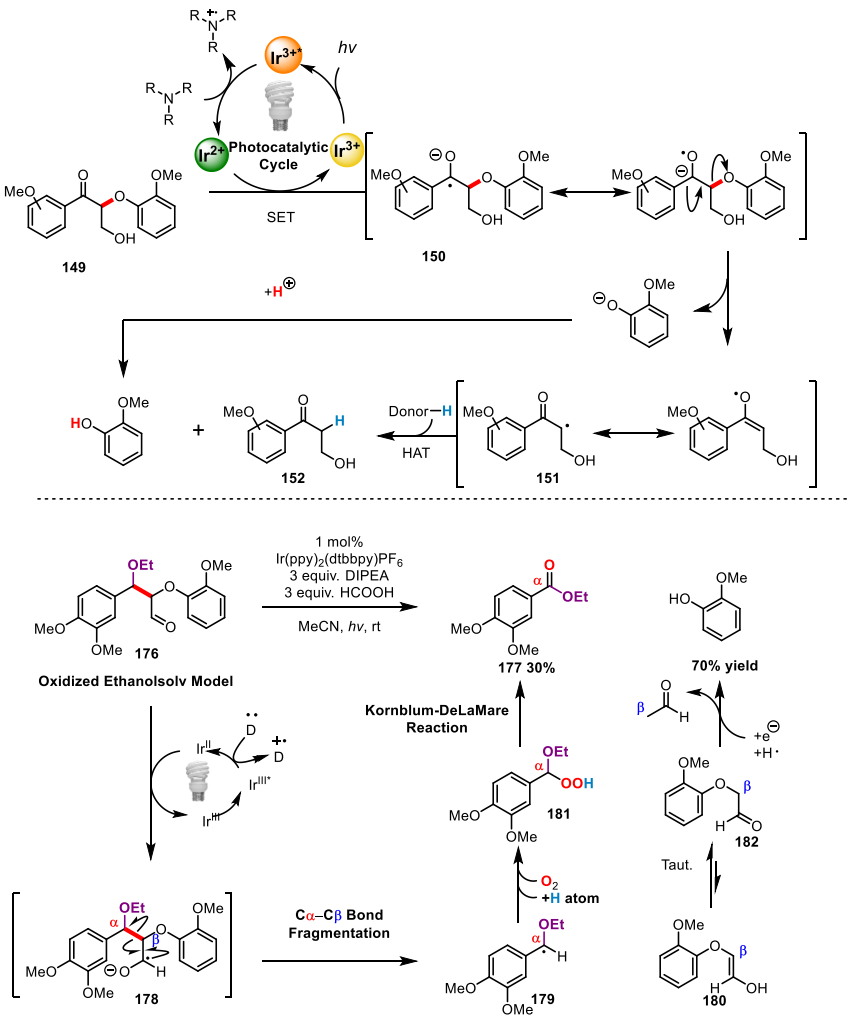

Figure 28, B). Benzylic radicals such as **179** typically readily undergo diffusion

The isolation 3,4-dimethoxyethylbenzoate from the reductive cleavage of **176** suggests an unusual mechanism of fragmentation. We propose that upon single electron reduction of **176** by $[Ir]^{2+}$, the resultant ketyl radical (**178**) undergoes a C–C bond cleaving β–scission, resulting in the formation stabilized radical **179** and of enol ether **180** (Figure 28controlled[143] radical addition of $^3O_2$ forming an alkylperoxyl radical which can subsequently abstract a hydrogen atom from a various H-atom donors such as solvent, DIPEA, or formic acid. The resultant peroxyl radical **181** can decompose via a Kornblum–DeLaMare type elimination, yielding 3,4-dimethoxyethylbenzoate (**177**). The

presence of the ethyl group in the product is significant, since there are no other sources of ethanol in the reaction except for the benzylic ether in the starting material. Tautomerization of **180** forms acetaldehyde aryl ether **182**, which can undergo a second photocatalytic fragmentation yielding acetaldehyde and guaiacol.

3.5 Conclusions and Outlook

In conclusion, John and I developed a novel approach toward the depolymerization of lignin which involves a two stage processing strategy. This was accomplished through the development of a room temperature, selective benzylic oxidation using Bobbitt's salt, followed by a mild reductive C_β–O fragmentation using the reductive quenching cycle of $[Ir(ppy)_2(dtbbpy)]PF_6$. The exceptionally mild conditions of this two-step approach ultimately enabled us to fragment β–O–4 model compounds in high overall yield while preserving the structure of the fragmentation products. This method was highly versatile, capable of fragmenting both benzylic ketones and substrates containing functionalized benzylic positions. Furthermore, this reaction was highly chemoselective and could competently cleave the C_β–O bond in the presence of free phenols. Using a flow reactor, it was possible to significantly reduce catalyst loading, accelerate reaction rate, and reductively cleave model compounds in the presence of actual lignin using solvent quantities of water. Although this approach possesses several advantages from a strategic standpoint, there are several challenges including issues with reagent stoichiometry, the use of a precious metal catalyst, and reaction scalability that remain to be addressed. Current efforts in our lab are focused on finding a more efficient photocatalytic benzylic oxidation and applying these reductive conditions on polymeric substrates including actual oxidized lignin. Our ultimate goal will be to develop a redox neutral depolymerization of lignin using electron shuttling reagents, obviating the need for any stoichiometric reagents.

3.6 Experimental Section

General Procedure A: Benzylic Oxidation with [4-AcNH-TEMPO]BF_4. (SI Table 2)

A 5 dram vial with a magnetic stir bar was charged with the corresponding benzylic alcohol (1.00 mmol, 1.00 equiv), dichloromethane (10.0 mL), silica gel (100 wt. % of benzylic alcohol), and [4-AcNH-TEMPO]BF_4 (1.05 mmol, 1.05 equiv). The vial was capped and the heterogenous mixture was stirred at room temperature until it was complete (as judged by TLC analysis). The reaction mixture was vacuum filtered through a pad of silica on a glass-fritted funnel (pore size C) and an additional 30 mL of dichloromethane (10 mL portions) was used to rinse the product from the silica. The filtrate was concentrated in vacuo and the crude residue can be used directly in General Procedure B or purified by chromatography on silica gel to afford the desired product.

General Procedure B: Reductive C–O Bond Cleavage. (Substrates 1–9)

A 5 dram vial with a magnetic stir bar was charged with the corresponding benzylic ketone (1.00 mmol, 1.00 equiv), MeCN (5.0 mL), *N*,*N*-diisopropylamine (3.0 mmol, 3.0 equiv), formic acid (3.0 mmol, 3.0 equiv) and $[Ir(ppy)_2(dtbbpy)]PF_6$ (0.010 mmol, 0.010 equiv). The vial was capped and the reaction mixture was stirred at room temperature until it was complete (as judged by TLC analysis). The solvent was removed from the crude mixture *in vacuo* and was dissolved in EtOAc. The contents were poured into a separatory funnel containing 25 mL of EtOAc and 25 mL of deionized water. The layers were separated and the aqueous layer was extracted with EtOAc (2 × 25 mL). The combined organic layers were washed with brine, dried (Na_2SO_4), and concentrated in vacuo. The residue was purified by chromatography on silica gel to afford the desired products.

General Procedure C: Two-Step Degradation Protocol. (Substrates 10-12)

A 5 dram vial with a magnetic stir bar was charged with the corresponding benzylic alcohol (1.00 mmol, 1.00 equiv), dichloromethane (10.0 mL), silica gel (100 wt. % of benzylic alcohol), and [4-AcNH-TEMPO]BF_4 (1.05 mmol, 1.05 equiv). The vial was capped and the heterogenous mixture was stirred at room temperature until it was complete (as judged by TLC analysis). The reaction mixture was vacuum filtered through a pad of silica on a glass-fritted funnel (pore size C) and an additional 30 mL of dichloromethane (10 mL portions) was used to rinse the product from the silica. The filtrate was concentrated in vacuo and the crude residue was combined with MeCN (5.0 mL), *N*,*N*-diisopropylamine (3.0 mmol, 3.0 equiv), formic acid (3.0 mmol, 3.0 equiv) and $[Ir(ppy)_2(dtbbpy)]PF_6$ (0.010 mmol, 0.010 equiv) in a 5 dram vial. The vial was capped and the reaction mixture was stirred at room temperature until it was complete (as judged by TLC analysis). The solvent was removed from the crude mixture in vacuo and was dissolved in EtOAc. The contents were poured into a separatory funnel containing 25 mL of EtOAc and 25 mL of deionized water. The layers were separated and the aqueous layer was extracted with EtOAc (2 × 25 mL). The combined organic layers were washed with brine, dried (Na_2SO_4), and concentrated in vacuo. The residue was purified by chromatography on silica gel to afford the desired products.

Compound Characterization

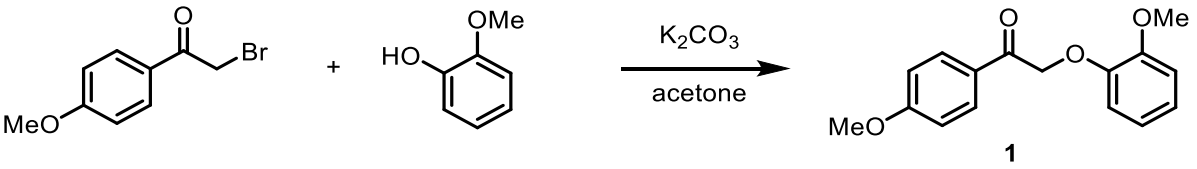

2-(2-methoxyphenoxy)-1-(4-methoxyphenyl)ethanone (1): Substrate **1** was prepared according to a literature procedure.[2] A round bottom flask equipped with a reflux condenser was charged with 2-bromo-1-(4-methoxyphenyl)ethanone (13.7 g, 60 mmol), potassium carbonate (12.3 g, 89 mmol), guaiacol (8.2 mL, 74 mmol), and acetone (250 mL). The resulting suspension was stirred and heated to reflux for 3 h, after which it was filtered through celite and concentrated in vacuo. The resulting solid purified by chromatography on SiO_2 (70:30, hexanes/EtOAc) afforded **1** (13.9 g, 51 mmol, 86%) as a colorless solid.

R_f (EtOAc/hexane 1:3): 0.20;

IR (neat): 2936, 2837, 1689, 1597, 1501, 1212, 1168, 1127, 1023, 832, 739 cm^{-1};

^1H NMR ($CDCl_3$, 400 MHz): δ 8.03 (d, *J* = 8.4 Hz, 2H), 6.97 (d, *J* = 8.4 Hz, 2H), 7.00–6.90 (m, 2H), 6.88–6.84 (m, 2H), 5.29 (s, 2H), 3.89 (s, 6H);

^{13}C NMR ($CDCl_3$, 175 MHz): δ 193.1, 163.9, 149.7, 147.6, 130.5, 127.7, 122.3, 120.8, 114.7, 113.9, 112.2, 72.0, 55.9, 55.5;

HRMS (ESI) *m/z* calculated for $C_{16}H_{16}O_4^+$ ($[M+1]^+$) 273.1121, found 273.1110.

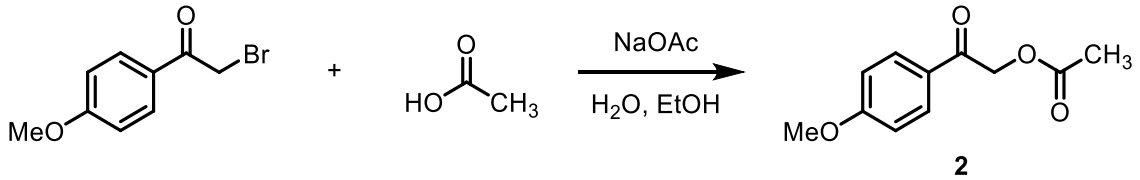

2-(4-methoxyphenyl)-2-oxoethyl acetate (2): Substrate **2** was prepared according to literature procedure.[3] A suspension of 2-bromo-1-(4-methoxyphenyl)ethanone (4.8 g, 21 mmol) in 22 mL of ethanol was prepared round-bottomed flask, and a solution of sodium acetate trihydrate (3.2 g, 24 mmol) in 11 mL of water and 1.1 mL of acetic acid was added. The mixture was heated at reflux for 2.5 h, then cooled to room temperature, and refrigerated overnight. In some cases, a solid separated that was collected by filtration and was found to be pure acetate. In other cases, most of the ethanol was removed under reduced pressure, and the resulting oily mixture was distributed between 30 mL EtOAc and 20 mL of a semisaturated, ice-cold $NaHCO_3$ solution. The organic extracts were washed in sequence with 10 mL of semisaturated brine, dried with sodium sulfate,

[2] *J. Am. Chem. Soc.* **2010**, *132*, 12554.
[3] *J. Med. Chem.* **2007**, *50*, 21.

and evaporated in vacuo. Purified by chromatography on SiO_2 (70:30, hexanes/EtOAc) afforded **2** (4.0 g, 19 mmol, 90%) as a colorless solid. Spectral data are consistent with those reported in the literature.[4]

R_f (EtOAc/hexanes 1:3): 0.20;

^{1}H NMR ($CDCl_3$, 400 MHz): δ 7.78 (d, *J* = 7.4 Hz, 2H), 6.83 (d, *J* = 7.3 Hz, 2H), 5.19 (s, 2H), 3.74 (s, 3H), 2.11 (s, 3H).

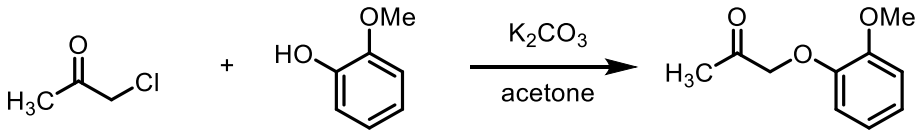

3

1-(2-methoxyphenoxy)propan-2-one (3): Substrate **3** was prepared according to a literature procedure.[5] A mixture of guaiacol (0.62 g, 5.0 mmol), chloroacetone (0.69 g, 7.5 mmol) and K_2CO_3 (1.0 g, 7.5 mmol) in acetone (10 mL) was stirred at 60 °C for 3 hours. Then, K_2CO_3 was filtered and the solvent removed under reduced pressure and purification by chromatography on SiO_2 (75:25, hexanes/EtOAc) afforded **3** (0.74 g, 4.1 mmol, 82%) as a clear and colorless oil.

R_f (EtOAc/hexanes 1:3): 0.25;

IR (neat): 2918, 2837, 1717, 1592, 1501, 1250, 1125, 1024, 965, 740 cm^{-1};

^{1}H NMR ($CDCl_3$, 400 MHz): δ 7.00 (dt, *J* = 8.2, 1.4 Hz, 1H), 6.94 (dd, *J* = 8.2, 1.8 Hz, 1H), 6.89 (dt, *J* = 8.0, 1.8 Hz, 1H), 6.79 (dd, *J* = 8.0, 1.4 Hz, 1H), 4.60 (s, 2H), 3.90 (s, 3H), 2.30 (s, 3H);

^{13}C NMR ($CDCl_3$, 175 MHz): δ 205.9, 149.4, 147.1, 122.3, 120.6, 114.1, 112.0, 74.1, 55.6, 26.2;

HRMS (ESI) *m/z* calculated for $C_{10}H_{12}O_3^+$ ($[M+1]^+$) 181.0859, found 181.0855.

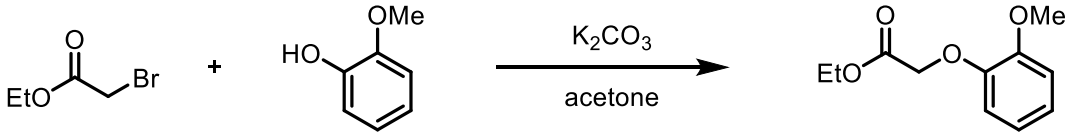

4

ethyl 2-(2-methoxyphenoxy)acetate (4): Substrate **4** was prepared according to a literature procedure.[6] 2-methoxyphenol (5.6 g, 45 mmol) and potassium carbonate (4.2 g, 30 mmol) were added to acetone (50 mL) forming a suspension. To this mixture was added ethylbromoacetate (5.0 g, 30 mmol) and the reaction was heated to reflux overnight to afford **4** (5.2 g, 82%) as a clear

[4] *Chin. J. Chem.* **2010**, *28*, 294.
[5] *Eur. J. Org. Chem.* **2012**, *2012*, 1499.
[6] *Med. Chem. Res.* **2010**, *19*, 33.

and colorless oil after purification by chromatography on SiO_2 (90:10, hexanes/EtOAc). Spectral data are consistent with those reported in the literature.[6]

R_f (hexanes/EtOAc 3:1): 0.54;

^{1}H NMR ($CDCl_3$, 500 MHz): δ 7.01–6.94 (m, 1H), 6.93–6.88 (m, 1H), 6.88–6.80 (m, 2H), 4.68 (s, 2H), 4.26 (q, *J* = 7.25 Hz, 2H), 3.88 (s, 3H), 1.28 (t, *J* = 7.21 Hz, 3H).

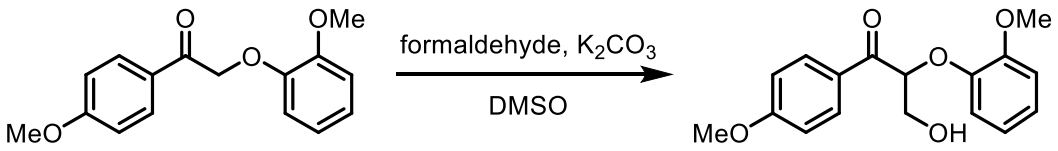

1 **6**

3-hydroxy-2-(2-methoxyphenoxy)-1-(4-methoxyphenyl)propan-1-one (6): Substrate **6** was prepared according to a literature procedure.[7] A solution of **1** (1.5 g, 5.5 mmol) in DMSO (30 mL) containing K_2CO_3 (1.5 g, 11 mmol) was stirred for 30 min at room temperature before adding formaldehyde (37 %) (0.82 mL, 11 mmol). The resulting solution was stirred for 3 h and 2 N NaOH (15 mL) was added and stirred for 1 h. After addition of 1 N HCl, the solution was extracted with ethyl acetate. The extracts were dried, concentrated in vacuo, and purification by chromatography on SiO_2 (50:50, hexanes/EtOAc) afforded **6** (0.83 g, 2.8 mmol, 50%) as a colorless solid.

R_f (EtOAc/hexanes 3:2): 0.31;

IR (neat): 3474, 2942, 2840, 1684, 1599, 1504, 1254, 1173, 1128, 1026, 974, 840, 742 cm^{-1};

^{1}H NMR ($CDCl_3$, 400 MHz): δ 8.06 (d, *J* = 8.6 Hz, 2H), 7.02 (t, *J* = 7.6 Hz, 1H), 6.98–6.89 (m, 4H), 6.83 (t, *J* = 7.2 Hz, 1H), 5.40–5.35 (m, 1H), 4.07 (t, *J* = 5.1 Hz, 2H), 3.89 (s, 3H), 3.87 (s, 3H), 3.00 (t, *J* = 5.6 Hz, 1H);

^{13}C NMR ($CDCl_3$, 175 MHz): δ 195.0, 164.0, 150.5, 146.9, 131.3, 127.9, 123.6, 121.1, 118.6, 114.0, 112.3, 84.7, 63.6, 55.8, 55.5;

HRMS (ESI) *m/z* calculated for $C_{17}H_{18}O_5^+$ ($[M+1]^+$) 303.1227, found 303.1225.

[7] *J. Org. Chem.* **2010**, *75*, 6549.

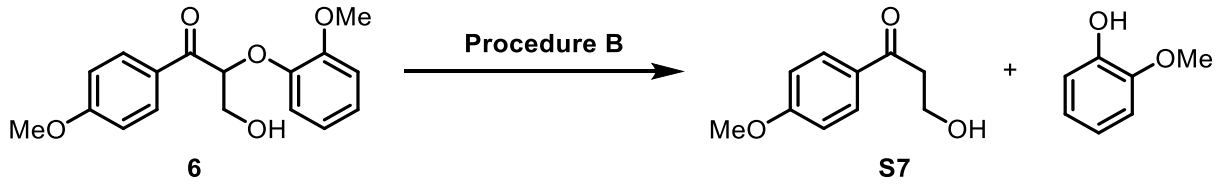

6 S7

3-hydroxy-1-(4-methoxyphenyl)propan-1-one (table 1, entry 6, product 1): According to General Procedure B, **6** (0.30 g, 1.0 mmol), DIPEA (0.52 mL, 0.39 g, 3.0 mmol), formic acid (0.11 mL, 0.14 g, 3.0 mmol) and $[Ir(ppy)_2(dtbbpy)]PF_6$ (9.2 mg, 10 μmol) in MeCN (5.0 mL) afforded **S7** (0.15 g, 0.85 mmol, 85%) and guaiacol (0.11 g, 0.88 mmol, 88%) after purification by chromatography on SiO_2 (50:50, hexanes/EtOAc). Spectral data are consistent with those reported in the literature.[8]

R_f (EtOAc/hexanes 3:2): 0.28;

^{1}H NMR ($CDCl_3$, 400 MHz): δ 7.93 (d, *J* = 9.0 Hz, 2H), 6.93 (d, *J* = 9.0 Hz, 2H), 4.00 (t, *J* = 5.5 Hz, 2H), 3.89 (s, 3H), 3.16 (t, *J* = 5.5 Hz, 2H,), 2.74 (br s, 1H).

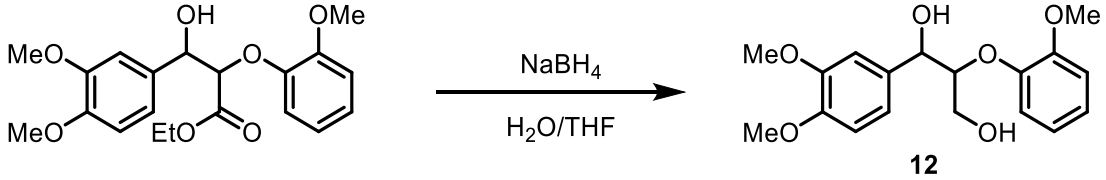

12

1-(3,4-dimethoxyphenyl)-2-(2-methoxyphenoxy)propane-1,3-diol (12): The synthesis of **12** was adapted from the literature procedure.[9] To a solution of β-hydroxyester[9] (3.4 g, 9.0 mmol) in THF/H_2O (5 mL, 3:1 ratio) was added sodium borohydride (1.7 g, 45 mmol) in portions. The reaction was allowed to stir at room temperature overnight. The reaction was diluted with ethyl acetate and washed with water and brine, then dried over sodium sulfate. The organic layer was then concentrated and purified by chromatography on SiO_2 (60:40, hexanes/EtOAc) afforded **12** (2.7 g, 89%) as a 2.5:1 mixture of diastereomers. Spectral data are consistent with those reported in the literature.[10]

R_f (hexanes/DCM/acetone/MeOH 6:2:1.5:0.5): 0.40;

^{1}H NMR ($CDCl_3$, 500 MHz): δ 7.14 (dd, *J* = 7.9, 1.5 Hz, 1H, minor diastereomer), 7.11-7.05 (m, 1H, major diastereomer, 1H minor diastereomer, overlap), 7.01-6.89 (m, 5H, major diastereomer, 2H, minor diastereomer, overlap), 6.87-6.83 (m, 1H, major diastereomer, 1H, minor diastereomer, overlap), 4.99 (d, *J* = 4.7 Hz, 1H, minor diastereomer), 4.98 (t, *J* = 4.7 Hz, 1H, major diastereomer), 4.16 (ddd, *J* = 6.0, 4.7, 3.4 Hz, 1H, major diastereomer), 4.04 (m, 1H, minor diastereomer), 3.95-3.89 (m, 1H, major diastereomer), 3.92 (s, 3H, minor diastereomer), 3.88 (s, 3H, major diastereomer, 3H, minor diastereomer), 3.88 (s, 3H, major diastereomer, 3H minor diastereomer),

[8] *Tetrahedron* **2010**, *66*, 3995.
[9] *Angew. Chem. Int. Ed.* **2012**, *51*, 3410.
[10] *Chem. Eur. J.* **2011**, *17*, 13877.

3.69 (m, 1H, minor diastereomer) 3.66 (m, 1H, major diastereomer), 3.63 (m, 1H minor diastereomer), 3.48 (dd, *J* = 12.5, 3.9 Hz, 1H, minor diastereomer).

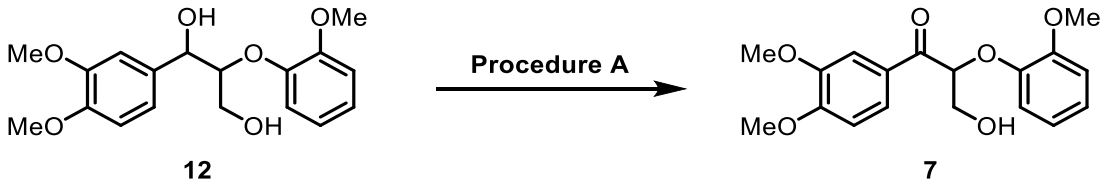

12 **7**

1-(3,4-dimethoxyphenyl)-3-hydroxy-2-(2-methoxyphenoxy)propan-1-one (7): According to General Procedure A, **12** (334 mg, 1.0 mmol), [4-AcNH-TEMPO]BF_4 (315 mg, 1.1 mmol), and silica (334 mg) in DCM (10 mL) afforded **7** (314 mg, 94%) after purification by chromatography on SiO_2 (60:40,hexanes/EtOAc). Spectral data are consistent with those reported in the literature.[11]

R_f (hexanes/DCM/acetone/MeOH 6:2:1.5:0.5): 0.36;

^{1}H NMR ($CDCl_3$, 500 MHz): δ 7.76 (dd, *J* = 8.6, 2.2 Hz, 1H), 7.62 (d, *J* = 2.0 Hz, 1H), 7.00 (td, *J* = 7.7, 7.7, 1.2 Hz, 1H), 6.91 (ddd, *J* = 8.3, 8.3, 1.5 Hz, 1H), 6.89 (d, *J* = 8.31 Hz, 1H), 6.83 (td, *J* = 7.26, 7.26 Hz, 1H), 5.40 (t, *J* = 5.4, 5.4 Hz, 1H), 4.07, (d, *J* = 5.4 Hz, 2H), 3.95 (s, 3H), 3.92 (s, 3H), 3.86 (s, 3H), 3.06 (br s, 1H).

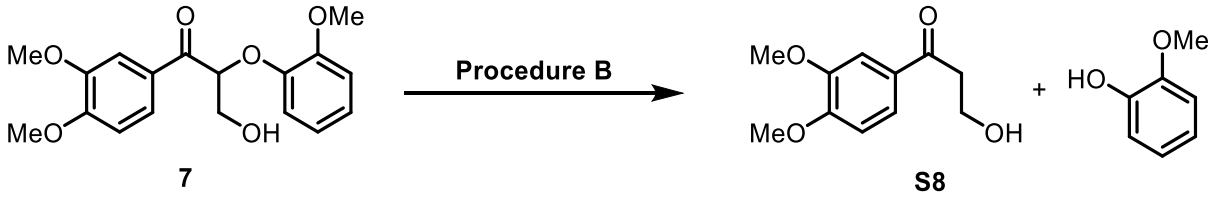

7 **S8**

1-(3,4-dimethoxyphenyl)-3-hydroxypropan-1-one (table 1, entry 7, product 1): According to General Procedure B, **7** (0.38 g, 1.14 mmol), DIPEA (0.60 mL, 0.44 g, 3.4 mmol), formic acid (0.13 mL, 0.16 g, 3.4 mmol) and [Ir(ppy)$_2$(dtbbpy)]PF_6 (10 mg, 11.0 μmol) in MeCN (10.0 mL) afforded **S8** (141 mg, 85%) and guaiacol (239 mg, 76%) after purification by chromatography on SiO_2 (70:20:5:5 hexanes/DCM/MeOH/acetone).

5.2 mmol Scale One-Pot Reductive Fragmentation of 12 to S8

According to General Procedure C, **12** (1.75 g, 5.22 mmol) in DCM (50.0 mL), silica gel (1.75 g, 100 wt. %), and [4-AcNH-TEMPO]BF_4 (1.65 g, 5.5 mmol). The vial was capped and the heterogenous mixture was stirred at room temperature until it was complete (as judged by TLC analysis). The reaction mixture was vacuum filtered through a pad of silica on a glass-fritted funnel (pore size C) and an additional 90 mL of DCM (30 mL portions) was used to rinse **7** from the silica. The organic layer was concentrated and then the crude was reacted with DIPEA (2.75 mL, 2.0 g, 16 mmol), formic acid (0.60 mL, 0.73 g, 16 mmol) and [Ir(ppy)$_2$(dtbbpy)]PF_6 (2 mg, 2.0 μmol) in MeCN (50 mL) afforded **S8** (1.05 g, 95%) and guaiacol (0.65 g, 99%) after purification by chromatography on SiO_2 (70:20:5:5 hexanes/DCM/MeOH/acetone).

[11] *J. Am. Chem. Soc.* **2013**, *135*, 6415.

R_f (hexanes/DCM/MeOH/acetone 7:2:0.5:0.5): 0.21;

IR (neat): 3437, 2938, 1667, 1586, 1514, 1464, 1418, 1347, 1264, 1201, 1150, 1021, 888, 808, 766 cm^{-1};

^1H NMR ($CDCl_3$, 700 MHz): δ 7.59 (d, *J* = 8.3 Hz, 1H), 7.52 (s, 1H), 6.89 (d, *J* = 8.3 Hz, 1H), 4.02 (m, 2H), 3.95 (s, 3H), 3.93 (s, 3H), 3.19 (t, *J* = 5.3 Hz, 2H);

^{13}C NMR ($CDCl_3$, 175 MHz): δ 231.5, 129.9, 123.0, 110.0, 109.9, 58.3, 56.1, 56.0, 39.8;

HRMS (ESI) *m/z* calculated for $C_{11}H_{15}O_4^+$ ($[M+1]^+$) 211.0965, found 211.0960.

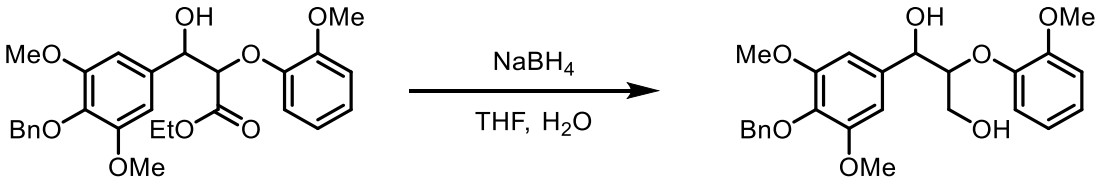

S3

1-(4-(benzyloxy)-3,5-dimethoxyphenyl)-2-(2-methoxyphenoxy)propane-1,3-diol (S3): Substrate **S3** was synthesized according the literature procedure.[9] To a solution of β-hydroxyester[9] (5.0 g, 9.5 mmol) in THF/H_2O (5 mL, 3:1 ratio) was added sodium borohydride (1.8 g, 47 mmol) in portions. The reaction was allowed to stir at room temperature overnight. The reaction was diluted with ethyl acetate and washed with water and brine, then dried over sodium sulfate. The organic layer was then concentrated and purified by chromatography on SiO_2 (60:40, hexanes/EtOAc) afforded **S3** (3.8 g, 91%, 2.5:1 diastereomeric ratio). Spectral data are consistent with those reported in the literature.[9]

R_f (hexanes:EtOAc 7:1): 0.10;

^1H NMR ($CDCl_3$, 500 MHz): δ 7.47 (d, *J* = 6.8 Hz, 2H, minor diastereomer), 7.47 (d, *J* = 6.8 Hz, 2H, major diastereomer), 7.33 (m, 2H, minor diastereomer), 7.33 (m, 2H, major diastereomer) 7.29 (d, *J* = 6.8 Hz, 1H, minor diastereomer), 7.29 (d, *J* = 6.8 Hz, 1H, major diastereomer), 7.10 (m, 1H, minor diastereomer), 6.95 (m, 3H), 6.67 (s, 0.82H, minor diastereomer), 6.60 (s, 2H, major diastereomer), 4.99 (m, 2H, major diastereomer), 4.97 (d, *J* = 4.4 Hz, 1.3H, minor diastereomer), 4.16 (m, 1H, major diastereomer), 4.02 (m, 0.6H, minor diastereomer), 3.92 (s, 1.4H, minor diastereomer), 3.90 (s, 3H, major diastereomer), 3.82 (s, 1.83H, minor diastereomer), 3.81 (s, 6H, major diastereomer), 3.66 (m, 1H, major diastereomer), 3.51 (m, 0.5H, minor diastereomer).

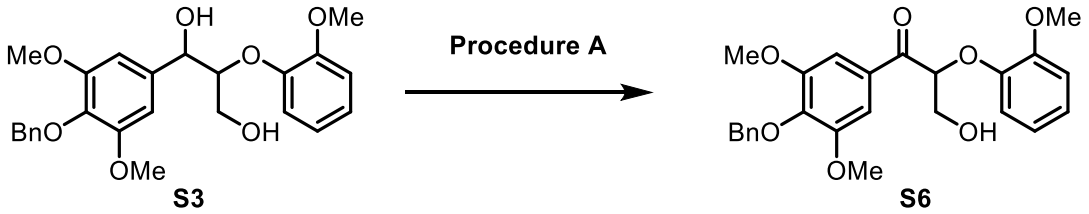

1-(4-(benzyloxy)-3,5-dimethoxyphenyl)-3-hydroxy-2-(2-methoxyphenoxy)propan-1-one (S6): According to General Procedure A, **S3** (1.0 g, 2.3 mmol), [4-AcNH-TEMPO]BF_4 (0.72 g, 2.4 mmol), and silica (1.0 g) in DCM (20 mL) afforded **S6** (0.94 g, 94%) after purification by chromatography on SiO_2 (60:40, hexanes/EtOAc). Spectral data are consistent with those reported in the literature.[12]

R_f (hexanes/EtOAc 4:1): 0.15;

^{1}H NMR ($CDCl_3$, 500 MHz): δ 7.46-7.43 (m, 2H), 7.34-7.31 (m, 2H), 7.32 (s, 2H), 7.02 (ddd, *J* = 7.8, 7.8, 1.6 Hz, 1H), 6.92 (ddd, *J* = 8, 1.5, 1.5 Hz, 2H), 6.85 (ddd, *J* = 7.7, 7.7, 1.5 Hz, 1H), 5.35 (d, *J* = 5.1, 5.1 Hz, 1H), 5.10 (s, 2H), 4.09-4.07 (m, 2H), 3.82 (s, 6H), 2.93 (dd, *J* = 6.0, 6.0 Hz, 1H).

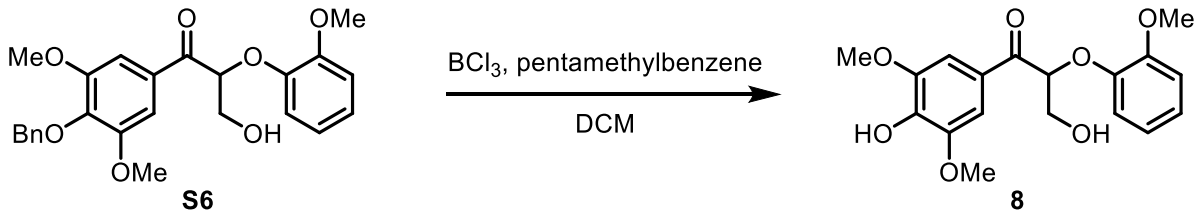

3-hydroxy-1-(4-hydroxy-3,5-dimethoxyphenyl)-2-(2-methoxyphenoxy)propan-1-one (8): A solution of **S6** (150 mg, 0.23 mmol) and pentamethylbenzene (101 mg, 0.69 mmol) in dicholoromethane was cooled to -78℃ in a dry ice/acetone bath. To this, BCl_3 (450 µL, 1M solution in DCM, 0.45 mmol) was added dropwise.[13] This was allowed to stir at -78℃ for 30 minutes upon which the reaction was quenched with MeOH. This organic layer was immediately loaded onto celite and purified by chromatography on SiO_2 (50:50, hexanes/EtOAc) to afford **8** (75 mg, 95%) as a colorless solid. Spectral data are consistent with those reported in the literature.[9]

R_f (hexanes/EtOAc, 8:2): 0.06;

^{1}H NMR ($CDCl_3$, 500 MHz): δ 7.41 (s, 2H), 7.01 (ddd, *J* = 8.1, 7.3, 1.5 Hz, 1H), 6.91 (ddd, *J* = 9.5, 8.5, 1.7 Hz, 2H), 6.83 (ddd, *J* = 7.6, 7.6, 1.5 Hz, 1H), 6.01 (br s, 1H), 5.34 (dd, *J* = 6.5, 4.3 Hz, 1H), 4.09 (d, *J* = 5.4 Hz, 1H), 4.08 (d, *J* = 3.2 Hz, 1H), 3.91 (s, 6H), 3.86 (s, 3H).

[12] *J. Photochem. Photobiol. A 2003, 156, 253.*
[13] *Synlett* **2008**, *13*, 1977.

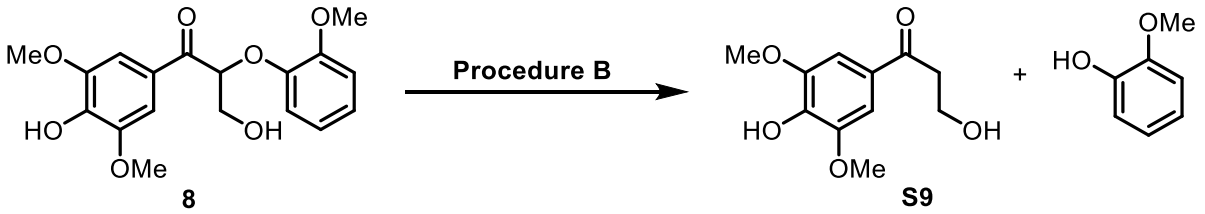

3-hydroxy-1-(4-hydroxy-3,5-dimethoxyphenyl)propan-1-one (table 1, entry 8, product 1): According to General Procedure B, **8**[14] (71 mg, 0.19 mmol), DIPEA (0.13 mL, 96 mg, 0.75 mmol), formic acid (28 µL, 34 mg, 0.75 mmol) and $[Ir(ppy)_2(dtbbpy)]PF_6$ (1.7 mg, 2.0 µmol) in MeCN (0.5 mL) afforded **S9** (41 mg, 80%) and guaiacol (22 mg, 95%) after purification by chromatography on SiO_2 (70:10:10:10, hexanes/DCM/MeOH/acetone). Spectral data are consistent with those reported in the literature.[14]

R_f (hexanes/DCM/acetone/MeOH 7:1:1:1) 0.05;

^{1}H NMR ($CDCl_3$, 700 MHz): δ 7.26 (s, 2H), 5.99 (br s, 1H), 4.03 (q, J = 8.4 Hz, 2H), 3.96 (s, 3H), 3.20 (t, J = 5.3 Hz, 2H), 2.67 (t, J = 6.3 Hz, 1H).

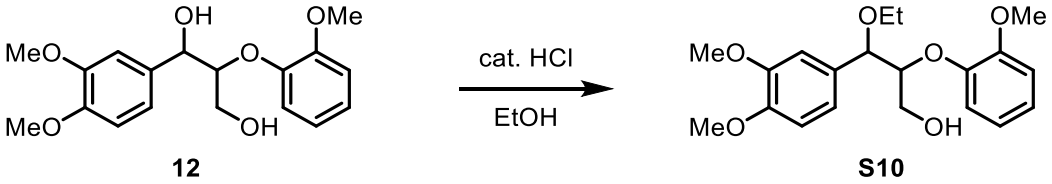

3-(3,4-dimethoxyphenyl)-3-ethoxy-2-(2-methoxyphenoxy)propan-1-ol (S10): Compound **S10** was made according to literature precedent.[15] 1 drop of conc. HCl was added a solution of **12** (0.75 g, 2.2 mmol) in ethanol (6 mL) and heated to 60°C for 3 hours. The reaction was concentrated and purified by chromatography over SiO_2 (75:25, hexanes/EtOAc) to afford **S10** (0.68 g, 84% 1:4:1 mixture of diastereomers) as a clear and colorless oil. Spectral data are consistent with those reported in the literature.[15]

R_f (hexanes/EtOAc 3:1): 0.26;

^{1}H NMR ($CDCl_3$, 500 MHz): δ 7.29 (dd, J = 7.8, 1.5 Hz, 1H, minor diastereomer), 7.02 (m, 1H, minor diastereomer), 6.97-6.89 (m, 3H, major diastereomer, 4H, minor diastereomer), 6.86-6.82 (m, 2H, major diastereomer, 1H, minor diastereomer), 6.75 (ddd, J = 7.7, 7.7, 1.7 Hz, 1H, major diastereomer), 6.50 (dd, J = 7.8, 1.5 Hz, 1H, major diastereomer), 4.53 (d, J = 7.3 Hz, 1H, major diastereomer), 4.50 (d, J = 7.3 Hz, 1H, minor diastereomer), 4.18 (ddd, J = 7.0, 7.0, 3.7 Hz, 1H, minor diastereomer), 4.08 (m, 1H, major diastereomer), 3.93 (br. s., 1H, major diastereomer), 3.89 (s, 3H, minor diastereomer), 3.88 (s, 3H, minor diastereomer), 3.88 (s, 3H, major diastereomer), 3.87 (s, 3H, minor diastereomer), 3.86 (s, 3H, major diastereomer), 3.82 (s, 3H, major diastereomer), 3.52-3.38 (m, 2H, major diastereomer, 2H, minor diastereomer), 3.39 (br. s., 1H,

[14] *J. Chem. Soc. Pak.* **2009**, *31*, 126.
[15] *Holzforschung* **1991**, *45*, 37.

major diastereomer), 3.23 (br. s., 1H, major diastereomer, 1H, minor diastereomer), 1.21 (t, *J* = 7, 7 Hz, 3H major diastereomer), 1.19 (t, *J* = 7, 7 Hz, 3H, minor diastereomer).

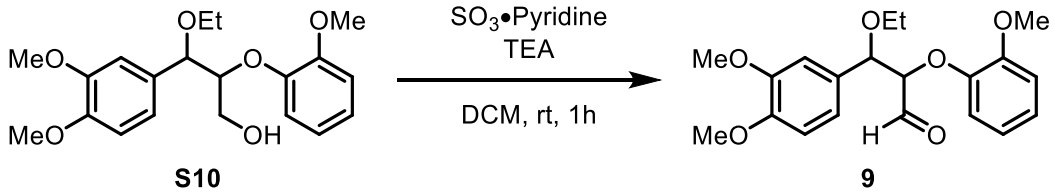

S10 **9**

3-(3,4-dimethoxyphenyl)-3-ethoxy-2-(2-methoxyphenoxy)propanal (9): To a solution of **S10** (108 mg, 0.30 mmol) in a 1:1 mixture of DCM/DMSO (2 mL), was added SO_3•Pyridine (190 mg, 1.2 mmol) and triethylamine (0.17 mL, 120 mg, 1.2 mmol). This reaction was allowed to stir at room temperature for 3 hours upon which it was diluted with ethyl acetate and washed with five portions of water and one portion of brine. The organic layer was dried over sodium sulfate and concentrated to afford **9** as a yellow oil (97 mg as a 1.5:1 mixture of diastereomers). This was found to be unstable to chromatography and was used directly in the next step.

R_f (hexanes/EtOAc 1:3): 0.25;

IR (neat): 3452, 2972, 2933, 1734, 1594, 1502, 1456, 1258, 1118, 1113, 1027, 750 cm^{-1};

^{1}H NMR ($CDCl_3$, 500 MHz): δ 9.88 (d, *J* = 2.0 Hz, 1H, minor diastereomer), 9.76 (d, *J* = 2.9, 1H, major diastereomer), 7.12 (d, *J* = 2.0 Hz, 1H, minor diastereomer), 7.00 (d, *J* = 2.0, 1H, major diastereomer), 6.97-6.91 (m, 2H, major diastereomer, 2H, minor diastereomer), 6.84 (dd, *J* = 8.3, 1.5 Hz, 2H, major diastereomer), 6.82 (dd, *J* = 8.3, 1.5 Hz, 2H, minor diastereomer), 6.75–6.79 (m, 1H, major diastereomer), 6.72–6.68 (m, 1H, major diastereomer, 1H minor diastereomer), 6.53 (dd, *J* = 8.3, 1.5, 1H, minor diastereomer), 4.77 (d, *J* = 3.4 Hz, 1H, minor diastereomer), 4.71 (d, *J* = 5.9 Hz, 1H, major diastereomer), 4.44 (dd, *J* = 5.9, 2.4 Hz, 1H, major diastereomer), 4.23 (dd, *J* = 3.2, 2.2 Hz, 1H, minor diastereomer), 3.90 (s, 3H, minor diastereomer), 3.87 (s, 6H, major diastereomer), 3.87 (3H, minor diastereomer), 3.75 (s, 3H, major diastereomer), 3.74 (s, 3, minor diastereomer), 3.51-3.36 (m, 2H, major diastereomer, 2H, minor diastereomer), 1.19 (t, *J* = 7.1 Hz, 3H, minor diastereomer), 1.18 (t, *J* = 7.1 Hz, 3H, major diastereomer);

^{13}C NMR ($CDCl_3$, 125 MHz): δ 203.0, 200.4, 150.3, 149.0, 147.4, 130.2, 130.0, 123.6, 123.5, 120.9, 120.9, 120.2, 119.8, 118.8, 118.7, 112.4, 112.2, 110.7, 110.7, 110.6, 88.4, 87.0, 82.1, 81.0, 65.2, 64.7, 55.9, 55.9, 55.9, 55.9, 55.6, 55.4, 15.1, 15.0;

HRMS (ESI) *m/z* calculated for $C_{20}H_{24}O_6Na^+$ ($[M+Na]^+$) 383.1471, found 383.1461.

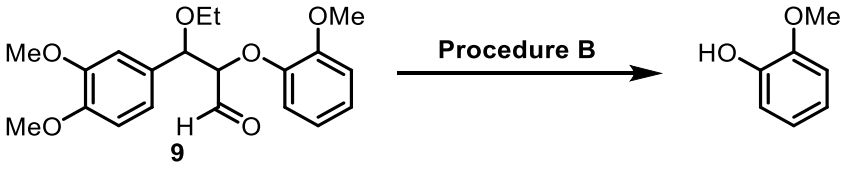

Fragmentation of Compound 9 (Table 1, Entry 9): According to General Procedure B crude aldehyde **9** (117 mg, 0.33 mmol), DIPEA (0.17 mL, 126 mg, 0.97 mmol), formic acid (0.04 mL, 45 mg, 0.97 mmol) and $[Ir(ppy)_2(dtbbpy)]PF_6$ (3 mg, 3.3 μmol) in MeCN (0.5 mL) afforded guaiacol (28 mg, 70%) after purification by chromatography on SiO_2 (70:20:5:5, hexanes/DCM/MeOH/acetone).

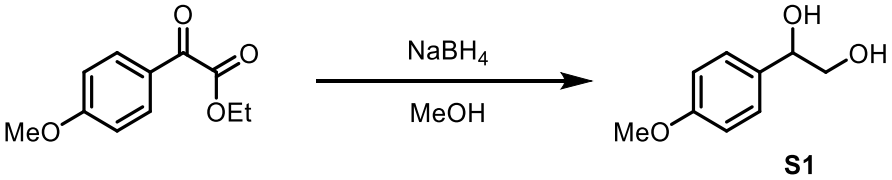

1-(4-methoxyphenyl)ethane-1,2-diol (S1): Substrate **S1** was prepared according to a literature procedure.[8] In a flask, the α-ketoester (1.0 mmol) was dissolved in methanol (5 mL). Then $NaBH_4$ (3.0 equiv) was added portion wise. The reaction mixture was stirred at room temperature until the reaction was completed based on TLC monitoring. Upon completion of the reaction, the mixture was acidified using 5.0 M HCl until pH 6. The solvent was then evaporated using rotary evaporator. The residue was dissolved in brine solution and the crude material was extracted using EtOAc. The organic layer was dried using anhydrous Na_2SO_4, filtered, and the solvent was evaporated. Purification by chromatography on SiO_2 (25:75, hexanes/EtOAc) afforded **S1** (0.17 g, 1.0 mmol, 100%). Spectral data are consistent with those reported in the literature.[16]

R_f (EtOAc/hexanes 3:2): 0.18;

^{1}H NMR ($CDCl_3$, 400 MHz): δ 7.30 (d, J = 8.4 Hz, 2H), 6.90 (d, J = 8.8 Hz, 2H), 4.83–4.74 (m, 1H), 3.81 (s, 3H), 3.76–3.63 (m, 2H), 2.51 (br s, 1H), 2.12 (br s, 1H).

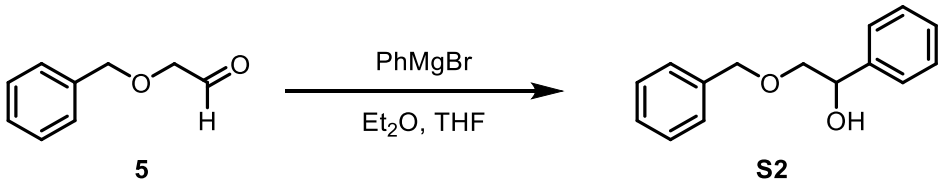

2-(benzyloxy)-1-phenylethanol (S2): Substrate **S2** was prepared according to a literature procedure.[17] To a solution of 2-(benzyloxy)acetaldehyde (**5**) (20 mmol) in THF (40 mL) was added PhMgBr 3.0 M in Et_2O (22 mmol. 1.1 eq.) at 0℃. After the mixture was stirred for 10 min at 0 °C, the mixture was warmed up to room temperature and was stirred for another 2 hours. The mixture was carefully quenched with saturated aq. NH_4Cl at 0℃, and the organic layer was separated and

[16] *J. Am. Chem. Soc.* **2010**, *132*, 14409.
[17] *J. Am. Chem. Soc.* **2012**, *134*, 10329.

aqueous layer was extracted with Et_2O twice. The combined organic layer was washed with brine and dried over anhydrous Na_2SO_4. The solvent was removed under reduced pressure and the residue was purified by chromatography on SiO_2 (90:10, hexanes/EtOAc) to afford **S2** (3.9 g, 17 mmol, 85%) as a clear and colorless oil. Spectral data are consistent with those reported in the literature.[17]

R_f (EtOAc/hexanes 1:3): 0.48;

^{1}H NMR ($CDCl_3$, 400 MHz): δ 7.40–7.29 (m, 10H), 4.98 (dd, *J* = 9.0, 3.3 Hz, 1H), 4.63 (d, *J* = 12.0 Hz, 1H), 4.59 (d, *J* = 12.0 Hz, 1H), 3.67 (dd, *J* = 9.6, 3.3 Hz, 1H), 3.54 (dd, *J* = 9.6, 9.0 Hz, 1H), 2.87 (br s, 1H).

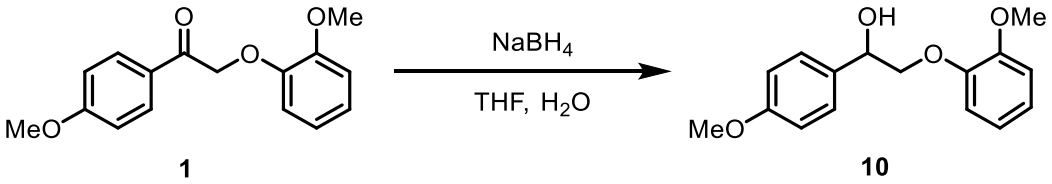

1 **10**

2-(2-methoxyphenoxy)-1-(4-methoxyphenyl)ethanol (10): Substrate **10** was prepared according to a literature procedure.[2] A round bottom flask was charged with **1** (1.7 g, 6.2 mmol), THF (28 mL), and water (7 mL). Sodium borohydride (0.47 g, 12.4 mmol) was added portion-wise to maintain a gentle evolution of gas over 5 minutes, after which the reaction mixture was stirred for 3 h at room temperature. The reaction was quenched with saturated aqueous NH_4Cl (50 mL) and then the reaction mixture was diluted with water (50 mL). The aqueous portion was extracted with Et_2O (3 x 50 mL). The combined organic extracts were washed twice with brine, dried over $MgSO_4$, filtered, and concentrated in vacuo. Purification by chromatography on SiO_2 (75:25, hexanes/EtOAc) afforded **10** (1.4 g, 5.0 mmol, 80%) as a clear and colorless oil.

R_f (EtOAc/hexanes 1:1): 0.43;

IR (neat): 3454, 2933, 2836, 1612, 1593, 1505, 1455, 1250, 1177, 1124, 1027, 832, 745 cm^{-1};

^{1}H NMR ($CDCl_3$, 400 MHz): δ 7.37 (d, *J* = 9.0 Hz, 2H) 7.03–6.88 (m, 6H), 5.06 (d, *J* = 9.0 Hz, 1H), 4.16 (dd, *J* = 10, 2.8 Hz, 1H), 4.01–3.93 (m, 1H), 3.90 (s, 3H), 3.82 (s, 3H), 3.38 (br s, 1H);

^{13}C NMR ($CDCl_3$, 175 MHz): δ 159.3, 150.0, 148.0, 131.7, 127.5, 122.4, 121.0, 115.8, 113.8, 111.9, 76.1, 71.9, 55.8, 55.2;

HRMS (ESI) *m/z* calculated for $C_{16}H_{18}O_4^+$ ($[M+1]^+$) 292.1543, found 292.1537.

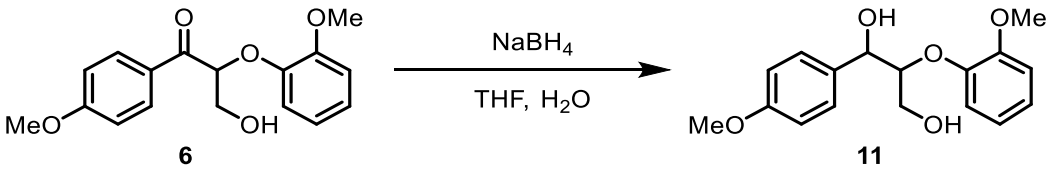

2-(2-methoxyphenoxy)-1-(4-methoxyphenyl)propane-1,3-diol (11): Substrate **11** was prepared according to a literature procedure.[11] Substrate **6** (1.1 g, 3.5 mmol) was dissolved in the mixture of THF:H_2O (5:1) (25 mL), and sodium borohydride (0.26 g, 7.0 mmol) was added portion-wise to maintain a gentle evolution of gas. Then, the mixture was stirred for 6 h at room temperature. The reaction mixture was quenched with saturated aqueous NH_4Cl (50 mL) and diluted with 30 mL water. The aqueous portion was extracted with ethyl acetate (3 × 30 mL). The organic portions were combined, dried over $MgSO_4$, filtered and concentrated in vacuo. Purification by chromatography on SiO_2 (40:60, hexanes/EtOAc) afforded **11** as a mixture of diastereomers (0.75: 1) and a thick colorless oil (0.80 g, 2.6 mmol, 75%). Spectral data are consistent with those reported in the literature.[10]

R_f (EtOAc/hexanes 3:2): 0.31;

^{1}H NMR ($CDCl_3$, 400 MHz): δ 7.38 (d, *J* = 7.8 Hz, 2H, major diastereomer), 7.32 (d, *J* = 7.4 Hz, 2H, minor diastereomer), 7.14 (d, *J* = 7.6 Hz, 1H, major diastereomer), 7.11–7.04 (m, 1H, both diastereomers), 7.01–6.87 (m, 4H, major diastereomer, 5H, minor diastereomer), 5.04–4.98 (m, 1H, both diastereomers), 4.20–4.14 (m, 1H, minor diastereomer), 4.07–4.01 (m, 1H, major diastereomer), 3.96–3.87 (m, 1H, minor diastereomer), 3.93 (s, 3H, major diastereomer), 3.90 (s, 3H, minor diastereomer), 3.82 (s, 3H, both diastereomers), 3.70–3.59 (m, 2H, major diastereomer, 1H, minor diastereomer), 3.51–3.39 (m, 1H, both diastereomers), 2.78–2.67 (m, 1H, both diastereomers).

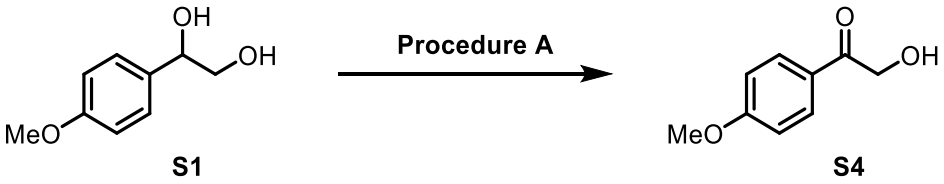

2-hydroxy-1-(4-methoxyphenyl)ethanone (S4): According to General Procedure A, **S1** (0.17 g, 1.0 mmol), [4-AcNH-TEMPO]BF_4 (0.32 g, 1.05 mmol), and silica (0.17 g) in DCM (10 mL) afforded **S4** (0.16 g, 95%) after purification by chromatography on SiO_2 (60:40, hexanes/EtOAc) as a colorless solid. Spectral data are consistent with those reported in the literature.[18]

R_f (EtOAc/hexanes 1:3): 0.13;

^{1}H NMR ($CDCl_3$, 400 MHz): δ 7.92 (d, *J* = 8.4 Hz, 2H), 6.98 (d, *J* = 8.4 Hz, 2H), 4.83 (s, 2H), 3.90 (s, 3H), 3.57 (br s, 1H).

[18] *J. Organomet. Chem*. **2009**, *694*, 3452.

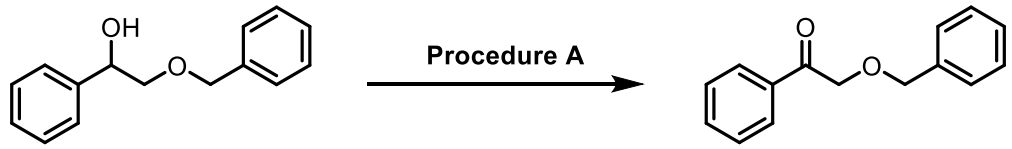

S2 **S5**

2-(benzyloxy)-1-phenylethanone (S5): According to General Procedure A, **S2** (0.23 g, 1.0 mmol), [4-AcNH-TEMPO]BF_4 (0.32 g, 1.05 mmol), and silica (0.23 g) in DCM (10 mL) afforded **S5** (0.21 g, 95%) after purification by chromatography on SiO_2 (75:25, hexanes/EtOAc) as a colorless solid. Spectral data are consistent with those reported in the literature.[19]

R_f (EtOAc/hexanes 3:2): 0.77;

^{1}H NMR ($CDCl_3$, 400 MHz): δ 7.93 (d, J = 7.6 Hz, 2H), 7.59 (t, J = 7.6 Hz, 1H), 7.47 (t, J = 8.0 Hz, 2H), 7.43–7.27 (m, 5H), 4.77 (s, 2H), 4.71 (s, 2H).

[19] *J. Org. Chem.* **2011**, *76*, 3576.

Batch to Flow Reaction:

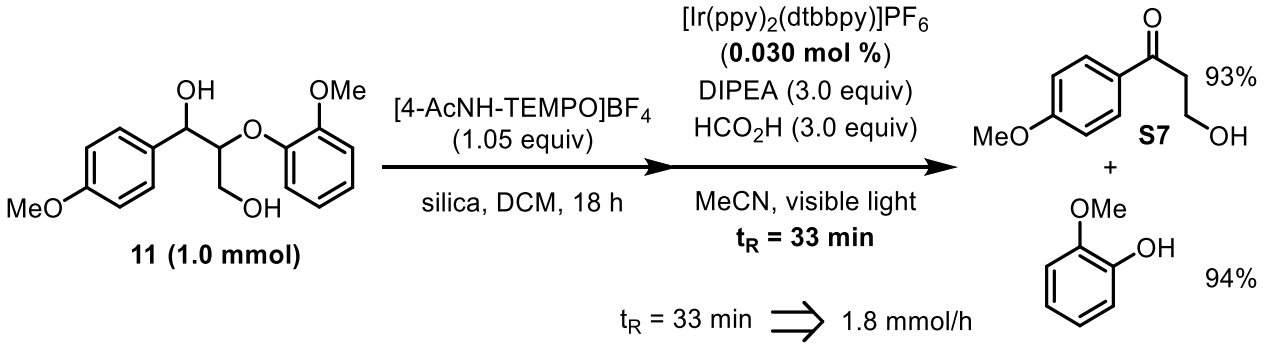

According to General Procedure A, **11** (0.30 g, 1.0 mmol), [4-AcNH-TEMPO]BF_4 (0.32 g, 1.05 mmol), and silica (0.30 g) in DCM (10 mL) afforded **6**, which was then mixed with DIPEA (0.52 mL, 0.39 g, 3.0 mmol), formic acid (0.11 mL, 0.14 g, 3.0 mmol) and $[Ir(ppy)_2(dtbbpy)]PF_6$ (0.27 mg, 0.30 μmol) in MeCN (5.0 mL) and submitted to the photoreactor at a flow rate of 0.41 μL/min (t_R = 33 min) to afford **S7** (0.17 g, 0.93 mmol, 93%) and guaiacol (0.12 g, 0.94 mmol, 94%) after purification by chromatography on SiO_2.

Chapter 4: The Scalable Synthesis and Antioxidant Evaluation of the Resveratrol Dimers Quadrangularin A and Pallidol

*Portions of this thesis were published in:
• Matsuura, B. S.†; Keylor, M. H.†; Li, B.; Lin, Y.; Allison, S.; Pratt, D. A.; Stephenson, C. R. J. *Angew. Chem.* **2015**, *127*, 3825–3828.

• Keylor, M. H.†; Matsuura, B. S.†; Stephenson, C. R. J. *Chem. Rev.* **2015**
DOI: 10.1021/cr500689b

4.1 Introduction

Cardiovascular disease (CVD) is the number one cause of death in the world and is responsible for 31% of overall deaths per annum. The prevalence of CVDs puts an enormous burden on the health system and those afflicted; therefore efforts to treat and prevent CVD are of significance to the scientific community, medical community and society at large. The risk factors contributing to the potential development of CVD are neither fully understood nor mutually exclusive. However, it has become increasingly apparent that populations from countries such as France, Japan, and Switzerland are significantly less likely to develop cardiovascular disease and enjoy longer average life spans.[144] The causative factors for this geographic disparity in CVD morbidity and mortality could, in part, be attributed to genetics, but other factors such as lifestyle and environmental influence may also play a role. Aside from differences in public health policy, modernization, and other societal factors, diet is the most important epidemiological variable to consider and is thought to be profoundly important in promoting a healthy life style.

During the early 1990's the correlation between diets high in saturated fats and cholesterol and CVDs was widely accepted.[145] However, this association could not account for the low

incidence of CVD experienced by the French despite the fact that their diet and lifestyle exposed the population to elevated risk factors. At this point, it was also recognized that moderate alcohol consumption was associated with lower rates of cardiovascular disease.[146] However, it was not known if this effect was universal, or if only certain types of alcoholic beverages were more effective than others.[147] In 1992, Siemann and Creasy reported that resveratrol (**1**) was present in significant concentrations in red wine.[148] This report was particularly timely, as work by Frankel and co-workers found that wine polyphenolics significantly inhibited fatty acid oxidation – a major contributor to arteriosclerosis.[149] The authors posited that polyphenolic constituents in red wine could act as "self-regenerating reducing components" (e.g. antioxidants), ameliorating arteriosclerosis, and thereby reducing cardiovascular mortality. The conclusions of these reports were staggering, providing a simple solution to this "French Paradox" and advancing the notion of a molecular basis for a healthy diet. Although the validity of the "French Paradox" has since come into question,[150,151] this work ignited vigorous interest in the field of phytochemicals, in particular resveratrol (**183**). Since then resveratrol has been described as possessing anticancer,[152] antidiabetic,[153,154]cardioprotective,[149] and even anti-aging properties.[155]

Despite the voluminous number of reports detailing its biological activity, little is known about the actual mode of action for a vast majority of its effects. It is perhaps unsurprising that resveratrol is a highly promiscuous molecule, given is simple structure and redox activity, and has the potential to interfere and modify several enzymatic processes or signaling pathways. The ambiguous mode of action of it biological activity has frustrated many efforts in developing resveratrol into an effective therapy. Resveratrol, however, is just member of a highly diverse family of oligostilbenoids that are prevalent within the foods we eat. Given the quantity of polyphenols present in the average human diet, it is highly likely that there are a multitude of

distinct chemical entities that can promote these beneficial effects. The biological activities of more complex resveratrol oligomers and other higher order polyphenols is poorly understood due to material scarcity, since these compounds can only be acquired through highly technical and laborious isolation from plant material. Therefore, the development of scalable synthetic strategies towards the resveratrol oligomers and other complex polyphenols is essential to further elucidate their biological activities and roles as dietary nutraceuticals.

4.2 Resveratrol Biosynthesis and Biological Role in the Plant

The resveratrol oligomers are plant phytoalexins – secondary metabolites that are not expressed constitutively, but rather are induced upon stimulation by pathogenic invasion or under environmentally stressing conditions, analogous to a mammalian immune response. As noted by Langcake and Pryce, resveratrol is not a particularly effective antifungal metabolite, however, the resveratrol dimer ε–viniferin (**185**) and cyclotrimer α–viniferin are much more efficacious.[156–158] Under certain criteria, resveratrol itself would not be considered a phytoalexin *per se*, however, it is clear that its expression is part of a greater phytoalexin response.

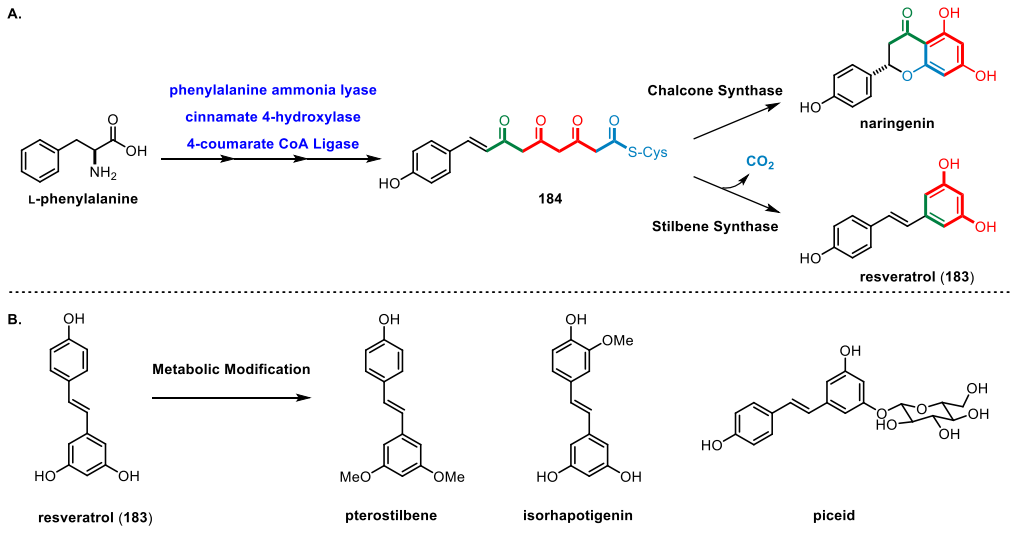

Figure 29 A) Resveratrol Biosynthesis and B) Post-synthetic Modification and Derivatization

Resveratrol is derived from the phenylpropanoid biosynthetic pathway shared by cinnamate and flavonoid natural products (Figure 29, A).[159] Phenylalanine, which is a product of the shikimate pathway, undergoes a series of enzymatic reactions resulting in the formation of linear tetraketide (**184**). Under normal conditions, **184** is converted into various flavonoids, such as naringenin, through chalcone synthase, which is expressed constitutively.[160] The gene encoding stilbene synthase is only transcribed under stressing conditions such as pathogenic invasion, physical trauma, UV irradiation, and oxidative stress. Resveratrol accumulates within lignified tissues in plant and are not in photosynthetic tissues where they have been shown to inhibit ion transport and redox processes associated with photosynthesis and cellular respiration. This reactivity of resveratrol protects the plant against oxidative stress and is at least, in part, responsible for its antipathogenic properties.

The resveratrol-derived natural products belong to a diverse family of >300 stilbenoids that have been isolated from 9 distantly related plant families. Like many secondary metabolites, resveratrol is chiefly expressed by plants as a chemical defense against invading pathogens. The oxidation of resveratrol frequently results in its radical oligomerization into polyphenolic secondary metabolites ranging from 2 to 8 units of resveratrol. The biological role of resveratrol was described in a series of publications by Lancake and Pryce in the early to mid 1970's.[156,157,161,162] During their studies, they identified resveratrol as the principle constituent of highly fluorescent lesions on grape (*Vitis vinifera)* leaves that have been infected with *Botrytis cinerea* (grey mold) and *Plasmapara viticola* (powdery mildew). They found that the expression of resveratrol was highly localized, increasing in concentration nearer to the lesion site. This fact, coupled with the observation that they could induce resveratrol expression by inoculating healthy leaves with *B.*

cinerea or by irradiation with UV light, suggested its role as a phytoalexin – a defensive compound in *V. vinifera*. Comparing the lesions of resistant and susceptible cultivars of *V. vinifera* revealed that lesions on resistant strains possessed high concentration of resveratrol oligomers including ε-viniferin (**185**) and α-viniferin whereas susceptible strains did not. These oligomeric derivatives possessed significantly more potent antifungal activity, as was evident qualitatively by their smaller, more compact lesions.[162] They concluded that resveratrol acted as a biogenic precursor to more potent antifungal compound through an oxidative process, a hypothesis that had previously been posited by Coggon and co-workers in their isolation of the resveratrol tetramer, hopeaphenol.[163,164] Inspired by the chemistry of the structurally similar lignan natural products, Langcake and Pryce demonstrated that the oxidation of resveratrol with horse radish peroxidase produced the resveratrol dimer δ-viniferin, which possessed superior fungicidal properties than resveratrol. Subsequent studies have shown that fungi are also able to mediate this dimerization reaction through extracellularly secreted laccases, a process that is highly reminiscent of the related process of lignin depolymerization. While it is widely recognized that plants produce the majority of the resveratrol oligomers, some of these compounds may in fact be of fungal origin. It is unclear at this time whether or not this is a phytoalexin counter-defense mechanism by the fungus to enable its proliferation or is the mechanism by which plants kill the pathogen by overwhelming important metabolic redox processes necessary for survival.

4.3 The Biosynthesis of Resveratrol Dimers

While the biosynthesis of resveratrol and other stilbenoids such as piceid, pterostilbene, and isorhapotigenin have been elucidated, several aspects of resveratrol oligomer biosynthesis are poorly understood. It is generally recognized that resveratrol oligomerization occurs through the intermolecular coupling of oxidatively generated phenoxyl radicals (**186–188**) as predicted

originally by Langcake and Pryce (Figure 30,A). These phenoxyl radicals generally dimerize through three regioisomeric pathways – 3–8’ coupling found in δ-viniferin (**194**), the 8–10’ coupling mode occurring for ampelopsin F(**195**)[165]

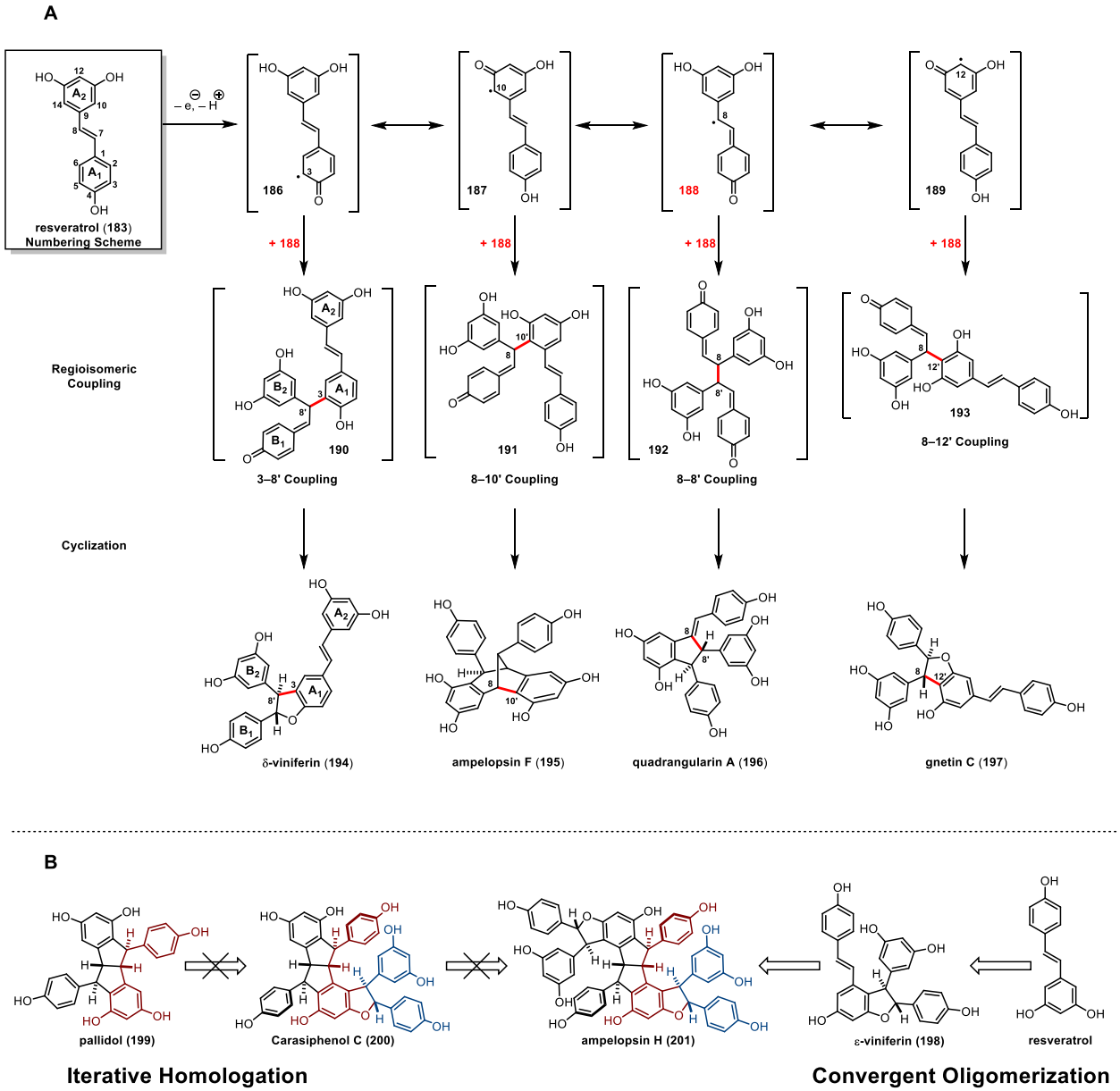

Figure 30 The Regioisomeric Modes of Resveratrol Dimerization

and ε-viniferin (**198**, Figure 30) , 8–8’ coupling found in quadrangularin A **196**[166,167] and pallidol **194**,[167,168] and. Other exotic regioisomers such as 8–12’ (gnetin C **197**[169]), 12–12’ (amurensin M)

have also been described, however they are exceedingly rare. The oxidative coupling of the phenoxyl radicals produces highly reactive *para*-quinone methide intermediates (**190**–**193**), which can undergo divergent Friedel–Crafts cyclization reactions and can yield several distinct molecular architectures from a single intermediate (Figure 30, A). The biosynthesis of higher order oligomers, such as trimers and tetramers arise from the same biosynthetic logic, arising from the crossed-dimerization of 8–10' ε-viniferin (**198**) to form trimers, or homocoupling to form tetramers (Figure 30, B) Through these two distinct reaction manifolds, plants are capable of quickly generating a large number of structurally complex architectures and despite this chemical diversity, their biosynthesis can generally be traced by these fundamental disconnections.

4.4 An Introduction to the Biomimetic Synthesis of the Resveratrol Oligomers

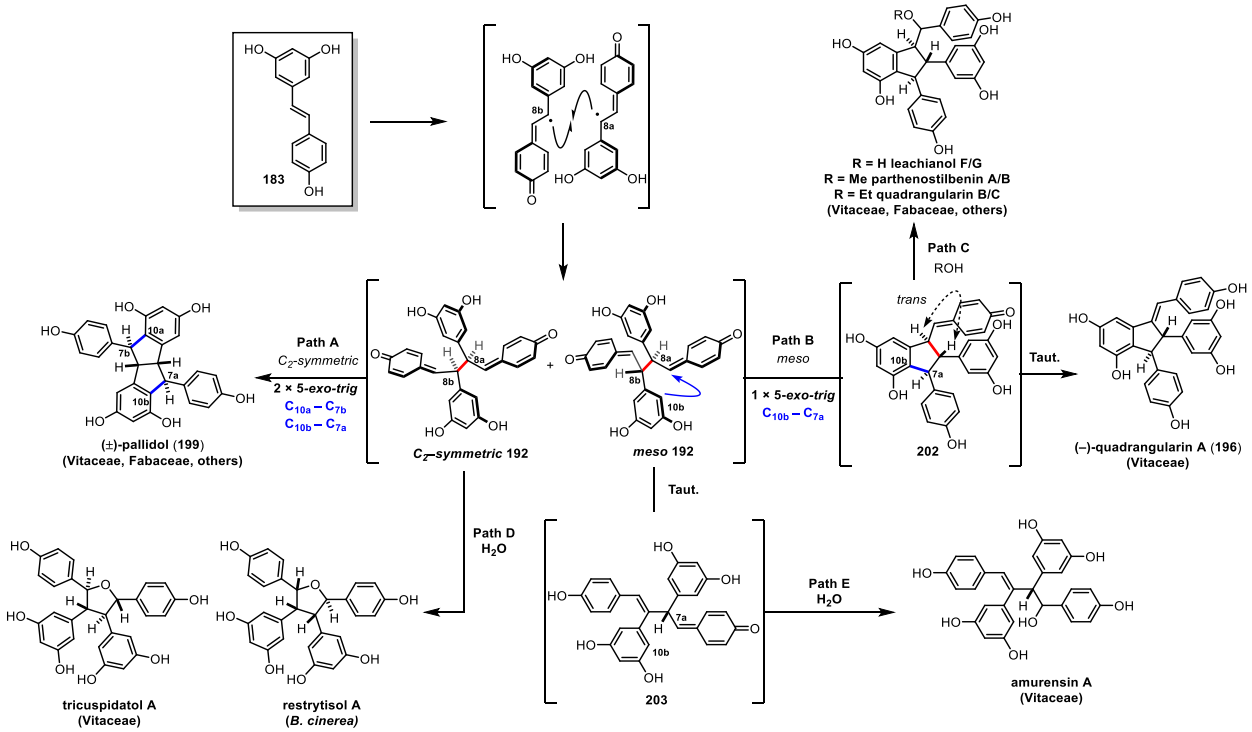

Figure 31 The biosynthesis of the 8–8' Dimers

The concept of a biomimetic synthesis was developed by Robinson following his historic synthesis of tropinone in 1917.[170,171] This strategy of imitating a biosynthetic reaction sequence has been used to support the plausibility of a given biosynthetic hypotheses, and in many cases, it is recognized as the most efficient means to synthesize complex natural products. The resveratrol natural products are particularly well-suited for biomimetic synthesis because the starting material is relatively easy to access and the convergent nature of their oligomerization can rapidly introduce molecular complexity. The challenge in designing a biomimetic synthesis of the resveratrol natural products is principally an issue of chemoselectivity, since the products of dimerization have similar electrochemical potentials as resveratrol itself and are prone to over-oxidation. Consider the biosynthesis of the 8–8' resveratrol dimers (Figure 31). The dimerization of resveratrol leads to the formation of two diastereomeric linear-*bis*-para-quinone methides *meso* and *rac* **192**. The double cyclization of *rac*-**192** leads to the formation of pallidol (**199**) (Path A), whereas the cyclization of *meso*-**192** leads to the formation of cyclized *para*-quinone methide **202** (Path B), an intermediate which then can undergo tautomerization to form quadrangularin A (**196**) or nucleophilic trapping to get leachinol B/C (**203**) parthenostilbenin A/B (**204**), or quadrangularin B/C (**205**, Path C) Both stereoisomers of **192** are capable of undergo separate multiple reaction pathways, reacting with water forms tricuspidatol A (**207**) or restrytisol A (**208**) (Path D) or tautomerization to form an intermediate linear-*mono*-quinone methide (**209**) *en route* towards amurensin A (Path E).[172] Although the biosynthesis of any one of these natural products is theoretically only two steps from resveratrol, the challenge of chemoselectivity becomes immediately obvious.

Although the resveratrol oligomers have been known since the 1960's, there was very little interest by the synthetic community towards their total synthesis. Most of the research within this class of compounds was concerned with using biomimetic oxidation chemistry as a means to support the proposed chemical structures of isolated natural products. These studies on biosynthesis highlighted significant challenges in achieving high chemoselectivity, regioselectivity, and useful yields. The most important advances made during this period were the understanding the subtle effects of oxidant,[173] solvent choice,[174] and pH on product selectivity.[175] However, given the fact that these reaction were unpredictable and difficult to control, research in this area were largely driven by empirical observation.

4.4.1 Early Studies on the Biomimetic Dimerization of Resveratrol

The biomimetic oxidative dimerization of resveratrol can be induced by electrochemically,[176] enzymatically, and with the use of stoichiometric oxidants. Under most reaction conditions, the biomimetic oxidation of resveratrol has a propensity to prefer 3–8' coupling, yielding δ-viniferin (**194**) as the major product.[173,177,178] Often, this product can be obtained in high chemical yield, since the formation of the dihydrobenzofuran attenuates the

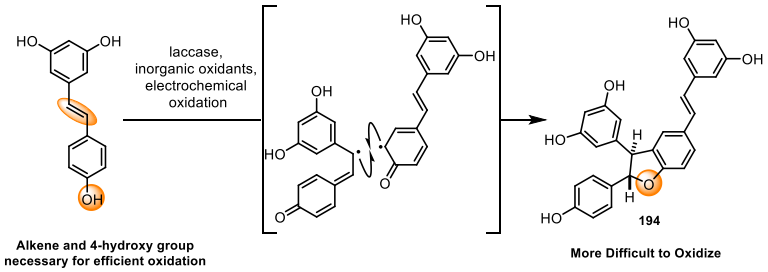

Figure 32 Alkylation of 4'-hydroxygroup prevents further oxidation

electron transfer potential through alkylation of the phenol, preventing over oxidation (Figure 32). Initially, the biomimetic oxidation of resveratrol was used as tool to understand the biosynthesis of the resveratrol natural products. In these cases, low chemical yield was acceptable, as along as

Table 8 A Summary of Biomimetic Oxidation of Resveratrol

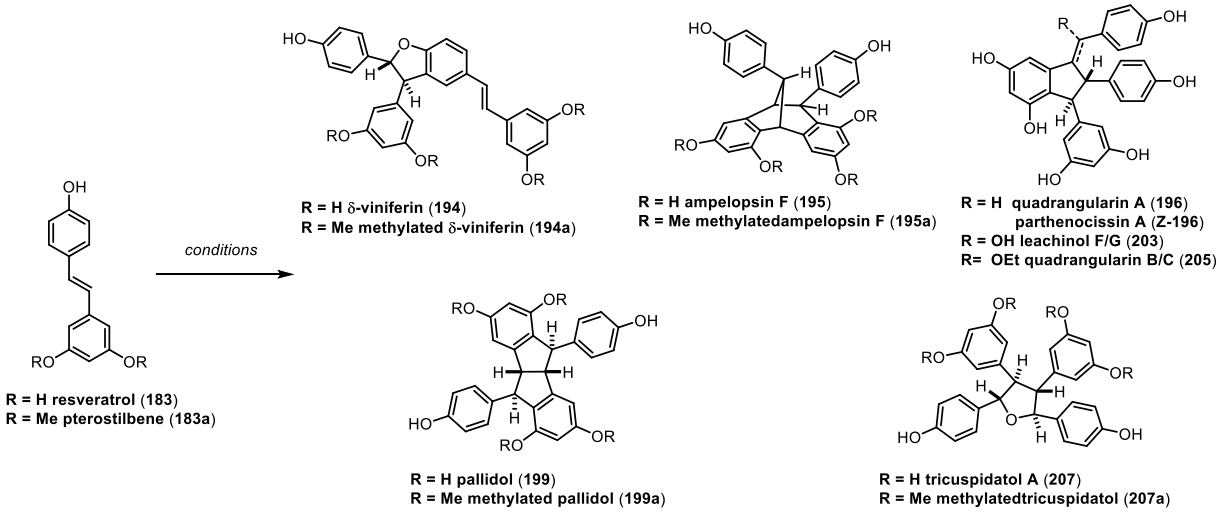

Entry	Reaction Conditions	194	195	203/205	199	207	Ref
1	$K_3Fe(CN)_6$, K_2CO_3, MeOH/H_2O, rt	23%	—	—	16%	—	[174]
2	Horseradish Peroxidase, aq. acetone	13%	—	—	10%	—	[174]
3	Soybean Peroxidase, aq. EtOH	12%	—	14%[b]	10%	—	[174]
4[a]	$FeCl_3$•$6H_2O$, CH_2Cl_2	—	7%	—	10%	—	[173]
5[a]	AgOAc, MeOH, 50 °C	—	—	—	—	86%	[179]
6[a]	$FeCl_3$•$6H_2O$, CH_2Cl_2/MeOH (7:3 v/v)	—	—	—	—	29%	[173]
7	Horseradish Peroxidase, acetone/pH 8.0 Buffer	93%[c] (89%)[d]	—	—	—	—	[175]
8	Horseradish Peroxidase, acetone/pH 6.0 Buffer	—	—	55%[c,e] (24%)[d,e]	—	—	[175]
9	Horseradish Peroxidase, acetone/pH 5.0 Buffer	—	—	—	20%[c] (19%)[d]	—	[175]
10	Horseradish Peroxidase, acetone/pH 4.0 Buffer	28%[c] (26%)[d,f]	—	—	—	—	[175]
11	$NaNO_2$/pH 3.0 Buffer, MeOH	2%	—	—	—	1%	[180]

[a] R=Me (pterostilbene, 18**3a**) [b] 2:1 Mixture of **203/205** [c]HPLC yield [d]isolated yield [e]Product was **203** [f]cis-δ-viniferin is major pdt

the desired product could be isolated. **Table 8** summarizes previous attempts at the direct dimerization of resveratrol using a variety of oxidation strategies. With few exceptions, these reaction occurred with very poor chemoselectivity. The Ito group was the first that was able to identify variable reaction conditions that afforded some degree of control over the product distribution between the 3–8' and 8–8' dimers (Table 8, Entries 1-3) .[174] Although the reaction yields were low and there was little control of product ratios, this was the first indication that non-3–8' dimers could be synthesized in a biomimetic fashion. In 2012, Pan and co-workers demonstrated that the chemoselective dimerization of resveratrol could be effected by careful control of the reaction pH using horse radish peroxidase as the oxidant. They found that they could selectively form δ-viniferin (**194**), a mixture of leachinol F/G (**203**), or pallidol (**199**) by

4.4.2 The Hou and Li Synthesis of Quadrangularin A via an Arene Protecting Group Strategy and Related Works

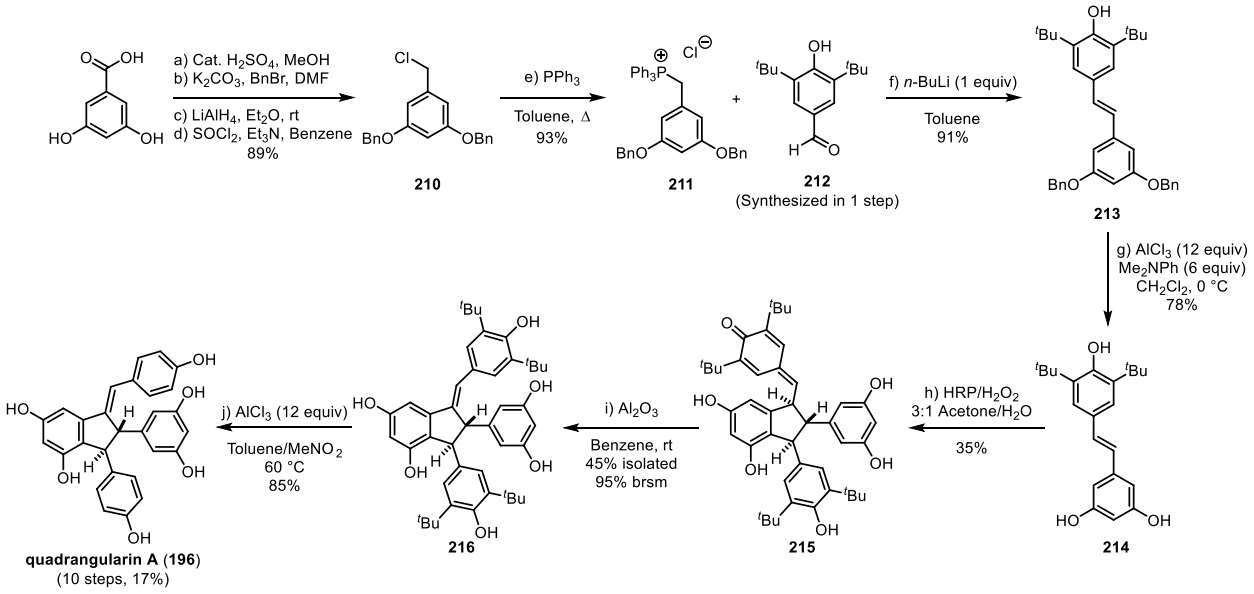

Figure 33 Hou and Li's biomimetic synthesis of quadrangularin A

successively lowering the reaction pH. They were able to report good isolated yields for **194**, but the other natural products suffered from poor mass recovery. These reaction conditions are the current state of the art for the chemoselective dimerization of resveratrol.

In 2006, Hou and Li reported the first biomimetic synthesis of the resveratrol dimer quadrangularin A (**196,** Figure 33). This report can be considered the first total synthesis of any resveratrol dimers, since previous biomimetic reactions were "shotgun" approaches and were discovered without a specific target in mind. Key to the success of their strategy was the use of flanking *tert*-butyl groups to protect the 4'-hydroxygroup of their resveratrol substrate **214**, which prevented undesired 3–8' coupling that thwarted previous synthetic efforts. The synthesis of **214** proceeded in 7 steps, starting from 3,5-dihydroxybenzoic acid to synthesize phosphonium salt (**211**) through the intermediacy of benzylchloride **210**. This was coupled with 4-hydroxy-2,6-di-*tert*-butyl benzaldehyde (**212**) via a Wittig reaction, followed by selective debenzylation of **213**,

Table 9 Chemoselective Dimerization of **214**

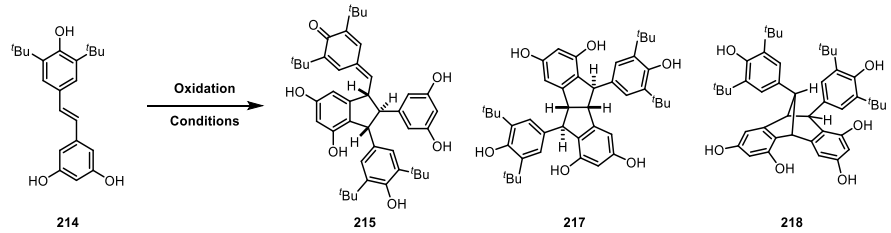

214 215 217 218

Entry	Reaction Conditions	215	217	218
1	Ag_2CO_3, CH_2Cl_2	59%[a]	—	—
2	MnO_2, CH_2Cl_2	54%[a]	—	—
3	$FeCl_3$•$6H_2O$, Benzene/Acetone 2:1	—	55%[a]	—
4	$FeCl_3$•$6H_2O$, CH_2Cl_2	—	—	45%[a]

[a] Reported as % conversion

yielding the desired stilbene **214** in ca. 59% overall yield. This substrate was subjected to the venerable horse radish peroxidase oxidation conditions described by Wallis,[181] affording the unusual hydroxylated cyclized *para*-quinone methide **215** in 35% yield.

Tautomerization of **215** to **216**, followed by de-*tert*-butylation with $AlCl_3$ afforded the desired natural product quadrangularin A (**196**) in 10 steps, in 17% overall yield. This seminal contribution highlighted several strategic advantages endowed by biomimetic synthesis. In particular, it was able to deliver **196** in high overall yield in just 10 steps. Expanding on their previous work, Li and co-workers reported a series of oxidations of chemoselective oxidation stilbene **214** using inorganic oxidants in several solvent systems.[182] This communication is in good agreement with the findings reported by Niwa and Velu, which suggest that solvent choice can have a profound effect on desired product distribution. This is undoubtedly improved by the presence of the *tert*-butyl groups found on **214**, which would aid in increasing product selectivity. When **214** was oxidized by 1 equivalent of either Ag_2CO_3 or MnO_2 in CH_2Cl_2, they observed 59% and 54% reaction conversion to quinone methide **215** with 64% and 76% recovered starting material, respectively (**Table 9**, Entries 1 and 2). Whereas $FeCl_3 \bullet H_2O$ in 2:1 mixture of benzene/acetone, produced a 55% reaction conversion to protected pallidol (**217**) with 45% recovery of starting material (Entry 3). Switching solvents from benzene/acetone to DCM, produced protected ampelopsin F (**218**) in 45% reaction conversion with 25% recovered starting material (Entry 4). In their disclosure, Li and co-workers report yields as reaction conversions and percent recovered starting material, but in several cases, these values add up to more than 100%, making yield estimation difficult. Deprotection of these adducts with $AlCl_3$, as previously described, cleanly converted these precursors to the desired natural products. The synthesis of ampelopsin F (**195**) is the first example of a selective, biomimetic synthesis of an 8–10’ dimer.

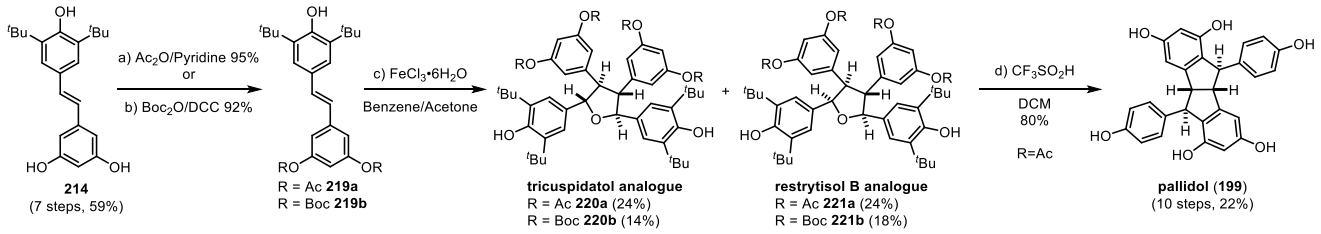

Figure 34 Li's synthesis of protected tetraarylfuran dimers

Finally, in 2014, the same group reported the synthesis of protected tricuspidatol/restrytisol analogues through the use of O–acylated protected congeners of stilbene **219** (Figure 34).[183] Using the dimerization conditions described in **Table 9**, entry 3, they were able to isolate the tetraaryl furan analogues of tricuspidatol (**220**) and restrytisol (**221**) as a 1:1 mixture of diastereoisomers in ~40% yield. Efforts to deprotect these intermediates were unsuccessful, only yielding the natural product pallidol (**199**) in 22% overall yield in 10 steps. The clean conversion of these protected analogues into pallidol may be of some biosynthetic relevance.

4.5 Introduction to the *De Novo* Synthesis of the Resveratrol Dimers

The previously described biomimetic syntheses provided very important insight to the reactions that are likely responsible for the generation of the resveratrol natural products in nature. From a synthetic point of view, however, this general strategy has failed to adequately address issues of reaction scalability as well as provide a reasonable route to further explore their development as pharmacologically active compounds. *De novo* synthesis provides key advantages over biomimetic approaches, since concerns over chemoselectivity and stereoselectivity are usually less problematic if the reaction sequence is properly designed. Shortly after the Hou and Li synthesis of quadrangularin A, Snyder and co-workers disclosed a series of

total syntheses of the resveratrol based natural product which raised the profile of resveratrol natural products in the general synthetic community. Since their initial publications, several groups have also made important contributions in the total synthesis of these natural products. The following sections will specifically highly *de novo* approaches towards the synthesis of indane containing dimers and oligomers, for a more comprehensive overview of the synthesis of other resveratrol natural products, please refer to the following reviews.[184–186]

4.5.1 Snyder's Synthesis of the Indane Containing Resveratrol Dimers

In 2007, Snyder and co-workers disclosed the a unified *de novo* synthesis of the indane containing resveratrol dimers quadrangularin A (**196**), pallidol (**199**), ampelopsin D (**222**), and ampelopsin F (**195**).[187,188] The strategy relied on the ionization triarylbenzhydyl alcohols (**223**/**224**) (prepared in 6 steps) with Brønsted acids to initiate an intramolecular cyclization as a means to rapidly generate the requite indane core (Figure 35, A). For the synthesis of quadrangularin A, benzhydryl alcohol **223** was ionized with TsOH generating indane cation **225** as an intermediate. This was intercepted by 4-methoxybenzylmercaptan yielding indane thioether **226** in 65% yield. Treatment with mCPBA oxidized **226** to the corresponding sulfone which was subsequently treated with KOH in *tert*-butanol/H_2O/CCl_4 under standard Ramberg–Bäcklund conditions, yielding permethyl quadrangularin A (**OMe-196**) in 39% yield. Treatment with BBr_3 afforded quadrangularin A (**196**) in 75%, in 10 steps with an overall yield of 13%. Permethyl quadrangularin A could be treated with NBS, to initiate a bromonium-mediated cyclization of **OMe-196,** through the intermediacy of quinone methide cation **227**, affording brominated permethyl pallidol (**228**) in 89% yield. Hydrogenation with Pd/C followed by alkylation afforded

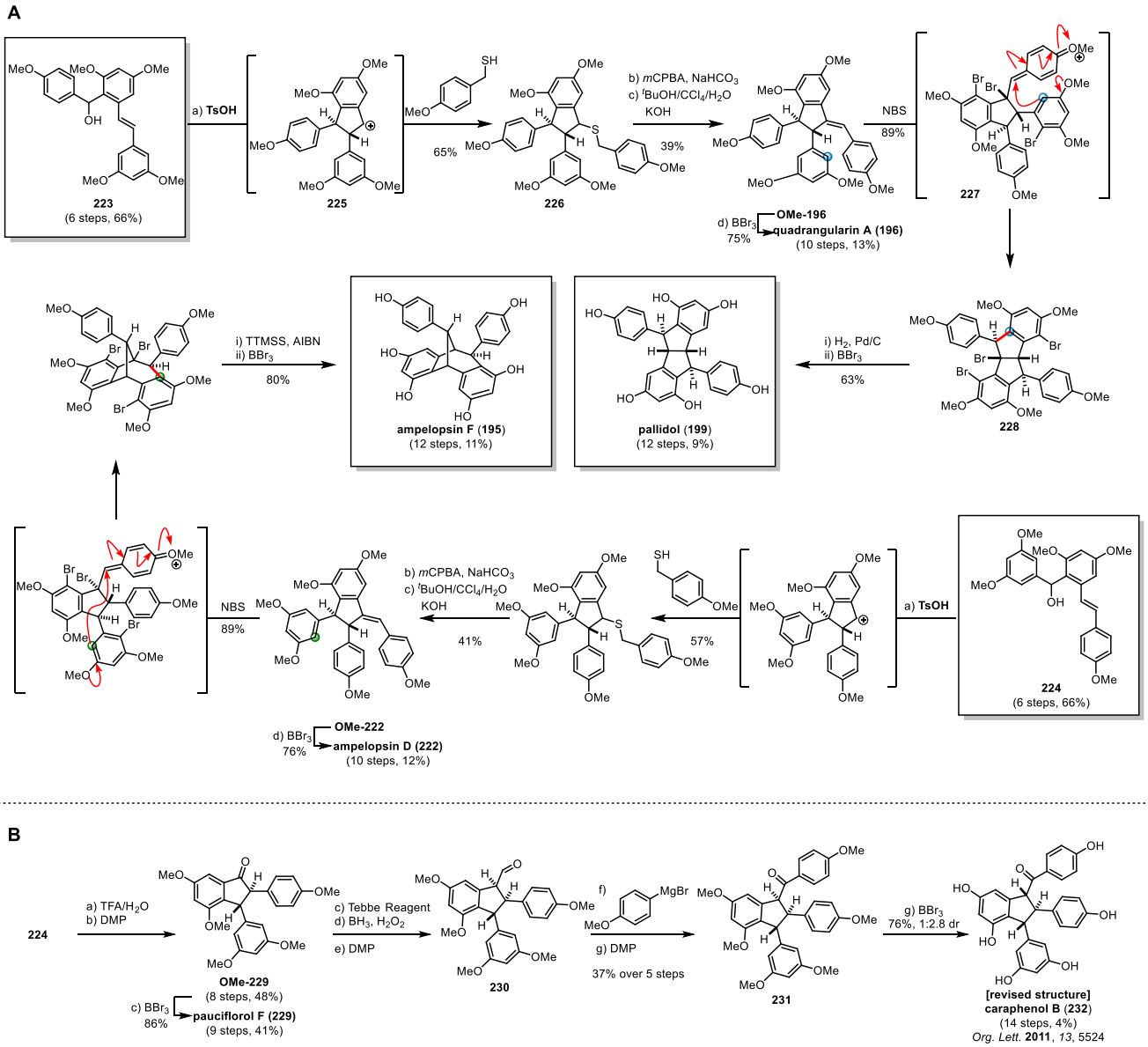

Figure 35 Snyder's unified approach to the 8–8' and 8–10' indane dimers

pallidol (**199**) in 12 steps in 9% overall yield. This strategy was applicable to the synthesis of ampelopsin D (**222**) and F (**195**) through an analogous approach starting from benzhydryl alcohol **224** affording ampelopsin D in 10 steps/12% overall yield and ampelopsin F in 12 steps in 11% overall yield. When treated with acid in the presence of water, followed by oxidation with Dess-Martin periodinane (DMP), **224** could be converted into the truncated indanone pauciflorol F (**229**, Figure 35, B) in 8 steps in 48% overall yield. Synthesis of its regioisomer isopauciflorol F (not depicted) was also synthesized in the same way. These indanone intermediates have been subsequently used in the synthesis of oxidized indane dimers caraphenols A and B through a formal homologation of **OMe-229** via a Tebbe olefination, followed by hydroboration/oxidation sequence yielding aldehyde **230**. Nucleophilic addition of 4-methoxyphenylmagnesium bromide to **230**, followed by DMP oxidation yields permethyl *epi*-caraphenol B (**231**). Treatment of **231** with BBr_3 initiates a global demethylation and epimerization of ketone **231** to the *trans,trans*-indane dimer caraphenol B (**232**, Figure 35, B). The same reaction sequence starting from benzyhydryl alcohol **223** affords caraphenol A in the same fashion. The flexibility granted by this route enable confirmation of the structures of caraphenols A and B, which had previously been misassigned.[189]

This clever strategy has since been employed in the synthesis of several non- indane containing resveratrol oligomers including hopeanol (**233**), hopeahainol A (**234**),[190] heimiol (**235**), hopeahainol D (**236**),[191] and ampelopsin G (**237**).[188] The highly modular nature of this approach also enable the synthesis of several structural analogues which would be difficult to synthesize in any other way. The influence of this work cannot be overstated and truly provided a framework by which this class of natural products could be synthesized rationally.

4.5.2 Sarpong's Palladium-Mediated Synthesis of the Cores of Quadrangularin A and Pallidol

Two years after the Snyder's seminal contribution, Sarpong and co-workers reported an alternate strategy towards the synthesis of quadrangularin A and pallidol using a Larock-type annulation. Starting from bromopermethyl resveratrol **238** and tolane **239**, Sarpong and co-workers anticipated that the benzofulvene **241** could be synthesized through a palladium-mediated cyclization cascade (Figure 36).[192] This was realized using a $Pd^{0/II}$ catalytic system wherein

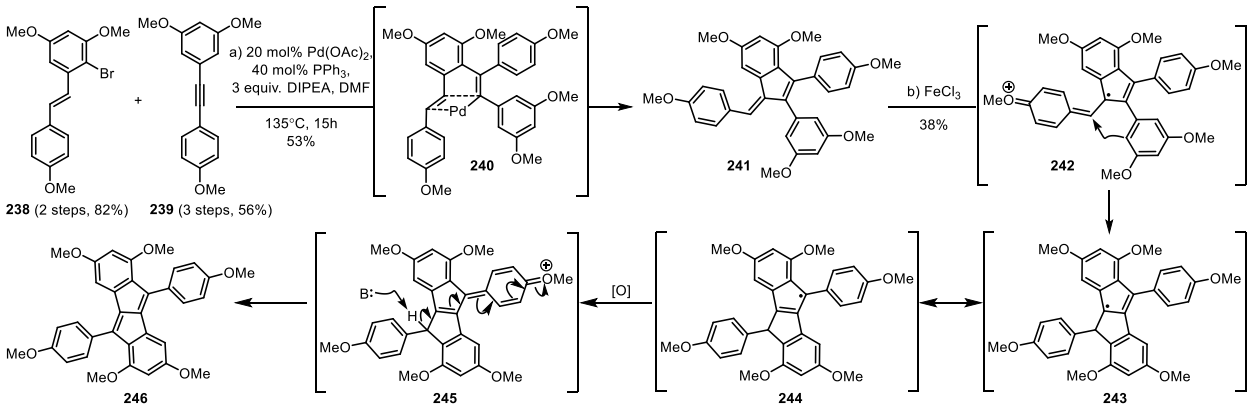

Figure 36 Sarpong's palladium-mediated cyclization cascade

palladium could oxidatively insert into C–Br bond of **238**, forming an aryl Pd(II) intermediate. This could then undergo an intermolecular migratory insertion with **239** forming intermediate **240**. A second, intramolecular cyclization on the pendant stilbene, followed by β–hydride elimination afforded permethylbenzofulvene **241** in 53% yield, a desaturated analogue of quadrangularin A. Reacting **241** with $FeCl_3$ induces an oxidative Scholl reaction in 38% (through intermediates **242**–**245**), producing tetradehydropermethyl pallidol (**246**). Although this particular synthetic strategy did not result in the synthesis of the actual natural products, they are a demonstration of a novel

approach towards the construction of these unusual molecular architectures. The judicious use of tolane **239** to differentiate between intermolecular heteroannulation with **238** vs homocoupling was particularly elegant from a strategic standpoint. They were able to extend this strategy towards the synthesis of pauciflorol F (**229**) in a later publication.[193]

4.5.3 Studer's Synthesis of the Indane Dimers via an Oxidative Heck Reaction

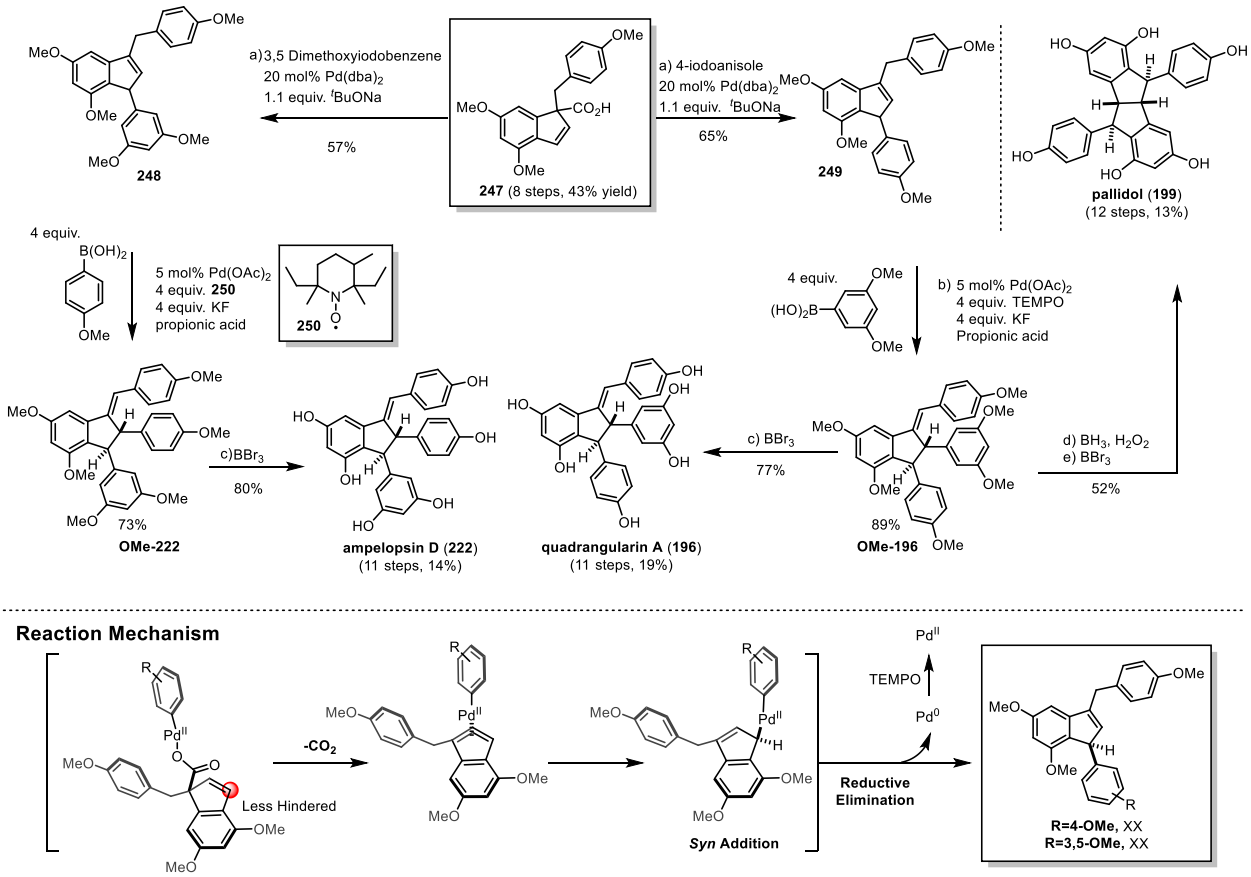

Figure 37 Studer's synthesis of the indane dimers via successive palladium-mediated arylation reactions

In 2014, Studer and co-workers described a novel *de novo* synthesis of the 8–8' and 8–10' indane dimers (Figure 37).[194] Their key reaction employed the use of a stereospecific, decarboxylative Heck reaction developed previously.[195] Starting from indene carboxylate **247**, they could divergently synthesize tetraaryl indenes **248** or **249** using $Pd(dba)_2$ and the corresponding aryliodide in 57–65% yield. A subsequent TEMPO or derivative **250**-mediated oxidative Heck reaction of indenes **248** and **249** occurs stereoselectively, presumably approaching from the less hindered face. The resulting β-hydride elimination only forms the *E*-alkene due to minimization of $A_{1,3}$ strain, affording permethyl ampelopsin D (**OMe-222**) or permethylquadrangularin A (**OMe-196**) in high yield. These intermediates can be deprotected[187] or in the case of **OMe-196**, interconverted[196] into other resveratrol through processes reported previously.

4.5.4 Concluding Remarks

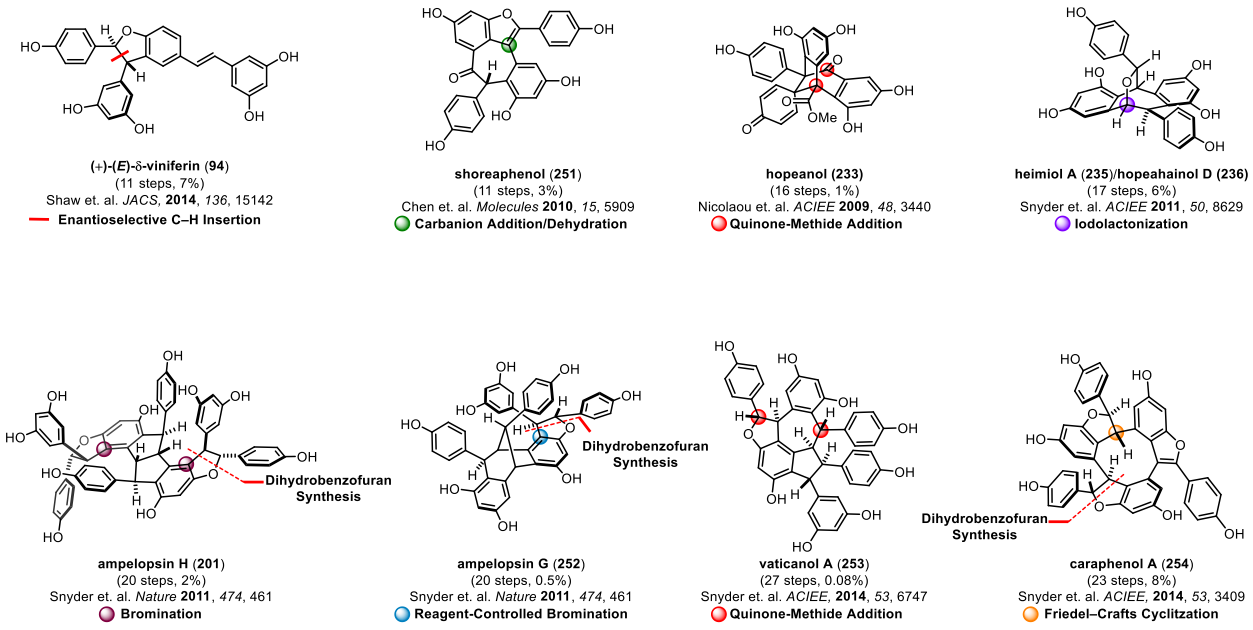

Figure 38 Selected synthesis of complex resveratrol oligomers

The last 10 years has witnessed a renaissance in the biomimetic and *de novo* synthesis of the resveratrol oligomers. Several creative strategies from leading synthetic groups have culminated in the synthesis of many of the molecular architectures found within this diverse class of natural products (Figure 38). While it is undeniable that many of these molecular architectures can be synthesized, there are several synthetic challenges that remain. For instance, the incorporation of the 2,3-diaryl-dihydrobenzofuran motif that is ubiquitous within the natural product family is a curiously difficult transformation that requires anywhere from 5 to 9 steps. Enantioselective synthesis of the resveratrol oligomers is also difficult, with Shaw[197] and Nicolaou[198] providing the only reports detailing enantioselective synthesis of complex dimers. Finally, the synthesis of higher order oligomers, while possible, still demands a relatively large number of synthetic steps. Nevertheless, the progress in both biomimetic and *de novo* syntheses will be instrumental in future research concerning their biological and antioxidant properties.

4.6 Our Synthetic Strategy Towards Quadrangularin A and Pallidol

Our interest in the synthesis of resveratrol oligomers was influenced by efforts within our group in the then nascent field of photoredox catalysis. During this period, research within the context of photocatalysis was primarily devoted to the development of redox neutral processes[17,19] and net reductions using the reductive quenching cycle.[21,139,199] Although there were reactions describing a net photocatalytic oxidation,[200,201] this strategy had been underdeveloped, particularly within the context of natural product synthesis. The oligomerization of resveratrol is known to occur through a radical coupling of phenoxyl radicals generated from by oxidation. Since polypyridyl photocatalysts such as $Ru(bpy)_3$ can be easily quenched by electron rich aromatic substrates,[24] the synthesis of the resveratrol oligomers presented an intriguing opportunity to implement oxidative photoredox catalysis in the context of complex molecule synthesis.

The use of a photosensitizer to oxidize resveratrol or a derivative therefrom presented a few significant challenges from a reaction design standpoint. Photocatalysts such as $Ru(bpy)_3$ can undergo unproductive side reactions with the substrate, readily isomerizing stilbenes,[202] sensitizing the formation of singlet oxygen,[203] which can cleave the electron rich alkene in stilbenes,[204] and undergoing uncontrolled over oxidation of both starting materials and products. Nonetheless, the use of photoredox catalysis was envisioned to address several problems associated with previous biomimetic synthetic endeavors. This usually entailed the introduction of the stoichiometric oxidant is one portion, making it difficult to control the oxidation reaction beyond reagent and/or solvent choice. Using photoredox catalysis, on the other hand, provides options to select the desired oxidation strength of the catalyst and properties of the desired terminal oxidant. Parallel research in the development of organic LEDs and water splitting catalyst by the broader chemical community resulted in the synthesis and characterization of hundreds of complexes that can act as effective photoredox catalysts. The photophysical properties such as excited state potentials, ground state potentials, excited state lifetimes and extinction coefficients have been rigorously characterized and catalogued for several photocatalysts. The oxidation step can either be achieved through the direct quenching of the excited state of a photocatalyst (PC*) or by oxidation of the substrate by the grounds state of the oxidized catalyst (PC^{n+1}) (Figure 1). Catalyst selection would therefore be dictated by the oxidation potentials of the photocatalysts excited state or its oxidized ground state. An additional consideration was choosing the appropriate terminal oxidant. There are several classes of electron acceptors including nitroarenes, viologens, alkylhalides, molecular oxygen, and others,[23,24] which upon reduction by the photocatalyst, can generate radical intermediates that have the potential to interfere with the desired dimerization reaction. Knowing

the mechanism of quenching, and the byproducts generated therefrom, can guide reagent selection, and mitigate unwanted side reactivity.

With these considerations in mind, our intention was to synthesize protected intermediates **256** and **258** (vida infra), which would undergo dealkylative deprotection to elaborate the natural products quadrangularin A **196** and pallidol **199**. This work would ultimately provide the framework for the biomimetic synthesis of more complex and biologically intriguing resveratrol timers and tetramers.

4.6.1 Development of a Highly Scalable, Biomimetic Dimerization of A Tert-Butylated Resveratrol Analogue

The dimerization of 2,6-di-*tert*-butyl resveratrol **215** was indeed possible but there were significant disadvantages concerning the scalability, yield, and chemoselectivity of the oxidation step. The use of enzymes or stoichiometric oxidants is not necessarily detrimental in its own right, unless they do not provide benefits in terms of yield or reaction selectivity. In this regard, there was an opportunity to significantly improve existing biomimetic strategies for a practical synthesis of these fascinating molecules. With these considerations in mind, we initiated our lab's synthetic research within this fascinating class of natural products, an endeavor which as subsequently joined by my exemplary colleague Mr. Mitchell Keylor, whose efforts were instrumental in the planning and execution of the following work.

Initial studies on the biomimetic synthesis of quadrangularin A began using alkylated resveratrol derivative **255**. This substrate was readily synthesized in two steps from commercially available 3,5-dimethoxybenzylbromide and 3,5-di-*tert*-butyl-4-hydroxybenzaldehyde through the Wittig reaction. Initial screening with $Ru(bpy)_3Cl_2$ using bromotrichloromethane or ammonium persulfate as oxidative quenchers revealed significant decomposition of **255** into an intractable

mixture of products (Entries 1 and 2, Table 10). This finding is perhaps unsurprising since the reduction of $BrCCl_3$ or persulfate by the excited state of $Ru(bpy)_3^{*2+}$ ($E_{1/2}^{II*/I}$ = -0.81V vs SCE)

Table 10 Optimization of the Oxidative Resveratrol Dimerization

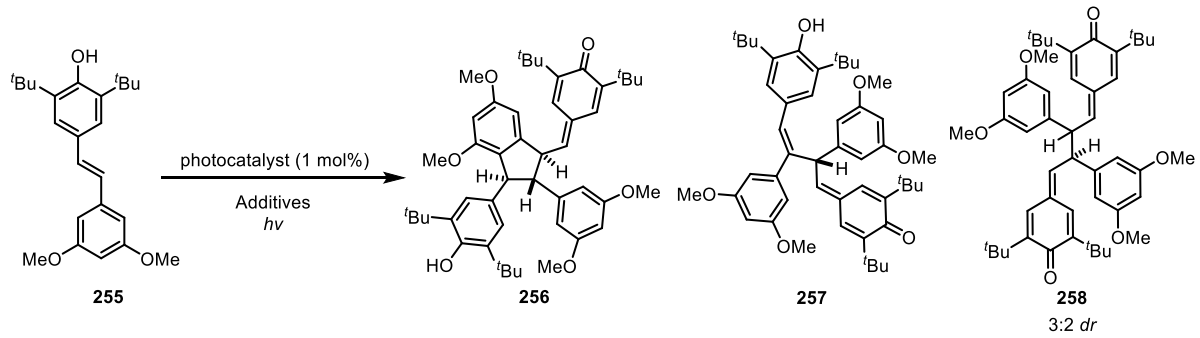

Entry	Photocatalyst	Solvent	Oxidant	Additive	Time	Yield	Product
1	$Ru(bpy)_3Cl_2$	MeCN	$BrCCl_3$	—	12h	Decomp.	—
2	$Ru(bpy)_3Cl_3$	MeCN	$(NH_4)_2S_2O_8$	—	2h	Decomp.	—
3	$Ir(tpy)_2(PF_6)_3$	MeCN	O_2	—	2d	7%[a]	**256**
4	$Ir(ttpy)(tpy)(PF_6)_3$	Acetone	O_2	—	2d	38%	**256**
5	$Ir(ttpy)(tpy)(PF_6)_3$	Acetone/MeOH	O_2	NaOMe	5h	47%	**257**
6	—	Acetone/MeOH	Degassed	NaOMe	2h	100%	E/Z **255**
7[b]	—	Acetone/MeOH	Degassed	NaOMe	2h	—	**255**
8[b]	$Ir(ttpy)(tpy)(PF_6)_3$	Acetone/MeOH	O_2	NaOMe	5h	45%	**257**
9[b]	—	Acetone/MeOH	O_2	NaOMe	2h	55%	**257**
10[b]	—	CCl_4	O_2	KO^{t}Bu	1h	60-80%	**258**
11[b]	—	THF	Cp_2FePF_6	KHMDS	30min	98%	**258**
12	$Ir(dF\{CF_3\}ppy)_2(dtbbpy)PF_6$	CCl_4	CCl_4	—	3d	0%	**—**

[a] Incomplete conversion
[b] Reaction was shielded from light

yields highly reactive, electron deficient trichloromethyl or sulfate radicals, respectively. These intermediates are expected to be indiscriminately reactive, operating through Fenton-type C–H abstraction of substrate, solvent, or catalyst.[205] Additionally, polyhaloalkyl radicals are known to be efficient substrates for atom transfer radical addition chemistry (ATRA) with stilbenes,[206] potentially diverting **255** from its desired reactivity. In order to circumvent this undesirable side reactions associated with the use of traditional oxidative quenchers, it was necessary to identify a suitable catalyst with an excited state that could directly oxidize substrate **255**. The first successful dimerization of **255** was realized using oxygen as the terminal oxidant and the triply cationic,

homoleptic iridium complex developed by Flamigni and co-workers, $[Ir(tpy)_2](PF_6)_3$ (Entry 3, Table 10).[207] This photocatalyst is well situated specifically for excited state oxidation since it possesses an extremely low excited state reduction potential ($E_{1/2}^{III*/IV}$ = -0.3V vs SCE) which is unlikely to reduce molecular oxygen ($E^{O_2/O_2^{\bullet-}}$ = -0.78V vs SCE in acetone)[208] but has a very strong excited state oxidation potential ($E_{1/2}^{IV/III*}$ = +1.9V vs SCE) which is more than sufficient for the oxidation of **255** (Figure 39). Accordingly, the return potential of the reduced ground state of $[Ir(tpy)_2](PF_6)_3$ can reduce O_2, regenerating the catalyst. Using 1 mol% $[Ir(tpy)_2](PF_6)_3$ in the presence of substrate **255** in acetone yielded **c**yclized ***para*-q**uinone **m**ethide (henceforth referred to as CPQM) **256** in only 7% yield with 37% recovered starting material over a period of 3 days. The sluggish reaction rate and low yield was attributed to the poor absorption of $[Ir(tpy)_2](PF_6)_3$ in the visible light region. In order to address this, we implemented a modified heteroleptic catalyst $[Ir(ttpy)(tpy)](PF_6)_3$ (Figure 39). This catalyst has a redshifted absorption spectra and higher extinction coefficient than $[Ir(tpy)_2](PF_6)_3$ due to the extended π system of the terpyridine ligand. Accordingly, this catalyst converted **255** to **256** in 38% yield within the same time period (Entry 4, **Table 10**).

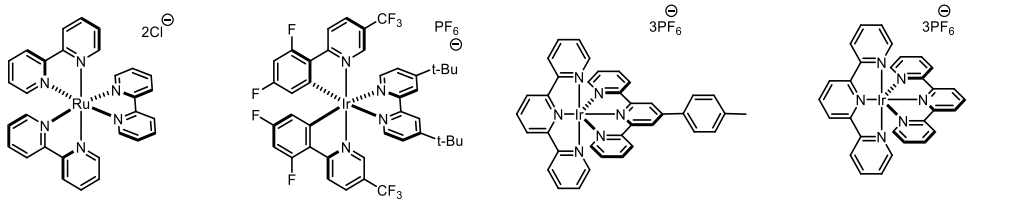

$Ru(bpy)_3Cl_2$

Excited State Potentials
$E_{1/2}^{II*/I}$ = +0.77V vs SCE
$E_{1/2}^{III/II*}$ = -0.81V vs SCE
Ground State Potentials
$E_{1/2}^{II/I}$ = -1.33V vs SCE
$E_{1/2}^{III/II}$ = +1.29V vs SCE

$Ir[(dF\{CF_3\}ppy)_2(dtbbpy)]PF_6$

Excited State Potentials
$E_{1/2}^{III*/II}$ = +1.21V vs SCE
$E_{1/2}^{IV/III*}$ = -0.89V vs SCE
Ground State Potentials
$E_{1/2}^{III/II}$ = -1.37V vs SCE
$E_{1/2}^{IV/III}$ = +1.69V vs SCE

$Ir[(ttpy)(tpy)](PF_6)_3$

Excited State Potentials
$E_{1/2}^{III*/II}$ = +1.79V vs SCE
$E_{1/2}^{IV/III*}$ = -0.7V vs SCE
Ground State Potentials
$E_{1/2}^{III/II}$ = -0.81V vs SCE
$E_{1/2}^{IV/III}$ = >+2.4V vs SCE (est.)

$Ir[(tpy)_2](PF_6)_3$

Excited State Potentials
$E_{1/2}^{III*/II}$ = +1.9V vs SCE
$E_{1/2}^{IV/III*}$ = -0.3V vs SCE
Ground State Potentials
$E_{1/2}^{III/II}$ = -0.77V vs SCE
$E_{1/2}^{IV/III}$ = >+2.4V vs SCE (est.)0

Figure 39 Catalyst structure and electrochemical potentials

Although the yield of the dimerization was competitive with precedented oxidations, the yield, scalability, and reaction rate were all aspects that needed improvement. The reasons for the poor reaction performance were likely due to the highly reversible nature of the single electron transfer chemistry. We hypothesized that this issue could be overcome through the deprotonation of **255** to its corresponding phenoxide, which would have a significantly lower reduction potential. The pH dependence on reduction potential of resveratrol had been previously reported by Corduneanu and co-workers, which shows that its redox potential decreases as the solution's pH increases and vice versa (Figure 40) .[209] This hypothesis proved to be fortuitous; when **255** was dissolved in a 4:1 mixture of acetone/MeOH and deprotonated with 4 equiv. NaOMe, the reaction proceeded in only 5 hours in 45% yield (Entry 5, Table 10). These conditions revealed an interesting solvent effect since the isolated product was not the CPQM **256**, but rather a **l**inear **m**ono**q**uinone **m**ethide **257** (henceforth referred to as LMQM).

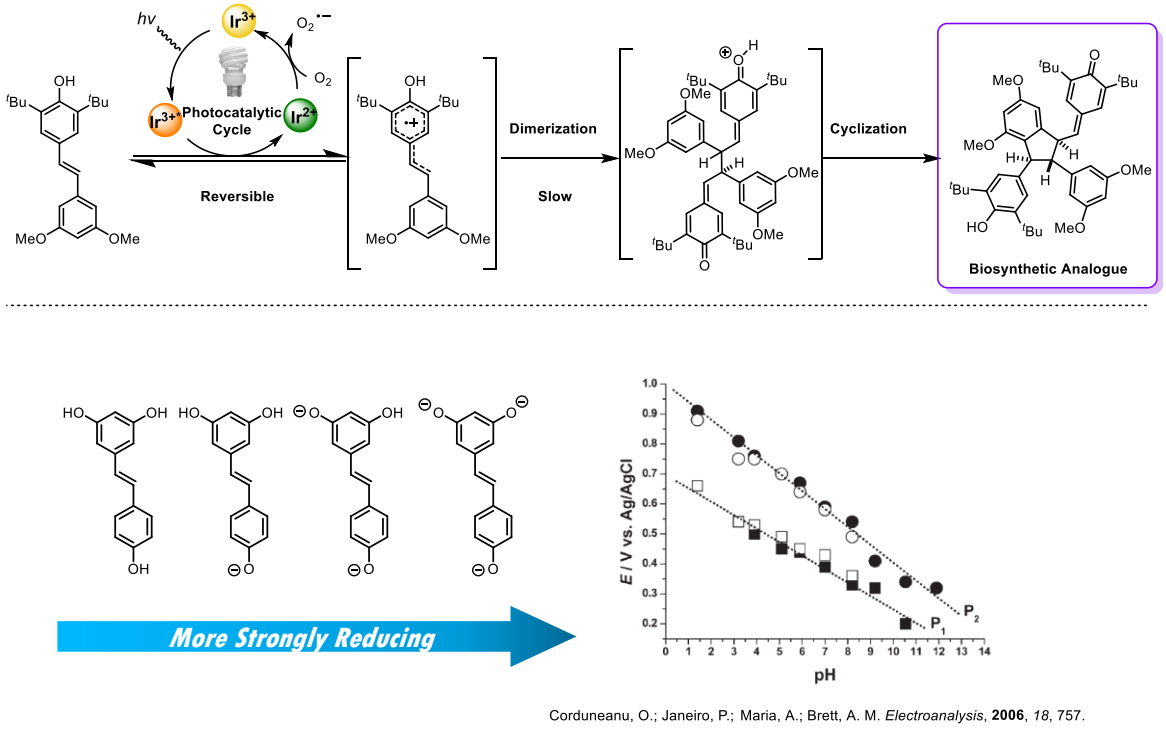

Corduneanu, O.; Janeiro, P.; Maria, A.; Brett, A. M. *Electroanalysis*, **2006**, *18*, 757.

Figure 40 pH Dependence on the oxidation potential of resveratrol

The deprotonation was accompanied by a dramatic change in reaction color from a light yellow to a dark green upon the addition of NaOMe. Intrigued by this observation, a series of control reactions were ran (Entries 6–9, Table 10). These experiments revealed that the photocatalyst *wasn't* needed in basic conditions and that the phenoxide of **255** was a sufficiently strong reductant to directly reduce molecular oxygen (Entry 8, Table 10). The phenoxide of **255** was also found to be photoactive in the visible region, and readily underwent E/Z isomerization (Entry 6, Table 10), and could also sensitize the formation of singlet oxygen resulting in oxidative cleavage of the stilbene into is constituent aldehydes (Not Depicted). This was observed qualitatively in previous photocatalytic reactions where the oxidative dimerization of **255** did not appear to occur until E/Z ratio of **255** achieved a photostationary state.[210] The exclusion of light and photocatalyst increased the reaction rate and yield significantly (Entry 9, Table 10), by suppressing singlet oxygen sensitization and stilbene isomerization. Using these principles, the aerobic oxidation of **255** using KO^{t}Bu as a base in CCl_4 dramatically decreased the reaction time to 1 hour, forming an unusual **l**inear **b**is-*para*-**q**uinone **m**ethide **258** (henceforth LBQM) in 60–80% yield(Entry10, Table 10). These benefits were attributed to the increased solubility of O_2 in non-polar, aprotic, halogenated solvents.[211]

Although these reaction conditions were capable of producing gram quantities of LBQM **258**, the aerobic oxidation of **255** in CCl_4 suffered from poor reliability. Since the terminal oxidant was O_2, reaction surface to volume ratio, oxygen presaturation, KO^{t}Bu water content, and even stirring rates could dramatically change the reaction profile. The solution to these limitations turned out to be surprisingly simple. Deprotonation of **255** with 1.05 equiv. of KHMDS in

degassed THF, followed by addition of 1.25 equiv. of the mild outer sphere oxidant, ferrocenium hexafluorophosphate, yielded the desired LBQM **258** in essentially quantitative yield as a 1.4:1 mixture of diastereomers. This reaction is highly scalable; the synthesis of 10 grams of **213** was achieved in a single batch reaction in 98% yield.

4.6.2 Studies on the Reactivity of Stable Quinone Methides and the Completion of the Syntheses of Quadrangularin A and Pallidol

The dimerization studies on substrate **255** revealed several interesting properties of the isomeric quinone methides **256**, **257**, and **258**. Dimerization of **255** in pH neutral, polar/aprotic solvents favored the formation of CPQM **256** as the major product, while dimerization in protic, basic media favored the formation LMQM **257**, and dimerization in basic conditions in non-polar solvents exclusively LBQM **258**. These structures represent stable synthetic analogues of the postulated biosynthetic intermediates of the 8–8' dimers (**192**, **202, 203**, Figure 31). These *para*-quinone methides possess remarkable stability – are resistant to nucleophilic attack by water and alcoholic solvents, and are indefinitely bench stable at room temperature. Although we had developed three separate reaction conditions that could selectively favor the formation of all three isomers **256**, **257**, and **258**, the only practical procedure of the three produced the LBQM. From the outset, this intermediate appeared to be ideal to synthesize pallidol through a double intramolecular Friedel–Crafts cyclization reaction. However, it was unclear whether LBQM **258** could be selectively isomerized to CPQM **256** or LMQM **257** en route to quadrangularin A **196**.

The reactivity of **258** was unexpectedly predictable and would readily cyclize upon exposure to simple Brønsted or Lewis acids. For instance, upon exposure to 4 equiv. of BF_3•OEt_2 in DCM at -78°C, OBn-**258** cyclizes into CPQM OBn-**256** and protected pallidol derivative **259** as a 60:40 mixture of isomers in nearly quantitative combined yield. This product distribution

presumably reflects the diastereomeric ratio of **OBn-258**. The Friedel–Crafts reaction highlights the unique reactivity of the *tert*-butylated quinone methides, which possess exceptional stability under neutral conditions but retain their electrophilic reactivity in the presence of an acid. For instance, when exposed to 1.25 equiv. of KHMDS in THF, LBQM **OBn-258** converts into LMQM **OBn-257** in essentially quantitative yield as a single alkene isomer, likely due to the minimization of allylic strain. Exposure of LMQM OBn-**257** to 4 equivalents BF_3•OEt_2 in DCM at -78°C initiates an intramolecular Friedel–Crafts cyclization generating protected quadrangularin A adduct **OBn-259** in quantitative yield. This approach to **OBn-259** circumvents the problem of isomerizing the protected CPQM **OBn-256** which occurs with poor conversion. When dissolved in 1µl/mL TFA in $MeNO_2$, LBQM OBn-**256** quantitatively converts to CPQM **OBn-256** as a single diastereoisomer (see below for mechanism).

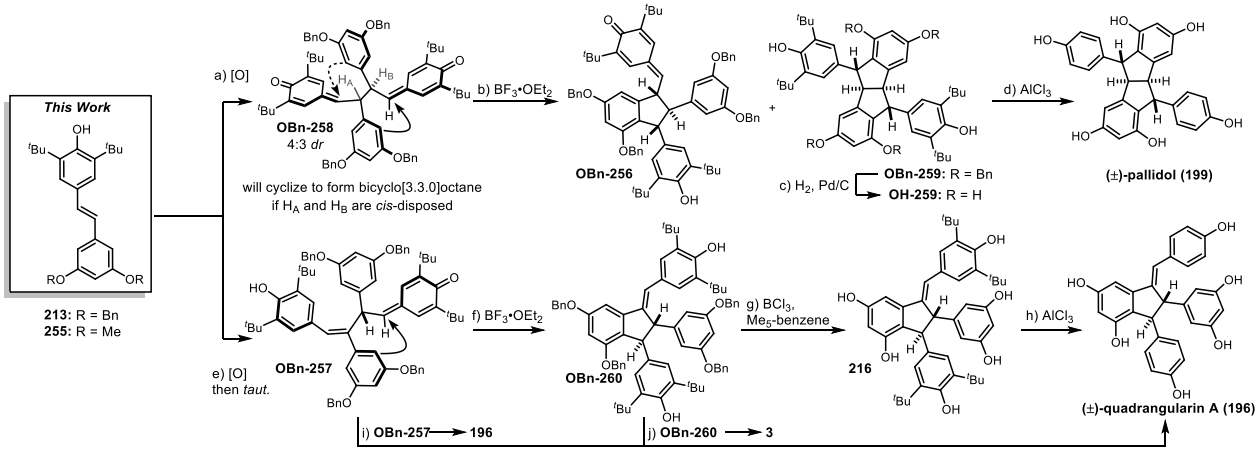

Figure 41 The synthesis of quadrangularin A and pallidol

With methods to convert stilbene **213** into all three isomeric dimers **OBn-258**, **OBn-257**, and **OBn-256**, we set out to complete the synthesis of quadrangularin A and pallidol through the

intermediacy of the LBQM (Figure 41). For this task, we elected to use the *O*-benzylated congeners for ease of deprotection. The synthesis of stilbene **213** was achieved starting from 3,5-dibenzyloxybenzyl bromide in 81% yield over two steps. **213** was deprotonated with 1.05 equiv. of KHMDS in THF followed by addition of 1.05 equiv. of ferrocenium hexafluorophosphate, yielding LBQM **OBn-258** in >95% yield as a 4:3 mixture of diastereomers. Addition of 4 equivalents of BF_3•OEt_2 in DCM at -78°C initiated the double Friedel–Crafts cyclization cascade forming the fully protected pallidol **OBn-259** core in 43% yield. Hydrogenolysis of the benzyl ethers with Pd/C followed by an $AlCl_3$-mediated de-*tert*-butylation of **OH-259** yielded pallidol **199** in 27% overall yield, starting from **213**. Quadrangularin A was synthesized in a similar fashion *via* the base mediated oxidative dimerization of **213**. We elected to synthesize protected quadrangularin A **(196)** through the intermediacy of LBQM **OBn-258** instead of CPQM **OBn-256**, since the isomerization of the latter suffers from poor reaction conversion.[212]

We found that the synthesis of LBQM **OBn-258** could be achieved in one step by adding an additional 1.25 equiv. of KHMDS the dimerization reaction after the addition of $FeCp_2PF_6$ with no loss in yield. This material was filtered over silica with hexanes, to wash out ferrocene, and used as a semicrude material for the subsequent BF_3•OEt_2 cyclization yielding the protected quadrangularin A derivative **OBn-260** in 90% yield over the two operations. At this stage, hydrogenolysis of the benzylethers was not possible due to the presence of the electron rich alkene. While Lewis acidic reagents such as BBr_3, $AlCl_3$, and TMSI were capable of debenzylating **OBn-260**, their use resulted in low yields, presumably due to O-to-C transfer and other degradation pathways via a Friedel–Crafts process. To circumvent this issue, we employed the use of BCl_3 in DCM using pentamethylbenzene as a cation scavenger. This reaction provided a remarkably clean reaction profile and could debenzylate **OBn-260** in 82% yield on large scale. Unlike other

commonly used cation scavengers such as *N,N*–dimethyl aniline, thiophenol, or dimethoxybenzene, pentamethylbenzene does not contain Lewis basic sites that can interact with the BCl_3 and therefore lower the reactivity of the reagent. De-*tert*-butylation of **216** occurred predictably using $AlCl_3$ in toluene/$MeNO_2$ affording quadrangularin A in 6 steps with a 48% overall yield.[213,214] The robust reactivity of the Lewis acid cyclization and deprotection chemistry led to the development of two shorter routes that using slightly modified deprotection conditions. For instance, the global deprotection of **OBn-260** using $AlCl_3$ and pentamethylbenzene in toluene/$MeNO_2$ afforded quadrangularin A in 88% yield as a 5:1 mixture of alkene isomers, for an overall yield of 54%. These reaction conditions were able to directly convert LBQM **OBn-257** in to the final product in 51% yield for a synthetic sequence of only four steps. With the completion of our synthesis of quadrangularin A and pallidol, we were now able to provide material for our collaborator Prof. Derek Pratt and evaluate the antioxidant properties of these resveratrol oligomers. Our synthetic strategy has the best overall yield and the fewest total steps for both

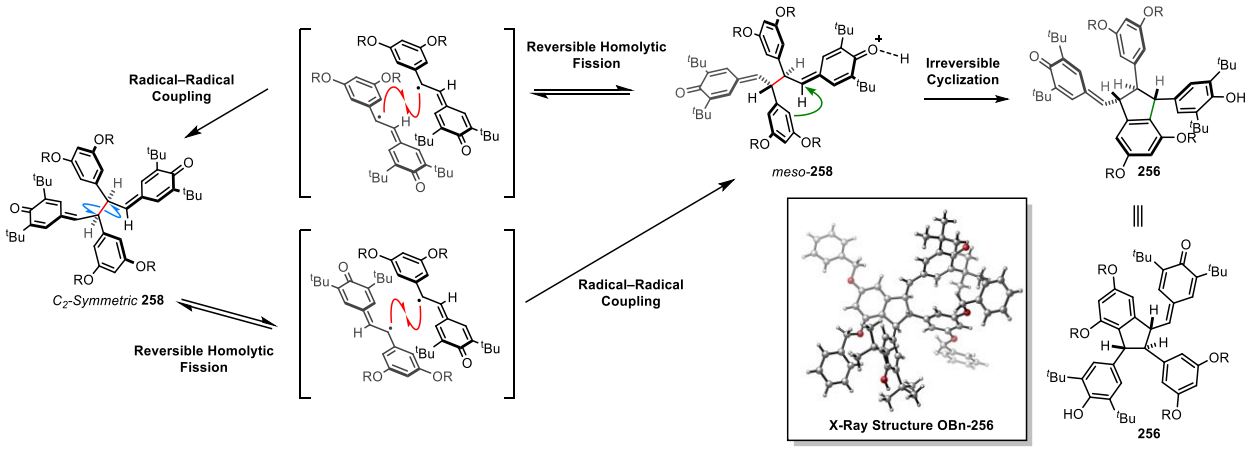

Figure 42 The mechanism of the stereoconvergent cyclization of **258** to **256**

pallidol and quadrangularin A. The scalability of all steps within the synthetic sequence was essential for the evaluation of the antioxidant properties of these compounds since getting reliable kinetic data for their oxidation rates required millimolar quantities of all intermediates.

The conversion of **258** into **256** is remarkable and is worth discussing. This process, which is performed on a 1.4:1 mixture of diastereomers is stereoconvergent (Figure 42). At a glance, the reaction mechanism appears to be the result of a Brønsted acid-mediated dynamic interconversion of *rac*-**258** into its *meso* diastereomer followed by intramolecular Friedel–Crafts cyclization yielding **256**. In this scenario, the epimerization of **258** would logically occur through the intermediacy of LMQM **257**. However, under the same conditions, independently prepared LMQM **257** is completely unreactive and is recovered quantitatively from the reaction mixture, suggesting that the epimerization mechanism that is not a simple tautomerization. During his studies on the reversible quinone oxidations, Becker described the synthesis and characterization of a series of linear bis *para*-quinone methides of 2,6-di-*tert*-butyl-4-hydroxyl stilbene.[215] He found that this linear bis *para*-quinone methides were paramagnetic in solution at room temperature due to a highly unusual equilibrium between the dimeric LBQM and the monomeric radical. The dimer–radical equilibrium was determined to be 2.0×10^{-2} favoring the dimer at room temperature. These results suggest that a similar process is operative here. The diastereomeric ratio between *C_2-symmetric* and *meso*-**258** is a reflection of the thermodynamic equilibrium of both stereoisomers at room temperature, and the cyclization of **258** to CPQM likely occurs through the selective cyclization of *meso*-**258**, funneling to a single product through an epimerization of the *C_2-symmetric* diastereomer via a homolytic cleavage/radical recombination mechanism.

4.7 Evaluation of the Antioxidant Properties of Resveratrol, Quadrangularin A, Pallidol, and its Congeners

Oxidative stress embodies a cellular or physiological imbalance between the generation reactive oxygen species such as free radicals and the ability of the biological system to prevent or repair the resulting damage. The cellular damage due to reactive oxygen species is implicated in the pathology of several major disease classes – ranging from cardiovascular disease[216] and cancer,[217] to Alzheimer's[218] and diabetes. On a cellular level, oxidative stress has been implicated in the disruption of numerous biological processes including cell signaling, gene regulation,[219] aging,[220] and mutagenesis. Although the pathology of these conditions are unimaginably complex, the conspicuous role of oxidative stress in disease progression has stimulated intense scientific research in the development of antioxidant therapies to offset the damage caused by reactive oxygen species. Despite these efforts, the efficacy of antioxidant therapy is highly controversial and it is unclear if they provide any beneficial effects. One the largest obstacles in developing effective antioxidant therapies is the lack of a standardized protocol to evaluate the antioxidant properties of small molecules, making the direct comparison between therapies difficult. Furthermore, there is an inadequate understanding of the mechanisms of action of these molecular therapies, hindering drug development and advancement within this field.

The introduction and identification of resveratrol as a therapeutic 'antioxidant' came at a particularly auspicious time when the connections between oxidative stress and degenerative diseases were being made. In particular, it appeared that the seemingly distant issues concerning alcohol consumption, oxidative stress in CVD, and the "French Paradox" could be explained by the consumption of dietary resveratrol and its ability to prophylactically prevent damage caused by oxidative stress. These results emboldened the notion that antioxidants, in particular dietary phytochemicals such as α-tocopherol, ascorbic acid or curcumin, could also be used to prevent or

treat other degenerative diseases through this same mode of action, resulting in an explosion in antioxidant research. Resveratrol itself received a nearly anointed status as a molecule that could be used to prevent cancer,[152] diabetes,[154] cardiovascular disease,[221] and even aging.[155] Over time, this groundswell of excitement was soon abated as research began to yield unreliable and contradictory results, leading many to question the validity of this therapeutic approach.[146,222,223] Although the are several reasons for this state of affairs, a particularly troubling explanation questions the ability of resveratrol to even act as an antioxidant under biologically relevant conditions.

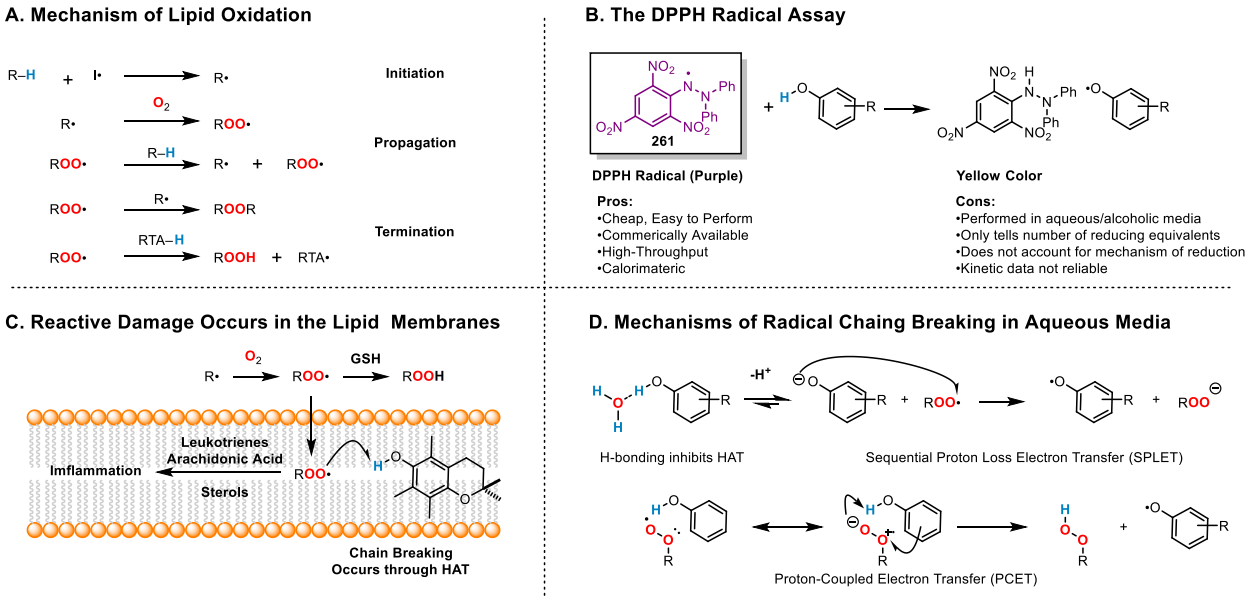

Figure 43 The mechanisms of radical trapping antioxidants

Key to the misunderstanding of this fundamental property of resveratrol and other phytochemical 'antioxidants' lies with the mechanisms of lipid peroxidation (Figure 43, A) and the popular assays used to determine the compound's antioxidant capacity.[224] By far the most prevalent assays use a calorimetric indicator, typically an oxidant such as DPPH (**261,** Figure 43, B), which is titrated into a solution of the antioxidant. The resulting redox reaction causes a color

change that can be quantified by a change in fluorescence or absorbance, reflecting the position of the reaction equilibrium between the indicator (oxidant) and the antioxidant (reductant). While the use of these assays is a fast and convenient way to assess the total reducing equivalents within a sample, they suffer from two drawbacks: 1) They generally do not provide any kinetic data on reaction between the peroxyl radical and the antioxidant. 2) They are often conducted in aqueous or highly ionizable media such as ethanol or methanol. This point is particularly salient, since in lipid bilayers or lipoproteins, where radical peroxidation typically occurs (Figure 43, C), peroxyl radicals react with antioxidants through a hydrogen atom transfer (HAT) mechanism. Whereas in H–bond accepting solvents, HAT is suppressed due to hydrogen bonding to the solvent and other mechanisms such as sequential proton loss electron transfer (SPLET) or proton coupled electron transfer (PCET) can become the dominant reaction pathway (Figure 43,D). A calorimetric indicator such as DPPH (**261**) cannot distinguish between these three mechanisms and at best can provide dubious information about the actual mechanisms and reaction kinetics between an antioxidant and peroxyl radicals.

In 2013, we initiated a collaboration with Professor Derek Pratt's group of the University of Ottawa to study and rigorously characterize the antioxidant properties of quadrangularin A, pallidol, resveratrol and their corresponding alkylated congeners. Prof. Pratt's research focuses on the development and characterization of radical trapping antioxidants, with a strong emphasis on physical organic chemistry to guide structure development. The synthetic route described above is particularly well suited for these purposes because the determination of k_{inh}, defined as the rate of reaction between an antioxidant and an alkylperoxyl radical, requires millimolar quantities of the compound in question. Furthermore, the antioxidant properties of the *tert*-butylated analogs were expected to have potentially superior antioxidant activities, since they possess a BHT (2,6-

di-*tert*-butyl-4-hydroxytoluene, a standard antioxidant) equivalent as a part of their structure. Our collaboration sought to determine the peroxyl radical trapping activities of the resveratrol based natural products in homogenous solution, phosphatidyl choline lipid bilayers, and in cell culture and benchmark these activities against well-known antioxidants α-tocopherol and BHT. The following findings were performed by our outstanding collaborators Bo Li, XuYuan Lin, and Shelby Allison.

4.7.1 Determination of k_{inh} in Homogenous Organic Media, Lipid Bilayers, and Cell Culture

Despite the scientific interest in resveratrol as a dietary antioxidant, there was very little kinetic data assessing its ability to trap peroxyl radicals. Several reports had suggested that resveratrol possessed comparable or even superior antioxidant capacity than α-tocopherol (α-TOH), nature's most effective chain-breaking antioxidant.[149,225225,226] Others suggested that resveratrol was still the main contributor of antioxidant activity in red wine despite the fact that it was not present in high concentrations. An intriguing hypothesis suggested the resveratrol, along with other polyphenols, was actually acting synergistically as a redox mediator for α-TOH and regenerating it *in vivo*. Despite these reports, very little was known about resveratrol's ability to trap alkyl peroxyl radicals, a key step in the inhibition of radical autoxidation within lipid bilayers. In 2003, Valgimigli and co-workers determined the k_{inh} of resveratrol to be 2.0×10^5 $M^{-1}s^{-1}$ with k_{inh} describing the rate constant for the reaction of a peroxyl radical with resveratrol.[227] For comparison, α-TOH was determined to have a $k_{inh} = 3.2 \times 10^6$ $M^{-1}s^{-1}$ suggesting that resveratrol was *not* kinetically competitive with α-TOH in homogenous solution and could not regenerate α-TOH in solution.

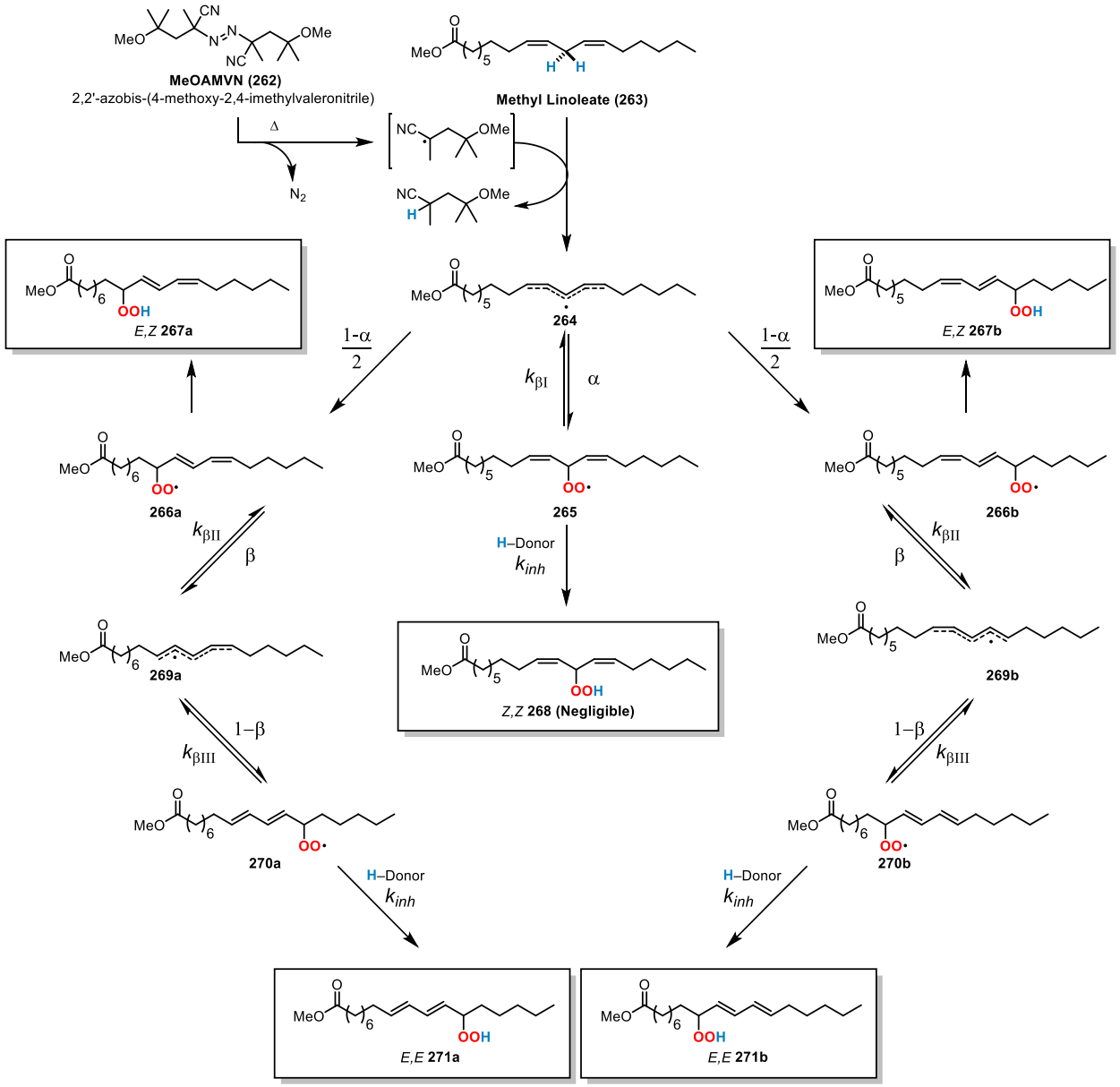

Figure 44 The methyl linoleate radical clock

We determined the rate constants (k_{inh}) of autoxidation using the methyl lineolate radical clock in chlorobenzene, using MeOAMVN (**262**) as an initiator (Figure 44) as described by Porter and co-workers.[228] Radical clock experiments are a means to measure the kinetics of an intermolecular radical reaction by a competition between an intramolecular (unimolecular) reaction with a known rate constant and an intermolecular (bimolecular) reaction of an unknown rate constant. The methyl linoleate (**263**) radical clock is a convenient means to measure the rate constants of antioxidants that possess both fast and slow k_{inh}. The autoxidation of methyl linoleate is typically initiated with AIBN or MeONMVN (**262**, Figure 44) generating delocalized pentadienyl radical **264**. The corresponding radical traps molecular oxygen at a diffusion controlled rate and is partitioned between non-conjugated peroxyl **265** and conjugated peroxyl adducts **266a** and **266b** in a 0.45:0.55 product ratio. The rate of β-fragmentation of **266a** and **266b** to the original pentadienyl radical **264** is not competitive with k_{inh} of fast reacting antioxidants and only lead to the formation of hydroperoxides **267a** and **267b**. Non-conjugated alkylperoxyl **265** undergoes β-fragmentation to the original pentadienyl radical **264** with a calibrated rate constant of $k_{\beta I} = 2.57 \times 10^6\ s^{-1}$ vs α-TOH. The k_{inh} can therefore be inferred from the ratios of **267a**+**267b** and **268** (Equation 1). For antioxidants that do not compete with $k_{\beta I}$, the rate of β-fragmentation of **266a** and **266b** to *E,E*-pentadienyl radicals **269a** and **269b** becomes kinetically relevant and subsequently only thermodynamic hydroperoxyls **270a** and **270b** are formed. Like in the previous case, the oxygen reacts with the *E,E*-pentadienyl radicals at a diffusion controlled rate, partitioning between conjugated E,Z-peroxylradicals **266a**/**266b** and *E,E*-peroxyl radicals **270a**/**270b** in a 0.69 : 0.31 ratio. The interconversion between **266a**/**266b** and **270a**/**270b** through pentadienyl radicals **269a**/**269b** can be described by rate constants $k_{\beta II}$ and $k_{\beta III}$ which were determined to be $690 s^{-1}$ and

$50s^{-1}$ respectively, calibrated against methyl lineolate itself. The k_{inh} can be inferred from the ratios of **267** and **271** (Equation 2).

$$\text{Equation 1}: \frac{[E,Z]}{[Z,Z]} = \frac{k_{\beta I}}{k_{inh}[Antioxidant}\left(\frac{1-\alpha}{\alpha}\right) + \left(\frac{1-\alpha}{\alpha}\right)$$

$$\text{Equation 2}: \frac{[E,Z]}{[E,E]} = \frac{k_{inh}[Antioxidant]}{k_{\beta II}(1-\beta)} + \frac{k_{\beta III}}{k_{\beta II}}\left(\frac{\beta}{1-\beta}\right)$$

The rate constants for pallidol (**199**) and quadrangularin A (**196**) were estimated from the k_{inh} of resveratrol[227] since they were poorly soluble in chlorobenzene. These estimated values for quadrangularin A and pallidol are expected to be comparable to resveratrol or BHT and inferior to α-TOH by an order of magnitude. The k_{inh} of **213**, **OBn-259**, and **OBn-260** were determined experimentally using Equation 2 to estimate the k_{inh} of the hydroxylated analogs due to their poor solubility in PhCl. These results, summarized in Table 11 (*vide infra*), demonstrated that all experimentally determined k_{inh} for the corresponding *tert*-butylated analogues were superior to their natural product counterparts. As expected, *tert*-butylated resveratrol (**214**) and *tert*-butylated quadrangularin A (**216**) both possessed better radical trapping ability than *tert*-butylated pallidol (**OH-259**) due to the presence of $C_{7–8}$ alkene. However, all tested compounds were inferior to α-TOH by a considerable degree (entries 4–7, Table 11).

Although the k_{inh} of these compounds were not competitive with α-TOH in homogenous solution, values derived from these experiments are poor predictors for antioxidant performance in biologically relevant contexts. The cellular milieu is a highly dynamic environment consisting of an aqueous phase possessing high ionic strength filled with proteins, dissolved salts, and other cellular components and a lipid phase that constitutes the lipid bilayers of the cell membrane and other membrane bound organelles. In this environment, peroxyl radicals cause the most damage in lipid membranes since the non-polar environment enhances radical propagation chain reaction.

To more accurately study the behavior of RTA's within this context, Bo evaluated the antioxidant activities of resveratrol, pallidol, quadrangularin A and their *tert*-butylated compounds in heterogeneous unilamellar phosphatidyl choline micelles and in cultured human erythroblasts. Niki[229] and Barclay[230] had demonstrated previously that the antioxidant activity of RTA's can be significantly altered in a heterogeneous environment despite what their k_{inh} (determined in homogenous organic medium) might suggest. This discrepancy is due to a contribution of several factors, particularly concerning RTA mobilization and localization, which is largely determined by its partition coefficient. This concept, which is a staple of medicinal chemistry, refers to the ratio of concentration of a compound in a mixture of two immiscible phases at equilibrium. This value is highly dependent on the lipophilicity of the molecule, the composition of the lipid bilayer, and the surface charge of its head groups. These properties can all affect the observed k_{inh}, since inefficient diffusion of the RTA into the lipid bilayer, for instance, lowers its probability to encounter the lipid soluble peroxyl radicals, whereas the phenolic O–H of the antioxidant can participate in hydrogen bonding with the phospholipid head group or with water at the membrane interface slowing the rate of H-atom transfer. Moreover, the reaction kinetics can be further perturbed by the identity of the radical initiator, where partitioning of hydrophilic (APPH, **272**) or hydrophobic (MeOAMVN, **262**) radical initiators can dramatically influence the rate of radical initiation (Figure 45). The combination of these compound dynamics can often overcome reactivity, where antioxidants possessing the same k_{inh} in homogenous organic media can have superior (or inferior) radical trapping properties in biologically relevant contexts.

The relative reactivity of resveratrol, quadrangularin A, pallidol, and their *tert*-butylated congeners in unilamellar micelles were measured using a fluorescence assay developed by Cosa

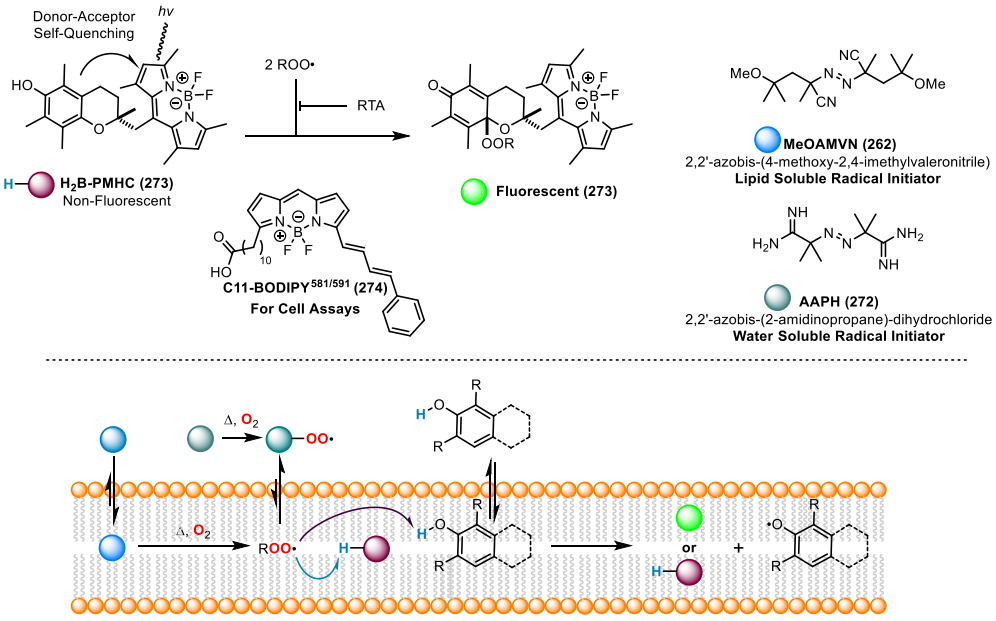

Figure 45 Determining the k_{rel} of antioxidants in heterogeneous mixtures

and co-workers which employs a lipophilic BODIPY-based probe H_2B-PMHC (**273**, Figure 45).[231,232] The fluorescent probe **273** possess a fluorescent BODIPY nucleus and a highly electron rich PMHC motif, which actively quenches the fluorescence of the fluorophore through an intramolecular photoinduced electron transfer. The chromanol motif therefore prevents emission of the BODIPY dye (dark state) until it reacts with a peroxylradical. This prevents the self-quenching mechanism, enabling fluorescence of the BODIPY nucleus, allowing simple detection by a fluorescence microplate reader. Addition of a competitive antioxidant should therefore prolong the induction period of the BODIPY luminescence through competitive quenching or peroxyl radicals in a concentration dependent manner (Figure 45). This assay enables the simple, high throughput evaluation of antioxidant activity in a parallel fashion using a multiwall setup using a fluorimeter to sample reaction progress over time. The observed k_{inh} of H_2B-BODIPY is the summation of several synergistic or antagonistic dynamic processes that can be affected by membrane composition. While quantitative values for k_{inh} and the partition coefficient may be

possible to determine experimentally for each of these reaction phases, this is a challenging and laborious task. Fortunately, Cosa and co-workers provided a simple means to calculate the relative reactivity of H_2B-PMHC with using the following equation where *t* equals the time at the initial rate of reaction, τ is the time at which maximum fluorescence is reached, and I_∞, I_t, and I_0 correspond to the intensity of fluorescence at its maximum, at time *t*, at the start of the reaction, respectively:

Equation 3: $$-ln\left(\frac{I_\infty - I_t}{I_\infty - I_0}\right) = \frac{k_{inh}^{H_2B-TOH}}{k_{inh}^{TOH}} ln\left(1 - \frac{t}{\tau}\right)$$

Our results indicated that resveratrol, pallidol, *tert*-butylated pallidol (**OH-259**), and quadrangularin A (**196**) were not effective radical trapping antioxidants in lipid bilayers. While this assay only gives information of the relative reactivity of these antioxidants compared to the fluorogenic probe, these results suggest that antioxidant activity is *not* responsible for their biological activity, contrary to popular belief. *Tert*-butylated resveratrol **214** and *tert*-butylated quadrangularin A (**216**) were very effective antioxidants compared to α-TOH and were roughly 10 to 16 times better for **214** and 4 fold better for **216** depending if lipophilic or hydrophilic radical initiators were used (Table 11, Entries 4,5 and 7). This is likely due to the presence of flanking *tert*-butyl groups which increase the compound's solubility in lipid bilayer and can preclude the formation of hydrogen bonds with phenolic O–H groups, which inhibit H-atom transfer.

Finally, the antioxidant activities of these compounds were tested in cultured human erythroblasts using the fluorogenic probe C11-BODIPY$^{581/591}$ (**274**)[233] as a reporter (Figure 45). Conceptually, this assay is very similar to the one developed by Cosa and co-workers. The highly lipophilic **274** is not fluorescent due to the presence of the vinyl stilbene, which quenches the

excited state of the fluorophore via electron transfer. As this motif gets oxidized by peroxyl radicals in the cell membrane, the corresponding oxidized **274** becomes a highly efficient fluorophore. Here, antioxidant activity is measured by incubating the cells with a solution of the antioxidant and BODIPY reporter. Oxidative stress is induced by the addition of diethylmaleate, which reacts with cellular glutathione – a major endogenous antioxidant that acts as a chain breaking RTA. With glutathione levels depleted, cellular concentrations of reactive oxygen species increases, which in turn can either react in the cell membrane with the supplemented antioxidant or with C11-BODIPY$^{581/591}$, which will then fluoresce. A dose response curve for a given antioxidant can be generated by measuring the fluorescence at different antioxidant concentrations, using cells untreated with DEM as a negative control and cells untreated with antioxidant as a positive control. Under the assay's conditions, the half maximal effective concentration (EC_{50}) values for resveratrol, pallidol and quadrangularin A were 13, 8, and 3.4 μM, roughly on par with butylated hydroxytoluene (BHT) (Entries 1–2,Table 11, Column 4). Their corresponding *tert*-butylated analogs **214, 216,** and **OH-259** were far superior, in the case of quadrangularin A and pallidol, the difference between **216** and **OH-259** was around 20 fold – 3.4 and 8.1 vs 0.21 and 0.39 μM, respectively. For *tert*-butylated resveratrol **214**, the EC_{50} value of 51 nM is nearly 250 fold higher than resveratrol. In fact, **214** was superior to α-TOH (150 nM) and is the most reactive radical-trapping antioxidant studied in cell culture. Although *tert*-butylated pallidol (**OH-259**) was not an effective antioxidant in lipid bilayers, it was an unexpectedly potent against lipid peroxidation in cell culture. This suggests that it can be acting through an alternative mechanism, possibly through modulation of the expression of genes controlled by the antioxidant response element (ARE).[234] The resveratrol oligomers, and presumably the *tert*-butylated analogies, have known cytotoxic activity. This is a particularly important detail because if these

compounds are toxic at the concentrations used in the assay, their antioxidant activities are irrelevant – since dead cells do not respire. Fortunately, the EC_{50} values for inducing cell deaths were 8.7 μM for **216** and 10.2 μM for **214**, 40 and 200 fold higher than their EC_{50} determined in the antioxidant assay.

Table 11 Evaluation of Antioxidant Activities of Resveratrol, Pallidol, Quadrangularin A and Their Derivatives

Radical-trapping antioxidant activity of resveratrol, pallidol and quadrangularin A and their synthetic precursors in solution (chlorobenzene), lipid bilayers (of egg phosphatidylcholine) and cell culture (human erythroblasts). Data are also given for benchmark phenolic antioxidants α-tocopherol and BHT (2,6-di-*tert*-butyl-4-methylphenol).

		Solution	*Lipid Bilayers*		*Cells*	*Cytotoxicity*
Entry		k_{inh}[a] (PhCl) / $M^{-1}s^{-1}$	k_{rel},[b] n[c] ($ROO\bullet_{lipid}$)[d]	k_{rel},[b] n[c] ($ROO\bullet_{aq}$)[d]	EC_{50} / μM	EC_{50} / μM
1	resveratrol (**183**)	2.0×10^{5} [e]	<0.01	<0.01	12.6±0.9	118±14
2	pallidol (199)[f]	8.5×10^{4} [g]	<0.01	<0.01	8.1±0.9	205±11
3	quadrangularin A (196)	2.3×10^{5} [g]	<0.01	<0.1	3.4±0.4	63.5±3.0
4	α-tocopherol (α-TOH)	3.2×10^{6} [f]	1.8±0.2, 2.0[h]	1.3±0.1, 2.0[h]	0.15±0.01	>100
5	$^{t}Bu_2$-resveratrol (**214**)	$(5.9\pm0.8)\times10^{4}$ [i]	17.9±3.3, 1.8±0.1	21.0±6.8, 1.8±0.1	0.051±0.004	10.2±0.3
6	$^{t}Bu_4$-pallidol (**OH-259**)[f]	$(2.1\pm0.3)\times10^{4}$ [i]	<0.01	<0.01	0.39±0.07	10.2±0.4
7	$^{t}Bu_4$-quadrangularinA (**216**)	$(6.2\pm0.9)\times10^{4}$ [i]	7.5±0.6, 1.9±0.1	<0.1	0.21±0.03	8.7±0.5
8	BHT	$(2.2\pm0.1)\times10^{4}$ [i]	<0.01	<0.01	12.7±1.5	49.5±2.0

[a] Second order rate constant for the reaction with (linoleyl) peroxyl radicals. [b] Second order rate constant for the reaction with peroxyl radicals relative to the fluorescent probe H_2B-PMHC. [c] Number of peroxyl radicals trapped per molecule of test compound. [d] Initiated with MeOAMVN and AAPH, respectively. [e] determined at 30 °C by the inhibited autoxidation of styrene, see ref. [88]. [f] Since two equivalent units exist on the same molecule, the observed rate constant has been divided by 2. [g]Estimated from the value for resveratrol and the relative reactivities of the corresponding synthetic precursors (*tert*-butylated analogs). [h]From ref. [230]. [i]Determined at 37°C by the peroxyl radical clock methodology on resorcinol ring-protected (benzyl) compounds.

4.8 Conclusions and Outlook

This work describes a collaborative effort between the Stephenson group and the Pratt group seeking to elucidate long-standing questions concerning the biological activity of resveratrol based natural products and their relevance as dietary antioxidants. What started as a humble exercise in photoredox catalysis and its applications in total synthesis, turned into a multidisciplinary collaboration culminating in the biomimetic synthesis of quadrangularin A and pallidol, producing the target compounds in the highest overall yields and fewest number of steps reported yet. The identification of the base promoted, oxidative dimerization of stilbene **255** using $FeCp_2PF_6$ enabled the synthesis of LBQM **258** in quantitative yield. This reaction, to our knowledge, is the most

scalable and highest yielding biomimetic dimerization of a resveratrol adduct reported thus far. The use of the *tert*-butyl groups – as pioneered by Hou and Li – was essential, enabling the highly selective manipulation of **258** into synthetic analogs of the two other postulated biogenic intermediates common to all 8–8' resveratrol dimers, eventually leading to the final natural products themselves. The described route was capable of procuring millimolar quantities of all synthetic intermediates necessary for the evaluation of their antioxidant properties. Furthermore, this synthetic endeavor further emphasizes the central role of total synthesis in the development of novel, pharmaceutically relevant compounds: although the inclusion of *tert*-butyl groups was not initially a design element from an SAR (structure-activity-relationship) point of view, the properties that made them good substrates for oxidative dimerization also dramatically improved their performance as radical trapping antioxidants.

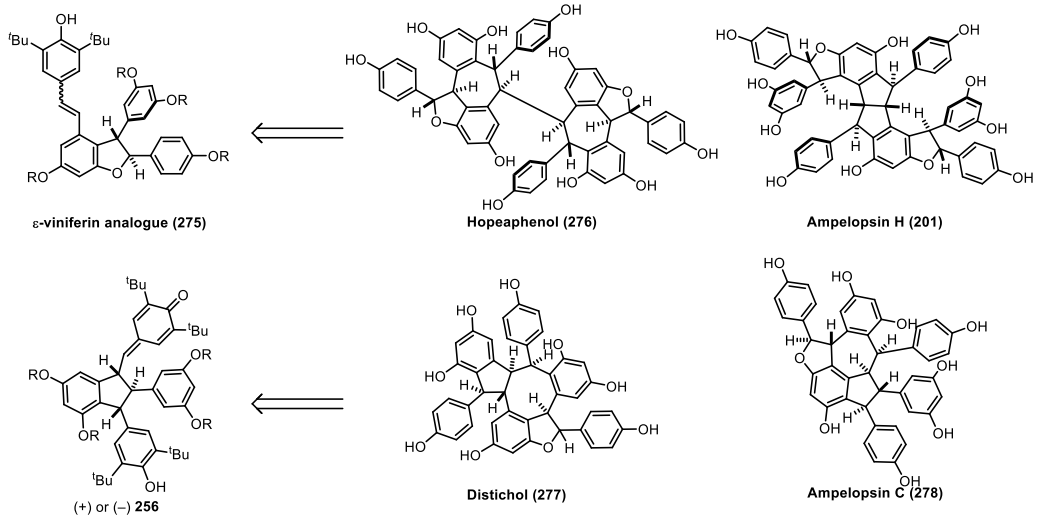

Figure 46 Future Directions

Our above delineated the behavior of the oxidative dimerization reaction using *tert*-butylated stilbenes and the reactivity of the subsequently generated *tert*-butylated *para*-quinone

methides. The reactivity of these reactions has proven to be scalable and highly predictable. Currently, the dimerization of butylated congeners of ε-viniferin (**275**) are being explored to synthesize more complex resveratrol tetramers hopeaphenol (**276**)[163] and ampelopsin H (**201,** Figure 46)[235]. CPQM **(256**) is a promising intermediate for the synthesis of several exotic resveratrol oligomers including distichol (**277**)[236] and ampelopsin C (**278**).[237] Furthermore, the dynamic interconversion of LBQM (**258**) to CPQM (**256**) occurs through its *meso* diastereomer, presenting the opportunity to develop a novel dynamic kinetic resolution of *rac/meso* **258** into enantiopure **256** through the intermediacy of a persistent quinone methide radical, which is also of synthetic value for the synthesis of more complex trimers and tetramers. The enantioselective synthesis of any resveratrol natural product has been limited to the dimers pauciflorol F (**229**) , δ-viniferin (**194**) and hopeanol (**233**) which are of limited value towards the synthesis of the vast majority of resveratrol derived natural products. The realization of these synthetic endeavors will be tied to their biological evaluation and development of these compounds into novel antioxidants.

4.9 Experimental Section

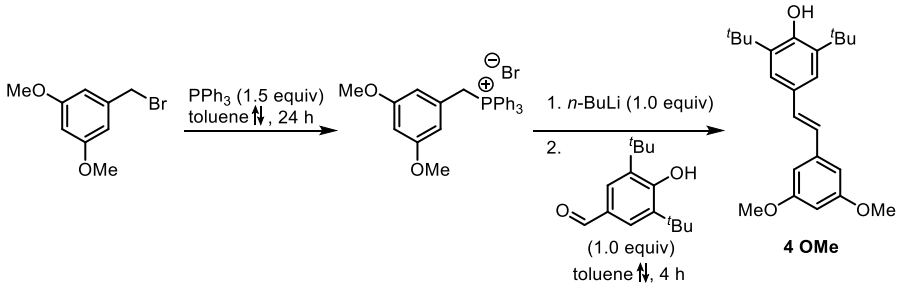

(*E*)-2,6-di-tert-butyl-4-(3,5-dimethoxystyryl)phenol (4 OMe): A round bottom flask equipped with a reflux condenser and magnetic stir bar was charged with commercially available 3,5-dimethoxy benzyl bromide (6.00 g, 26.0 mmol, 1.00 equiv). The material was dissolved in anhydrous toluene (60 mL, 0.43 M) at room temperature under N_2. To the stirring mixture, PPh_3 (10.2 g, 38.9 mmol, 1.5 equiv) was added in a single portion and the solution was heated to reflux for 24 h. The reaction mixture was allowed to cool to room temperature and the product collected by vacuum filtration. The solid was washed with hexanes and dried under vacuum to give the desired phosphonium salt as a crystalline white solid (12.8 g, 26.0 mmol 99% yield). The phosphonium salt (5.00 g, 10.1 mmol, 1.00 equiv) was suspended in anhydrous toluene (200 mL, 0.05 M) in a flame-dried, 3-neck 500 mL round bottom flask equipped with a reflux condenser and magnetic stir bar. To the stirring suspension at room temperature under N_2, *n*-BuLi (4.00 mL, 2.5 M soln. in hexanes, 1.00 equiv) was added slowly, turning the mixture a brilliant red. The mixture was allowed to equilibrate at this temperature for 30 minutes, at which point the solution of the ylide was heated to reflux. Once reflux temperature was reached, 3,5-di-*tert*-butyl-4-hydroxybenzaldehyde (2.38 g, 10.1 mmol, 1.00 equiv, recrystallized from toluene and dried from benzene 3x prior to use) was added as a solid, portion wise under a stream of N_2. The reaction was allowed to stir at this temperature for 4 hours; reaction progress was monitored by TLC in 9:1 Hexanes/EtOAc. At 4 h, the reaction was quenched with methanol and the solvent removed by rotary evaporation. The crude residue was treated with cold diethyl ether to precipitate triphenylphosphine oxide, and filtered through a fritted funnel packed with Celite and a filter paper. The crude filtrate was then dried onto Celite and purified by flash chromatography using 97:2:1 Hexanes/EtOAc/CH_2Cl_2 as the mobile phase. The desired stilbene (**4 OMe**) was obtained as an amorphous white solid (2.90 g, 7.87 mmol, 78% yield).

Rf (Hexanes/EtOAc, 9:1): 0.35

IR (Neat): 3624, 2956, 1590, 1456, 1436, 1358, 1236, 1204, 1150, 1066 cm^{-1};

^1H NMR ($CDCl_3$, 500 MHz): δ 7.34 (s, 2H), 7.05 (d, J = 16.1 Hz, 1H), 6.87 (d, J = 16.1 Hz, 1H), 6.66 (d, J = 2.2 Hz, 2H), 6.37 (t, J = 2.2 Hz, 1H), 5.29 (s, 1H), 3.84 (s, 6H), 1.48 (s, 18H);

^{13}C NMR ($CDCl_3$, 125 MHz): δ 161.2, 154.2, 140.2, 136.4, 130.3, 128.6, 126.0, 123.7, 104.4, 99.8, 55.6, 34.6, 30.5;

HRMS (ESI) *m/z* calculated for $C_{24}H_{33}O_3^+$ ($[M+H]^+$) 369.2244, found 369.2426.

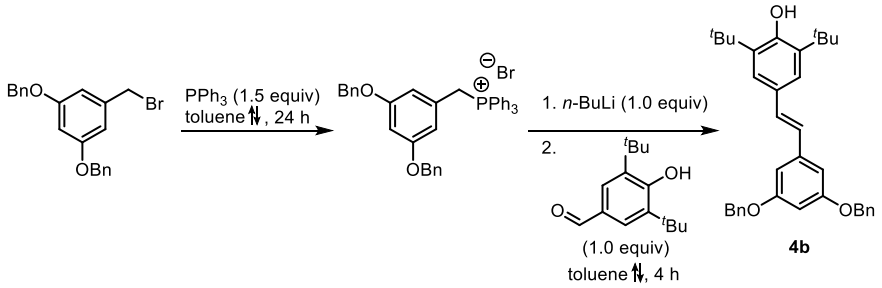

(*E*)-4-(3,5-bis(benzyloxy)styryl)-2,6-di-tert-butylphenol (4b): A round bottom flask equipped with a reflux condenser and magnetic stir bar was charged with commercially available 3,5-dibenzyloxy benzyl bromide (10.1 g, 26.4 mmol, 1.00 equiv). The material was dissolved in anhydrous toluene (60 mL, 0.44 M) at room temperature under N_2. To the stirring mixture, PPh_3 (10.4 g, 39.6 mmol, 1.50 equiv) was added in a single portion and the solution was heated to reflux for 24 h. The reaction mixture was allowed to cool to room temperature and the product collected by vacuum filtration. The solid was washed with hexanes and dried under vacuum to give the desired phosphonium salt as a crystalline white solid (16.9 g, 26.2 mmol 99% yield). The phosphonium salt (13.5 g, 22.4 mmol, 1.00 equiv) was suspended in anhydrous toluene (225 mL, 0.10 M) in a flame-dried, 3-neck 500 mL round bottom flask equipped with a reflux condenser and magnetic stir bar. To the stirring suspension at room temperature under N_2, *n*-BuLi (9.39 mL, 2.5 M soln. in hexanes, 1.05 equiv) was added slowly, turning the mixture a brilliant red. The mixture was allowed to equilibrate at this temperature for 30 minutes, at which point the solution of the ylide was heated to reflux. Once reflux temperature was reached, 3,5-di-*tert*-butyl-4-hydroxybenzaldehyde (5.77 g, 24.6 mmol, 1.10 equiv, recrystallized from toluene and dried from benzene 3x prior to use) was added as a solid, portionwise under a stream of N_2. The reaction was allowed to stir at this temperature for 4 hours; reaction progress was monitored by TLC in 9:1 Hexanes/EtOAc. At 4 h, the reaction was quenched with methanol and the solvent removed by rotary evaporation. The crude residue was treated with cold diethyl ether to precipitate triphenylphosphine oxide, and filtered through a fritted funnel packed with Celite and a filter paper. The crude filtrate was then dried onto Celite and purified by flash chromatography using 97:2:1 Hexanes/EtOAc/CH_2Cl_2 as the mobile phase. The desired stilbene (**4b**) was obtained as an amorphous white solid (9.57 g, 18.4 mmol, 82% yield), which was further purified to a crystalline white powder by sonication in ^{i}PrOH and collected by vacuum filtration.

Rf (Hexanes/EtOAc, 9:1): 0.35;

^{1}H NMR ($CDCl_3$, 500 MHz): δ 7.46 – 7.32 (m, 10H), 7.04 (d, *J* = 16.1 Hz, 1H), 6.87 (d, *J* = 16.1 Hz, 1H), 6.77 (d, *J* = 2.2 Hz, 2H), 6.52 (t, *J* = 2.2 Hz, 1H), 5.29 (s, 1H), 5.08 (s, 4H), 1.48 (s, 18H).

For additional characterization data, see:

W. Li, H. Li, Y. Li, Z. Hou, *Angew. Chem. Int. Ed.* **2006**, *45*, 7609–7611; *Angew. Chem.* **2006**, *118*, 7771–7773.

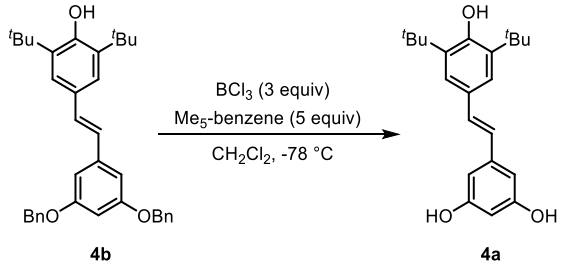

4b **4a**

(*E*)-5-(3,5-di-tert-butyl-4-hydroxystyryl)benzene-1,3-diol (4a): A round bottom flask equipped with a septum and magnetic stir bar was charged with starting **4b** (1.75 g, 3.36 mmol, 1.00 equiv) and Me_5-benzene (2.49 g, 16.8 mmol, 5 equiv). The mixture was dissolved in anhydrous CH_2Cl_2 (57 mL, 0.05 M) at room temperature under N_2 and cooled to -78 °C. To the stirring mixture, BCl_3 (10.1 mL, 1.0 M soln. in CH_2Cl_2, 3 equiv) was added slowly, turning the reaction deep maroon. Upon completion of the addition, the reaction was quickly transferred to a 0 °C ice bath and stirred for an additional 40 minutes at this temperature, over which the reaction turned a bright transparent red color. The reaction was quenched at -78 °C by pipetwise addition of a 4:1 THF/sat. aq. $NaHCO_3$ mixture and the solution stirred vigorously under N_2 for several minutes as it decolorized. The contents were then transferred to a separatory funnel containing DI H_2O and the organic layer separated. The aqueous phase was extracted with CH_2Cl_2 (2x) and organic layers combined, dried over Na_2SO_4, and concentrated *in vacuo*. The resulting residue was purified by flash chromatography using a gradient 5% to 15% EtOAc in $CHCl_3$ mobile phase to give **4a** as an amorphous white solid (1.05 g, 0.81 mmol, 91% yield) along with 45 mg (4%) of the corresponding (*Z*)-stilbene isomer. NOTE: **4a** is unstable to prolonged storage in air at room temperature, but could be stored indefinitely at -20 °C in a container sealed under N_2.

Rf (CH_2Cl_2/MeOH, 9:1): 0.48;

^{1}H NMR ($CDCl_3$, 500 MHz): δ 7.31 (s, 2H), 7.02 (d, *J* = 16.4 Hz, 1H), 6.79 (d, *J* = 16.4 Hz, 1H), 6.56 (d, *J* = 2.2 Hz, 2H), 6.24 (t, *J* = 2.2 Hz, 1H), 5.30 (s, 1H), 4.66 (s, 2H), 1.47 (s, 18H).

For additional characterization data, see:

W. Li, H. Li, Y. Li, Z. Hou, *Angew. Chem. Int. Ed.* **2006**, *45*, 7609–7611; *Angew. Chem.* **2006**, *118*, 7771–7773.

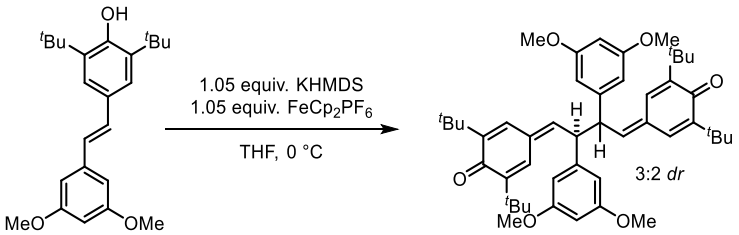

4 OMe **5/5' OMe**

4,4'-(2,3-bis(3,5-dimethoxyphenyl)butane-1,4-diylidene)bis(2,6-di-tert-butylcyclohexa-2,5-dien-1-one) (5 OMe): In a round bottom flask equipped with a septum and magnetic stir bar, a solution of **4 OMe** (2.00 g, 5.43 mmol, 1.00 equiv) in anhydrous THF (55 mL, 0.1 M) was cooled to 0 °C in an ice bath under inert atmosphere. To this, KHMDS (5.7 mL, 1.0 M soln. in THF, 1.05 equiv) was added slowly, turning the pale yellow solution a dark forest green. The solution was allowed to stir at temperature for 10 minutes, upon which the septum was removed and ferrocenium hexafluorophosphate (1.9 g, 97% purity, 5.70 mmol, 1.05 equiv.) was added in two 950 mg portions, separated by 15 minutes. The heterogeneous reaction slowly turns from blue-green to a dark yellow/orange color as the ferrocenium is reduced. After the reaction was deemed complete by TLC (ca. 30 min), the reaction mixture was dried on to Celite and the solvent removed completely under reduced pressure. The crude material was purified by flash chromatography over SiO_2 (100:0 Hexanes/EtOAc [to elute ferrocene], then gradient 95:2.5:2.5 to 90:5:5 Hexanes/EtOAc/CH_2Cl_2) to afford **5/5' OMe** as an amorphous yellow solid (1.94 g, 2.64 mmol, 97% yield), which further purified to a crystalline yellow powder by trituration from a minimum of CH_2Cl_2 with MeOH.

Rf (Hexanes/EtOAc, 9:1): 0.3;

IR (Neat): 2953, 1602, 1461, 1350, 1201, 1156, 1059, 925, 831, 696 cm^{-1};

^1H NMR ($CDCl_3$, 700 MHz): δ β-H's of quinone methides: 7.13 (major diastereomer, d, *J* = 1.9 Hz, 2H), 7.09 (minor diastereomer, d, *J* = 2.0 Hz, 2H), 6.82 (minor diastereomer, d, *J* = 2.2 Hz, 2H), 6.71 (major diastereomer, d, *J* = 2.2 Hz, 2H); δ-H's of quinone methides: 6.43 (minor diastereomer, m, 2H), 6.33 (major diastereomer, m, 2H); 6.35 (Ar-H major diastereomer, d, *J* = 2.1 Hz, 4H), 6.31 (Ar-H major diastereomer, t, *J* = 2.1 Hz, 2H), 6.29-6.27 (Ar-H's minor diastereomer, overlap, 6H), 4.34 – 4.30 (minor diastereomer sp^3 methines, m, 2H), 4.30 – 4.26 (major diastereomer sp^3 methines, m, 2H), 3.74 (major diastereomer –OMe's, s, 12H), 3.70 (minor diastereomer –OMe's, s, 12H), 1.25 (minor diastereomer ^{t}Bu's, s, 18H), 1.24 (major diastereomer ^{t}Bu's, s, 18H), 1.23 (minor diastereomer ^{t}Bu's, s, 18H), 1.22 (major diastereomer ^{t}Bu's, s, 18H);

^{13}C NMR ($CDCl_3$, 175 MHz): δ 186.67, 186.65, 161.3, 161.2, 149.2, 149.0, 147.7, 147.3, 145.3, 144.1, 143.3, 142.9, 134.8, 134.7, 133.1, 132.1, 126.1, 126.0, 106.9, 106.8, 99.0, 98.8, 55.54, 55.52, 51.6, 51.2, 35.6, 35.5, 35.1, 35.0, 29.7, 29.63, 29.62, 29.60;

HRMS (ESI) *m/z* calculated for $C_{48}H_{63}O_6^+$ ($[M+H]^+$) 735.4619, found 735.4613.

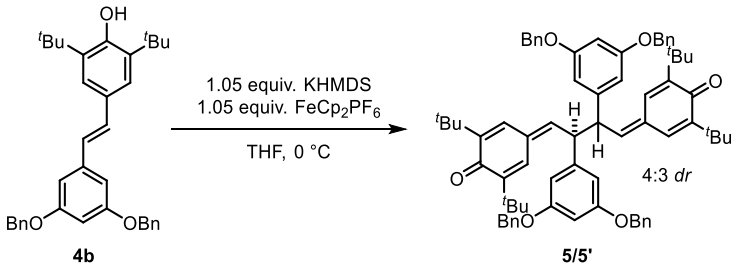

4,4'-(2,3-bis(3,5-bis(benzyloxy)phenyl)butane-1,4-diylidene)bis(2,6-di-tert-butylcyclohexa-2,5-dien-1-one) (5): In a round bottom flask equipped with a septum and magnetic stir bar, a solution of **4b** (1.88 g, 3.61 mmol, 1.00 equiv) in anhydrous THF (30 mL, 0.1 M) was cooled to 0 °C in an ice bath under inert atmosphere. To this, KHMDS (3.8 mL, 1.0 M soln. in THF, 1.05 equiv) was added slowly, turning the pale yellow solution a dark forest green. The solution was allowed to stir at temperature for 10 minutes, upon which the septum was removed and ferrocenium hexafluorophosphate (1.25 g, 97% purity, 3.79 mmol, 1.05 equiv) was added in two 625 mg portions, separated by 15 minutes. The heterogeneous reaction turns from blue-green to a dark yellow/orange color as the ferrocenium is reduced. After the reaction was complete by TLC (ca. 30 min), the reaction mixture was dried on to Celite and the solvent removed completely under reduced pressure. The crude material was purified by flash chromatography over SiO_2 (100% Hexanes [to elute ferrocene], then gradient 95:2.5:2.5 to 90:5:5 Hexanes/EtOAc/CH_2Cl_2) to afford **5/5'** (1.87 g, 1.81 mmol, 99% yield) as an amorphous yellow solid, which was further purified to a crystalline yellow powder by sonication in pH neutral CH_3NO_2. When ran on 10 gram scale, isolated 9.49 g of **5** (95% yield).

Rf (Hexanes/EtOAc, 9:1): 0.35;

IR (Neat): 2954, 1593, 1453, 1361, 1292, 1254, 1160, 1054, 930, 822, 734, 695 cm^{-1};

^1H NMR ($CDCl_3$, 500 MHz): δ 7.40 – 7.40 (m, 20H), β-H's of quinone methides: 7.12 (major diastereomer, d, *J* = 2.2 Hz, 2H), 7.02 (minor diastereomer, d, *J* = 2.0 Hz, 2H), 6.82 (minor diastereomer, d, *J* = 2.2 Hz, 2H), 6.72 (major diastereomer, d, *J* = 2.0 Hz, 2H); δ-H's of quinone methides: 6.41 – 6.37 (minor diastereomer, m, 2H), 6.33 – 6.29 (major diastereomer, m, 2H); 6.48 (major diastereomer, t, *J* = 2.1 Hz, 2H), 6.47 (minor diastereomer, t, *J* = 2.2 Hz, 2H), 6.45 (major diastereomer, d, *J* = 2.1 Hz, 4H), 6.38 (minor diastereomer, d, *J* = 2.2 Hz, 4H), 4.96 (major diastereomer, d, *J* = 11.5 Hz, 4H), 4.94 (major diastereomer, d, *J* = 11.5 Hz, 4H), 4.91 (minor diastereomer, d, *J* = 11.5 Hz, 4H), 4.89 (minor diastereomer, d, *J* = 11.5 Hz, 4H), 4.28 (m, overlap, sp^3 methines of both diastereomers, 4H), 1.26 (minor diastereomer ^{t}Bu's, s, 18H), 1.24 (major diastereomer ^{t}Bu's, s, 36H), 1.23 (minor diastereomer ^{t}Bu's, s, 18H).

^{13}C NMR ($CDCl_3$, 175 MHz): δ 186.70, 186.66, 160.5, 160.4, 149.2. 149.1, 147.7, 147.4, 145.2, 143.9, 143.3, 142.9, 136.7, 136.6, 134.9, 134.7, 133.2, 132.2, 128.85 (2C), 128.4, 127.81, 127.79, 126.2, 126.0, 108.2, 108.0, 100.6, 100.57, 100.54, 70.5, 51.8, 51.2, 35.57, 35.55, 35.11, 35.05, 29.7, 29.64, 29.62;

HRMS (ESI) *m/z* calculated for $C_{72}H_{79}O_6^+$ ([M+H]$^+$) 1039.5832, found 1039.5871.

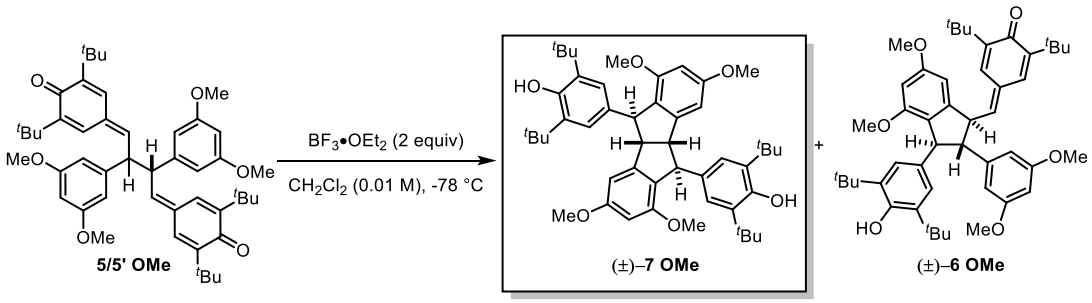

4,4'-((4bS,5S,9bS,10S)-1,3,6,8-tetramethoxy-4b,5,9b,10-tetrahydroindeno[2,1-a]indene-5,10-diyl)bis(2,6-di-tert-butylphenol) (7 OMe): A solution of **5 OMe** (20 mg, 0.027 mmol, 1.00 equiv) in anhydrous CH_2Cl_2 (10 mL, 0.003 M) was cooled to -78 °C in a dry ice/acetone bath under inert atmosphere. To this, BF_3•OEt_2 (14 μL, 46.5% in diethyl ether, 2 equiv) was added dropwise, turning the reaction a brilliant magenta color. Temperature control is critical for the success of this reaction. The reaction was allowed to run for 40 minutes upon which the reaction was quenched with sat. aq. $NaHCO_3$ at temperature and allowed to warm to room temperature under vigorous stirring. The reaction was diluted with CH_2Cl_2 and transferred to a separatory funnel. The phases were separated and the aqueous layer was extracted with portions of CH_2Cl_2. The organic layers were combined, washed with sat. aq. $NaHCO_3$, brine, dried over sodium sulfate and concentrated *in vacuo*. The crude material was purified by column chromatography over SiO_2 (90:5:5 Hexanes/EtOAc/CH_2Cl_2) to afford **7 OMe** (8.5 mg, 0.012 mmol 43% yield) as a white amorphous solid. The remaining material was identified as compound **6 OMe** (see S13 for characterization data).

Rf (Hexanes/EtOAc 9:1): 0.1;

IR (Neat): 3646, 2988, 1600, 1436, cm^{-1};

^{1}H NMR ($CDCl_3$, 700 MHz): δ 7.12 (s, 4H), 6.66 (s, 2H), 6.23 (s, 2H), 5.03 (s, 2H, OH), 4.57 (s, 2H), 4.25 (s, 2H), 3.83 (s, 6H), 3.66 (s, 6H), 1.42 (s, 36H);

^{13}C NMR ($CDCl_3$, 175 MHz): δ 161.1, 157.1, 152.0, 148.5, 136.3, 135.4, 125.9, 124.3, 100.8, 97.6, 59.6, 55.7, 55.3, 54.2, 34.5, 30.6;

HRMS (ESI) *m/z* calculated for $C_{68}H_{63}O_6^+$ ([M+H]$^+$) 735.4650, found 735.4625.

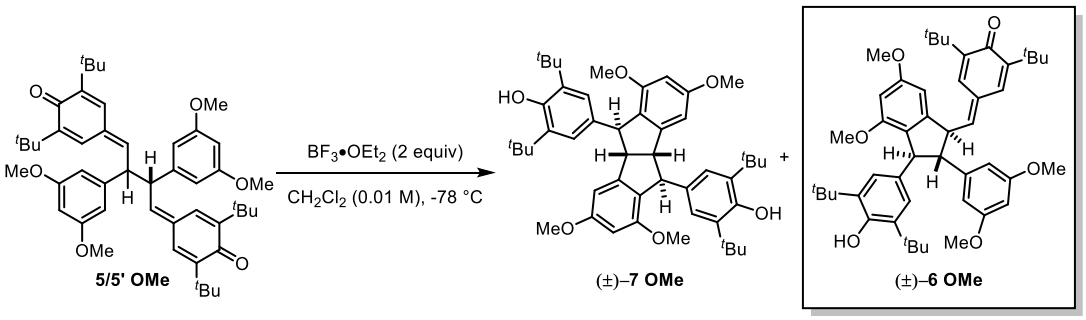

2,6-di-tert-butyl-4-(((1S,2S,3S)-3-(3,5-di-tert-butyl-4-hydroxyphenyl)-2-(3,5-dimethoxyphenyl)-4,6-dimethoxy-2,3-dihydro-1H-inden-1-yl)methylene)cyclohexa-2,5-dien-1-one (6 OMe)

Rf (Hexanes/THF, 90:10): 0.33;

IR (Neat): 3640, 2953, 1594, 1460, 1434, 1360, 1202, 1152, 1070, 934, 882, 832 cm^{-1};

^{1}H NMR ($CDCl_3$, 500 MHz): δ 6.97 (d, *J* = 2.2 Hz, 1H), 6.85 (d, *J* = 2.2 Hz, 1H), 6.70 (s, 2H), 6.42 (d, *J* = 2.0 Hz, 1H), 6.39 (d, *J* = 10 Hz, 1H), 6.34 – 6.30 (m, 4H), 4.96 (s, 1H), 4.58 (dd, *J* = 9.2, 9.2 Hz, 1H), 4.48 (d, *J* = 7.8 Hz, 1H), 3.83 (s, 3H), 3.70 (s, 6H), 3.61 (s, 3H), 3.08 (dd, *J* = 8.1, 8.1 Hz, 1H), 1.32 (s, 18H), 1.26 (s, 9H), 1.16 (s, 9H);

^{13}C NMR ($CDCl_3$, 125 MHz): δ 186.8, 161.6, 161.0, 157.5, 152.1, 148.7, 147.8, 147.1, 146.7, 144.8, 135.1, 134.9, 133.9, 132.8, 127.0, 124.0, 123.8, 106.5, 100.9, 98.9, 98.7, 65.1, 56.6, 55.8, 55.5, 55.4, 52.9, 35.4, 35.0, 34.5, 30.6, 29.61, 29.56;

HRMS (ESI) *m/z* calculated for $C_{48}H_{63}O_6^+$ ($[M+H]^+$) 735.4619, found 735.4620.

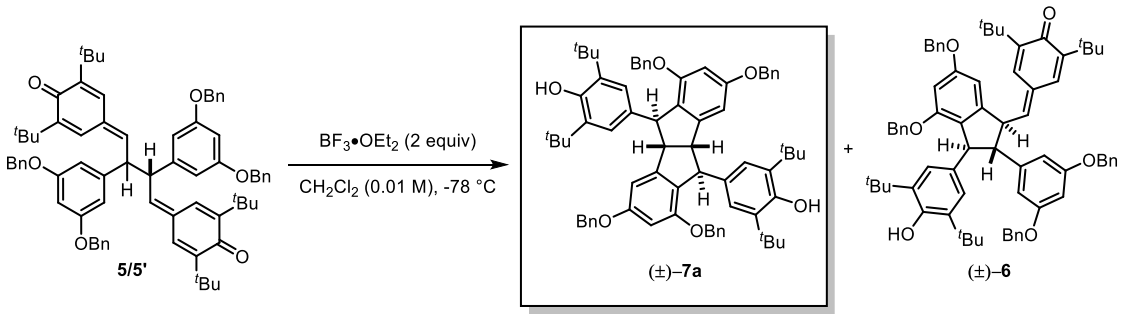

4,4'-((4bS,5S,9bS,10S)-1,3,6,8-tetrakis(benzyloxy)-4b,5,9b,10-tetrahydroindeno[2,1-a]indene-5,10-diyl)bis(2,6-di-tert-butylphenol) (7a): A solution of **5** (800 mg, 0.77 mmol, 1.00 equiv) in CH_2Cl_2 (77 mL, 0.01M) was cooled to -78 °C in a dry ice/acetone bath under inert atmosphere. To this, BF_3•OEt_2 (390 μL, 46.5% in diethyl ether, 2 equiv) was added dropwise, turning the reaction a brilliant magenta color. Temperature control is critical for the success of this reaction. The reaction was allowed to run for 40 minutes upon which the reaction was quenched with sat. aq. $NaHCO_3$ at temperature and allowed to warm to room temperature under vigorous stirring. The reaction was diluted with CH_2Cl_2 and transferred to a separatory funnel. The phases were separated and the aqueous layer was extracted with portions of CH_2Cl_2. The organic layers were combined, washed with sat. aq. $NaHCO_3$, brine, dried over sodium sulfate and concentrated *in vacuo*. The crude material was purified by column chromatography over SiO_2 (95:5 Hexanes/THF gradient to 90:10 Hexanes/THF) to afford **7a** (340 mg, 0.33 mmol, 43% yield) as a white amorphous solid. The remaining material was identified as compound **6** (see S15 for characterization data).

Rf (Hexanes/THF, 95:5): 0.19;

IR (Neat): 3636, 2954, 2908, 2870, 1598, 1433, 1316, 1135, 905, 727, 695 cm^{-1};

^1H NMR ($CDCl_3$, 500 MHz): δ 7.42 (d, *J* = 7.5 Hz, 4H), 7.35 (m, 5H), 7.29 (m, 2H), 7.22 (m, 5H), 7.03 (s, 4H), 7.01 (m, 4H), 6.73 (d, *J* = 2.0 Hz), 6.33 (d, *J* = 2.0 Hz), 5.04 (d, *J* = 11.2 Hz, 2H), 5.02 (d, *J* = 11.2 Hz, 2H), 5.01 (s, 2H, OH), 4.88 (d, *J* = 11.7 Hz, 2H), 4.82 (d, *J* = 11.7 Hz, 2H), 4.55 (s, 2 H), 4.24 (s, 2H), 1.36 (s, 36H);

^{13}C NMR ($CDCl_3$, 175 MHz): δ 160.2, 156.0, 152.1, 148.8, 137.3, 136.9, 135.6, 128.8, 128.6, 128.2, 127.9, 127.7, 127.1, 126.7, 124.3, 102.4, 99.5, 70.6, 69.6, 60.1, 55.4, 34.47 (2C), 30.6;

HRMS (ESI) *m/z* calculated for $C_{72}H_{79}O_6^+$ ($[M+H]^+$) 1039.5871, found 1039.5843.

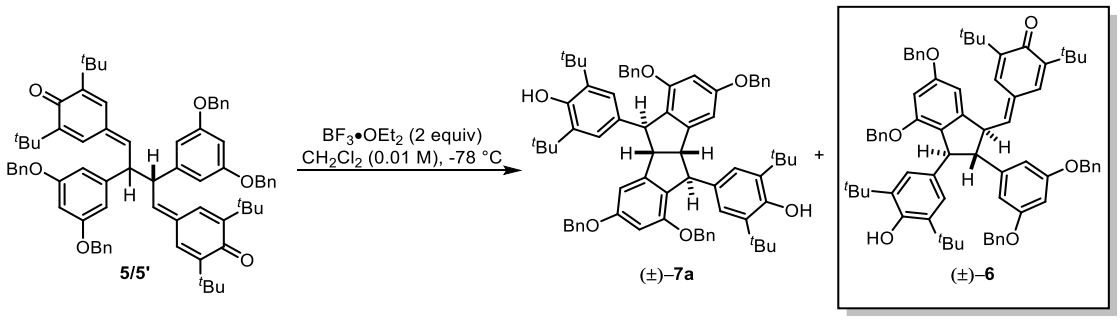

4-(((1S,2S,3S)-4,6-bis(benzyloxy)-2-(3,5-bis(benzyloxy)phenyl)-3-(3,5-di-tert-butyl-4-hydroxyphenyl)-2,3-dihydro-1H-inden-1-yl)methylene)-2,6-di-tert-butylcyclohexa-2,5-dien-1-one (6):

Rf (Hexanes/CH_2Cl_2/EtOAc, 85:10:5): 0.25;

IR (Neat): 3639, 2956, 1603, 1559, 1434, 1378, 1308, 1157, 1054, 1029 cm^{-1};

^1H NMR ($CDCl_3$, 500 MHz): δ 7.47 – 7.28 (m, 15H), 7.14 – 7.10 (m, 3H), 7.02 (d, *J* = 2 Hz, 1H), 6.89 (d, *J* = 2.4 Hz, 1H), 6.80 (S, 2H), 6.68 (d, *J* = 2.0 Hz, 1H), 6.66 (d, *J* = 2.0 Hz, 1H) 6.59 (d, *J* = 2.0 Hz, 1H), 6.47 (t, *J* = 2.2 Hz, 1H), 6.46 – 6.43 (m, overlap, 2H), 6.42 (d, *J* = 2.2 Hz, 2H), 5.08 (d, *J*= 11.2 Hz, 1H), 5.05 (d, *J*= 11.2 Hz, 1H), 5.03 (s, 1H), 4.91 (d, *J* = 11.2 Hz, 1H), 4.90 (d, *J* = 11.2 Hz, 2H), 4.87 (d, *J* = 11.2 Hz, 2H), 4.84 (d, *J* = 12.0 Hz, 1H), 4.65 (dd, *J* = 9.4, 9.4 Hz, 1H), 4.52 (d, *J* = 8.5 Hz, 1H), 3.14 (dd, *J* = 8.8, 8.8 Hz, 1H), 1.31 (s, 18H), 1.28 (s, 9H), 1.18 (s, 9H);

^{13}C NMR ($CDCl_3$, 175 MHz): δ 186.8, 160.7, 160.2, 156.2, 152.3, 148.8, 147.6, 147.2, 146.8, 144.0, 137.0, 136.9, 136.8, 135.5, 134.9, 134.2, 133.1, 128.82, 128.75, 128.4, 128.3, 128.2, 127.9, 127.8, 127.5, 127.1, 126.4, 124.8, 124.1, 107.6, 102.3, 100.5, 100.4, 70.7, 70.3, 69.6, 65.5, 57.0, 52.5, 35.4, 35.1, 34.5, 30.6, 29.66, 29.65;

HRMS (ESI) *m/z* calculated for $C_{72}H_{79}O_6^+$ ($[M+H]^+$) 1039.5871, found 1039.5849.

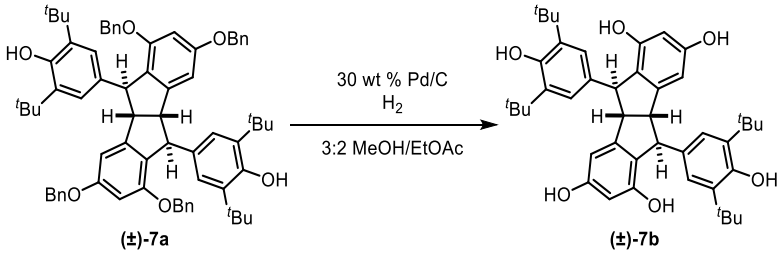

(4bS,5S,9bS,10S)-5,10-bis(3,5-di-tert-butyl-4-hydroxyphenyl)-4b,5,9b,10-tetrahydroindeno[2,1-a]indene-1,3,6,8-tetraol (7b): A heterogenous solution of **7a** (250 mg, 0.24 mmol, 1 equiv) and 30 wt % Pd/C (770 mg) in 5 mL of 3:2 EtOAc/MeOH was sparged with hydrogen gas for 30 min at room temperature. The walls of the vessel were rinsed down with a minimum of MeOH and the septum fitted with a full balloon of H_2. The reaction was allowed to stir at room temperature overnight under an atmosphere of hydrogen. The reaction solution was filtered over a pad of celite and concentrated to provide **7b** (155 mg, 0.23 mmol, 95% yield) as an amorphous white solid without need for further purification. NOTE: **7b** is unstable to prolonged storage in air at room temperature, but could be stored indefinitely at -20 °C in a container sealed under N_2.

Rf (CH_2Cl_2/MeOH, 95:5): 0.09;

IR (Neat): 3367, 2956, 1600, 1458, 1435, 1254, 1233, 1126, 1042 cm^{-1};

^1H NMR (Acetone d_6, 700 MHz): δ 7.09 (s, 4H), 6.64 (s, 2H), 6.21 (s, 2H), 4.61 (s, 2H), 3.94 (s, 2H), 1.38 (s, 36H);

^{13}C NMR (Acetone d_6, 175 MHz): δ 159.2, 155.3, 152.7, 150.3, 137.8, 124.5, 123.4, 103.4, 102.3, 60.7, 54.6, 35.1, 30.8;

HRMS (ESI) *m/z* calculated for $C_{44}H_{55}O_6^+$ ($[M+H]^+$) 679.3993, found 679.3989.

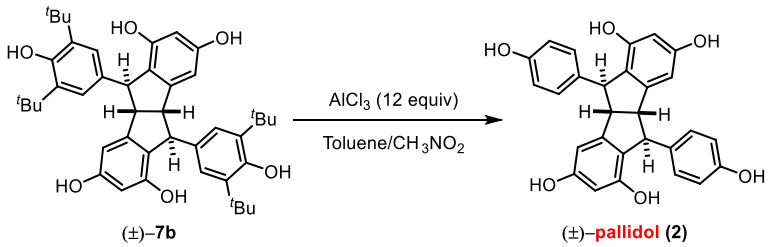

Pallidol (2): The following procedure was adapted from Hou et. al.[4] To a solution of **7b** (150 mg, 0.22 mmol, 1 equiv) in anhydrous toluene (10.8 mL, 0.02 M) at room temperature under inert atmosphere, $AlCl_3$ (354 mg, 0.28 mmol, 12 equiv) was added as a solution in CH_3NO_2 (1.2 mL, 2.25 M). The reaction was immediately heated to 60 °C for 30 min upon which the reaction was removed from the heat source and transferred to a separatory funnel containing 1:1 ice/1 N HCl. The reaction flask was rinsed with EtOAc several times and the contents transferred to the separatory funnel. The phases were separated and the aqueous layer extracted with additional ethyl acetate (2x). The organic layers were combined, washed with sat. aq. $NaHCO_3$, brine, dried over Na_2SO_4, and concentrated *in vacuo*. The crude material was purified by flash chromatography over SiO_2 (95:5 CH_2Cl_2/MeOH gradient to 90:10 CH_2Cl_2/MeOH) to afford pallidol (**2**) (80 mg, 0.17 mmol, 80%) as white amorphous solid.

Rf (CH_2Cl_2/MeOH, 95:5): 0.09;

IR (Neat): 3296, 1598, 1508, 1464, 1334, 1238, 1128, 1147, 995, 831 cm^{-1};

^1H NMR (Acetone d_6, 500 MHz): δ8.02 (s, 2H, OH), 8.00 (s, 2H, OH), 7.77 (s, 2H, OH), 6.98 (d, J = 8.5 Hz, 4H), 6.70 (d, J = 8.5 Hz, 4H), 6.62 (d, J = 2.0 Hz, 2H), 6.19 (d, J = 2.2 Hz, 2H) 4.57 (s, 2H), 3.81 (s, 2H);

^{13}C NMR (Acetone d_6, 175 MHz): δ 159.4, 156.4, 155.4, 150.4, 137.8, 129.1, 123.3, 115.9, 103.4, 102.6, 60.6, 54.0;

HRMS (ESI) *m/z* calculated for $C_{28}H_{23}O_6^+$ ($[M+H]^+$) 455.1450, found 455.1457.

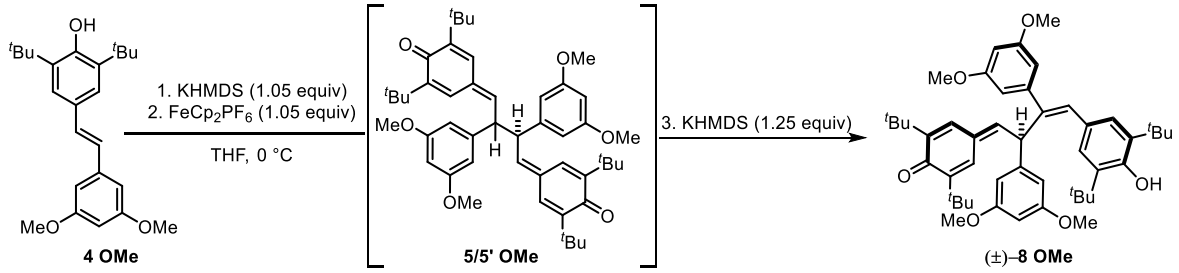

(*E*)-2,6-di-tert-butyl-4-(4-(3,5-di-tert-butyl-4-hydroxyphenyl)-2,3-bis(3,5-dimethoxyphenyl)but-3-en-1-ylidene)cyclohexa-2,5-dien-1-one (8 OMe): In a round bottom flask equipped with a septum and magnetic stir bar, a solution of **4 OMe** (1.88 g, 2.60 mmol, 1.00 equiv) in anhydrous THF (75 mL, 0.02 M) was cooled to 0 °C in an ice bath under inert atmosphere. To this, KHMDS (2.73 mL, 1.0 M soln. in THF, 1.05 equiv) was added slowly. The solution was allowed to stir at temperature for 10 minutes, upon which the septum was removed and ferrocenium hexafluorophosphate (932 mg, 97% purity, 2.73 mmol, 1.05 equiv) was added in two 466 mg portions, separated by 15 minutes. After the reaction was deemed complete by TLC (ca. 30 min), KHMDS (3.25 mL, 1.0 M soln. in THF, 1.25 equiv), was added, turning the solution from yellow-orange to opaque. After 15 min, the reaction mixture was quenched by the addition of sat. aq. NH_4Cl, turning the organic phase bright red. The reaction was diluted with EtOAc and transferred to a separatory funnel containing DI H_2O. The phases were separated and the aqueous layer extracted with additional EtOAc (2x). The organic layers were combined and washed with brine, dried over Na_2SO_4, and concentrated *in vacuo*. The crude residue was taken up in CH_2Cl_2 and dried on to Celite and the solvent removed completely under reduced pressure. The crude material was purified by flash chromatography over a short plug of SiO_2 (100:0 Hexanes/EtOAc [to elute ferrocene] then 100% CH_2Cl_2) to afford **8** (1.88 g, 1.30 mmol, crude), which was taken directly on to the next step (see S18). For characterization, the material can instead be eluted with a gradient 95:2.5:2.5 to 90:5:5 Hexanes/EtOAc/CH_2Cl_2 mobile phase.

Rf (Hexanes/EtOAc, 95:5): 0.17;

IR (Neat): 3630, 2956, 2359, 1653, 1590, 1457, 1356, 1204, 1153, 1065, 833, 738 cm^{-1};

^1H NMR ($CDCl_3$, 500 MHz): δ 6.92 (s, 2H), 6.73 (d, *J* = 2.9 Hz, 1H), 6.52 (d, *J* = 2.2 Hz, 2H), 6.39 (d, *J* = 2.2 Hz, 2H), 6.31 (t, *J* = 2.2 Hz, 1H), 6.24 (d, *J* = 2.7 Hz, 1H), 6.23 (t, *J* = 2.2 Hz, 1H), 5.80 (d, *J* = 1.7 Hz, 1H), 5.00 (s, 1H), 4.97 (dd, *J* = 9.6, 1.8 Hz, 1H), 3.7 (s, 6H), 3.68 (s, 6H), 1.37 (s, 18H), 1.30 (s, 9H), 0.91 (s, 9H);

^{13}C NMR ($CDCl_3$, 175 MHz): δ 186.6, 160.9, 160.7, 152.8, 147.6, 146.6, 146.22, 146.15, 144.5, 141.6, 137.5, 135.4, 130.8, 127.8, 124.0, 106.9, 105.0, 100.2, 98.2, 65.3, 56.6, 55.5, 55.4, 54.6, 35.0, 34.8, 34.5, 30.5, 30.0, 29.3;

HRMS (ESI) *m/z* calculated for $C_{48}H_{63}O_6^+$ ($[M+H]^+$) 735.4619, found 735.4616.

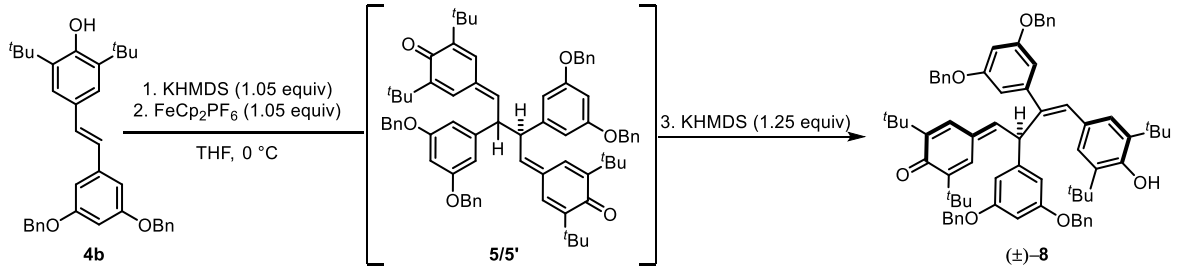

(*E*)-4-(2,3-bis(3,5-bis(benzyloxy)phenyl)-4-(3,5-di-tert-butyl-4-hydroxyphenyl)but-3-en-1-ylidene)-2,6-di-tert-butylcyclohexa-2,5-dien-1-one (8): In a round bottom flask equipped with a septum and magnetic stir bar, a solution of **4b** (1.00 g, 1.92 mmol, 1.00 equiv) in anhydrous THF (75 mL, 0.02 M) was cooled to 0 °C in an ice bath under inert atmosphere. To this, KHMDS (1 M solution in THF, 1.61 mL, 1.05 equiv) was added slowly. The solution was allowed to stir at temperature for 10 minutes, upon which the septum was removed and ferrocenium hexafluorophosphate (655 mg, 97% purity, 2.04 mmol, 1.05 equiv) was added in two 328 mg portions, separated by 15 minutes. After the reaction was complete by TLC (ca. 30 min), KHMDS (1.92 mL, 1.0 M soln. in THF, 1.25 equiv), was added, turning the solution from yellow-orange to opaque. After 15 min, the reaction mixture was quenched by the addition of sat. aq. NH_4Cl. The reaction was diluted with EtOAc and transferred to a separatory funnel containing DI H_2O. The phases were separated and the aqueous layer extracted with EtOAc (2x). The organic layers were combined and washed with brine, dried over Na_2SO_4, and concentrated *in vacuo*. The crude residue was taken up in CH_2Cl_2 and dried on to Celite and the solvent removed under reduced pressure. Purification by flash chromatography over a short plug of SiO_2 (100% Hexanes [to elute ferrocene], then 100% CH_2Cl_2) afforded **8** (1.00 g, 0.96 mmol, crude), which was taken directly on to the next step (see S19). For characterization, the material can instead be eluted with a gradient 95:2.5:2.5 to 90:5:5 Hexanes/EtOAc/CH_2Cl_2 mobile phase.

Rf (Hexanes/EtOAc/CH_2Cl_2, 85:10:5): 0.25;

IR (Neat): 3641, 2952, 1654, 1590, 1435, 1373, 1264, 1151, 1054, 1028, 834, 733, 696 cm^{-1};

^1H NMR ($CDCl_3$, 500 MHz): δ 7.39 – 7.29 (m, 20H), 6.91 (s, 2H), 6.71 (d, *J* = 2.7 Hz, 1H), 6.64 (d, *J* = 2.2 Hz, 2H), 6.52 (d, *J* = 2.2 Hz, 2H), 6.50 (t, *J* = 2.2 Hz, 1H), 6.42 (t, *J* = 2.2 Hz, 1H), 6.23 (d, *J* = 2.7 Hz, 1H), 5.79 (d, *J* = 2.0 Hz, 1H), 5.02 (s, 1H), 4.95 (d, *J* = 11.5 Hz, 2H), 4.94 (d, *J* = 11.5 Hz, 2H), 4.89 (d, *J* = 11.5 Hz, 2H), 4.88 (d, *J* = 11.5 Hz, 2H), 3.66 (d, *J* = 9.8 Hz, 1H), 1.38 (s, 18 H), 1.31 (s, 9H), 0.92 (s, 9H);

^{13}C NMR ($CDCl_3$, 175 MHz): δ 186.6, 160.2, 159.9, 152.9, 147.6, 146.5, 146.2, 144.4, 141.6, 137.5, 137.0, 136.9, 135.4, 130.9, 128.80, 128.78, 128.76, 128.2, 127.9, 127.82, 127.76, 127.7, 124.0, 108.2, 106.3, 102.0, 100.3, 70.32, 70.27, 65.2, 56.6, 54.7, 35.0, 34.8, 34.5, 30.5, 30.0, 29.3;

HRMS (ESI) *m/z* calculated for $C_{72}H_{79}O_6^+$ ($[M+H]^+$) 1039.5832, found 1039.5838.

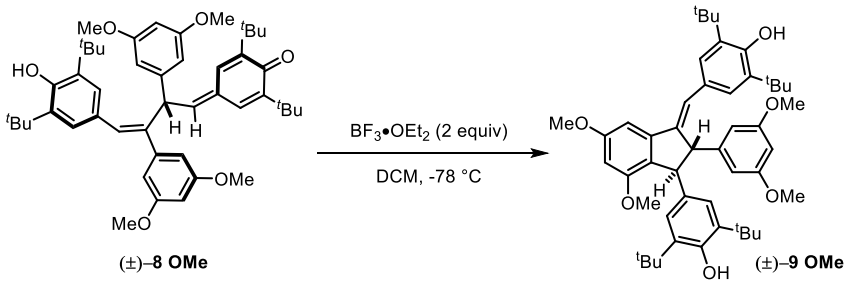

2,6-di-tert-butyl-4-((1S,2S)-3-((E)-3,5-di-tert-butyl-4-hydroxybenzylidene)-2-(3,5-dimethoxyphenyl)-5,7-dimethoxy-2,3-dihydro-1H-inden-1-yl)phenol (9 OMe): A solution of crude **8 OMe** (S12) (260 mg, 0.35 mmol, 1.00 equiv) in anhydrous CH_2Cl_2 (35 mL, 0.01 M) was cooled to -78 °C in a dry ice/acetone bath. To this, BF_3•OEt_2 (175 μL, 46.5% in diethyl ether, 2 equiv) was added dropwise, turning the solution into a deep ruby red color. After 5 min, the reaction was quenched with sat. aq. $NaHCO_3$ at -78 °C and allowed to warm to room temperature with vigorous stirring. The reaction mixture was diluted with CH_2Cl_2 and transferred to a separatory funnel containing additional sat. aq. $NaHCO_3$. The phases were separated and the aqueous layer was extracted with additional CH_2Cl_2 (2x). The organic layers were combined, washed with brine, dried over sodium sulfate and concentrated *in vacuo*. The crude residue was purified by flash chromatography using a 90:5:5 Hexanes/EtOAc/CH_2Cl_2 mobile phase to afford **9 OMe** (235 mg, 0.32 mmol, 90% yield over 3 steps) as a pale yellow amorphous solid.

Rf (Hexanes/EtOAc, 90:10): 0.33;

IR (Neat): 3633, 2965, 1593, 1435, 13783, 1304, 1234, 1153, 1050, 1028, 736 cm^{-1};

^1H NMR ($CDCl_3$, 500 MHz): δ 7.13 (s, 1H), 7.08 (s, 2H), 7.06 (s, 2H), 6.83 (d, *J* = 1.7 Hz, 1H), 6.50 (d, *J* = 2.2 Hz, 2H), 6.29 (d, *J* = 2.0 Hz, 2H), 5.18 (s, 1H), 4.99 (s, 1H), 4.49 (s, 1H), 4.32 (s, 1H), 3.92 (s, 3H), 3.73 (s, 6H), 3.65 (s, 3H), 1.35 (s, 18H), 1.31 (s, 18H);

^{13}C NMR ($CDCl_3$, 175 MHz): δ 161.3, 161.0, 160.8, 157.5, 153.1, 152.0, 147.9, 145.1, 142.5, 136.3, 135.8, 135.3, 128.9, 127.2, 126.3, 125.9, 124.1, 123.9, 106.0, 104.9, 98.9, 98.3, 95.5, 58.8, 57.0, 55.8, 55.4, 55.3, 34.50, 34.45, 30.5, 30.4;

HRMS (ESI) *m/z* calculated for $C_{48}H_{63}O_6^+$ ($[M+H]^+$) 735.4625, found 735.4648.

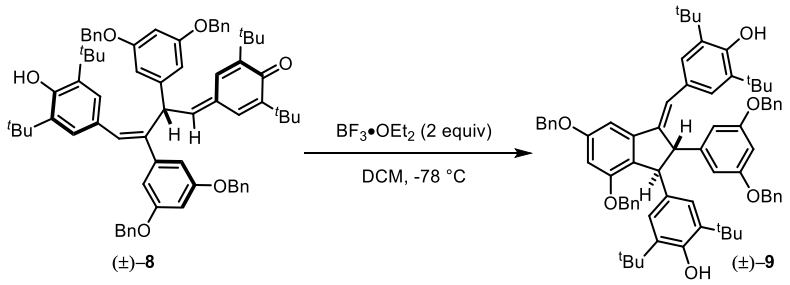

4-((1S,2S)-5,7-bis(benzyloxy)-2-(3,5-bis(benzyloxy)phenyl)-3-((E)-3,5-di-tert-butyl-4-hydroxybenzylidene)-2,3-dihydro-1H-inden-1-yl)-2,6-di-tert-butylphenol (9): A solution of crude **8** (S13) (1.00 g, 0.96 mmol, 1.00 equiv) in anhydrous CH_2Cl_2 (96 mL, 0.01 M) was cooled to -78 °C in a dry ice/acetone bath under inert atmosphere. To this, BF_3•OEt_2 (511 μL, 46.5% in diethyl ether 2 equiv) was added dropwise, turning the solution into a deep ruby red color. After 5 min, the reaction was quenched with sat. aq. $NaHCO_3$ at -78 °C and allowed to warm to room temperature with vigorous stirring. The reaction mixture was diluted with CH_2Cl_2 and transferred to a separatory funnel containing additional sat. aq. $NaHCO_3$. The phases were separated and the aqueous layer was extracted with additional CH_2Cl_2 (2x). The organic layers were combined, washed with brine, dried over sodium sulfate and concentrated *in vacuo*. The crude residue was purified by flash chromatography using a 90:5:5 Hexanes/EtOAc/CH_2Cl_2 mobile phase to afford **9** (898 mg, 0.86 mmol, 90% yield over 3 steps) as a pale yellow amorphous solid.

Rf (Hexanes/CH_2Cl_2/EtOAc, 85:10:5): 0.27;

IR (Neat): 3632, 2953, 1592, 1451, 1434, 1372, 1304, 1154, 1048, 774, 696 cm^{-1};

^1H NMR ($CDCl_3$, 500 MHz): δ 7.50 (m, 2H), 7.41 – 7.28 (m, 13H, benzyl group overlap), 7.21 (m, 3H), 7.14 (d, *J* = 0.7 Hz, 1H), 7.04 (s, 2H), 7.03-7.01 (m, 2H, benzyl group H's), 7.00 (s, 2H), 6.95 (d, *J* = 1.7 Hz, 1H), 6.59 (d, *J* = 2.2 Hz, 2H), 6.42 (t, *J* = 2.2 Hz, 1H), 6.41 (d, *J* = 1.7 Hz, 1H), 5.30 (s, 2H), 5.16 (s, 1H, OH), 5.15 (s, 2H), 4.99 (s, 1H, OH), 4.95 (d, *J* = 12.2 Hz, 2H), 4.93 (d, *J* = 12.2 Hz, 2H), 4.90 (d, *J* = 12.0 Hz, 1H), 4.84 (d, *J* = 12.0Hz, 1H), 4.40 (s, 1H), 4.32 (s, 1H), 1.31 (s, 18H), 1.29 (s, 18H);

^{13}C NMR ($CDCl_3$, 175 MHz): δ 160.5, 160.2, 156.4, 153.2, 152.1, 148.1, 145.3, 142.5, 137.3, 137.20, 137.16, 136.6, 135.7, 135.5, 128.9, 128.80, 128.77, 128.7, 128.6, 128.5, 128.21, 128.18, 128.1, 128.0, 127.9, 127.8, 127.7, 127.2, 127.1, 126.0, 124.2, 124.1, 107.1, 100.8, 100.1, 97.0, 70.6, 70.2, 69.6, 58.9, 57.6, 34.5, 34.4, 30.6, 30.5, 30.4;

HRMS (ESI) *m/z* calculated for $C_{72}H_{79}O_6^+$ ($[M+H]^+$) 1039.5871, found 1039.5829.

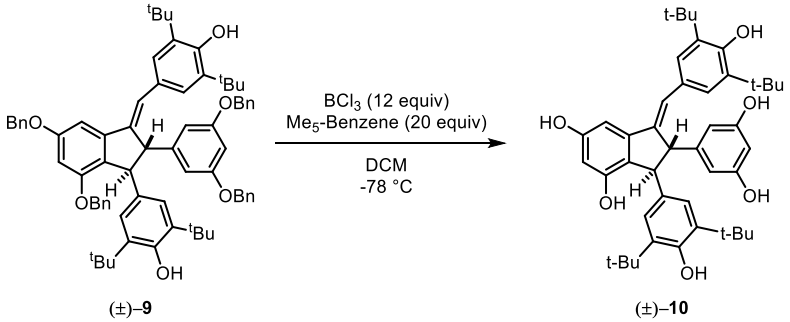

(±)–**9** (±)–**10**

(2S,3S)-1-((E)-3,5-di-tert-butyl-4-hydroxybenzylidene)-3-(3,5-di-tert-butyl-4-hydroxyphenyl)-2-(3,5-dihydroxyphenyl)-2,3-dihydro-1H-indene-4,6-diol: A solution of **9** (460 mg, 0.44 mmol, 1.00 equiv) and pentamethylbenzene (1.30 g, 8.8 mmol, 20 equiv) in anhydrous CH_2Cl_2 (22 mL, 0.02 M) was cooled to -78 °C in a dry ice/acetone bath under inert atmosphere. To this, BCl_3 (5.3 mL, 1.0 M soln. in CH_2Cl_2, 12 equiv) was added dropwise turning the yellow solution a brilliant magenta color. Reaction was maintained at -78 °C until deemed complete by TLC (ca. 2h). At this point, the reaction was quenched with a 4:1 THF/sat. aq. $NaHCO_3$ mixture at -78 °C and allowed to warm to room temperature while stirring vigorously. Upon thawing, the solution returned to a yellow color. The reaction was diluted with ethyl acetate (50 mL) and transferred to a separatory funnel containing additional sat. aq. $NaHCO_3$. The phases were separated and the aqueous layer extracted with additional EtOAc (2x). The organic layers were combined and washed with brine, dried over Na_2SO_4, and concentrated *in vacuo*. The crude residue was purified by flash chromatography over SiO_2 (98:2 CH_2Cl_2/MeOH gradient to 90:10 CH_2Cl_2/MeOH) to afford **10** (245 mg, 0.36 mmol, 82% yield) as a white amorphous solid. NOTE: **10** is unstable to prolonged storage in air at room temperature, but could be stored indefinitely at -20 °C in a container sealed under N_2.

Rf (CH_2Cl_2/MeOH, 95:5): 0.09;

IR (Neat): 3376, 2957, 1599, 1547, 1467, 1434, 1341, 1237, 1157, 1006, 838 cm^{-1};

^1H NMR (Acetone d_6, 700 MHz): δ 8.13 (br. s., 4H, OH), 7.86 (br. s., 2H, OH), 7.15 (s, 2H), 7.12 (s, 1H), 7.05 (s, 2H), 6.80 (s, 1H), 6.38 (s, 2H), 6.29 (s, 1H), 6.20 (s, 1H), 5.99 (s, 1H), 5.73 (s, 1H), 4.33 (s, 1H), 4.26 (s, 1H), 1.34 (s, 18H), 1.31 (s, 18H);

^{13}C NMR (Acetone d_6, 175 MHz): δ 159.6, 159.5, 155.9, 154.0, 152.9, 148.8, 147.2, 143.0, 137.9, 137.8, 137.6, 130.0, 126.6, 124.4, 107.0, 103.6, 101.5, 98.8, 60.5, 58.0, 35.2, 30.8, 30.7;

HRMS (ESI) *m/z* calculated for $C_{44}H_{55}O_6^+$ ($[M+H]^+$) 679.3993, found 679.3989.

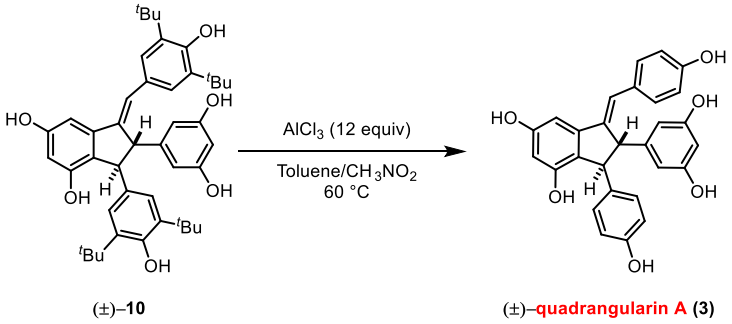

Quadrangularin A (3): The following procedure was adapted from Hou et. al.[4] To a solution of **10** (80.0 mg, 0.12 mmol, 1.00 equiv) in anhydrous toluene (5.4 mL, 0.022 M) at room temperature under inert atmosphere, $AlCl_3$ (190 mg, 1.44 mmol, 12.0 equiv) was added as a solution in CH_3NO_2 (600 µL, 2.33 M). The reaction was immediately heated to 60 °C for 30 min upon which the reaction was removed from the heat source and transferred to a separatory funnel containing 1:1 ice/1 N HCl. The reaction flask was rinsed with EtOAc several times and the contents transferred to the separatory funnel. The phases were separated and the aqueous layer extracted with additional ethyl acetate (2x). The organic layers were combined, washed with brine, dried over Na_2SO_4, and concentrated *in vacuo*. The crude material was purified by flash chromatography over SiO_2 (95:5 CH_2Cl_2/MeOH gradient to 90:10 CH_2Cl_2/MeOH) to afford quadrangularin A (**3**) (43 mg, 0.095 mmol 80%) as a tan amorphous solid.

Rf (CH_2Cl_2/MeOH, 95:5): 0.09;

IR (Neat): 3245, 1596, 1509, 1446, 1334, 1233, 1172, 1147, 1005, 831 cm^{-1};

^1H NMR (Acetone d_6, 500 MHz): δ 8.16 (s, 6H), 7.21 (d, J = 8.5 Hz, 2H), 7.05 (d, J = 1.0 Hz, 1H), 6.92 (d, J = 8.5 Hz), 6.79 (d, J = 2.0 Hz, 1H), 6.68 (d, J = 5.4 Hz, 2H), 6.67 (d, J = 5.4 Hz, 2H), 6.31 (d, J = 2.2 Hz, 2H), 6.30 (d, J = 2.0 Hz, 1H), 6.19 (t, J = 2.2 X 2 Hz, 1H), 4.27 (s, 1H), 4.14 (s, 1H);

^{13}C NMR (Acetone d_6, 175 MHz): δ 159.7, 159.7, 157.4, 156.6, 155.9, 149.1, 147.1, 142.7, 137.8, 131.1, 129.8, 128.8, 124.6, 123.0, 116.0, 115.9, 106.3, 103.7, 101.6, 98.4, 60.7, 57.7;

HRMS (ESI) *m/z* calculated for $C_{28}H_{23}O_6^+$ ($[M+H]^+$) 455.1489, found 455.1485.

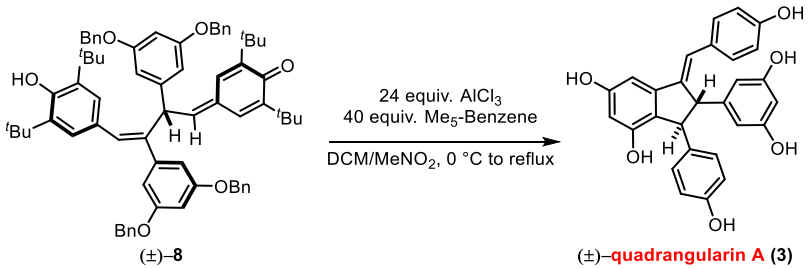

Friedel-Crafts Cyclization – Global Deprotection of 8 with $AlCl_3$

A solution of **8** (370 mg, 0.34 mmol, 1 equiv) and pentamethylbenzene (2.1 g, 14.1 mmol, 40 equiv) in anhydrous CH_2Cl_2 (57 mL, 0.005 M) was cooled to 0 °C in an ice bath under inert atmosphere. To this, $AlCl_3$ (1.14 g, 8.6 mmol, 25 equiv) was added slowly as a solution in CH_3NO_2 (14 mL, 0.6 M) via syringe turning the clear yellow solution a deep red color. Upon addition, the reaction flask was fitted with a reflux condenser and heated to 60 °C, allowing the reaction to stir at this temperature for 15 minutes. The reaction was removed from the heat and the contents transferred to a separatory funnel containing 1:1 ice/1N HCl. The reaction flask was rinsed with EtOAc several times and the contents transferred to the separatory funnel. The phases were separated and the aqueous layer extracted with additional ethyl acetate (2x). The organic layers were combined, washed with sat. aq. $NaHCO_3$, brine, dried over Na_2SO_4, and concentrated *in vacuo*. The dry crude material was dissolved in a minimal amount of diethyl ether using sonication. Then hexane was added dropwise to the sonicating material to precipitate out crude quadrangularin A as a brown amorphous solid, which was collected by vacuum filtration. This crude material (nearly pure by NMR), was purified via flash chromatography (95:2.5:2.5 gradient to 90:5:5 Chloroform/Acetone/MeOH) to yield quadrangularin A (**3**) (82 mg, 0.18 mmol, 51%) as a tan amorphous solid (see S23 for characterization data).

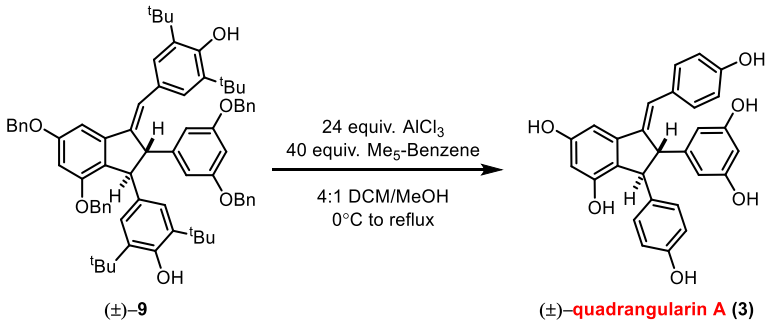

(±)–**9** (±)–**quadrangularin A (3)**

Global Deprotection of 9 with $AlCl_3$

A solution of **9** (30 mg, 0.03 mmol, 1 equiv) and pentamethylbenzene (170 mg, 1.14 mmol, 40 equiv.) in CH_2Cl_2 (4.5 mL, 0.005 M) was cooled to 0 °C in an ice bath under inert atmosphere. To this, $AlCl_3$ (92 mg, 0.70 mmol, 24 equiv) was added as a solution in CH_3NO_2 (1.5 mL, 0.48 M) via syringe, turning the clear yellow solution a deep red color. Upon addition, the reaction flask was fitted with a reflux condenser and heated to 60 °C, allowing the reaction to stir at this temperature for 1 hour. The reaction was cooled down to 0 °C, quenched with sat. aq. $NaHCO_3$, and stirred until the solution turned from red to clear yellow. The reaction was transferred to a separatory funnel and washed with ice cold 1N HCl (CO_2 evolution). The organic layer was removed and the aqueous layer was extracted with EtOAc (2x). The organic layers were combined, washed with sat. aq. $NaHCO_3$, brine, dried over Na_2SO_4, and concentrated *in vacuo*. The crude residue was purified by flash chromatography over SiO_2 (17:2:1 Chloroform/MeOH/Acetone) to yield quadrangularin A (**3**) (11.5 mg, 88%, 5:1 ratio of quadrangularin A and its internal alkene isomer) as a tan amorphous solid (see S23 for characterization data).

Radical Clock Experiments with 4b, 7a, 9, and BHT

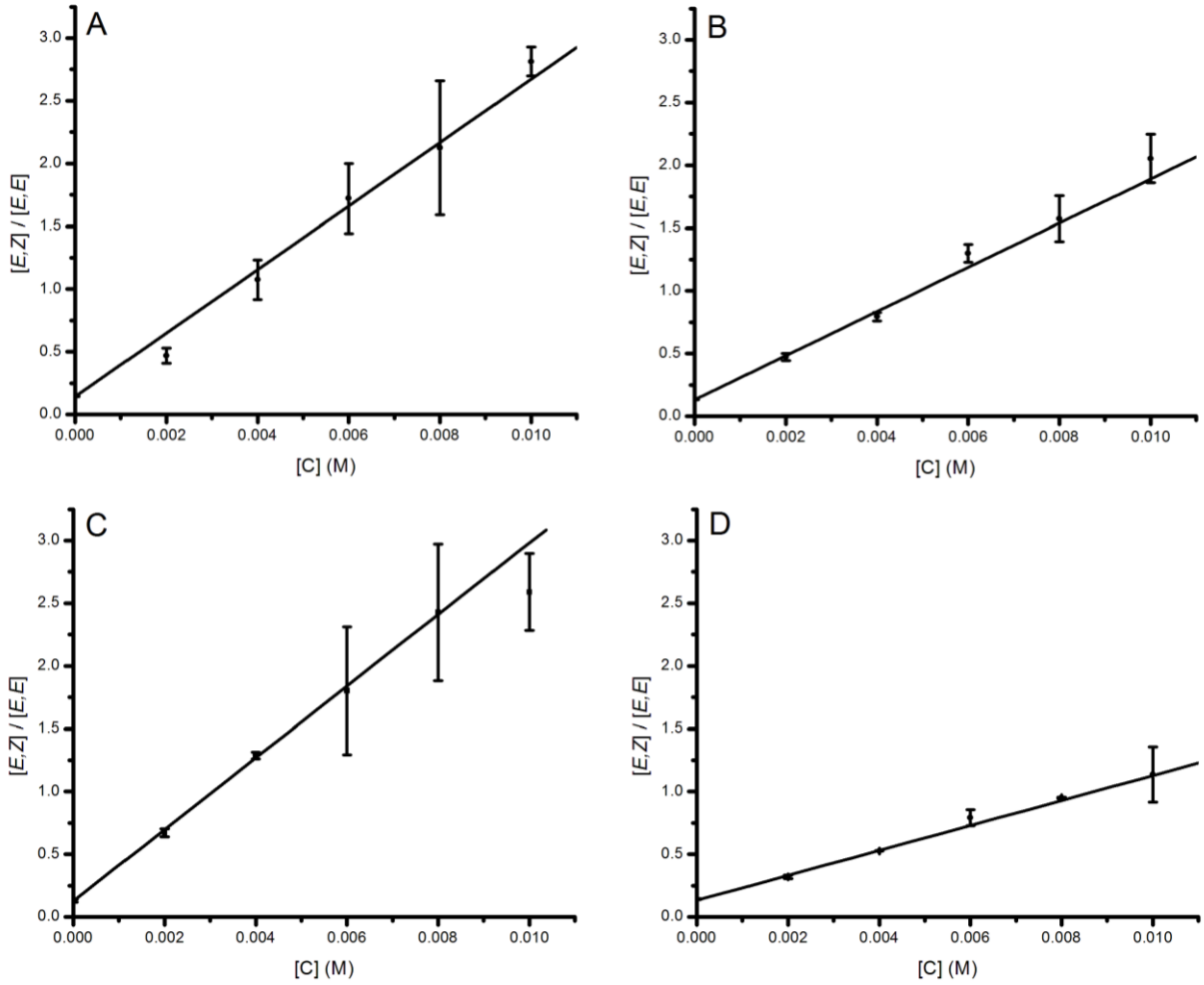

Figure S1. Ratio of [*E*,*Z*]:[*E*,*E*] products versus concentration of *t*-Bu$_2$-resveratrol (**4b**) (A), *t*-Bu$_2$-pallidol (**7a**) (B), *t*-Bu$_2$-quadrangularin A B (**9**) (C), and BHT (D) in the MeOAMVN-initiated (0.01 M) autoxidation of methyl linoleate (0.1 M) in chlorobenzene at 37°C.

Inhibited Oxidations of Phosphatidylcholine Liposomes

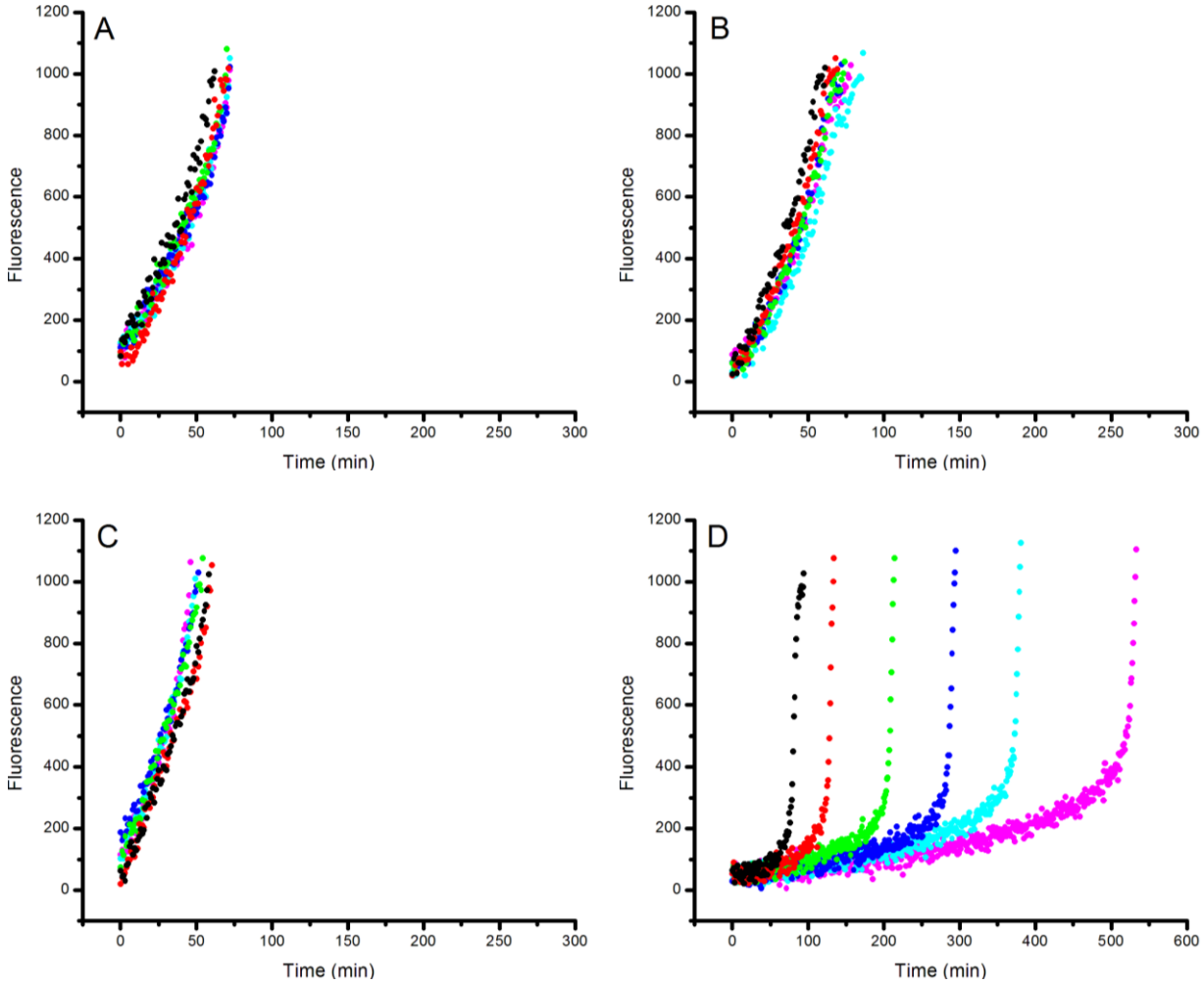

Figure S2. Representative fluorescence intensity-time profiles from MeOAMVN-mediated (0.68 mM) oxidations of egg phosphatidylcholine liposomes (1 mM in pH 7.4 PBS buffer) containing 0.15 μM H_2B-PMHC probe and increasing concentrations (2.5 μM, 5.0 μM, 10 μM, 15 μM, 20 μM, 30 μM) of resveratrol (**1**) (A), pallidol (**2**) (B), quadrangularin A (**3**) (C) and PMHC (D). Fluorescence (λ_{ex} = 485 nm, λ_{em} = 520 nM) was recorded every 60s.

Inhibited Oxidations of Phosphatidylcholine Liposomes Cont'd

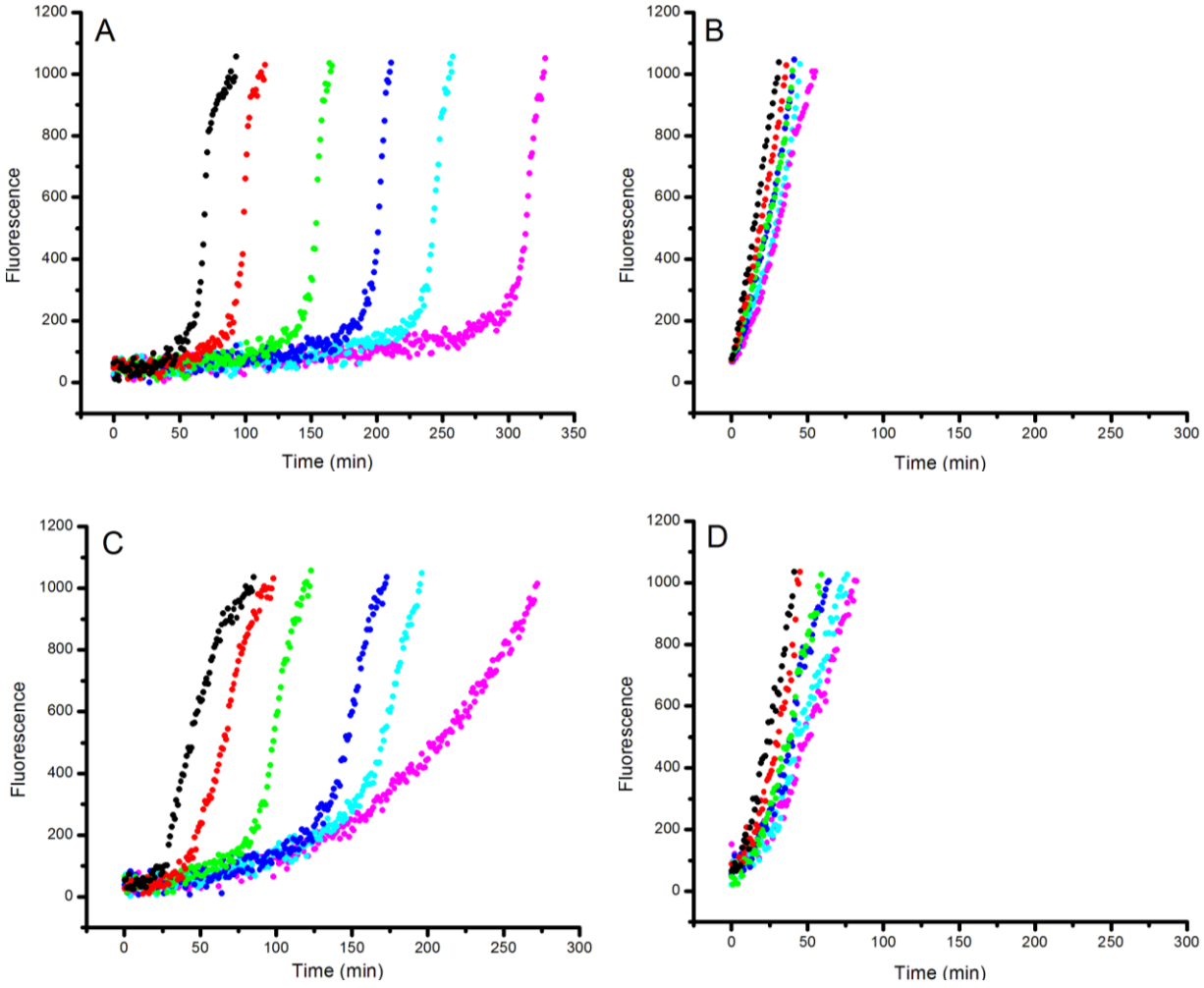

Figure S3. Representative fluorescence intensity-time profiles from MeOAMVN-mediated (0.68 mM) oxidations of egg phosphatidylcholine liposomes (1 mM in pH7.4 PBS buffer) containing 0.15 μM H_2B-PMHC and increasing concentrations (2.5 μM, 5.0 μM, 10 μM, 15 μM, 20 μM, 30 μM) of *t*-Bu_2-resveratrol (**4a**) (A), *t*-Bu_2-pallidol (**7b**) (B), *t*-Bu_2-quadrangularin A (**10**) (C) and BHT (D). Fluorescence (λ_{ex} = 485 nm; λ_{em} = 520 nM) was recorded every 60s.

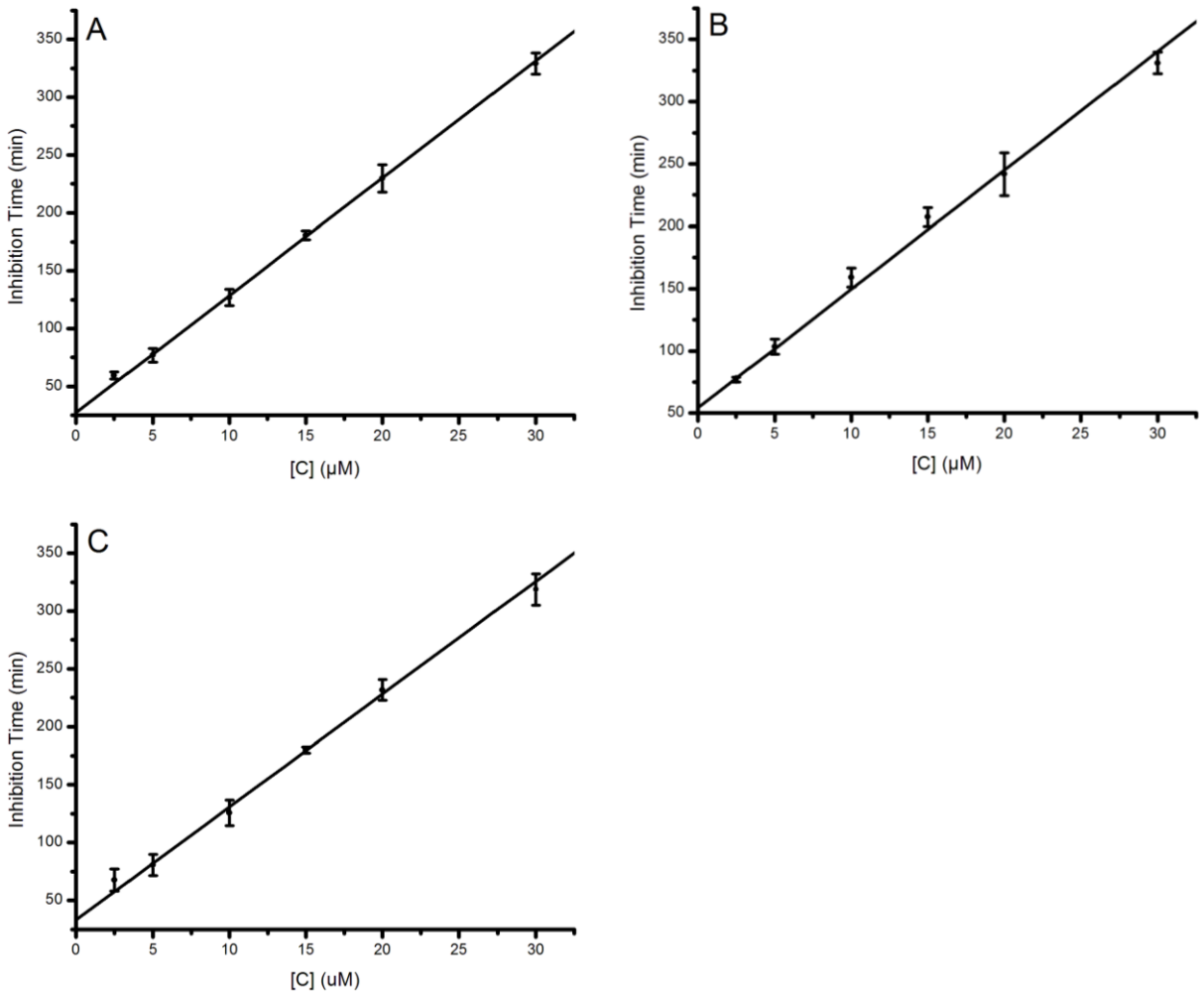

Figure S4. Inhibition time-concentration profiles from MeOAMVN-mediated (0.68 mM) oxidations of egg phosphatidylcholine liposomes (1 mM in pH 7.4 PBS buffer) containing 0.15 μM H_2B-PMHC and increasing concentrations (2.5 μM, 5.0 μM, 10 μM, 15 μM, 20 μM, 30 μM) of the inhibitors which display a clear inhibited period: PMHC (A), *t*-Bu_2-resveratrol (**4**) (B), and *t*-Bu_2-quadrangularin A (**10**) (C). The stoichiometric numbers (*n*) were calculated based on the slopes of the line of best fit relative to PMHC, for which *n*=2.

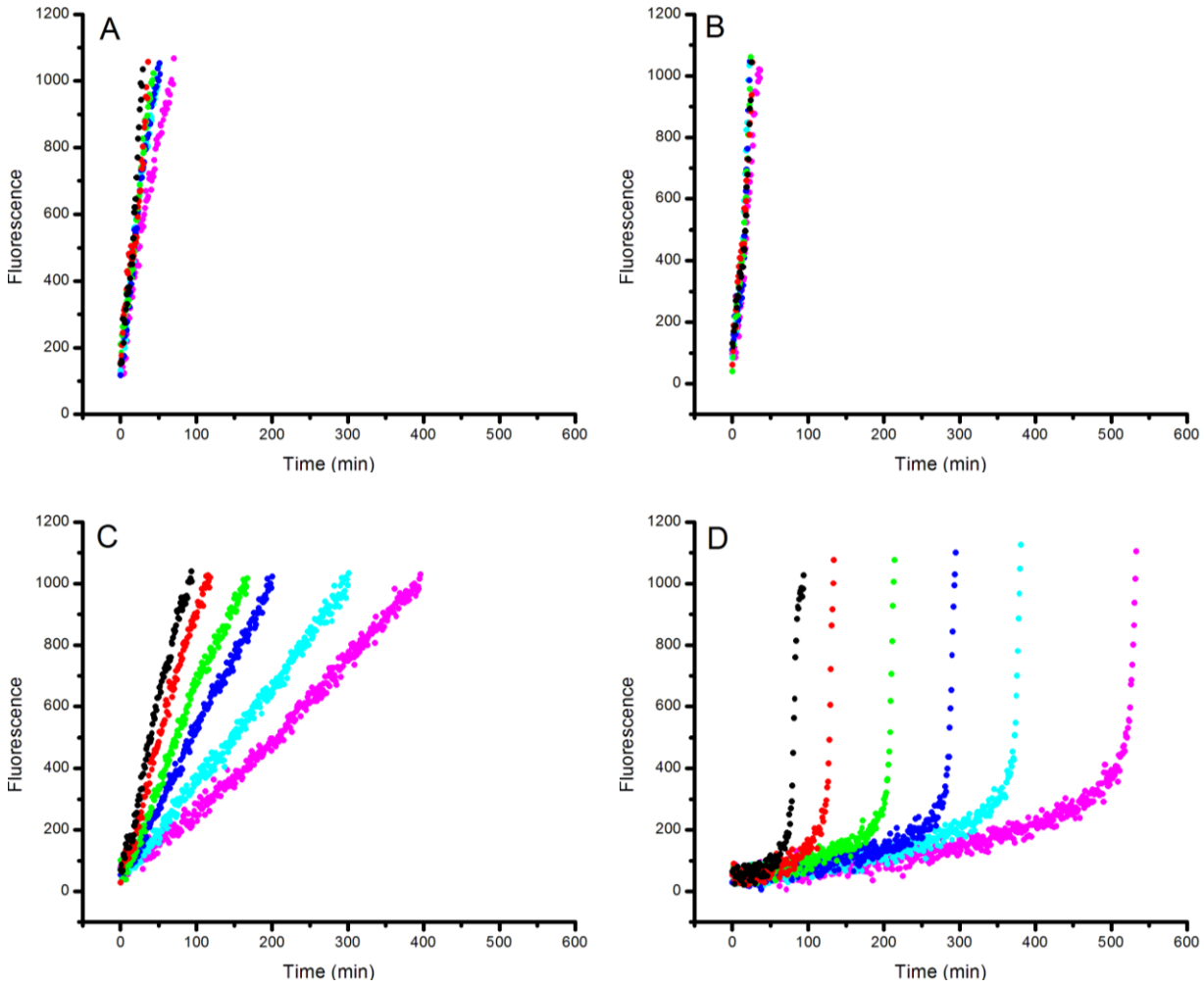

Figure S5. Representative fluorescence intensity-time profiles from AAPH-mediated (2.7 mM) oxidations of egg phosphatidylcholine liposomes (1 mM in pH 7.4 PBS buffer) containing 0.15 μM H_2B-PMHC and increasing concentrations (2.5 μM, 5.0 μM, 10 μM, 15 μM, 20 μM, 30 μM) of resveratrol (**1**) (A), pallidol (**2**) (B), quadrangularin A (**3**) (C) and PMHC (D). Fluorescence (λ_{ex} = 485 nm; λ_{em} = 520 nM) was recorded every 60s.

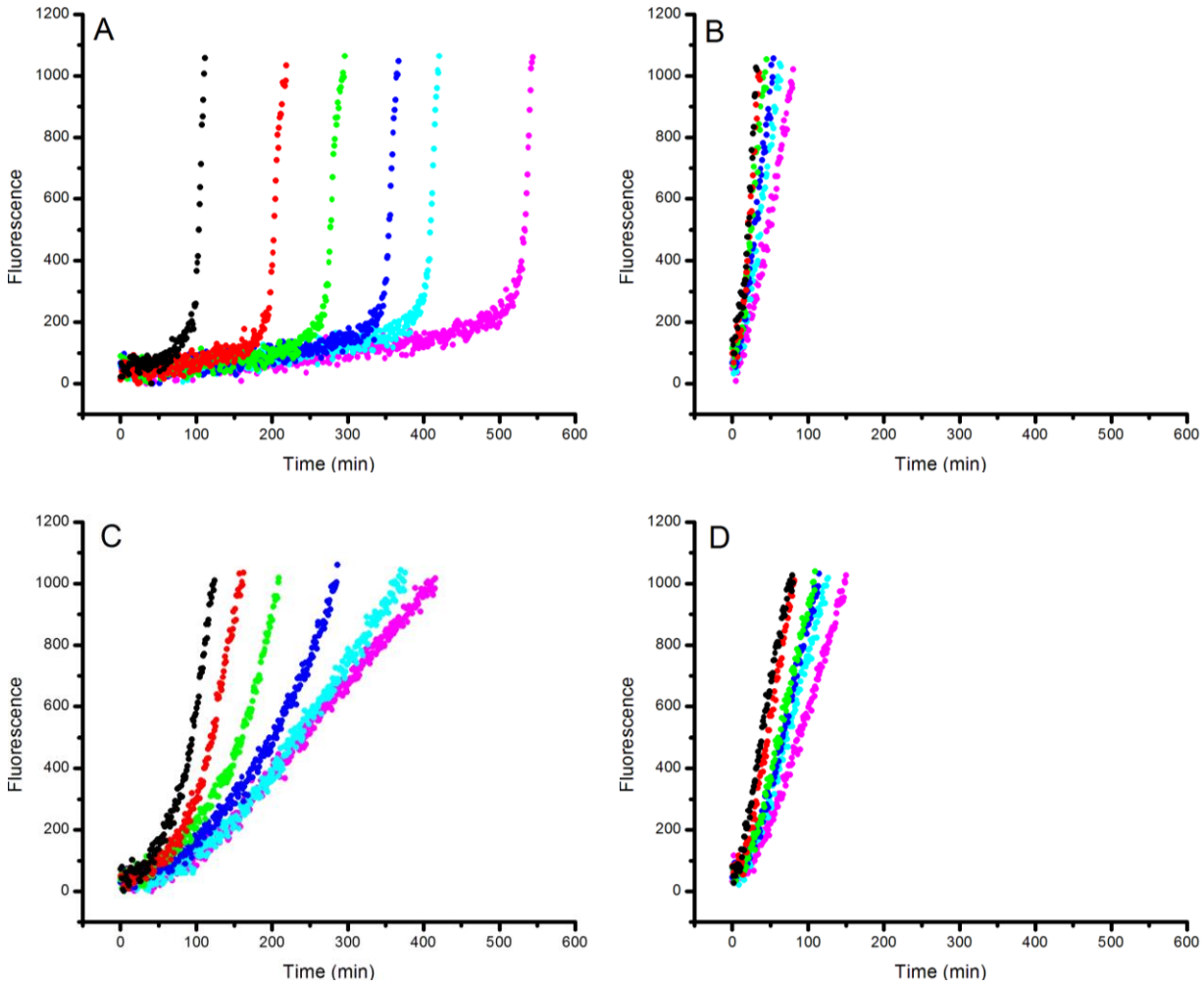

Figure S6. Representative fluorescence intensity-time profiles from AAPH-mediated (2.7 mM) oxidations of egg phosphatidylcholine liposomes (1 mM in pH 7.4 PBS buffer) containing 0.15 μM H_2B-PMHC and increasing concentrations (2.5 μM, 5.0 μM, 10 μM, 15 μM, 20 μM, 30 μM) of *t*-Bu_2-resveratrol (**4a**) (A), *t*-Bu_2-pallidol (**7b**) (B), *t*-Bu_2-quadrangularin A (**10**) (C) and BHT (D). Fluorescence (λ_{ex} = 485 nm; λ_{em} = 520 nM) was recorded every 60s.

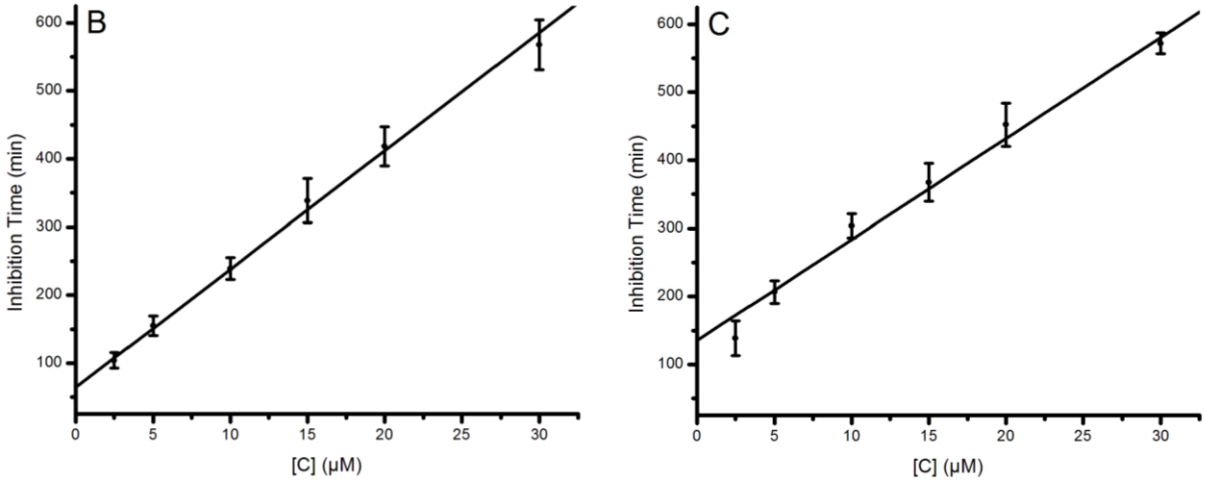

Figure S7. Inhibition time-concentration profiles from AAPH-mediated (2.7 mM) oxidations of egg phosphatidylcholine liposomes (1 mM in pH 7.4 PBS buffer) containing 0.15 μM H_2B-PMHC and increasing concentrations (2.5 μM, 5.0 μM, 10 μM, 15 μM, 20 μM, 30 μM) of the inhibitors which display a clear inhibited period: PMC (B) and *t*-Bu_2-resveratrol (**4a**) (C). The stoichiometric numbers (*n*) were calculated based on the slopes of the line of best fit relative to PMHC, for which *n*=2.

Cellular Lipid Peroxidation Assay

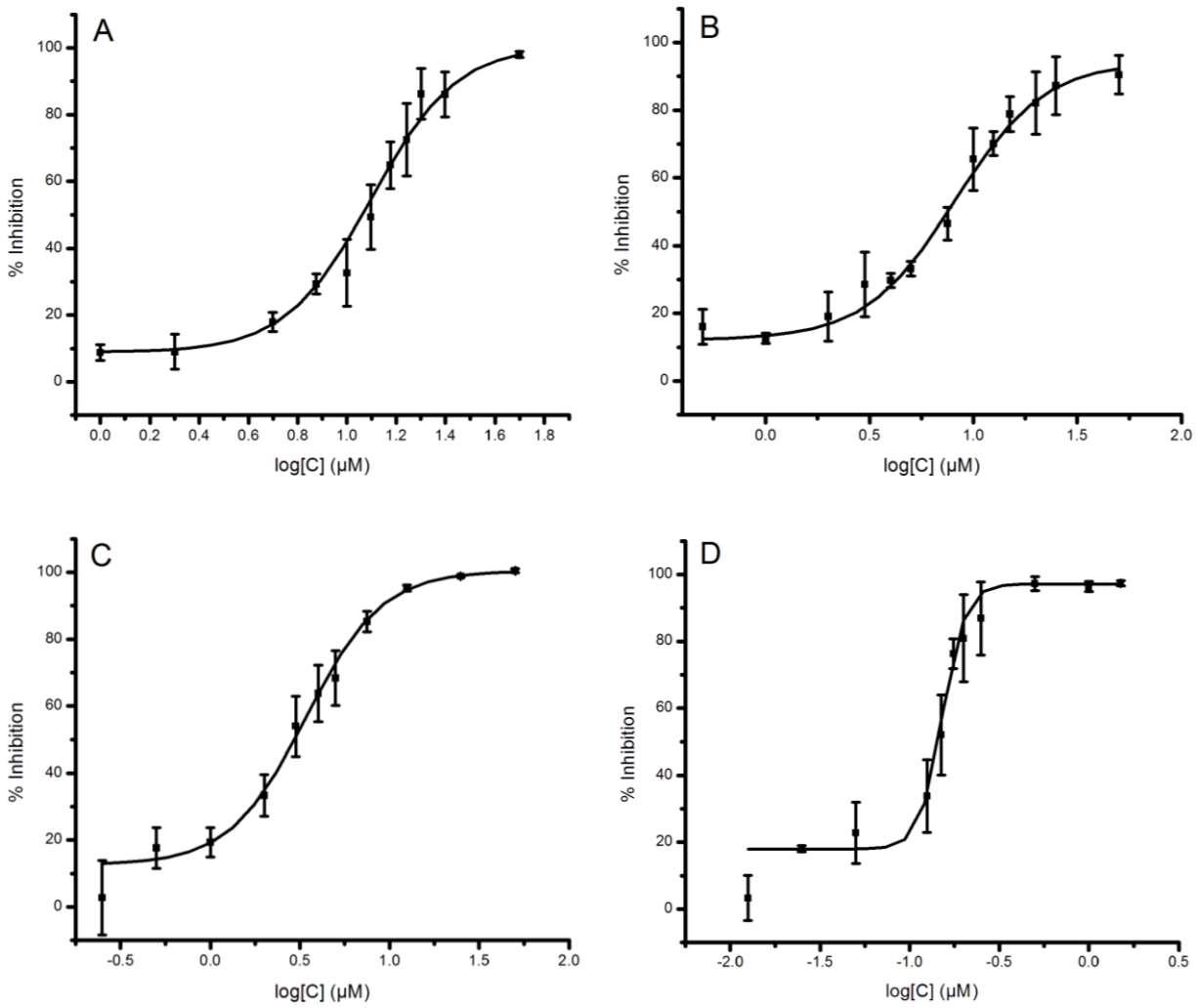

Figure S8. Dose-response curves obtained from flow cytometry (5×10^5 cells/ mL; λ_{ex} = 488 nm, λ_{em} = 525±25 nm; 10,000 events) following induction of oxidative stress with diethylmaleate (DEM, 9 mM) in TF1a cells grown in media containing resveratrol (**1**) (A), pallidol (**2**) (B), quadrangularin A (**3**) (C) and α-tocopherol (D) (0.015-50 μM) for 22 hours at 37 °C. Cells were incubated with the lipid peroxidation reporter C11-BODIPY$^{581/591}$ (1 μM) for 30 minutes prior to DEM treatment.

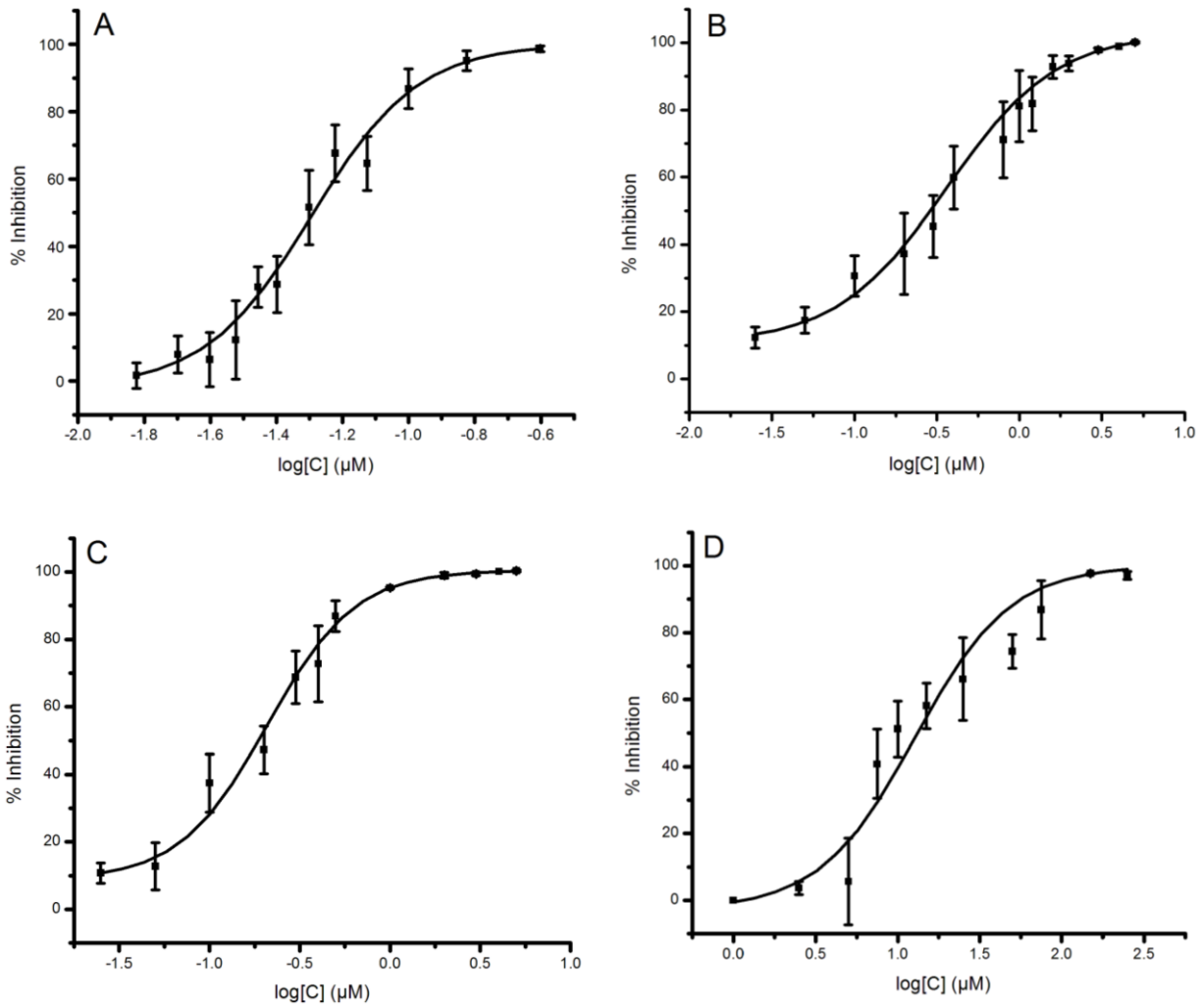

Figure S9. Dose-response curves obtained from flow cytometry (5×10^5 cells/ mL; λ_{ex} = 488 nm, λ_{em} = 525±25 nm; 10,000 events) following induction of oxidative stress with diethylmaleate (DEM, 9 mM) in TF1a cells grown in media containing *t*-Bu_2-resveratrol (**4a**) (A), *t*-Bu_2-pallidol (**7b**) (B), *t*-Bu_2-quadrangularin A (**10**) (C) and BHT (D) (0.015-50 μM) for 22 hours at 37 °C. Cells were incubated with the lipid peroxidation reporter C11-BODIPY$^{581/591}$ (1 μM) for 30 minutes prior to DEM treatment.

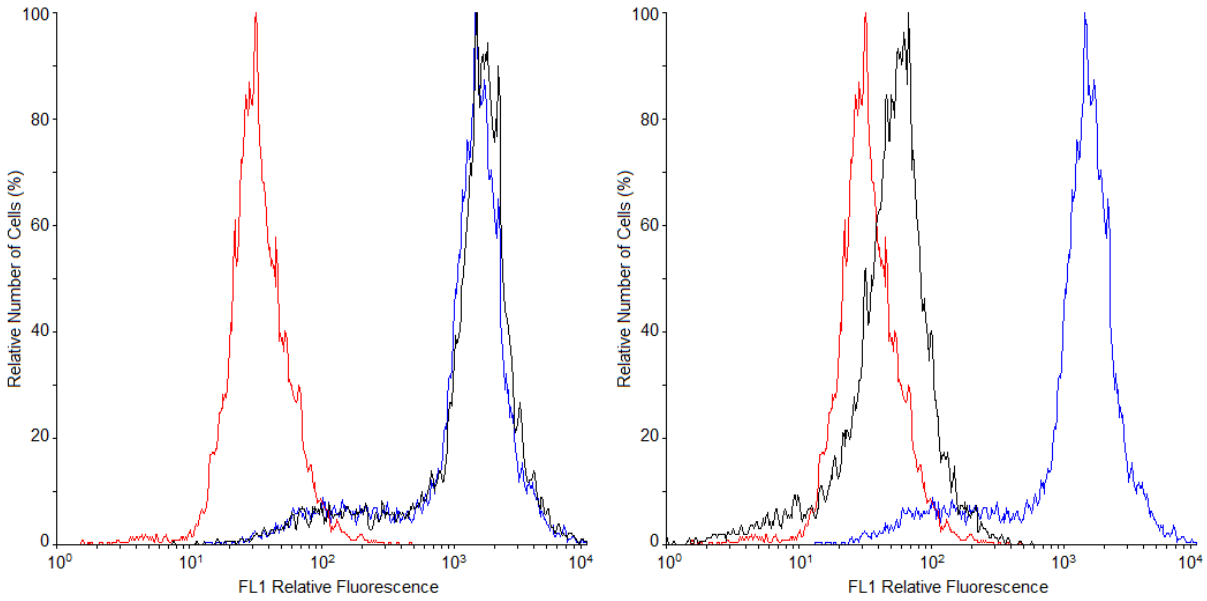

Figure S10. Representative histograms obtained from flow cytometry (5×10^5 cells/ mL; λ_{ex} = 488 nm, λ_{em} = 525±25 nm; 10,000 events) following induction of oxidative stress with diethylmaleate (DEM, 9 mM) in TF1a cells grown in media containing resveratrol (left black: 5 μM, right black: 50 μM) for 22 hours at 37 °C. Cells were incubated with the lipid peroxidation reporter C11-BODIPY$^{581/591}$ (1 μM) for 30 minutes prior to DEM treatment. Cells not treated with DEM were used as negative control (red). Cells not treated with antioxidants were used as positive control (blue).

Cell Viability Studies

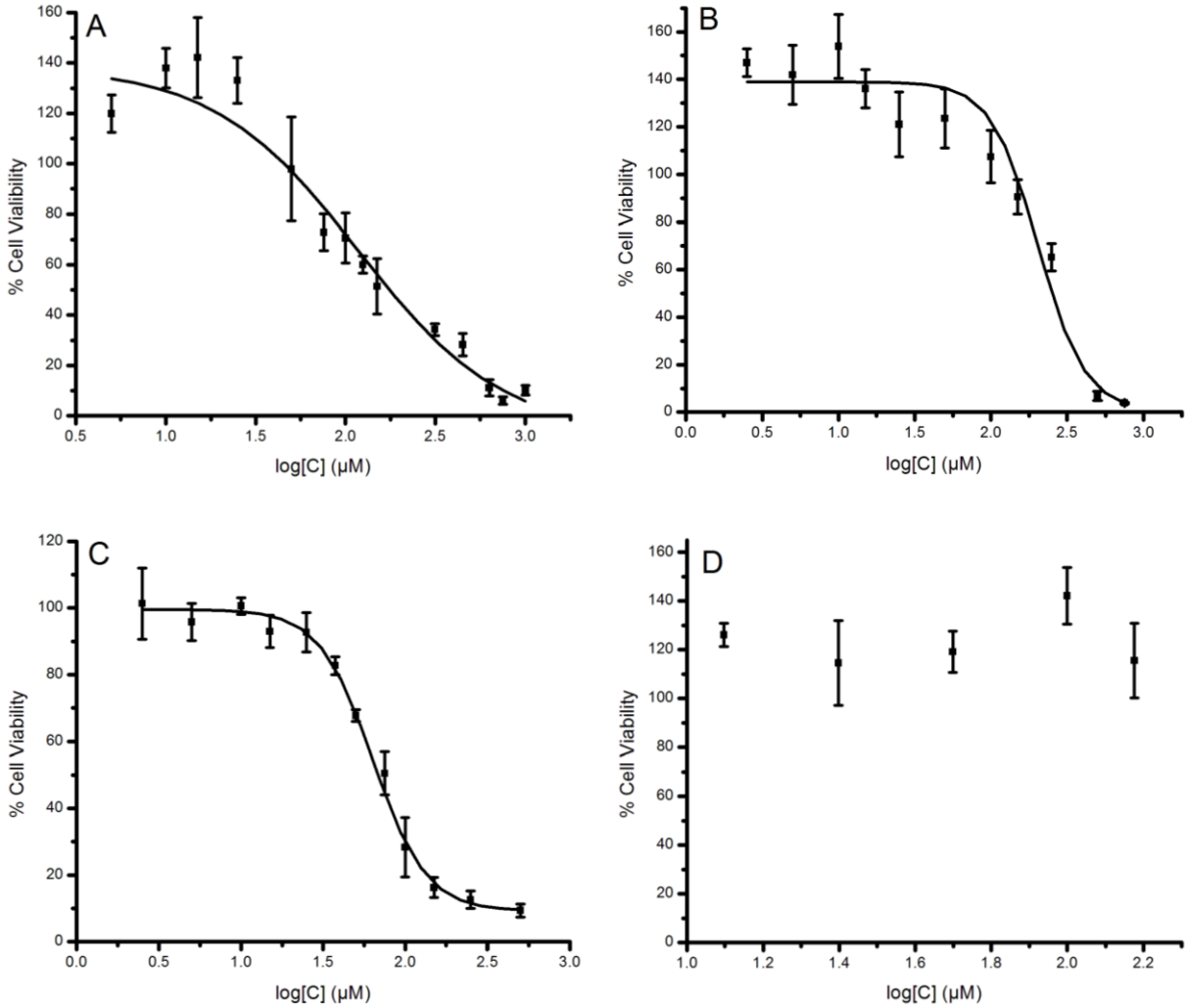

Figure S11. Dose-response curves obtained from MTT cell viability studies with TF1a erythroblasts (0.2 × 10^6 cells/ mL) containing varying concentrations of resveratrol (**1**) (A), pallidol (**2**) (B), quadrangularin A (**3**) (C), α-tocopherol (D) incubated at 37 °C for 22h.

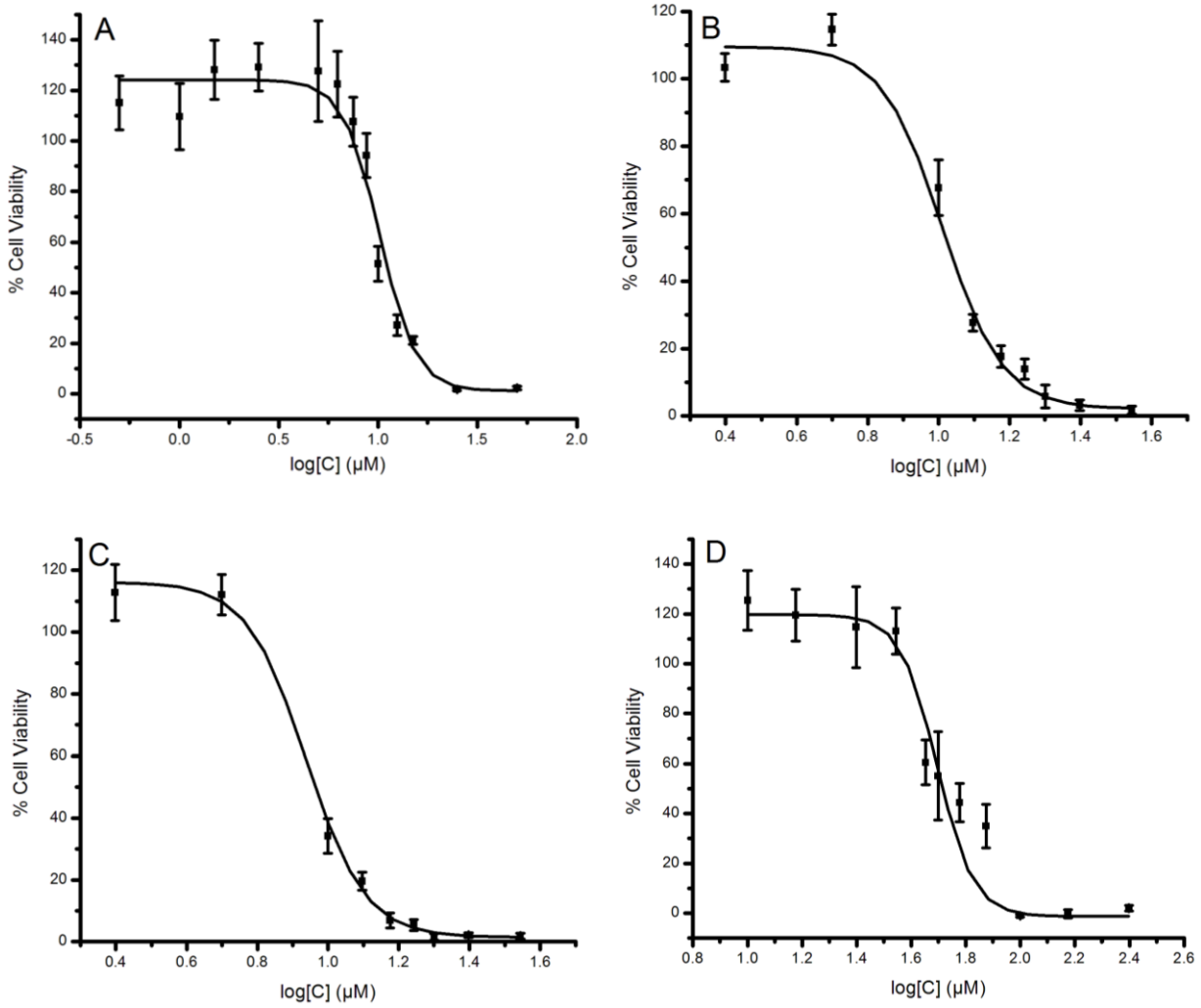

Figure S12. Dose-response curves obtained from MTT cell viability studies with TF1a erythroblasts (0.2×10^6 cells/ mL) containing varying concentrations of *t*-Bu$_2$-resveratrol (**4a**) (A), *t*-Bu$_2$-pallidol (**7b**) (B), *t*-Bu$_2$-quadrangularin A (**10** (C), BHT (D) incubated at 37 °C for 22h.

Compound Structures for Antioxidant Studies

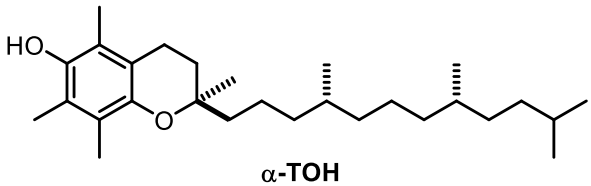

α-TOH
α-Tocopherol

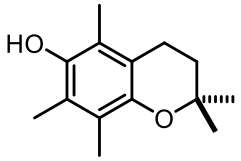

PMHC
2,2,5,7,8-pentamethyl-6-hydroxy-chromane

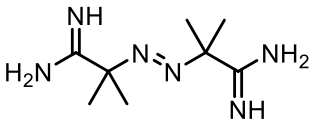

AAPH
2,2'-azobis-(2-amidinopropane)-dihydrochloride

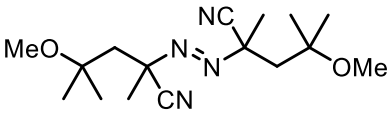

MeOAMVN
2,2'-azobis-(4-methoxy-2,4-imethylvaleronitrile)

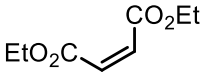

DEM
Diethylmaleate

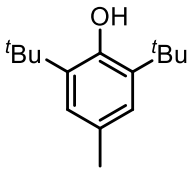

BHT
2,6-di-*tert*-butyl-4-hydroxytoluene

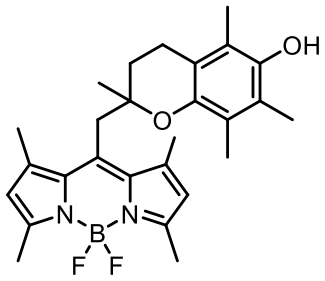

H_2B-PMHC
BODIPY-2,2,5,7,8-pentamethyl-6-hydroxy-chromane

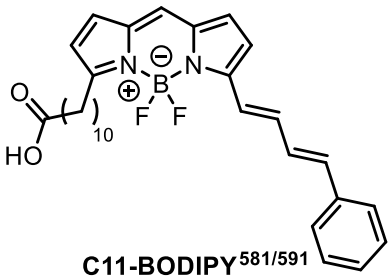

C11-BODIPY$^{581/591}$

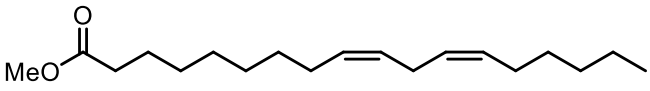

Methyl Linoleate

Bibliography

(1) Burstall, F. H. 34. Optical Activity Dependent on Co-Ordinated Bivalent Ruthenium. *J. Chem. Soc. Resumed* **1936**, No. 0, 173–175.

(2) Hagfeldt, A.; Boschloo, G.; Sun, L.; Kloo, L.; Pettersson, H. Dye-Sensitized Solar Cells. *Chem. Rev.* **2010**, *110* (11), 6595–6663.

(3) Kärkäs, M. D.; Verho, O.; Johnston, E. V.; Åkermark, B. Artificial Photosynthesis: Molecular Systems for Catalytic Water Oxidation. *Chem. Rev.* **2014**, *114* (24), 11863–12001.

(4) Hains, A. W.; Liang, Z.; Woodhouse, M. A.; Gregg, B. A. Molecular Semiconductors in Organic Photovoltaic Cells. *Chem. Rev.* **2010**, *110* (11), 6689–6735.

(5) You, Y.; Nam, W. Photofunctional Triplet Excited States of Cyclometalated Ir(III) Complexes: Beyond Electroluminescence. *Chem. Soc. Rev.* **2012**, *41* (21), 7061–7084.

(6) Kalyanasundaram, K. Photophysics, Photochemistry and Solar Energy Conversion with tris(bipyridyl)ruthenium(II) and Its Analogues. *Coord. Chem. Rev.* **1982**, *46*, 159–244.

(7) Jasperse, C. P.; Curran, D. P.; Fevig, T. L. Radical Reactions in Natural Product Synthesis. *Chem. Rev.* **1991**, *91* (6), 1237–1286.

(8) Curran, D. P.; Chen, M.-H. Radical-Initiated Polyolefinic Cyclizations in Condensed Cyclopentanoid Synthesis. Total Synthesis of (±)-Δ9(12)-Capnellene. *Tetrahedron Lett.* **1985**, *26* (41), 4991–4994.

(9) Cismesia, M. A.; Yoon, T. P. Characterizing Chain Processes in Visible Light Photoredox Catalysis. *Chem. Sci.* **2015**.

(10) Tucker, J. W.; Stephenson, C. R. J. Shining Light on Photoredox Catalysis: Theory and Synthetic Applications. *J. Org. Chem.* **2012**, *77* (4), 1617–1622.

(11) Flamigni, L.; Barbieri, A.; Sabatini, C.; Ventura, B.; Barigelletti, F. Photochemistry and Photophysics of Coordination Compounds: Iridium. In *Photochemistry and Photophysics of Coordination Compounds II*; Balzani, V., Campagna, S., Eds.; Topics in Current Chemistry; Springer Berlin Heidelberg, 2007; pp 143–203.

(12) Armaroli, N.; Accorsi, G.; Cardinali, F.; Listorti, A. Photochemistry and Photophysics of Coordination Compounds: Copper. In *Photochemistry and Photophysics of Coordination Compounds I*; Balzani, V., Campagna, S., Eds.; Topics in Current Chemistry; Springer Berlin Heidelberg, 2007; pp 69–115.

(13) Cano-Yelo, H.; Deronzier, A. Photocatalysis of the Pschorr Reaction by Tris-(2,2′-bipyridyl)ruthenium(II) in the Phenanthrene Series. *J. Chem. Soc. Perkin Trans. 2* **1984**, No. 6, 1093–1098.

(14) Van Bergen, T. J.; Hedstrand, D. M.; Kruizinga, W. H.; Kellogg, R. M. Chemistry of Dihydropyridines. 9. Hydride Transfer from 1,4-Dihydropyridines to sp3-Hybridized Carbon in Sulfonium Salts and Activated Halides. Studies with NAD(P)H Models. *J. Org. Chem.* **1979**, *44* (26), 4953–4962.

(15) Okada, K.; Okamoto, K.; Morita, N.; Okubo, K.; Oda, M. Photosensitized Decarboxylative Michael Addition through N-(acyloxy)phthalimides via an Electron-Transfer Mechanism. *J. Am. Chem. Soc.* **1991**, *113* (24), 9401–9402.
(16) Fukuzumi, S.; Mochizuki, S.; Tanaka, T. Photocatalytic Reduction of Phenacyl Halides by 9,10-Dihydro-10-Methylacridine: Control between the Reductive and Oxidative Quenching Pathways of Tris(bipyridine)ruthenium Complex Utilizing an Acid Catalysis. *J. Phys. Chem.* **1990**, *94* (2), 722–726.
(17) Nicewicz, D. A.; MacMillan, D. W. C. Merging Photoredox Catalysis with Organocatalysis: The Direct Asymmetric Alkylation of Aldehydes. *Science* **2008**, *322* (5898), 77–80.
(18) Nagib, D. A.; Scott, M. E.; MacMillan, D. W. C. Enantioselective A-Trifluoromethylation of Aldehydes via Photoredox Organocatalysis. *J. Am. Chem. Soc.* **2009**, *131* (31), 10875–10877.
(19) Ischay, M. A.; Anzovino, M. E.; Du, J.; Yoon, T. P. Efficient Visible Light Photocatalysis of [2+2] Enone Cycloadditions. *J. Am. Chem. Soc.* **2008**, *130* (39), 12886–12887.
(20) Du, J.; Yoon, T. P. Crossed Intermolecular [2+2] Cycloadditions of Acyclic Enones via Visible Light Photocatalysis. *J. Am. Chem. Soc.* **2009**, *131* (41), 14604–14605.
(21) Narayanam, J. M. R.; Tucker, J. W.; Stephenson, C. R. J. Electron-Transfer Photoredox Catalysis: Development of a Tin-Free Reductive Dehalogenation Reaction. *J. Am. Chem. Soc.* **2009**, *131* (25), 8756–8757.
(22) Tucker, J. W.; Narayanam, J. M. R.; Krabbe, S. W.; Stephenson, C. R. J. Electron Transfer Photoredox Catalysis: Intramolecular Radical Addition to Indoles and Pyrroles. *Org. Lett.* **2010**, *12* (2), 368–371.
(23) Narayanam, J. M. R.; Stephenson, C. R. J. Visible Light Photoredox Catalysis: Applications in Organic Synthesis. *Chem. Soc. Rev.* **2010**, *40* (1), 102–113.
(24) Prier, C. K.; Rankic, D. A.; MacMillan, D. W. C. Visible Light Photoredox Catalysis with Transition Metal Complexes: Applications in Organic Synthesis. *Chem. Rev.* **2013**, *113* (7), 5322–5363.
(25) Schultz, D. M.; Yoon, T. P. Solar Synthesis: Prospects in Visible Light Photocatalysis. *Science* **2014**, *343* (6174), 1239176.
(26) Ishikura, M.; Abe, T.; Choshi, T.; Hibino, S. Simple Indole Alkaloids and Those with a Nonrearranged Monoterpenoid Unit. *Nat. Prod. Rep.* **2015**.
(27) Chuang, C.-P.; Tsai, A.-I.; Lin, C.-H. Manganese(III) Acetate Mediated Oxidative Free Radical Reactions between Indole Derivatives and 1,3-Dicarbonyl Compounds. *Heterocycles* **2005**, *65* (10), 2381.
(28) Richter, J. M.; Whitefield, B. W.; Maimone, T. J.; Lin, D. W.; Castroviejo, M. P.; Baran, P. S. Scope and Mechanism of Direct Indole and Pyrrole Couplings Adjacent to Carbonyl Compounds: Total Synthesis of Acremoauxin A and Oxazinin 3. *J. Am. Chem. Soc.* **2007**, *129* (42), 12857–12869.
(29) Antos, J. M.; McFarland, J. M.; Iavarone, A. T.; Francis, M. B. Chemoselective Tryptophan Labeling with Rhodium Carbenoids at Mild pH. *J. Am. Chem. Soc.* **2009**, *131* (17), 6301–6308.
(30) Chan, W.-W.; Yeung, S.-H.; Zhou, Z.; Chan, A. S. C.; Yu, W.-Y. Ruthenium Catalyzed Directing Group-Free C2-Selective Carbenoid Functionalization of Indoles by A-Aryldiazoesters. *Org. Lett.* **2010**, *12* (3), 604–607.

(31) Freeman, D. B.; Furst, L.; Condie, A. G.; Stephenson, C. R. J. Functionally Diverse Nucleophilic Trapping of Iminium Intermediates Generated Utilizing Visible Light. *Org. Lett.* **2012**, *14* (1), 94–97.
(32) Beatty, J. W.; Stephenson, C. R. J. Amine Functionalization via Oxidative Photoredox Catalysis: Methodology Development and Complex Molecule Synthesis. *Acc. Chem. Res.* **2015**, *48* (5), 1474–1484.
(33) Shirota, Y.; Kageyama, H. Charge Carrier Transporting Molecular Materials and Their Applications in Devices. *Chem. Rev.* **2007**, *107* (4), 953–1010.
(34) Bellville, D. J.; Wirth, D. W.; Bauld, N. L. Cation-Radical Catalyzed Diels-Alder Reaction. *J. Am. Chem. Soc.* **1981**, *103* (3), 718–720.
(35) Bauld, N. L.; Bellville, D. J.; Pabon, R.; Chelsky, R.; Green, G. Theory of Cation-Radical Pericyclic Reactions. *J. Am. Chem. Soc.* **1983**, *105* (8), 2378–2382.
(36) Drew, S. L.; Lawrence, A. L.; Sherburn, M. S. Total Synthesis of Kingianins A, D, and F. *Angew. Chem. Int. Ed.* **2013**, *52* (15), 4221–4224.
(37) Alexanian, E. J.; Lee, C.; Sorensen, E. J. Palladium-Catalyzed Ring-Forming Aminoacetoxylation of Alkenes. *J. Am. Chem. Soc.* **2005**, *127* (21), 7690–7691.
(38) Liu, G.; Stahl, S. S. Highly Regioselective Pd-Catalyzed Intermolecular Aminoacetoxylation of Alkenes and Evidence for Cis-Aminopalladation and SN2 C−O Bond Formation. *J. Am. Chem. Soc.* **2006**, *128* (22), 7179–7181.
(39) Desai, L. V.; Sanford, M. S. Construction of Tetrahydrofurans by PdII/PdIV-Catalyzed Aminooxygenation of Alkenes. *Angew. Chem. Int. Ed.* **2007**, *46* (30), 5737–5740.
(40) Li, Y.; Song, D.; Dong, V. M. Palladium-Catalyzed Olefin Dioxygenation. *J. Am. Chem. Soc.* **2008**, *130* (10), 2962–2964.
(41) Wang, A.; Jiang, H.; Chen, H. Palladium-Catalyzed Diacetoxylation of Alkenes with Molecular Oxygen as Sole Oxidant. *J. Am. Chem. Soc.* **2009**, *131* (11), 3846–3847.
(42) Streuff, J.; Hövelmann, C. H.; Nieger, M.; Muñiz, K. Palladium(II)-Catalyzed Intramolecular Diamination of Unfunctionalized Alkenes. *J. Am. Chem. Soc.* **2005**, *127* (42), 14586–14587.
(43) Iglesias, Á.; Pérez, E. G.; Muñiz, K. An Intermolecular Palladium-Catalyzed Diamination of Unactivated Alkenes. *Angew. Chem. Int. Ed.* **2010**, *49* (44), 8109–8111.
(44) Åkermark, B.; Bäckvall, J. E.; Hegedus, L. S.; Zetterberg, K.; Siirala-Hansén, K.; Sjöberg, K. Palladium-Promoted Addition of Amines to Isolated Double Bonds. *J. Organomet. Chem.* **1974**, *72* (1), 127–138.
(45) Hegedus, L. S.; Allen, G. F.; Waterman, E. L. Palladium Assisted Intramolecular Amination of Olefins. A New Synthesis of Indoles. *J. Am. Chem. Soc.* **1976**, *98* (9), 2674–2676.
(46) Hegedus, L. S.; McKearin, J. M. Palladium-Catalyzed Cyclization of .omega.-Olefinic Tosamides. Synthesis of Nonaromatic Nitrogen Heterocycles. *J. Am. Chem. Soc.* **1982**, *104* (9), 2444–2451.
(47) Hegedus, L. S.; Williams, R. E.; McGuire, M. A.; Hayashi, T. Palladium-Assisted Alkylation of Olefins. *J. Am. Chem. Soc.* **1980**, *102* (15), 4973–4979.
(48) Hegedus, L. S.; Darlington, W. H. Palladium-Assisted Carboacylation of Olefins. *J. Am. Chem. Soc.* **1980**, *102* (15), 4980–4983.
(49) Semmelhack, M. F.; Bodurow, C. Intramolecular Alkoxypalladation/carbonylation of Alkenes. *J. Am. Chem. Soc.* **1984**, *106* (5), 1496–1498.

(50) Semmelhack, M. F.; Zhang, N. Stereoselective Formation of Tetrahydrofuran Rings via Intramolecular Alkoxycarbonylation of Hydroxyalkenes. *J. Org. Chem.* **1989**, *54* (19), 4483–4485.
(51) Semmelhack, M. F.; Epa, W. R. Catalytic Tandem Oxy-Palladation and Vinylation. *Tetrahedron Lett.* **1993**, *34* (45), 7205–7208.
(52) Semmelhack, M. F.; Zask, A. Synthesis of Racemic Frenolicin via Organochromium and Organopalladium Intermediates. *J. Am. Chem. Soc.* **1983**, *105* (7), 2034–2043.
(53) Carpenter, J.; Northrup, A. B.; Chung, deMichael; Wiener, J. J. M.; Kim, S.-G.; MacMillan, D. W. C. Total Synthesis and Structural Revision of Callipeltoside C. *Angew. Chem. Int. Ed.* **2008**, *47* (19), 3568–3572.
(54) Marshall, J. A.; Yanik, M. M. Stereoselective Synthesis of Substituted Ketopyranose Subunits of Polyketide Natural Products by Intramolecular Alkoxycarbonylation of Δ-Alkynyl Alcohols. *Tetrahedron Lett.* **2000**, *41* (24), 4717–4721.
(55) Hegedus, L. S.; Akermark, B.; Zetterberg, K.; Olsson, L. F. Palladium-Assisted Amination of Olefins. A Mechanistic Study. *J. Am. Chem. Soc.* **1984**, *106* (23), 7122–7126.
(56) Desai, L. V.; Hull, K. L.; Sanford, M. S. Palladium-Catalyzed Oxygenation of Unactivated sp3 C−H Bonds. *J. Am. Chem. Soc.* **2004**, *126* (31), 9542–9543.
(57) Camasso, N. M.; Pérez-Temprano, M. H.; Sanford, M. S. C(sp3)–O Bond-Forming Reductive Elimination from PdIV with Diverse Oxygen Nucleophiles. *J. Am. Chem. Soc.* **2014**, *136* (36), 12771–12775.
(58) Racowski, J. M.; Gary, J. B.; Sanford, M. S. Carbon(sp3)□Fluorine Bond-Forming Reductive Elimination from Palladium(IV) Complexes. *Angew. Chem. Int. Ed.* **2012**, *51* (14), 3414–3417.
(59) Rosewall, C. F.; Sibbald, P. A.; Liskin, D. V.; Michael, F. E. Palladium-Catalyzed Carboamination of Alkenes Promoted by N-Fluorobenzenesulfonimide via C−H Activation of Arenes. *J. Am. Chem. Soc.* **2009**, *131* (27), 9488–9489.
(60) Sibbald, P. A.; Rosewall, C. F.; Swartz, R. D.; Michael, F. E. Mechanism of N-Fluorobenzenesulfonimide Promoted Diamination and Carboamination Reactions: Divergent Reactivity of a Pd(IV) Species. *J. Am. Chem. Soc.* **2009**, *131* (43), 15945–15951.
(61) Sibbald, P. A.; Michael, F. E. Palladium-Catalyzed Diamination of Unactivated Alkenes Using N-Fluorobenzenesulfonimide as Source of Electrophilic Nitrogen. *Org. Lett.* **2009**, *11* (5), 1147–1149.
(62) Nicolai, S.; Erard, S.; González, D. F.; Waser, J. Pd-Catalyzed Intramolecular Oxyalkynylation of Alkenes with Hypervalent Iodine. *Org. Lett.* **2010**, *12* (2), 384–387.
(63) Charpentier, J.; Früh, N.; Togni, A. Electrophilic Trifluoromethylation by Use of Hypervalent Iodine Reagents. *Chem. Rev.* **2015**, *115* (2), 650–682.
(64) Nicolai, S.; Piemontesi, C.; Waser, J. A Palladium-Catalyzed Aminoalkynylation Strategy towards Bicyclic Heterocycles: Synthesis of (±)-Trachelanthamidine. *Angew. Chem. Int. Ed.* **2011**, *50* (20), 4680–4683.
(65) Wolfe, J. P.; Rossi, M. A. Stereoselective Synthesis of Tetrahydrofurans via the Palladium-Catalyzed Reaction of Aryl Bromides with Γ-Hydroxy Alkenes: Evidence for an Unusual Intramolecular Olefin Insertion into a Pd(Ar)(OR) Intermediate. *J. Am. Chem. Soc.* **2004**, *126* (6), 1620–1621.

(66) Wolfe, J. P. Palladium-Catalyzed Carboetherification and Carboamination Reactions of Γ-Hydroxy- and Γ-Aminoalkenes for the Synthesis of Tetrahydrofurans and Pyrrolidines. *Eur. J. Org. Chem.* **2007**, *2007* (4), 571–582.
(67) Zhu, R.; Buchwald, S. L. Combined Oxypalladation/C□H Functionalization: Palladium(II)-Catalyzed Intramolecular Oxidative Oxyarylation of Hydroxyalkenes. *Angew. Chem. Int. Ed.* **2012**, *51* (8), 1926–1929.
(68) Lira, R.; Wolfe, J. P. Palladium-Catalyzed Synthesis of N-Aryl-2-Benzylindolines via Tandem Arylation of 2-Allylaniline: Control of Selectivity through in Situ Catalyst Modification. *J. Am. Chem. Soc.* **2004**, *126* (43), 13906–13907.
(69) Leathen, M. L.; Rosen, B. R.; Wolfe, J. P. New Strategy for the Synthesis of Substituted Morpholines. *J. Org. Chem.* **2009**, *74* (14), 5107–5110.
(70) Wolfe, J. P.; Wagaw, S.; Marcoux, J.-F.; Buchwald, S. L. Rational Development of Practical Catalysts for Aromatic Carbon−Nitrogen Bond Formation. *Acc. Chem. Res.* **1998**, *31* (12), 805–818.
(71) Surry, D. S.; Buchwald, S. L. Dialkylbiaryl Phosphines in Pd-Catalyzed Amination: A User's Guide. *Chem. Sci. R. Soc. Chem. 2010* **2011**, *2* (1), 27–50.
(72) Schultz, D. M.; Wolfe, J. P. Recent Developments in Pd-Catalyzed Alkene Aminoarylation Reactions for the Synthesis of Nitrogen Heterocycles. *Synthesis* **2012**, *44* (3), 351–361.
(73) Wang, J.; Soisson, S. M.; Young, K.; Shoop, W.; Kodali, S.; Galgoci, A.; Painter, R.; Parthasarathy, G.; Tang, Y. S.; Cummings, R.; Ha, S.; Dorso, K.; Motyl, M.; Jayasuriya, H.; Ondeyka, J.; Herath, K.; Zhang, C.; Hernandez, L.; Allocco, J.; Basilio, Á.; Tormo, J. R.; Genilloud, O.; Vicente, F.; Pelaez, F.; Colwell, L.; Lee, S. H.; Michael, B.; Felcetto, T.; Gill, C.; Silver, L. L.; Hermes, J. D.; Bartizal, K.; Barrett, J.; Schmatz, D.; Becker, J. W.; Cully, D.; Singh, S. B. Platensimycin Is a Selective FabF Inhibitor with Potent Antibiotic Properties. *Nature* **2006**, *441* (7091), 358–361.
(74) Tiefenbacher, K.; Mulzer, J. Synthesis of Platensimycin. *Angew. Chem. Int. Ed.* **2008**, *47* (14), 2548–2555.
(75) Furuya, T.; Kaiser, H. M.; Ritter, T. Palladium-Mediated Fluorination of Arylboronic Acids. *Angew. Chem. Int. Ed.* **2008**, *47* (32), 5993–5996.
(76) Hull, K. L.; Anani, W. Q.; Sanford, M. S. Palladium-Catalyzed Fluorination of Carbon−Hydrogen Bonds. *J. Am. Chem. Soc.* **2006**, *128* (22), 7134–7135.
(77) Chan, K. S. L.; Wasa, M.; Wang, X.; Yu, J.-Q. Palladium(II)-Catalyzed Selective Monofluorination of Benzoic Acids Using a Practical Auxiliary: A Weak-Coordination Approach. *Angew. Chem. Int. Ed.* **2011**, *50* (39), 9081–9084.
(78) Ball, N. D.; Kampf, J. W.; Sanford, M. S. Aryl−CF3 Bond-Forming Reductive Elimination from Palladium(IV). *J. Am. Chem. Soc.* **2010**, *132* (9), 2878–2879.
(79) Engle, K. M.; Mei, T.-S.; Wang, X.; Yu, J.-Q. Bystanding F+ Oxidants Enable Selective Reductive Elimination from High-Valent Metal Centers in Catalysis. *Angew. Chem. Int. Ed.* **2011**, *50* (7), 1478–1491.
(80) Pérez-Temprano, M. H.; Racowski, J. M.; Kampf, J. W.; Sanford, M. S. Competition between sp3-C–N vs sp3-C–F Reductive Elimination from PdIV Complexes. *J. Am. Chem. Soc.* **2014**, *136* (11), 4097–4100.
(81) Kalyani, D.; McMurtrey, K. B.; Neufeldt, S. R.; Sanford, M. S. Room-Temperature C–H Arylation: Merger of Pd-Catalyzed C–H Functionalization and Visible-Light Photocatalysis. *J. Am. Chem. Soc.* **2011**, *133* (46), 18566–18569.

(82) Ye, Y.; Sanford, M. S. Merging Visible-Light Photocatalysis and Transition-Metal Catalysis in the Copper-Catalyzed Trifluoromethylation of Boronic Acids with CF3I. *J. Am. Chem. Soc.* **2012**, *134* (22), 9034–9037.
(83) Zuo, Z.; Ahneman, D. T.; Chu, L.; Terrett, J. A.; Doyle, A. G.; MacMillan, D. W. C. Merging Photoredox with Nickel Catalysis: Coupling of A-Carboxyl sp3-Carbons with Aryl Halides. *Science* **2014**, *345* (6195), 437–440.
(84) Tellis, J. C.; Primer, D. N.; Molander, G. A. Single-Electron Transmetalation in Organoboron Cross-Coupling by Photoredox/nickel Dual Catalysis. *Science* **2014**, *345* (6195), 433–436.
(85) Vennestrøm, P. N. R.; Osmundsen, C. M.; Christensen, C. H.; Taarning, E. Beyond Petrochemicals: The Renewable Chemicals Industry. *Angew. Chem. Int. Ed.* **2011**, *50* (45), 10502–10509.
(86) Vanholme, R.; Demedts, B.; Morreel, K.; Ralph, J.; Boerjan, W. Lignin Biosynthesis and Structure. *Plant Physiol.* **2010**, *153* (3), 895–905.
(87) Ralph, J.; Peng, J.; Lu, F.; Hatfield, R. D.; Helm, R. F. Are Lignins Optically Active? *J. Agric. Food Chem.* **1999**, *47* (8), 2991–2996.
(88) Zakzeski, J.; Bruijnincx, P. C. A.; Jongerius, A. L.; Weckhuysen, B. M. The Catalytic Valorization of Lignin for the Production of Renewable Chemicals. *Chem. Rev.* **2010**, *110* (6), 3552–3599.
(89) Bozell, J. J. Alternative, Renewable, and Novel Feedstocks for Producing Chemicals. *US Dep. Energy Oak Ridge Natl. Lab. Oak Ridge TN* **2006**, 204–209.
(90) Anbarasan, P.; Baer, Z. C.; Sreekumar, S.; Gross, E.; Binder, J. B.; Blanch, H. W.; Clark, D. S.; Toste, F. D. Integration of Chemical Catalysis with Extractive Fermentation to Produce Fuels. *Nature* **2012**, *491* (7423), 235–239.
(91) Ahuja, R.; Punji, B.; Findlater, M.; Supplee, C.; Schinski, W.; Brookhart, M.; Goldman, A. S. Catalytic Dehydroaromatization of N-Alkanes by Pincer-Ligated Iridium Complexes. *Nat. Chem.* **2011**, *3* (2), 167–171.
(92) Pandey, M. P.; Kim, C. S. Lignin Depolymerization and Conversion: A Review of Thermochemical Methods. *Chem. Eng. Technol.* **2011**, *34* (1), 29–41.
(93) Khodakov, A. Y.; Chu, W.; Fongarland, P. Advances in the Development of Novel Cobalt Fischer−Tropsch Catalysts for Synthesis of Long-Chain Hydrocarbons and Clean Fuels. *Chem. Rev.* **2007**, *107* (5), 1692–1744.
(94) Clark, J. H.; Luque, R.; Matharu, A. S. Green Chemistry, Biofuels, and Biorefinery. *Annu. Rev. Chem. Biomol. Eng.* **2012**, *3* (1), 183–207.
(95) Fargues, C.; Mathias, Á.; Rodrigues, A. Kinetics of Vanillin Production from Kraft Lignin Oxidation. *Ind. Eng. Chem. Res.* **1996**, *35* (1), 28–36.
(96) Luterbacher, J. S.; Rand, J. M.; Alonso, D. M.; Han, J.; Youngquist, J. T.; Maravelias, C. T.; Pfleger, B. F.; Dumesic, J. A. Nonenzymatic Sugar Production from Biomass Using Biomass-Derived Γ-Valerolactone. *Science* **2014**, *343* (6168), 277–280.
(97) Tien, M.; Kirk, T. K. Lignin-Degrading Enzyme from the Hymenomycete Phanerochaete Chrysosporium Burds. *Science* **1983**, *221* (4611), 661–663.
(98) Lim, S. H.; Nahm, K.; Ra, C. S.; Cho, D. W.; Yoon, U. C.; Latham, J. A.; Dunaway-Mariano, D.; Mariano, P. S. Effects of Alkoxy Groups on Arene Rings of Lignin B-O-4 Model Compounds on the Efficiencies of Single Electron Transfer-Promoted Photochemical and Enzymatic C–C Bond Cleavage Reactions. *J. Org. Chem.* **2013**, *78* (18), 9431–9443.

(99) Dordick, J. S.; Marletta, M. A.; Klibanov, A. M. Peroxidases Depolymerize Lignin in Organic Media but Not in Water. *Proc. Natl. Acad. Sci. U. S. A.* **1986**, *83* (17), 6255–6257.
(100) Kirk, T. K.; Connors, W. J.; Bleam, R. D.; Hackett, W. F.; Zeikus, J. G. Preparation and Microbial Decomposition of Synthetic [14C]ligins. *Proc. Natl. Acad. Sci.* **1975**, *72* (7), 2515–2519.
(101) Kutsuki, H.; Enoki, A.; Gold, M. H. Riboflavin-Photosensitized Oxidative Degradation of a Variety of Lignin Model Compounds. *Photochem. Photobiol.* **1983**, *37* (1), 1–7.
(102) Shimada, M.; Habe, T.; Umezawa, T.; Higuchi, T.; Okamoto, T. The CC Bond Cleavage of a Lignin Model Compound, 1,2-Diarylpropane-1,3-Diol, with a Heme-Enzyme Model Catalyst Tetraphenylporphyrinatoiron (III) Chloride in the Presence of Tert-Butylhydroperoxide. *Biochem. Biophys. Res. Commun.* **1984**, *122* (3), 1247–1252.
(103) DiCosimo, R.; Szabo, H. C. Oxidation of Lignin Model Compounds Using Single-Electron-Transfer Catalysts. *J. Org. Chem.* **1988**, *53* (8), 1673–1679.
(104) Voitl, T.; Rudolf von Rohr, P. Oxidation of Lignin Using Aqueous Polyoxometalates in the Presence of Alcohols. *ChemSusChem* **2008**, *1* (8-9), 763–769.
(105) Cho, D. W.; Parthasarathi, R.; Pimentel, A. S.; Maestas, G. D.; Park, H. J.; Yoon, U. C.; Dunaway-Mariano, D.; Gnanakaran, S.; Langan, P.; Mariano, P. S. Nature and Kinetic Analysis of Carbon−Carbon Bond Fragmentation Reactions of Cation Radicals Derived from SET-Oxidation of Lignin Model Compounds. *J. Org. Chem.* **2010**, *75* (19), 6549–6562.
(106) Sedai, B.; Díaz-Urrutia, C.; Baker, R. T.; Wu, R.; Silks, L. A. "Pete"; Hanson, S. K. Comparison of Copper and Vanadium Homogeneous Catalysts for Aerobic Oxidation of Lignin Models. *ACS Catal.* **2011**, *1* (7), 794–804.
(107) Hanson, S. K.; Wu, R.; Silks, L. A. "Pete." C□C or C□O Bond Cleavage in a Phenolic Lignin Model Compound: Selectivity Depends on Vanadium Catalyst. *Angew. Chem. Int. Ed.* **2012**, *51* (14), 3410–3413.
(108) Zhang, G.; Scott, B. L.; Wu, R.; Silks, L. A. "Pete"; Hanson, S. K. Aerobic Oxidation Reactions Catalyzed by Vanadium Complexes of Bis(Phenolate) Ligands. *Inorg. Chem.* **2012**, *51* (13), 7354–7361.
(109) Sedai, B.; Díaz-Urrutia, C.; Baker, R. T.; Wu, R.; Silks, L. A. "Pete"; Hanson, S. K. Aerobic Oxidation of B-1 Lignin Model Compounds with Copper and Oxovanadium Catalysts. *ACS Catal.* **2013**, *3* (12), 3111–3122.
(110) Biannic, B.; Bozell, J. J. Efficient Cobalt-Catalyzed Oxidative Conversion of Lignin Models to Benzoquinones. *Org. Lett.* **2013**, *15* (11), 2730–2733.
(111) Biannic, B.; Bozell, J. J.; Elder, T. Steric Effects in the Design of Co-Schiff Base Complexes for the Catalytic Oxidation of Lignin Models to Para-Benzoquinones. *Green Chem.* **2014**, *16* (7), 3635–3642.
(112) Freudenberg, K.; Meister, M.; Flickinger, E. Fichtenlignin (XVI. Mitteil. Über Lignin). *Berichte Dtsch. Chem. Ges. B Ser.* **1937**, *70* (3), 500–514.
(113) Cramer, A. B.; Hunter, M. J.; Hibbert, H. Studies on Lignin and Related Compounds. XXXV. The Ethanolysis of Spruce Wood. *J. Am. Chem. Soc.* **1939**, *61* (2), 509–516.
(114) Harris, E. E.; D'Ianni, J.; Adkins, H. Reaction of Hardwood Lignin with Hydrogen. *J. Am. Chem. Soc.* **1938**, *60* (6), 1467–1470.
(115) J. M. PEPPER, W. F. STECK, R. SWOBODA, J. C. KARAPALLY. Hydrogenation of Lignin Using Nickel and Palladium Catalysts. In *Lignin Structure and Reactions*;

Advances in Chemistry; AMERICAN CHEMICAL SOCIETY, 1966; Vol. 59, pp 238–248.
(116) Pepper, J. M.; Hibbert, H. Studies on Lignin and Related Compounds. LXXXVII. High Pressure Hydrogenation of Maple Wood1. *J. Am. Chem. Soc.* **1948**, *70* (1), 67–71.
(117) Sergeev, A. G.; Hartwig, J. F. Selective, Nickel-Catalyzed Hydrogenolysis of Aryl Ethers. *Science* **2011**, *332* (6028), 439–443.
(118) Sergeev, A. G.; Webb, J. D.; Hartwig, J. F. A Heterogeneous Nickel Catalyst for the Hydrogenolysis of Aryl Ethers without Arene Hydrogenation. *J. Am. Chem. Soc.* **2012**, *134* (50), 20226–20229.
(119) Ren, Y.; Yan, M.; Wang, J.; Zhang, Z. C.; Yao, K. Selective Reductive Cleavage of Inert Aryl C□O Bonds by an Iron Catalyst. *Angew. Chem. Int. Ed.* **2013**, *52* (48), 12674–12678.
(120) Desnoyer, A. N.; Fartel, B.; MacLeod, K. C.; Patrick, B. O.; Smith, K. M. Ambient-Temperature Carbon–Oxygen Bond Cleavage of an A-Aryloxy Ketone with Cp2Ti(BTMSA) and Selective Protonolysis of the Resulting Ti–OR Bonds. *Organometallics* **2012**, *31* (21), 7625–7628.
(121) Nguyen, J. D.; Matsuura, B. S.; Stephenson, C. R. J. A Photochemical Strategy for Lignin Degradation at Room Temperature. *J. Am. Chem. Soc.* **2013**, *136* (4), 1218–1221.
(122) Son, S.; Toste, F. D. Non-Oxidative Vanadium-Catalyzed C□O Bond Cleavage: Application to Degradation of Lignin Model Compounds. *Angew. Chem. Int. Ed.* **2010**, *49* (22), 3791–3794.
(123) Radosevich, A. T.; Musich, C.; Toste, F. D. Vanadium-Catalyzed Asymmetric Oxidation of A-Hydroxy Esters Using Molecular Oxygen as Stoichiometric Oxidant. *J. Am. Chem. Soc.* **2005**, *127* (4), 1090–1091.
(124) Nichols, J. M.; Bishop, L. M.; Bergman, R. G.; Ellman, J. A. Catalytic C−O Bond Cleavage of 2-Aryloxy-1-Arylethanols and Its Application to the Depolymerization of Lignin-Related Polymers. *J. Am. Chem. Soc.* **2010**, *132* (36), 12554–12555.
(125) Wu, A.; Patrick, B. O.; Chung, E.; James, B. R. Hydrogenolysis of B-O-4 Lignin Model Dimers by a Ruthenium-Xantphos Catalyst. *Dalton Trans.* **2012**, *41* (36), 11093–11106.
(126) Wu, A.; Patrick, B. O.; James, B. R. Inactive ruthenium(II)-Xantphos Complexes from Attempted Catalyzed Lignin Reactions. *Inorg. Chem. Commun.* **2012**, *24*, 11–15.
(127) Vom Stein, T.; Weigand, T.; Merkens, C.; Klankermayer, J.; Leitner, W. Trimethylenemethane-Ruthenium(II)-Triphos Complexes as Highly Active Catalysts for Catalytic C□O Bond Cleavage Reactions of Lignin Model Compounds. *ChemCatChem* **2013**, *5* (2), 439–441.
(128) Wu, A.; Lauzon, J. M.; James, B. R. Hydrogenolysis of a Γ-Acetylated Lignin Model Compound with a Ruthenium–Xantphos Catalyst. *Catal. Lett.* **2014**, *145* (2), 511–518.
(129) Vom Stein, T.; den Hartog, T.; Buendia, J.; Stoychev, S.; Mottweiler, J.; Bolm, C.; Klankermayer, J.; Leitner, W. Ruthenium-Catalyzed C□C Bond Cleavage in Lignin Model Substrates. *Angew. Chem. Int. Ed.* **2015**, n/a – n/a.
(130) Kim, S.; Chmely, S. C.; Nimlos, M. R.; Bomble, Y. J.; Foust, T. D.; Paton, R. S.; Beckham, G. T. Computational Study of Bond Dissociation Enthalpies for a Large Range of Native and Modified Lignins. *J. Phys. Chem. Lett.* **2011**, *2* (22), 2846–2852.
(131) Hasegawa, E.; Takizawa, S.; Seida, T.; Yamaguchi, A.; Yamaguchi, N.; Chiba, N.; Takahashi, T.; Ikeda, H.; Akiyama, K. Photoinduced Electron-Transfer Systems Consisting of Electron-Donating Pyrenes or Anthracenes and Benzimidazolines for

Reductive Transformation of Carbonyl Compounds. *Tetrahedron* **2006**, *62* (27), 6581–6588.
(132) Larraufie, M.-H.; Pellet, R.; Fensterbank, L.; Goddard, J.-P.; Lacôte, E.; Malacria, M.; Ollivier, C. Visible-Light-Induced Photoreductive Generation of Radicals from Epoxides and Aziridines. *Angew. Chem. Int. Ed.* **2011**, *50* (19), 4463–4466.
(133) Chakar, F. S.; Ragauskas, A. J. Review of Current and Future Softwood Kraft Lignin Process Chemistry. *Ind. Crops Prod.* **2004**, *20* (2), 131–141.
(134) Slinker, J. D.; Gorodetsky, A. A.; Lowry, M. S.; Wang, J.; Parker, S.; Rohl, R.; Bernhard, S.; Malliaras, G. G. Efficient Yellow Electroluminescence from a Single Layer of a Cyclometalated Iridium Complex. *J. Am. Chem. Soc.* **2004**, *126* (9), 2763–2767.
(135) Rahimi, A.; Azarpira, A.; Kim, H.; Ralph, J.; Stahl, S. S. Chemoselective Metal-Free Aerobic Alcohol Oxidation in Lignin. *J. Am. Chem. Soc.* **2013**, *135* (17), 6415–6418.
(136) Rahimi, A.; Ulbrich, A.; Coon, J. J.; Stahl, S. S. Formic-Acid-Induced Depolymerization of Oxidized Lignin to Aromatics. *Nature* **2014**, *515* (7526), 249–252.
(137) Nguyen, J. D.; Reiß, B.; Dai, C.; Stephenson, C. R. J. Batch to Flow Deoxygenation Using Visible Light Photoredox Catalysis. *Chem. Commun.* **2013**, *49* (39), 4352–4354.
(138) Bobbitt, J. M. Oxoammonium Salts. 6.1 4-Acetylamino-2,2,6,6-Tetramethylpiperidine-1-Oxoammonium Perchlorate: A Stable and Convenient Reagent for the Oxidation of Alcohols. Silica Gel Catalysis. *J. Org. Chem.* **1998**, *63* (25), 9367–9374.
(139) Tucker, J. W.; Nguyen, J. D.; Narayanam, J. M. R.; Krabbe, S. W.; Stephenson, C. R. J. Tin-Free Radical Cyclization Reactions Initiated by Visible Light Photoredox Catalysis. *Chem. Commun.* **2010**, *46* (27), 4985–4987.
(140) Nguyen, J. D.; D'Amato, E. M.; Narayanam, J. M. R.; Stephenson, C. R. J. Engaging Unactivated Alkyl, Alkenyl and Aryl Iodides in Visible-Light-Mediated Free Radical Reactions. *Nat. Chem.* **2012**, *4* (10), 854–859.
(141) Tucker, J. W.; Zhang, Y.; Jamison, T. F.; Stephenson, C. R. J. Visible-Light Photoredox Catalysis in Flow. *Angew. Chem. Int. Ed.* **2012**, *51* (17), 4144–4147.
(142) Bou-Hamdan, F. R.; Seeberger, P. H. Visible-Light-Mediated Photochemistry: Accelerating Ru(bpy)32+-Catalyzed Reactions in Continuous Flow. *Chem. Sci.* **2012**, *3* (5), 1612–1616.
(143) Olah, G. A.; Molnár, Á. *Hydrocarbon Chemistry*; John Wiley & Sons, 2003.
(144) Kinsella, K. G. Changes in Life Expectancy 1900-1990. *Am. J. Clin. Nutr.* **1992**, *55* (6), 1196S – 1202S.
(145) *Diet and Health: Implications for Reducing Chronic Disease Risk*.
(146) Soleas, G. J.; Diamandis, E. P.; Goldberg, D. M. Resveratrol: A Molecule Whose Time Has Come? And Gone? *Clin. Biochem.* **1997**, *30* (2), 91–113.
(147) Rimm, E. B.; Klatsky, A.; Grobbee, D.; Stampfer, M. J. Review Of Moderate Alcohol Consumption And Reduced Risk Of Coronary Heart Disease: Is The Effect Due To Beer, Wine, Or Spirits? *BMJ* **1996**, *312* (7033), 731–736.
(148) Siemann, E. H.; Creasy, L. L. Concentration of the Phytoalexin Resveratrol in Wine. *Am. J. Enol. Vitic.* **1992**, *43* (1), 49–52.
(149) Frankel, E. N.; Waterhouse, A. L.; Kinsella, J. E. Inhibition of Human LDL Oxidation by Resveratrol. *The Lancet* **1993**, *341* (8852), 1103–1104.
(150) Law, M.; Stampfer, M.; Barker, D. J. P.; Mackenbach, J. P.; Wald, N.; Rimm, E.; Kunst, A. E. Why Heart Disease Mortality Is Low in France: The Time Lag explanationCommentary: Alcohol and Other Dietary Factors May Be

importantCommentary: Intrauterine Nutrition May Be importantCommentary: Heterogeneity of Populations Should Be Taken into accountAuthors' Response. *BMJ* **1999**, *318* (7196), 1471–1480.
(151) Fuchs, F. D.; Chambless, L. E. Is the Cardioprotective Effect of Alcohol Real? *Alcohol* **2007**, *41* (6), 399–402.
(152) Jang, M.; Cai, L.; Udeani, G. O.; Slowing, K. V.; Thomas, C. F.; Beecher, C. W. W.; Fong, H. H. S.; Farnsworth, N. R.; Kinghorn, A. D.; Mehta, R. G.; Moon, R. C.; Pezzuto, J. M. Cancer Chemopreventive Activity of Resveratrol, a Natural Product Derived from Grapes. *Science* **1997**, *275* (5297), 218–220.
(153) Banks, A. S.; Kon, N.; Knight, C.; Matsumoto, M.; Gutiérrez-Juárez, R.; Rossetti, L.; Gu, W.; Accili, D. SirT1 Gain of Function Increases Energy Efficiency and Prevents Diabetes in Mice. *Cell Metab.* **2008**, *8* (4), 333–341.
(154) Milne, J. C.; Lambert, P. D.; Schenk, S.; Carney, D. P.; Smith, J. J.; Gagne, D. J.; Jin, L.; Boss, O.; Perni, R. B.; Vu, C. B.; Bemis, J. E.; Xie, R.; Disch, J. S.; Ng, P. Y.; Nunes, J. J.; Lynch, A. V.; Yang, H.; Galonek, H.; Israelian, K.; Choy, W.; Iffland, A.; Lavu, S.; Medvedik, O.; Sinclair, D. A.; Olefsky, J. M.; Jirousek, M. R.; Elliott, P. J.; Westphal, C. H. Small Molecule Activators of SIRT1 as Therapeutics for the Treatment of Type 2 Diabetes. *Nature* **2007**, *450* (7170), 712–716.
(155) Baur, J. A.; Pearson, K. J.; Price, N. L.; Jamieson, H. A.; Lerin, C.; Kalra, A.; Prabhu, V. V.; Allard, J. S.; Lopez-Lluch, G.; Lewis, K.; Pistell, P. J.; Poosala, S.; Becker, K. G.; Boss, O.; Gwinn, D.; Wang, M.; Ramaswamy, S.; Fishbein, K. W.; Spencer, R. G.; Lakatta, E. G.; Le Couteur, D.; Shaw, R. J.; Navas, P.; Puigserver, P.; Ingram, D. K.; de Cabo, R.; Sinclair, D. A. Resveratrol Improves Health and Survival of Mice on a High-Calorie Diet. *Nature* **2006**, *444* (7117), 337–342.
(156) Langcake, P.; Pryce, R. J. A New Class of Phytoalexins from Grapevines. *Experientia* **1977**, *33* (2), 151–152.
(157) Pryce, R. J.; Langcake, P. A-Viniferin: An Antifungal Resveratrol Trimer from Grapevines. *Phytochemistry* **1977**, *16* (9), 1452–1454.
(158) Langcake, P.; McCarthy, W. V. The Relationship of Resveratrol Production to Infection of Grapevine Leaves by Botrytis Cinerea. *Vitis* **1979**, *18*, 244–253.
(159) Vogt, T. Phenylpropanoid Biosynthesis. *Mol. Plant* **2010**, *3* (1), 2–20.
(160) Schöppner, A.; Kindl, H. Purification and Properties of a Stilbene Synthase from Induced Cell Suspension Cultures of Peanut. *J. Biol. Chem.* **1984**, *259* (11), 6806–6811.
(161) Langcake, P.; Pryce, R. J. The Production of Resveratrol by Vitis Vinifera and Other Members of the Vitaceae as a Response to Infection or Injury. *Physiol. Plant Pathol.* **1976**, *9* (1), 77–86.
(162) Langcake, P. Disease Resistance of Vitis Spp. and the Production of the Stress Metabolites Resveratrol, E-Viniferin, A-Viniferin and Pterostilbene. *Physiol. Plant Pathol.* **1981**, *18* (2), 213–226.
(163) Coggon, P.; King, T. J.; Wallwork, S. C. The Structure of Hopeaphenol. *Chem. Commun. Lond.* **1966**, No. 13, 439–440.
(164) Coggon, P.; McPhail, A. T.; Wallwork, S. C. Structure of Hopeaphenol: X-Ray Analysis of the Benzene Solvate of Dibromodeca-O-Methylhopeaphenol. *J. Chem. Soc. B Phys. Org.* **1970**, No. 0, 884–897.

(165) Oshima, Y.; Ueno, Y.; Hisamichi, K.; Takeshita, M. Ampelopsins F and G, Novel Bridged Plant Oligostilbenes from Ampelopsis Brevipedunculata Var. Hancei Roots (vitaceae). *Tetrahedron* **1993**, *49* (26), 5801–5804.
(166) Adesanya, S. A.; Nia, R.; Martin, M.-T.; Boukamcha, N.; Montagnac, A.; Païs, M. Stilbene Derivatives from Cissus Quadrangularis. *J. Nat. Prod.* **1999**, *62* (12), 1694–1695.
(167) Ducrot, P.-H.; Kollmann, A.; Bala, A. E.; Majira, A.; Kerhoas, L.; Delorme, R.; Einhorn, J. Cyphostemmins A-B, Two New Antifungal Oligostilbenes from Cyphostemma Crotalarioides (Vitaceae). *Tetrahedron Lett.* **1998**, *39* (52), 9655–9658.
(168) Khan, M. A.; Nabi, S. G.; Prakash, S.; Zaman, A. Pallidol, a Resveratrol Dimer from Cissus Pallida. *Phytochemistry* **1986**, *25* (8), 1945–1948.
(169) Lins, A. P.; Ribeiro, M. N. D. S.; Gottlieb, O. R.; Gottlieb, H. E. Gnetins: Resveratrol Oligomers From Gnetum Species. *J. Nat. Prod.* **1982**, *45* (6), 754–761.
(170) Robinson, R. LXIII.—A Synthesis of Tropinone. *J. Chem. Soc. Trans.* **1917**, *111* (0), 762–768.
(171) Robinson, R. LXXV.—A Theory of the Mechanism of the Phytochemical Synthesis of Certain Alkaloids. *J. Chem. Soc. Trans.* **1917**, *111* (0), 876–899.
(172) Huang, K. A New Oligostilbene from the Roots of Vitis Amurensis. *Chin. Chem. Lett.* **1999**, *10* (9), 775.
(173) Velu, S. S.; Buniyamin, I.; Ching, L. K.; Feroz, F.; Noorbatcha, I.; Gee, L. C.; Awang, K.; Wahab, I. A.; Weber, J.-F. F. Regio- and Stereoselective Biomimetic Synthesis of Oligostilbenoid Dimers from Resveratrol Analogues: Influence of the Solvent, Oxidant, and Substitution. *Chem. - Eur. J.* **2008**, *14* (36), 11376–11384.
(174) Takaya, Y.; Terashima, K.; Ito, J.; He, Y.-H.; Tateoka, M.; Yamaguchi, N.; Niwa, M. Biomimic Transformation of Resveratrol. *Tetrahedron* **2005**, *61* (43), 10285–10290.
(175) Li, C.; Lu, J.; Xu, X.; Hu, R.; Pan, Y. pH-Switched HRP-Catalyzed Dimerization of Resveratrol: A Selective Biomimetic Synthesis. *Green Chem.* **2012**, *14* (12), 3281–3284.
(176) Hong, F.-J.; Low, Y.-Y.; Chong, K.-W.; Thomas, N. F.; Kam, T.-S. Biomimetic Oxidative Dimerization of Anodically Generated Stilbene Radical Cations: Effect of Aromatic Substitution on Product Distribution and Reaction Pathways. *J. Org. Chem.* **2014**, *79* (10), 4528–4543.
(177) Langcake, P.; Pryce, R. J. Oxidative Dimerisation of 4-Hydroxystilbenes in Vitro: Production of a Grapevine Phytoalexin Mimic. *J. Chem. Soc. Chem. Commun.* **1977**, No. 7, 208–210.
(178) Ponzoni, C.; Beneventi, E.; Cramarossa, M. R.; Raimondi, S.; Trevisi, G.; Pagnoni, U. M.; Riva, S.; Forti, L. Laccase-Catalyzed Dimerization of Hydroxystilbenes. *Adv. Synth. Catal.* **2007**, *349* (8-9), 1497–1506.
(179) Sako, M.; Hosokawa, H.; Ito, T.; Iinuma, M. Regioselective Oxidative Coupling of 4-Hydroxystilbenes: Synthesis of Resveratrol and E-Viniferin (E)-Dehydrodimers. *J. Org. Chem.* **2004**, *69* (7), 2598–2600.
(180) Panzella, L.; De Lucia, M.; Amalfitano, C.; Pezzella, A.; Evidente, A.; Napolitano, A.; d' Ischia, M. Acid-Promoted Reaction of the Stilbene Antioxidant Resveratrol with Nitrite Ions: Mild Phenolic Oxidation at the 4'-Hydroxystiryl Sector Triggering Nitration, Dimerization, and Aldehyde-Forming Routes. *J. Org. Chem.* **2006**, *71* (11), 4246–4254.
(181) Sarkanen, K. V.; Wallis, A. F. A. Oxidative Dimerizations of (E)- and (Z)-Isoeugenol (2-Methoxy-4-pro-Penylphenol) and (E)- and (Z)-2,6-Dimethoxy-4-Propenylphenol. *J. Chem. Soc. [Perkin 1]* **1973**, No. 0, 1869–1878.

(182) Li, W.; Li, H.; Luo, Y.; Yang, Y.; Wang, N. Biosynthesis of Resveratrol Dimers by Regioselective Oxidative Coupling Reaction. *Synlett* **4**, *2010* (EFirst), 1247–1250.
(183) Yang, Y.; Liu, Q.; Chen, P.; Li, W. FeCl3·6H2O Oxidation of Protected Resveratrol for the Synthesis of Tetraarylfuran-Type Oligostilbenes. *Tetrahedron Lett.* **2014**, *55* (32), 4455–4457.
(184) Snyder, S. A.; ElSohly, A. M.; Kontes, F. Synthetic Approaches to Oligomeric Natural Products. *Nat. Prod. Rep.* **2011**, *28* (5), 897–924.
(185) Velu, S. S. Strategies and Methods for the Syntheses of Natural Oligomeric Stilbenoids and Analogues. *Curr. Org. Chem.* **2012**, *16* (5), 605–662.
(186) Keylor, M. H.; Matsuura, B. S.; Stephenson, C. R. J. Chemistry and Biology of Resveratrol-Derived Natural Products. *Chem. Rev.* **2015**.
(187) Snyder, S. A.; Zografos, A. L.; Lin, Y. Total Synthesis of Resveratrol-Based Natural Products: A Chemoselective Solution. *Angew. Chem. Int. Ed.* **2007**, *46* (43), 8186–8191.
(188) Snyder, S. A.; Breazzano, S. P.; Ross, A. G.; Lin, Y.; Zografos, A. L. Total Synthesis of Diverse Carbogenic Complexity within the Resveratrol Class from a Common Building Block. *J. Am. Chem. Soc.* **2009**, *131* (5), 1753–1765.
(189) Luo, H.-F.; Zhang, L.-P.; Hu, C.-Q. Five Novel Oligostilbenes from the Roots of Caragana Sinica. *Tetrahedron* **2001**, *57* (23), 4849–4854.
(190) Snyder, S. A.; Thomas, S. B.; Mayer, A. C.; Breazzano, S. P. Total Syntheses of Hopeanol and Hopeahainol A Empowered by a Chiral Brønsted Acid Induced Pinacol Rearrangement. *Angew. Chem. Int. Ed.* **2012**, *51* (17), 4080–4084.
(191) Snyder, S. A.; Wright, N. E.; Pflueger, J. J.; Breazzano, S. P. Total Syntheses of Heimiol A, Hopeahainol D, and Constrained Analogues. *Angew. Chem. Int. Ed.* **2011**, *50* (37), 8629–8633.
(192) Jeffrey, J. L.; Sarpong, R. An Approach to the Synthesis of Dimeric Resveratrol Natural Products via a Palladium-Catalyzed Domino Reaction. *Tetrahedron Lett.* **2009**, *50* (17), 1969–1972.
(193) Jeffrey, J. L.; Sarpong, R. Concise Synthesis of Pauciflorol F Using a Larock Annulation. *Org. Lett.* **2009**, *11* (23), 5450–5453.
(194) Klotter, F.; Studer, A. Total Synthesis of Resveratrol-Based Natural Products Using a Palladium-Catalyzed Decarboxylative Arylation and an Oxidative Heck Reaction. *Angew. Chem. Int. Ed.* **2014**, *53* (9), 2473–2476.
(195) Chou, C.-M.; Chatterjee, I.; Studer, A. Stereospecific Palladium-Catalyzed Decarboxylative C(sp3)□C(sp2) Coupling of 2,5-Cyclohexadiene-1-Carboxylic Acid Derivatives with Aryl Iodides. *Angew. Chem. Int. Ed.* **2011**, *50* (37), 8614–8617.
(196) Zhong, C.; Zhu, J.; Chang, J.; Sun, X. Concise Total Syntheses of (±)isopaucifloral F, (±)quadrangularin A, and (±)pallidol. *Tetrahedron Lett.* **2011**, *52* (22), 2815–2817.
(197) Soldi, C.; Lamb, K. N.; Squitieri, R. A.; González-López, M.; Di Maso, M. J.; Shaw, J. T. Enantioselective Intramolecular C–H Insertion Reactions of Donor–Donor Metal Carbenoids. *J. Am. Chem. Soc.* **2014**, *136* (43), 15142–15145.
(198) Nicolaou, K. C.; Kang, Q.; Wu, T. R.; Lim, C. S.; Chen, D. Y.-K. Total Synthesis and Biological Evaluation of the Resveratrol-Derived Polyphenol Natural Products Hopeanol and Hopeahainol A. *J. Am. Chem. Soc.* **2010**, *132* (21), 7540–7548.
(199) Furst, L.; Matsuura, B. S.; Narayanam, J. M. R.; Tucker, J. W.; Stephenson, C. R. J. Visible Light-Mediated Intermolecular C−H Functionalization of Electron-Rich Heterocycles with Malonates. *Org. Lett.* **2010**, *12* (13), 3104–3107.

(200) Condie, A. G.; González-Gómez, J. C.; Stephenson, C. R. J. Visible-Light Photoredox Catalysis: Aza-Henry Reactions via C−H Functionalization. *J. Am. Chem. Soc.* **2010**, *132* (5), 1464–1465.
(201) Tucker, J. W.; Narayanam, J. M. R.; Shah, P. S.; Stephenson, C. R. J. Oxidative Photoredox Catalysis: Mild and Selective Deprotection of PMB Ethers Mediated by Visible Light. *Chem. Commun.* **2011**, *47* (17), 5040–5042.
(202) Wrighton, M.; Markham, J. Quenching of the Luminescent State of tris(2,2'-bipyridine)ruthenium(II) by Electronic Energy Transfer. *J. Phys. Chem.* **1973**, *77* (26), 3042–3044.
(203) Mulazzani, Q. G.; Sun, H.; Hoffman, M. Z.; Ford, W. E.; Rodgers, M. A. J. Quenching of the Excited States of Ruthenium(II)-Diimine Complexes by Oxygen. *J. Phys. Chem.* **1994**, *98* (4), 1145–1150.
(204) Lechner, R.; Kümmel, S.; König, B. Visible Light Flavin Photo-Oxidation of Methylbenzenes, Styrenes and Phenylacetic Acids. *Photochem. Photobiol. Sci.* **2010**, *9* (10), 1367–1377.
(205) Dai, C.; Meschini, F.; Narayanam, J. M. R.; Stephenson, C. R. J. Friedel–Crafts Amidoalkylation via Thermolysis and Oxidative Photocatalysis. *J. Org. Chem.* **2012**, *77* (9), 4425–4431.
(206) Yasu, Y.; Koike, T.; Akita, M. Three-Component Oxytrifluoromethylation of Alkenes: Highly Efficient and Regioselective Difunctionalization of C□C Bonds Mediated by Photoredox Catalysts. *Angew. Chem. Int. Ed.* **2012**, *51* (38), 9567–9571.
(207) Collin, J.-P.; Dixon, I. M.; Sauvage, J.-P.; Williams, J. A. G.; Barigelletti, F.; Flamigni, L. Synthesis and Photophysical Properties of Iridium(III) Bisterpyridine and Its Homologues: A Family of Complexes with a Long-Lived Excited State. *J. Am. Chem. Soc.* **1999**, *121* (21), 5009–5016.
(208) Wei, Y.; Shao, C.; Hufeng. Voltammetric Response and Electrochemical Properties of the O2/O 2 •− Couple in Acetone. *Russ. J. Electrochem.* **2007**, *43* (2), 178–183.
(209) Corduneanu, O.; Janeiro, P.; Brett, A. M. O. On the Electrochemical Oxidation of Resveratrol. *Electroanalysis* **2006**, *18* (8), 757–762.
(210) Hammond, G. S.; Saltiel, J. Photosensitized Cis-Trans Isomerization of the Stilbenes. *J. Am. Chem. Soc.* **1962**, *84* (24), 4983–4984.
(211) Turro, N. J. *Modern Molecular Photochemistry of Organic Molecules*, 1st edition.; University Science Books: Sausalito, Calif, 2010.
(212) Li, W.; Li, H.; Li, Y.; Hou, Z. Total Synthesis of (±)-Quadrangularin A. *Angew. Chem. Int. Ed.* **2006**, *45* (45), 7609–7611.
(213) Sartori, G.; Bigi, F.; Maggi, R.; Porta, C. Metal-Template Ortho-Regioselective Mono- and Bis-de-Tert-Butylation of Poly-Tert-Butylated Phenols. *Tetrahedron Lett.* **1994**, *35* (38), 7073–7076.
(214) Saleh, S. A.; Tashtoush, H. I. De-Tert-Butylation of Substituted Arenes. *Tetrahedron* **1998**, *54* (47), 14157–14177.
(215) Becker, H. D. New Stable Phenoxy Radicals. Oxidation of Hydroxystilbenes. *J. Org. Chem.* **1969**, *34* (5), 1211–1215.
(216) Dhalla, N. S.; Temsah, R. M.; Netticadan, T. Role of Oxidative Stress in Cardiovascular Diseases. *J. Hypertens.* **2000**, *18* (6), 655–673.

(217) Reuter, S.; Gupta, S. C.; Chaturvedi, M. M.; Aggarwal, B. B. Oxidative Stress, Inflammation, and Cancer: How Are They Linked? *Free Radic. Biol. Med.* **2010**, *49* (11), 1603–1616.
(218) Markesbery, W. R. Oxidative Stress Hypothesis in Alzheimer's Disease. *Free Radic. Biol. Med.* **1997**, *23* (1), 134–147.
(219) Allen, R. .; Tresini, M. Oxidative Stress and Gene Regulation. *Free Radic. Biol. Med.* **2000**, *28* (3), 463–499.
(220) Finkel, T.; Holbrook, N. J. Oxidants, Oxidative Stress and the Biology of Ageing. *Nature* **2000**, *408* (6809), 239–247.
(221) Das, M.; Das, D. K. Resveratrol and Cardiovascular Health. *Phytochem. Cardiovasc. Prot.* **2010**, *31* (6), 503–512.
(222) Vatassery, G. T.; Bauer, T.; Dysken, M. High Doses of Vitamin E in the Treatment of Disorders of the Central Nervous System in the Aged. *Am. J. Clin. Nutr.* **1999**, *70* (5), 793–801.
(223) Jha, P.; Flather, M.; Lonn, E.; Farkouh, M.; Yusuf, S. The Antioxidant Vitamins and Cardiovascular Disease: A Critical Review of Epidemiologic and Clinical Trial Data. *Ann. Intern. Med.* **1995**, *123* (11), 860–872.
(224) Li, B.; Pratt, D. A. Methods for Determining the Efficacy of Radical-Trapping Antioxidants. *Free Radic. Biol. Med.* **2015**, *82*, 187–202.
(225) Frankel, E. N.; German, J. B.; Kinsella, J. E.; Parks, E.; Kanner, J. Inhibition of Oxidation of Human Low-Density Lipoprotein by Phenolic Substances in Red Wine. *The Lancet* **1993**, *341* (8843), 454–457.
(226) Rice-evans, C. A.; Miller, N. J.; Bolwell, P. G.; Bramley, P. M.; Pridham, J. B. The Relative Antioxidant Activities of Plant-Derived Polyphenolic Flavonoids. *Free Radic. Res.* **1995**, *22* (4), 375–383.
(227) Amorati, R.; Ferroni, F.; Pedulli, G. F.; Valgimigli, L. Modeling the Co-Antioxidant Behavior of Monofunctional Phenols. Applications to Some Relevant Compounds. *J. Org. Chem.* **2003**, *68* (25), 9654–9658.
(228) Roschek, B.; Tallman, K. A.; Rector, C. L.; Gillmore, J. G.; Pratt, D. A.; Punta, C.; Porter, N. A. Peroxyl Radical Clocks. *J. Org. Chem.* **2006**, *71* (9), 3527–3532.
(229) Niki, E.; Noguchi, N. Dynamics of Antioxidant Action of Vitamin E. *Acc. Chem. Res.* **2004**, *37* (1), 45–51.
(230) Barclay, L. R. C.; Locke, S. J.; MacNeil, J. M.; VanKessel, J.; Burton, G. W.; Ingold, K. U. Autoxidation of Micelles and Model Membranes. Quantitative Kinetic Measurements Can Be Made by Using Either Water-Soluble or Lipid-Soluble Initiators with Water-Soluble or Lipid-Soluble Chain-Breaking Antioxidants. *J. Am. Chem. Soc.* **1984**, *106* (8), 2479–2481.
(231) Krumova, K.; Friedland, S.; Cosa, G. How Lipid Unsaturation, Peroxyl Radical Partitioning, and Chromanol Lipophilic Tail Affect the Antioxidant Activity of A-Tocopherol: Direct Visualization via High-Throughput Fluorescence Studies Conducted with Fluorogenic A-Tocopherol Analogues. *J. Am. Chem. Soc.* **2012**, *134* (24), 10102–10113.
(232) Li, B.; Harjani, J. R.; Cormier, N. S.; Madarati, H.; Atkinson, J.; Cosa, G.; Pratt, D. A. Besting Vitamin E: Sidechain Substitution Is Key to the Reactivity of Naphthyridinol Antioxidants in Lipid Bilayers. *J. Am. Chem. Soc.* **2013**, *135* (4), 1394–1405.

(233) Drummen, G. P. C.; van Liebergen, L. C. M.; Op den Kamp, J. A. F.; Post, J. A. C11-BODIPY581/591, an Oxidation-Sensitive Fluorescent Lipid Peroxidation Probe: (micro)spectroscopic Characterization and Validation of Methodology. *Free Radic. Biol. Med.* **2002**, *33* (4), 473–490.
(234) Forman, H. J.; Davies, K. J. A.; Ursini, F. How Do Nutritional Antioxidants Really Work: Nucleophilic Tone and Para-Hormesis versus Free Radical Scavenging in Vivo. *Free Radic. Biol. Med.* **2014**, *66*, 24–35.
(235) Oshima, Y.; Ueno, Y. Ampelopsins E, E, H and Cis-Ampelopsin E, Oligostilbenes from Ampelopsis Brevipedunculata Var. Hancei Roots. *Phytochemistry* **1993**, *33* (1), 179–182.
(236) Oshima, Y.; Ueno, Y.; Hikino, H.; Ling-Ling, Y.; Kun-Ying, Y. Ampelopsins A, B and C, New Oligostilbenes of Ampelopsis Brevipedunculata VAR. Hancei. *Tetrahedron* **1990**, *46* (15), 5121–5126.
(237) Sultanbawa, M. U. S.; Surendrakumar, S.; Bladon, P. Distichol an Antibacterial Polyphenol from Shorea Disticha. *Phytochemistry* **1987**, *26* (3), 799–801.